Dynamic wind turbine models in power system simulation tool DIgSILENT

Hansen, Anca Daniela; Iov, F.; Sørensen, Poul Ejnar; Cutululis, Nicolaos Antonio; Jauch, Clemens; Blaabjerg, Frede

Publication date:
2007

Document Version
Publisher's PDF, also known as Version of record

Dynamic wind turbine models in power system simulation tool DIgSILENT

Anca D. Hansen, Florin Iov, Poul Sørensen, Nicolaos Cutululis, Clemens Jauch, Frede Blaabjerg

Risø-R-1400(ed.2)(EN)

Risø National Laboratory
Technical University of Denmark
Roskilde, Denmark
August 2007

Author: Anca D. Hansen, Florin Iov, Poul Sørensen, Nicolaos Cutululis, Clemens Jauch, Frede Blaabjerg
Title: Dynamic wind turbine models in power system simulation tool DIgSILENT
Department: Wind Energy Department

Risø-R-1400(ed.2)(EN)
August 2007

Abstract (max. 2000 char.):
This report presents a collection of models and control strategies developed and implemented in the power system simulation tool PowerFactory DIgSILENT for different wind turbine concepts. It is the second edition of Risø-R-1400(EN) and it gathers and describes a whole wind turbine model database built-op and developed during several national research projects, carried out at Risø DTU National Laboratory for Sustainable Energy and Aalborg University, in the period 2001-2007. The overall objective of these projects was to create a wind turbine model database able to support the analysis of the interaction between the mechanical structure of the wind turbine and the electrical grid during different operational modes.
The report provides thus a description of the wind turbines modelling, both at a component level and at a system level. The report contains both the description of DIgSILENT built-in models for the electrical components of a grid connected wind turbine (e.g. induction generators, power converters, transformers) and the models developed by the user, in the dynamic simulation language DSL of DIgSILENT, for the non-electrical components of the wind turbine (wind model, aerodynamic model, mechanical model). The initialisation issues on the wind turbine models into the power system simulation are also presented.
The main attention in the report is drawn to the modelling at the system level of the following wind turbine concepts:

1. Fixed speed active stall wind turbine concept
2. Variable speed doubly-fed induction generator wind turbine concept
3. Variable speed multi-pole permanent magnet synchronous generator wind turbine concept

These wind turbine concept models can be used and even extended for the study of different aspects, e.g. the assessment of power quality, control strategies, connection of the wind turbine at different types of grid and storage systems. Different control strategies have been developed and implemented for these wind turbine concepts, their performance in normal or fault operation being assessed and discussed by means of simulations. The described control strategies have different goals e.g. fast response over disturbances, optimum power efficiency over a wider range of wind speeds, voltage ride-through capability including grid support. A dynamic model of a DC connection for active stall wind farms to the grid including the control is also implemented and presented.

ISSN 0106-2840
ISBN 978-87-550-3553-9

Contract no.:
ENS 1363/04-0008

Group's own reg. no.:
1115043-01

Sponsorship:

Cover :

Pages: 190
Tables: 7
References: 74

Information Service Department
Risø National Laboratory
Technical University of Denmark
P.O.Box 49
DK-4000 Roskilde
Denmark
Telephone +45 46774004
bibl@risoe.dk
Fax +45 46774013
www.risoe.dk

Contents

Preface

This report describes the modelling and control work carried out during two projects, i.e. “Simulation platform for modelling, optimization and design of wind turbines”, and "Electrical Design and Optimisation of Wind Turbines". These projects, carried out in a cooperation between Risø DTU National Laboratory for Sustainable Energy and Aalborg University, were funded by the Danish Energy Agency contract numbers ENS 1363/04-0008 and ENS-1363/01-0013.

1 Introduction

The present report describes the dynamic wind turbine models implemented in the power system simulation tool DIgSILENT, which provides both an extensive library for grid components and a dynamic simulation language (DSL) for the modelling of each wind turbine component. The development of these models is a part of the results of a national Danish research project, whose overall objective is to create a model database of electrical components mainly, in different simulation tools in order to enhance the design and the optimisation of the wind turbines.

The developed model database is able to support the analysis of the interaction between the mechanical structure of the wind turbine and the electrical grid both during normal operation of the wind turbine and during transient grid fault events. Such models make it possible to simulate the dynamic interaction between a wind turbine/wind farm and a power system. They enable both the potential wind turbine owners and the grid utility technical staff to perform the necessary studies before investing and connecting wind turbines (farms) to the grid. Simulation of the wind turbine interaction with the grid may thus provide valuable information and may even lower the overall grid connection costs.

The motivation for this research work is the ever-increasing wind power penetration into power networks. In recent years the trend has been moved from installations with a few wind turbines to the planning of large wind farms with several hundred MW of capacity. This increased and concentrated penetration makes the power network more dependent on, and vulnerable to, the wind energy production. This situation means that future wind farms must be able to replace conventional power stations, and thus be active controllable elements in the power supply network. In other words, wind farms must develop power plant characteristics (Sørensen P. et al., 2000). The two utilities responsible for the transmission systems in Denmark, Eltra and Elkraft System, have issued requirements (Eltra, 2000) that focus on the influence of wind farms on grid stability and power quality, and on the control capabilities of wind farms.

Another consequence of the increased future size of wind farms is that the large wind farms will be connected directly to the high voltage transmission grid. Until now, wind turbines and wind farms have been connected to the distribution system, which typically has either 10/20 kV or 50/60 kV grids. Therefore, the main focus has been on the influence of the wind farms on the power quality of the distribution system. For example in Denmark, this has been regulated by the Danish Utilities Research Institute (DEFU) requirements for grid connection of wind turbines to the distribution system (DEFU, 1998). However, the transmission system operators in Denmark now issue more strict connection requirements for large wind farms if they are connected directly to the transmission system. Moreover, national standards for power quality of wind turbines have recently been supplemented by a new standard for measurement and assessment of power quality of grid connected wind turbines, namely (IEC 61400-21,2001).

A large part of the report is dedicated to the modelling and control of three wind turbine concepts, namely:

1. Fixed speed active stall wind turbine concept

2. Variable speed doubly-fed induction generator wind turbine concept
3. Variable speed multi-pole permanent magnet synchronous generator wind turbine concept

The report is organised as follows. First, the power system simulation tool DIgSILENT is shortly described. Then the wind turbine modelling in DIgSILENT is presented. The modelling and control of the mentioned wind turbine concepts in the power simulation tool DIgSILENT are then presented, their performance being assessed and analysed by means of simulations. Different control strategies are presented and designed for both normal and fault operation, based on goals such as fast response over disturbances, optimum power efficiency over a wider range of wind speeds, voltage ride-through and grid support capabilities.

2 Wind turbine modelling in DIgSILENT

After a short description of the power system simulation tool, the goal of this chapter is to describe the wind turbine modelling in DIgSILENT at component level, namely the modelling of each wind turbine component.

2.1 Power system simulation tool - DIgSILENT

The increasing capacity of wind power penetration is one of today's most challenging aspects in power-system control. Computer models of power systems are widely used by power-system operators to study load flow, steady state voltage stability, dynamic and transient behaviour of power systems. Today these tools must incorporate extensive modelling capabilities with advanced solution algorithms for complex power-system studies, as in the case of wind power applications. An example of such a tool is the power system simulation tool DIgSILENT (DIgSILENT, 2006).

DIgSILENT has the ability to simulate load flow, RMS fluctuations and transient events in the same software environment. It provides models on a different level of detailing. It combines models for electromagnetic transient simulations of instantaneous values with models for electromechanical simulations of RMS values. This makes the models useful for studies of both (transient) grid fault and (longer-term) power quality and control issues.

DIgSILENT provides a comprehensive library of models of electrical components in power systems. The library includes models of e.g. generators, motors, controllers, dynamic loads and various passive network elements (e.g. lines, transformers, static loads and shunts). Therefore, in the present work, the grid model and the electrical components of the wind turbine model are included as standard components in the existing library. The models of the wind speed, the mechanics, aerodynamics and the control systems of the wind turbines are written in the dynamic simulation language DSL of DIgSILENT. The DSL makes it possible for users to create their own blocks either as modifications of existing models or as completely new models. These new models can be collected into a library, which can be easily used further in the modelling of other wind farms with other wind turbines.

The program DIgSILENT has been extended and further developed for wind power applications, based on extensive communication and collaboration between DIgSILENT and Risø DTU National Laboratory for Sustainable Energy.

In the following, the two types of models in DIgSILENT are presented:

1. Built-in models, which are standard electrical component models, already existing in the DIgSILENT library.
2. DSL models, which are created by the user in the dynamic simulation language DSL.

2.2 Grid component built-in models in DIgSILENT

The built-in models are standard models existing in DIgSILENT for different electrical components. The internal details of these models (e.g. equations, assumptions, approximations) are not directly accessible for the user and therefore they can only be used as black boxes with predefined inputs and outputs.

During the implementation of different wind turbine models in DIgSILENT, different built-in models are used for the grid components and for the electrical wind turbine components, e.g. generators, power converters, transformers and capacitors. The simulation results depend strongly on these built-in component models and they are therefore briefly described below, based on DIgSILENT documentation.

A grid can be modelled in a graphical programming environment, see Figure 1, where the power system component models (built-in models) are dragged, dropped and connected.

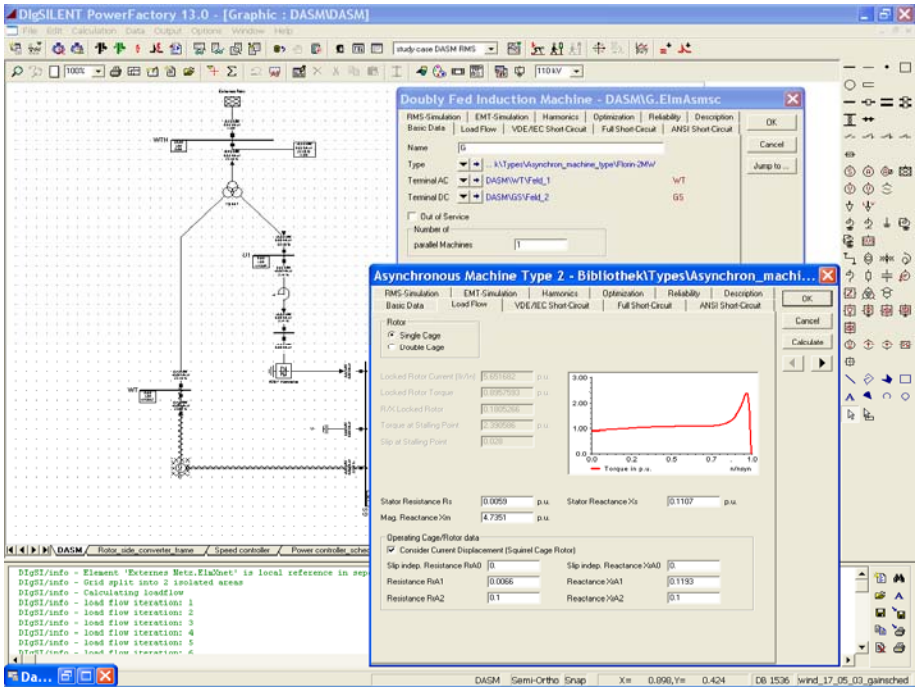

Figure 1: DIgSILENT graphical programming environment.

2.2.1 Electrical machinery

DIgSILENT provides models for induction (asynchronous) machines as well as for synchronous machines.

DIgSILENT machine models are black boxes with predefined inputs and outputs. Figure 2 illustrates the built-in blocks, with the most relevant input and output signals for squirrel cage induction generator (SCIG), doubly-fed induction generator (DFIG) and synchronous generator (SG).

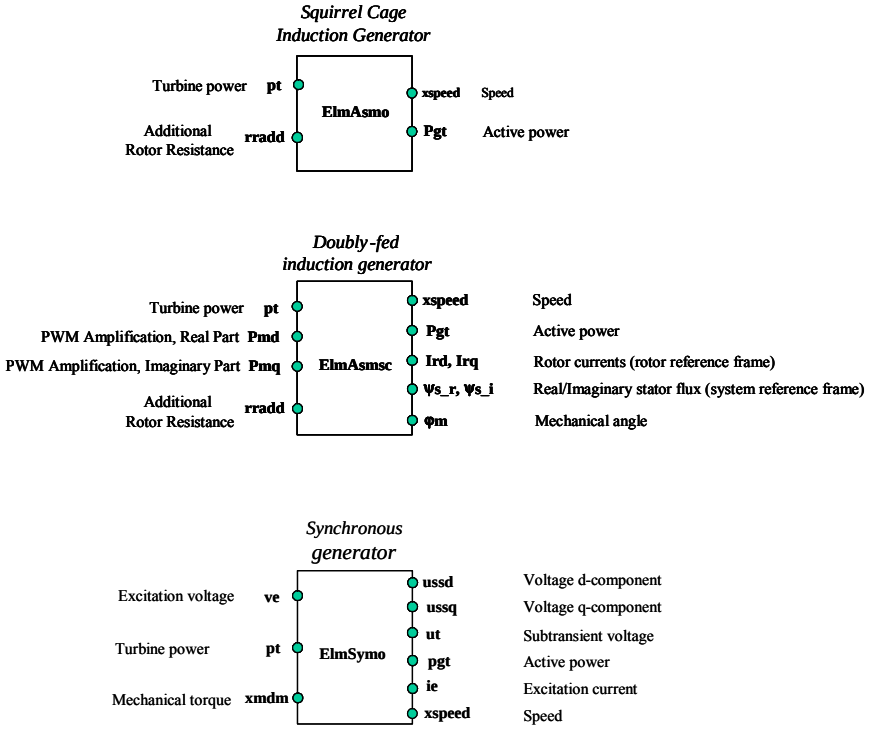

Figure 2: Squirrel cage induction generator (SCIG), doubly-fed induction generator (DFIG) and synchronous generator (SG) blocks.

1. *Squirrel cage induction generator model* (*ElmAsmo* asynchronous machine block model) – has the mechanical power of the wind turbine as primer mover input. An additional rotor resistance can be inserted if it is necessary. The outputs are the generator speed and the electrical power. In the load flow calculation, used in the initialisation process of the system, the information on the generators active power has to be specified.
2. *Doubly-fed induction generator model* (*ElmAsmsc* slip controlled asynchronous machine block model) – has as inputs the mechanical power of the wind turbine, the pulse width modulation factors *Pmd*, *Pmq* and the additional rotor resistance. As outputs, besides the speed and the active power, the rotor currents, the stator flux and the mechanical angle of the rotor can be delivered. In the load flow calculation, the active power for the stator, the reactive power and the slip have to be specified. Internally, the corresponding modulation factors of the converter are calculated and together with power balance between the AC and DC side of the converter, DC voltage and DC current are obtained.
3. *Synchronous generator* (ElmSymo – synchronous machine block model) – has as inputs the excitation voltage and the mechanical power of the wind turbine. The outputs are the generator speed, the electrical power and the excitation current. In the load flow calculation, used in the initialisation process of the system, the information on the generators active power has to be specified.

2.2.1.1 *Squirrel cage induction generator (SCIG)*

DIgSILENT uses different equivalent circuits to define the parameters in the induction generator model, as illustrated in Figure 3. It consists of a general model for the stator, which can be combined with three different rotor models, depending on the type of the generator. The model is thus basically a classical induction machine model including a slip dependent rotor impedance *Zrot.*

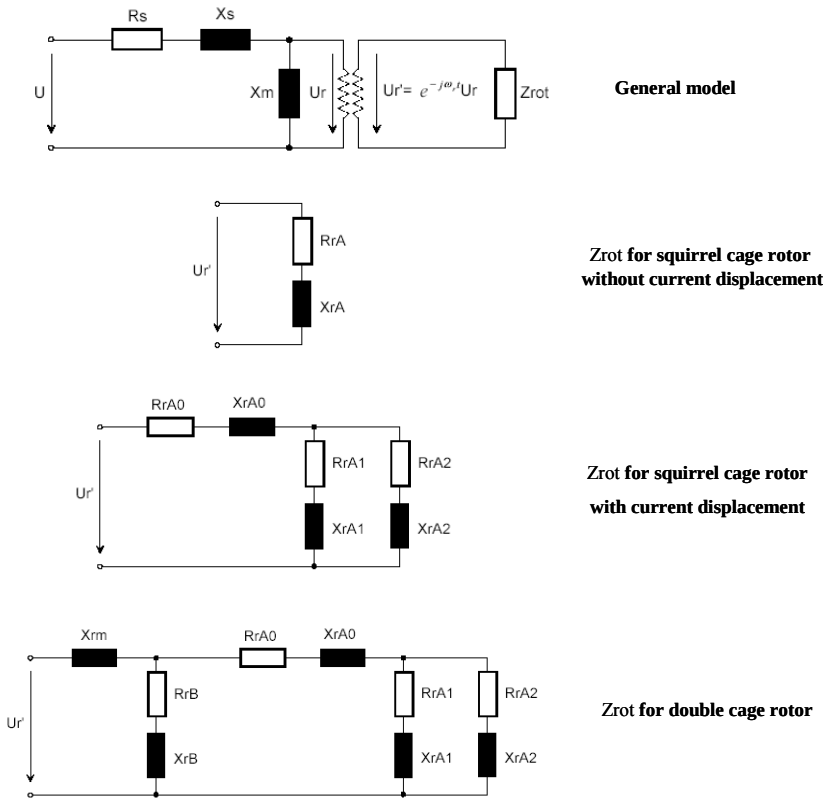

Figure 3: Squirrel cage induction generator diagram with the different definitions for the rotor impedance Zrot.

The model is characterized by the stator winding resistance R_s, the stator leakage reactance X_s, the magnetizing reactance X_m and the rotor impedance Z_{rot}. The rotor impedance Z_{rot} is frequency dependent and allows therefore the modeling over a wide speed/slip range. The rotor impedance can be approximated by parallel R-L elements. Different rotor circuit designs, depending on the rotor geometry, can thus be modeled by selecting a specific rotor impedance Z_{rot}.

Three different squirrel cage rotor types, as illustrated in Figure 3, can be used:

- Squirrel cage rotor without current displacement
- Squirrel cage rotor with current displacement
- Double cage rotor

The input parameters of the generator can be entered either by directly specifying the resistances and reactances of the equivalent circuit diagrams (if they are known e.g. from tests or other simulation programs) or by specifying characteristic points on the slip-torque and slip-current characteristic of the generator. When the electrical parameters are not available, they are automatically

calculated from the nominal operation point and slip-torque/slip-current characteristics. The nominal operation point is specified by the rated mechanical power, the rated power factor, the efficiency at nominal operation and the nominal speed.

The dynamic model of the induction generator uses the steady state parameters defined in the equivalent diagram depicted in Figure 3. DIgSILENT provides a d-q model, expressed in the rotor reference frame:

$$\begin{aligned} u_s &= R_s\, i_s + j\,\omega_{syn}\,\psi_s + \frac{d\psi_s}{dt} \\ 0 &= R_r\, i_r + j\,(\omega_{syn} - \omega_r)\,\psi_r + \frac{d\psi_r}{dt} \end{aligned} \tag{1}$$

where u, i, and ψ are space vectors for the voltage, current and flux, respectively. ω_{syn} is the synchronous speed, while ω_r is the angular speed of the rotor.

As the rotor is short-circuited in the squirrel-cage induction generator, the rotor voltage is set to zero. The voltage equations are used in DIgSILENT in per unit quantities, as follows:

$$\begin{aligned} \underline{u}_s &= \underline{R}_s\, \underline{i}_s + j\,\frac{\omega_{syn}}{\omega_n}\,\underline{\psi}_s + \frac{1}{\omega_n}\,\frac{d\underline{\psi}_s}{dt} \\ 0 &= \underline{R}_r\, \underline{i}_r + j\,\frac{(\omega_{syn} - \omega_r)}{\omega_n}\,\underline{\psi}_r + \frac{1}{\omega_n}\,\frac{d\underline{\psi}_r}{dt} \end{aligned} \tag{2}$$

where ω_n is the nominal electrical frequency of the network.

As mentioned before, DIgSILENT provides models with different detailing levels. Depending on the goal of the analysis, it is possible to select the models of an appropriate detailing level, by choosing the type of simulation method. For stability analysis, power quality and control issues, RMS simulations are used. RMS simulations are based on simplified electromechanical transient models. In the case of induction generators, the RMS simulation is using a third order generator model, where the stator transients are neglected. For the analysis of the wind turbine's behavior during grid faults, electromagnetic transient EMT simulations of instantaneous values are used. For this purpose, models of higher detailing level e.g. a fifth order generator model are used.

The generator inertia is modeled inside the built-in induction machine model. The generator inertia is specified in the form of an acceleration time constant in the induction generator type.

The dynamic model of the induction generator is completed by the mechanical equation:

$$J\,\dot{\omega}_r = T_e - T_m \tag{3}$$

where J is generator inertia, T_e is the electrical torque, T_m is the mechanical torque. The mechanical equation can be rated to the nominal torque:

$$T_n = P_n / \left[\omega_n\,(1 - s_n)\right] \tag{4}$$

and thus the acceleration time constant T_{ag} can be expressed as:

$$T_{ag} = \frac{J\,(1 - s_n)\,\omega_n^2}{P_n} \tag{5}$$

where ω_n is the nominal electrical frequency of the network and s_n is the nominal slip.

2.2.1.2 *Doubly-fed induction generator (DFIG)*

The doubly-fed induction generator (DFIG) model in DIgSILENT, illustrated in Figure 3, extends the usual induction generator by a PWM rotor-side converter in series to the rotor impedance Z_{rot} (DIgSILENT, 2006).

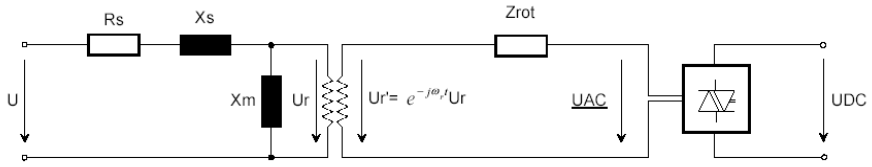

Figure 4: Doubly-fed induction machine with rotor-side converter.

The PWM converter inserted in the rotor circuit allows for a flexible and fast control of the machine by modifying the magnitude and phase angle of the generator's AC voltage output U_{AC} on the rotor side. This is done by modifying the modulation factor *PWM*. Based on the power balance between the AC and DC side of the converter, the DC voltage and DC current can be then calculated (DIgSILENT, 2006). The AC-DC relationship of the PWM converter is the following (the AC voltage is expressed as line-to-line voltage):

$$U_{ACr} = \frac{\sqrt{3}}{2\sqrt{2}} \cdot PWM_r \cdot U_{DC}$$
$$U_{ACi} = \frac{\sqrt{3}}{2\sqrt{2}} \cdot PWM_i \cdot U_{DC} \qquad (6)$$

where PWM_r and PWM_i are the real and imaginary components of the modulation factor, respectively.

It is assumed that a standard bridge consisting of six transistors builds the converter and that an ideal sinusoidal pulse width modulation is applied. The relationship between AC and DC currents can be found by assuming that the PWM converter is loss free:

$$P_{AC} = \mathrm{Re}(U_{AC}\ I_{AC}^{*}) = U_{DC}\, I_{DC} = P_{DC} \qquad (7)$$

During time domain simulations the converter is controlled through the pulse width modulation factors PWM_d and PWM_q, which define the ratio between DC-voltage and the AC-voltage at the slip rings.

The model equations of the doubly-fed machine can be derived from the normal induction machine equations by modifying the rotor-voltage equations:

$$\underline{u}_s = \underline{R}_s \underline{i}_s + j\frac{\omega_{syn}}{\omega_n}\underline{\psi}_s + \frac{1}{\omega_n}\frac{d\underline{\psi}_s}{dt}$$
$$\underline{u}_r\, e^{-j(\omega_{syn}-\omega_r)t} = \underline{R}_r \underline{i}_r + j\frac{(\omega_{syn}-\omega_r)}{\omega_n}\underline{\psi}_r + \frac{1}{\omega_n}\frac{d\underline{\psi}_r}{dt} \qquad (8)$$

The per unit rotor voltage that appears in the above equation is related to the DC- voltage as follows:

$$\underline{u}_{rd} = \frac{\sqrt{3}}{2\sqrt{2}} \cdot PWM_d \cdot \frac{U_{DC}}{U_{rnom}}$$
$$\underline{u}_{rq} = \frac{\sqrt{3}}{2\sqrt{2}} \cdot PWM_q \cdot \frac{U_{DC}}{U_{rnom}} \qquad (9)$$

where U_{rnom} is the nominal rotor voltage.

In the case of faults near the generator, rotor currents are increasing and risk to damage the rotor-side converter. The rotor-side PWM-converter is therefore protected against such high rotor currents by a bypass-circuit (Pöller, M., 2003). If the rotor current exceeds the maximum allowed value, a bypass R-L-circuit is immediately inserted and the rotor-side converter is blocked. All parameters of the bypass protection, including the time for its automatic removal can directly be entered in the input dialogue of the doubly-fed induction machine (element).

Figure 5 illustrates the single line diagram of DFIG configuration in DIgSILENT.

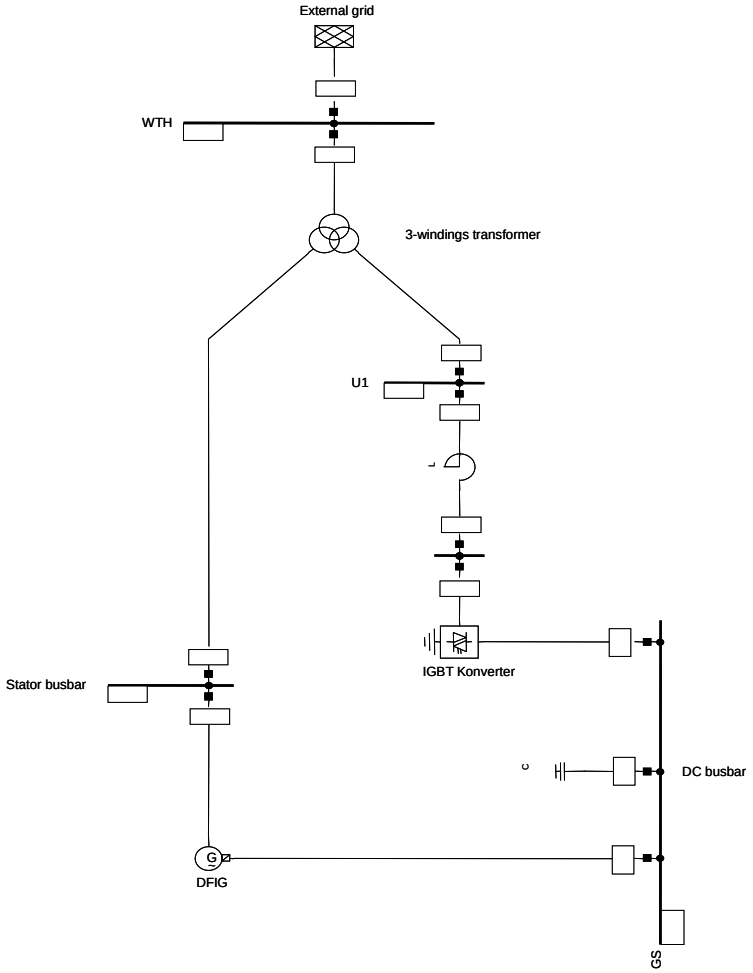

Figure 5: Single line diagram of the DFIG in DIgSILENT.

It contains a DFIG built-in model (the usual induction machine model extended with the PWM rotor-side converter), a common DC – busbar, an IGBT grid-side converter (independent component in DIgSILENT's library) and an inductor in series with the grid converter, used to smooth the converter currents. This inductor may also be integrated into the transformer.

The controllers of the rotor-side converter and of the grid-side converter are implemented as DSL models in DIgSILENT – see for details in Chapter 4.

2.2.1.3 *Synchronous generator*

A DC excited synchronous generator can be electrically represented by the one phase equivalent circuit shown in Figure 6. In addition to that, the phasor diagram of the synchronous generator is plotted for an arbitrary operational point. The rotor field is generated by the excitation current I_f, which induces the voltage E (electromotive force EMF) in the stator windings. The total magnetic field is represented with the main inductance X_h.

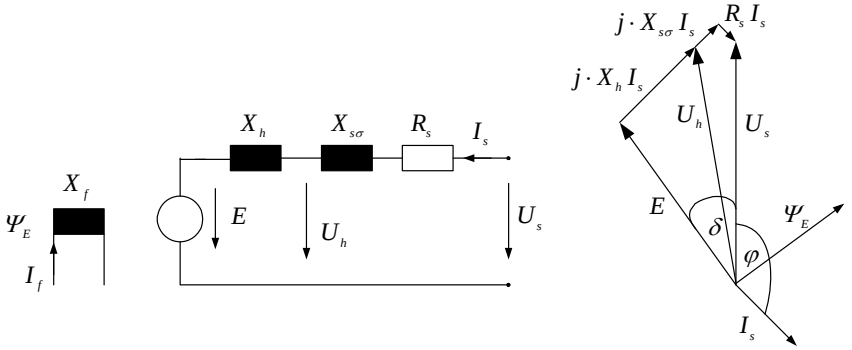

Figure 6: One phase equivalent circuit and phasor diagram of a DC excited synchronous generator

If the stator windings resistance R_s and the leakage reactance $X_{\sigma s}$ are neglected the equivalent circuit can be simplified. A simplified equivalent circuit is shown in Figure 7 for a permanent magnet induction generator. The voltage E is now induced by permanent magnets.

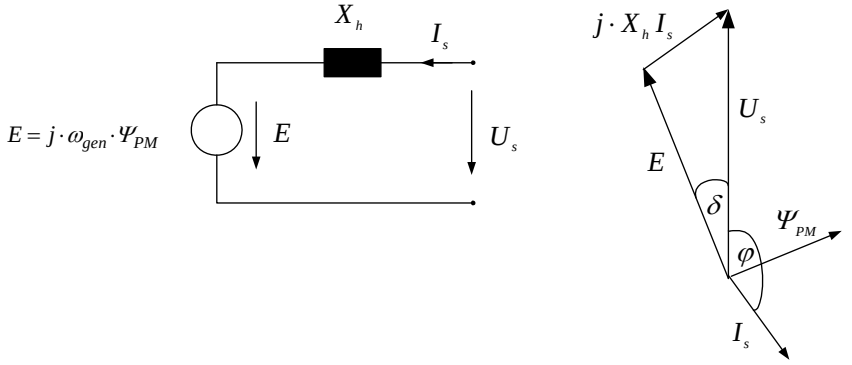

Figure 7: Simplified equivalent circuit a phasor diagram of a PM excited synchronous generator.

E	electromotive force (induced voltage)	X_f	field winding reactance
U_s	stator voltage	X_h	main reactance
U_h	voltage, representing the main field	$X_{s\sigma}$	stator leakage reactance
I_s	stator current	R_s	stator reactance
Ψ_{PM}	Permanent magnet flux	δ	load angle
Ψ_E	DC excited flux	φ	power factor
I_f	excitation current	ω_{gen}	generator rotational speed

Both, frequency and amplitude of the induced voltage E depend on the actual rotor speed $\omega_{gen} = p \cdot \Omega_{gen}$. The difference between the two voltage vectors E and U_s, which is mainly caused by the load angle δ, drives the stator current I_s. Based on this, a dependency between the machine torque, the voltages E and U_s and the load angle δ can be derived:

$$\begin{aligned} P_{gen} &= m \cdot \Re\left\{U_s \cdot I_s^*\right\} = m \cdot \Re\left\{U_s \cdot \frac{U_s - E \cdot (\cos\delta - j\sin\delta)}{-jX_h}\right\} \\ &= -m \cdot \frac{U_s \cdot E}{X_h} \sin\delta \\ T_e &= \frac{P_e}{\Omega_{gen}} = \frac{-m}{\Omega_{gen}} \cdot \frac{U_s \cdot E}{X_h} \sin\delta \end{aligned} \tag{10}$$

The reactive power of the generator is determined by:

$$\begin{aligned} Q_{gen} &= m \cdot \Im\left\{U_s \cdot I_s^*\right\} = m \cdot \Im\left\{U_s \cdot \frac{U_s - E \cdot (\cos\delta - j\sin\delta)}{-jX_h}\right\} \\ &= m \cdot \frac{U_s^2 - U_s \cdot E\cos\delta}{X_h} \end{aligned}$$

m	number of phases	P_{gen}	Generator active power
T_e	Electromagnetic torque	Q_{gen}	Generator reactive power
p	number of pole pairs	Ω_{gen}	Mechanical generator speed

Under load conditions, the stator current I_s and the stator reactance X_h also cause a magnetic field, which is superposed to the field of the rotor. Thus, the voltage U_s corresponds to the voltage induced by the total magnetic field (Grauers, 1999). The voltage drop over the machine's reactance X_h provokes a phase delay between the electromotive force E and the stator voltage U_s, which are equal only for no-load.

An increasing torque of the generator increases the load angle (the phase shift between Us and E) and thus also the reactive power of the machine. While electrical excited machines are controlled to be reactive neutral (reducing the converter rating to the active power value), permanent magnet machines, with their fixed excitation, work generally underexcited (Jöckel, 2002).

Synchronous machine models for power system analysis are usually based on the assumption that the magnetic flux distribution in the rotor is sinusoidal. With this assumption the flux can entirely be described by a vector and thus the internal voltage E induced in the stator by the permanent magnets can be expressed as follows:

$$E = \omega_{gen} \Psi_{PM} = 2\pi f \cdot \Psi_{PM} \tag{11}$$

where ω_{gen} is the electrical generator rotational speed, Ψ_{PM} is the magnitude of the flux provided by the permanent magnets of the rotor, and f is the electrical frequency. The excitation voltage E is proportional with the electrical speed of the generator.

The equations of a PMSG can be expressed directly from the equations of a DC excited SG, with the simplification that a PMSG does not have damper windings (Kundur, 1994). The voltage equations of the generator, expressed in

the rotor-oriented dq-reference frame RRF (the reference frame d-axis is aligned with the vector of the permanent magnet flux), can be expressed as follows:

$$\begin{aligned} u_{sd} &= R_s\, i_{sd} - \omega_e\, \psi_{sq} + \dot{\psi}_{sd} \\ u_{sq} &= R_s\, i_{sq} + \omega_e\, \psi_{sd} + \dot{\psi}_{sq} \end{aligned} \tag{12}$$

With the stator flux components:

$$\begin{aligned} \psi_{sd} &= L_d\, i_{sd} + \psi_{PM} \\ \psi_{sq} &= L_q\, i_{sq} \end{aligned} \tag{13}$$

Where u_{ds} and u_{qs} are the terminal stator voltages, i_{ds} and i_{qs} are the stator currents, L_d and L_q are the stator inductances in the dq reference frame. In stability studies, where the stator transients can be neglected, the stator voltage equations can be reduced to:

$$\begin{aligned} u_{sd} &= R_s\, i_{sd} - \omega_e\, \psi_{sq} \\ u_{sq} &= R_s\, i_{sq} + \omega_e\, \psi_{sd} \end{aligned} \tag{14}$$

The electrical torque of the generator is:

$$T_e = \frac{3}{2}\, p\, \mathrm{Im}\left[\bar{\psi}_s^{*}\, \bar{i}_s\right] = \frac{3}{2}\, p\, \left[\psi_{sd}\, i_{sq} - \psi_{sq}\, i_{sd}\right] \tag{15}$$

Expressing further the stator flux components, the electrical torque can be calculated by:

$$T_e = \frac{3}{2}\, p\, \left[(L_d - L_q)\, i_{sd}\, i_{sq} + \psi_{PM}\, i_{sq}\right] \tag{16}$$

If the generator is a round rotor machine, where L_d=L_q, the equation for the electrical torque results only from the permanent magnet flux and the q-component of the stator current:

$$T_e = \frac{3}{2}\, p\, \psi_{PM}\, i_{sq} \tag{17}$$

The active and reactive power of the synchronous generator can be then expressed as:

$$\begin{aligned} P_{gen} &= T_e\, \omega_m = \frac{3}{2}\left[u_{sd}\, i_{sd} + u_{sq}\, i_{sq}\right] \\ Q_{gen} &= \frac{3}{2}\left[u_{sq}\, i_{sd} - u_{sd}\, i_{sq}\right] \end{aligned} \tag{18}$$

As multipole permanent magnet generators are low speed applications and generally connected to the grid through a frequency converter system, the generator has no damper winding in the rotor core. Moreover, due to the permanent excitation a PMSG has no field windings, in which transient currents could be induced or damped, respectively. Hence, in case of load changes the field windings would not contribute to damping either.

As neither a damper nor field winding exists in a PMSG, no transient or subtransient reactances, as known for wound rotor SGs, can be defined for the PMSG.

$$x_d = x'_d = x''_d$$
$$x_q = x'_q = x''_q \quad (19)$$

x_d Synchronous reactance x_d' Transient reactance
x_d'' Subtransient reactance

However, as the multipole PMSG is a low speed application with slow dynamics, a damper winding is less important (Akhmatov, 2003). Nevertheless, a damping of the system must then be applied by means of the converter control.

2.2.2 Power converters

DIgSILENT provides models for different power converters such as: rectifiers/inverters, PWM converters, softstarter. They are briefly described below.

Rectifier/Inverter

The rectifier/inverter model is used to create DC power links, or for building power electronic devices such as variable speed drives (DIgSILENT, 2006). The rectifier and inverter models allow modelling of different types of frequency converters. For example, in the doubly-fed induction generator concept, the rotor circuit is connected to the grid through two PWM converters working back-to-back.

PWM converter

The power converters used in wind turbines are usually realised by self-commutated pulse-width modulated circuits, voltage source AC/DC converter based on the equivalent circuit shown in Figure 8. The DC-link capacitor is not included in the converter model.

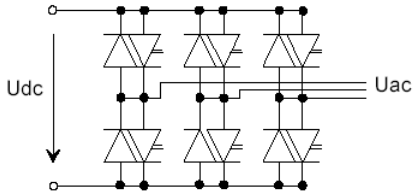

Figure 8: Generic PWM converter model.

These circuits are built by six valves with turn-off capability and six anti-parallel diodes. The valves are typically realised by IGBTs (insulated gate bipolar transistors) because they allow for higher switching frequencies than classical GTOs.

The general model of the PWM converter, that usually operated as a voltage source converter, is illustrated in Figure 9.

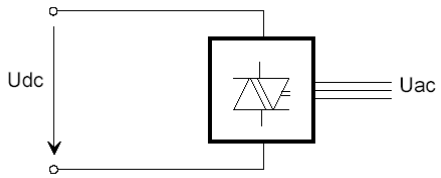

Figure 9: PWM converter - general model.

In load flow analysis, PWM converter model supports several control conditions. The initial value of the PWM modulation index results from the load flow calculation. The supported control conditions are as follows:

- V_{ac}-phi – Specifies magnitude and phase of the AC terminal. Typical control mode for motor-side converters in variable speed applications.
- V_{DC}-phi – Specifies the DC-voltage and the AC-voltage phase. No typical application;
- PWM-phi – Load flow setup without control. The PWM index is directly set in magnitude and phase.
- V_{DC}-Q – Specifies DC-voltage and reactive power. Typical applications: STATCOM, UPFC, grid-side converter for doubly-fed induction machine, VSC-HVDC applications.
- V_{ac}-P - Specifies AC-voltage magnitude and active power. This mode is equivalent to a PV characteristic of synchronous generators. Typical applications: Grid-side converter of converter driven synchronous machines, VSC-HVDC;
- P-Q – Specifies P and Q at the AC-side. This control is equivalent to a PQ characteristic of synchronous machines. Typical applications: Grid-side converter of converter driven synchronous machines, VSC-HVDC.

Since the model is based on the fundamental frequency approach, the load flow calculations will assume always a 50 Hz frequency on the bus bars. Then, the voltage angle for each bus bar is calculated in respect with the global reference frame as shown in Figure 10. This is the reason that for all the control conditions in the load flow analysis the frequency is not a controlled variable.

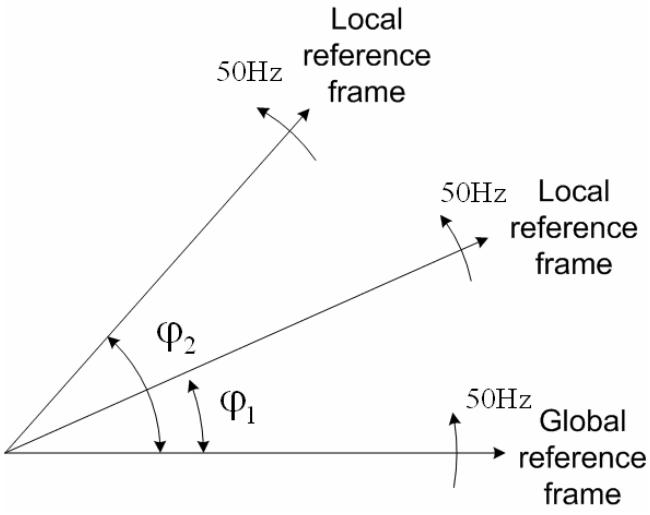

Figure 10. Reference systems in DIgSILENT.

Moreover, for the same reason the doubly-fed induction machine model in DIgSILENT includes the generator side PWM converter. In this case the frequency of the rotor voltage depends on the mechanical speed. If a separate model for the PWM converter is used and connected to the machine terminals via a bus bar, terminal or point terminal the load flow calculation will not be possible. In this situation the fundamental frequency of 50 Hz is used for the

PWM converter from the rotor-side and the modulation index cannot be calculated according with the mechanical speed of the machine.

For both RMS and EMT simulations, the PMW converter model is based on a fundamental frequency approach. The *PWM* index (magnitude and phase) can be defined in different ways depending on the application.

The model supports sinusoidal and rectangular modulation. Saturation and losses are taking into account. An equivalent resistance between the DC terminals models the losses in the converter. At fundamental frequency, the ideal, loss-less converter can be modelled by a DC voltage controlled AC voltage source conserving active power between AC and DC side. For values $|PWM|<1$, the model equations are expressed as follows:

$$\begin{aligned} U_{ACr} &= K_0 \cdot PWM_r \cdot U_{DC} \\ U_{ACi} &= K_0 \cdot PWM_i \cdot U_{DC} \end{aligned} \qquad (20)$$

where U_{ACr} , U_{ACi} are the real and the imaginary parts of the AC voltage, corresponding to the positive sequence component. PWM_r, PWM_i are the real and the imaginary modulation factors, while K_0 is the modulation factor, defined as follows:

- $K_0 = \dfrac{\sqrt{3}}{2\sqrt{2}}$ for a sinusoidal *PWM*
- $K_0 = \dfrac{\sqrt{2}\,\sqrt{3}}{\pi}$ for a rectangular *PWM* or for no modulation

For EMT simulations, DIgSILENT provides an additional modelling option, namely a switching model of the converter using a switching frequency and on and off resistances.

The input parameters for the converter are the rated AC or DC voltage, the rated power and the modulation factor K_0, which relates the fundamental component of the line to line AC voltage to the DC voltage. The equation (10) is valid for modulation factor $0 \leq |PWM| < 1$. For values higher than 1, the converter starts to saturate and the level of low-order harmonics starts increasing. In order to avoid the low-order harmonics the controllers of the converters usually limit the pulse-width modulation factor to 1.

Assuming the PWM to be loss-less, the converter equation can be completed by the power conservation equation:

$$P_{AC} = \mathrm{Re}(U_{AC}\, I_{AC}^{*}) = U_{DC}\, I_{DC} = P_{DC} \qquad (21)$$

As the switching frequency of PWM converters is usually very high (5-10kHz), the switching losses are the predominant type of losses.

The input definitions of the stability model (RMS) are presented in Table 1.

Name	Unit	Description
Pm_in	p.u.	Magnitude of PWM Index
f0	p.u.	Input frequency
F0Hz	Hz	Input frequency
dphiu	rad	Voltage angle
Pmr		Real part of PWM index
Pmi		Imaginary part of PWM Index
cosref		Cos of reference angle
sinref		Sin of reference angle
Pmd		PWM Index in d-axis
Pmq		PWM Index in q-axis
id_ref	p.u.	Current reference in d-axis
iq_ref	p.u.	Current reference in q-axis

Table 1: Input definition of the stability model.

The control variables for the stability model are defined in 4 ways depending on the applications (DIgSILENT, 2006):

A. *Pmr*, *Pmi* – Real and imaginary part of the PWM index. The reference system in this case is the global reference frame, which is usually defined by a reference-machine, external network, voltage source or a PWM converter. This sets of inputs must be always used in combination with phase measurement devices e.g. Phase Locked Loop (PLL) and transformation between reference frames.

B. *Pmd, Pmq*, *cosref*, *sinref* – This set of input is used in grid-connected applications. The PWM Index-vector is specified with a reference to a reference system, which is defined by *cosref* and *sinref*. For example the output from the current controllers are connected to *Pmd* and *Pmq* while the voltage is measured using a PLL and its output gives the *cosref* and *sinref* signals.

C. *Pm_in*, dphiu – magnitude and phase of the PWM Index. This representation is equivalent to Pmr, Pmi. The phase of PWM Index *dphiu* is expressed with reference to the global reference frame.

D. *Pm_in*, *f0* (*F0Hz*) – *Pm_in* is the magnitude of the PWM index and *f0* permits varying the frequency of the output voltage. The control variable *f0* defines the frequency in p.u., while *F0Hz* in Hz. According with (DIgSILENT, 2006) this input pair "is especially useful in variable speed-drive applications, in which a PWM converter is used for driving an induction machine".

Based on these available control variables for the PWM-converter model it can be concluded the following:

- Options A to C can only be used in grid-connected applications. In order to obtain the right angle for the output voltage these options requires a phase measurement device (e.g. PLL). Transformations between reference frames should be made for option A and B. ***The frequency of the output voltage cannot be varied using these options!*** This will be in all the cases around 50 Hz. The control schemes associated with these options will control only the magnitude and the phase of the output voltage.
- Option D is the only possibility to vary the frequency of the output voltage in a wide range. So, using this option is not possible to use vector control schemes. The only control scheme associated with this input pair should be similar with the scalar control (V/f control) for drives.

Softstarter

The softstarter is a simple and cheap power electric component, used in the fixed speed wind turbine during connection or disconnection to the grid of its generator. The softstarter's function is to reduce the in-rush current and thereby limit the disturbances to the grid. Without a softstarter, the in-rush current can be up to 7-8 times the rated current, which can cause severe voltage disturbance in the grid.

The softstarter contains two thyristors, as commutation devices in each phase. They are connected in anti-parallel for each phase. The smooth connection of the generator to the grid, during a predefined number of grid periods, is done by adjusting the firing angle (α) of the thyristors. The relationship between the firing angle (α) and the resulting amplification of the softstarter is highly non-linear and depends additionally on the power factor of the connected element. After in-rush, the thyristors are bypassed in order to reduce the losses of the overall system.

The softstarter model in DIgSILENT is a dqo model, considering one phase and an RL source.

There are many configurations of softstarters, which fed an induction machine, as for example: a) star connection b) delta connection and c) branch-delta connection. In wind turbine applications mainly the delta connection for the induction machine is used because the current rating of the stator windings can be reduced, and the third harmonic in the line currents is eliminated in this case.

In delta branch connection, the softstarter is not in series to the induction generator lines, but it is built inside the delta of the generator, reducing thus the power rating of the thyristors. As in DIgSILENT, the softstarter and the generator blocks are two independent components, it is not possible directly to model the generator with delta branch softstarter. However, the delta branch connection could be possibly equivalent with an ideal delta/star transformer in series with the softstarter and a star connected induction generator.

Capacitor bank

The capacitor bank is an electrical component, which is supplying reactive power (i.e. to the induction generators or to the grid). Thus the reactive power absorbed by the generator from the grid is reduced.

The general compensation device is modelled in DIgSILENT by a series connection of a capacitor *C*, a reactor *L* and a resistance *R*. The user can choose between different types of shunt, e.g.: *C, R-L* or *R-L-C*. The capacitor can be connected in a star or delta configuration.

To represent a parallel connection of capacitors, several compensators in parallel must be connected to the same busbar, as illustrated in Figure 11.

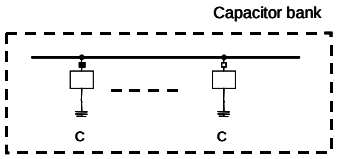

Figure 11: Capacitor bank in DIgSILENT.

The capacitor bank system is combinations of shunt capacitors, which can be switched on and off individually, depending on the load situation in response to changes in reactive power demands.

2.2.3 Transformer

DIgSILENT provides model blocks both for 2-windings transformer and for 3-windings transformer. The two/three winding transformer is a two/three -port element connecting two/three cubicles, respectively, in the power system. Both transformers include manual and automatic tap changers with voltage, active power or reactive power control.

In the following, the model of the 3- windings transformer is briefly illustrated. The representation of the positive sequence equivalent diagram is shown in Figure 12 and includes a generalised tap-changer model.

The magnetisation current may be chosen to be linear or piecewise linear, which is defined with a knee-current, a linear current and a saturated current.

The zero sequence equivalent models for three common winding connections are illustrated in Figure 13 to Figure 15.

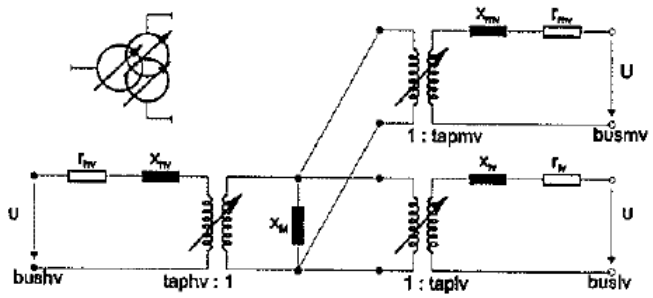

Figure 12: Positive sequence - three windings transformer equivalent model. Source: DIgSILENT Power Factory Manual (DIgSILENT, 2006).

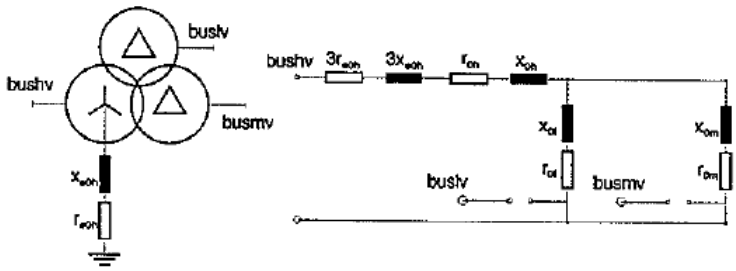

Figure 13: Zero sequence - grounded star/delta/delta connection. Source: DIgSILENT Power Factory Manual (DIgSILENT ,2003).

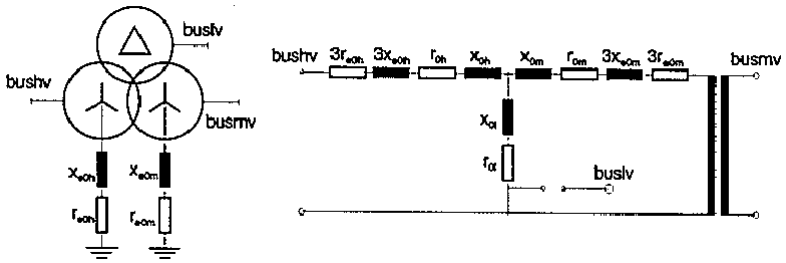

Figure 14: Zero sequence - grounded star/grounded star/delta connection. Source: DIgSILENT Power Factory Manual (DIgSILENT, 2006).

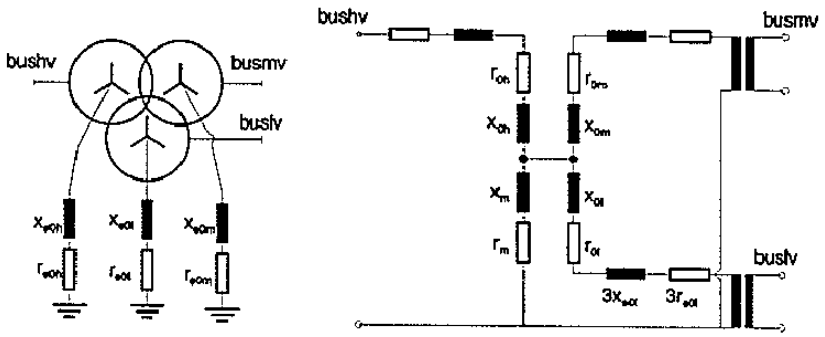

Figure 15: Zero sequence - grounded star/grounded star/ grounded star connection. DIgSILENT Power Factory Manual (DIgSILENT, 2006).

2.3 DSL models of wind turbine in DIgSILENT

Besides the models of the electrical components, already existing in DIgSILENT, as described in Section 2.2, the modelling of the wind turbine also requires models for wind speed, aerodynamic system, mechanical system and control system.

The Dynamic Simulation Language (DSL) is a powerful feature of DIgSILENT. It allows dynamic modelling of linear and non-linear systems. Thus, besides the modelling non-electrical wind turbine components (i.e. wind speed, aerodynamic system, mechanical system), DSL is also used to design and implement different types of controllers, such as capacitor bank (reactive power) controller, doubly-fed induction generator DFIG controller, active stall wind turbine controller and variable speed/variable pitch wind turbine controller.

In contrast to the built-in electrical models with initialisation procedures based on the load flow calculation, the initialisation of DSL models has to be carried out carefully by the user. Such initialisation is very useful to be able to evaluate the performance of the whole system (grid connected wind turbine), both during normal operation and during transient faults. The wind turbine and the electrical power system must be treated as a unified system, despite their formal separation at initialisation.

For illustration, a directly grid-connected blade angle-controlled wind turbine is used. Figure 16 depicts the overall structure of such a grid-connected wind turbine model. It contains (i) the wind speed model, (ii) the aerodynamic, mechanical, generator and grid model, and (iii) the control system models (i.e. blade angle control model, capacitor bank control model).

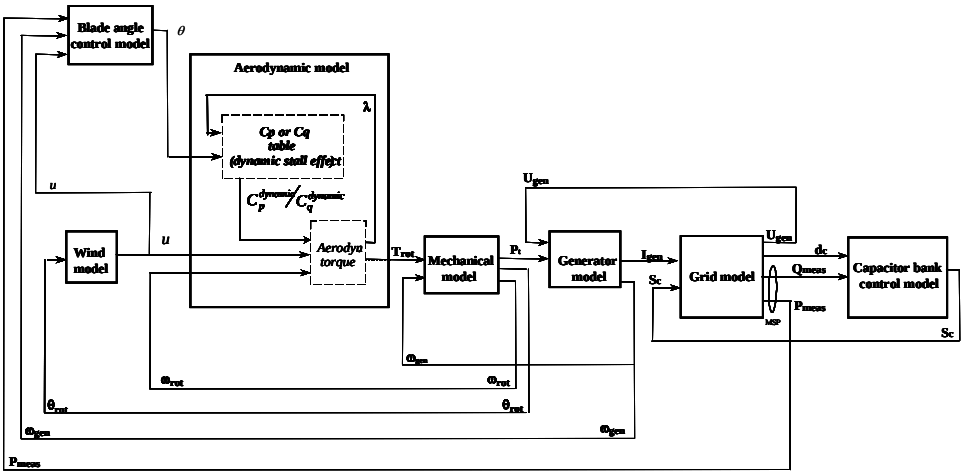

Figure 16: Example of grid-connected wind turbine model.

The aerodynamic model, extended with the dynamic stall effect, is fed with the equivalent wind speed u from the wind model, the rotor speed ω_{rot} from the mechanical model and the blade angle θ from the control model. The mechanical model describes the dynamics of the drive train and delivers the mechanical turbine power P_t to the generator model. Beside the mechanical turbine power P_t, the generator model has as input the voltage U_{gen} from the grid model. It delivers the rotational speed ω_{gen} and the current I_{gen} as outputs. The blade angle-control and capacitor-bank control systems constitute the overall control. The blade angle-control model delivers the blade angle θ to the aerodynamic model, by using information on the measured active power P_{meas}, the generator speed ω_{gen} and the wind speed u. The capacitor-bank control model generates the capacitor switch control signals S_C to the grid model, based on information on the measured reactive power Q_{meas} and on the capacitor status signals d_c. The active and the reactive power P_{meas} and Q_{meas}, measured at the main switch point MSP of the wind turbine, are used by the control system.

2.3.1 Initialisation issues on the wind turbine DSL models

In this section, the initialisation procedure and the initialisation of each DSL component model of a wind turbine is presented. The initialisation procedure is described by using a blade angle-controlled wind turbine with a directly connected squirrel-cage induction generator, as an example. However, during the description of the initialisation procedure, some comments regarding the variable speed wind turbine are also made.

To integrate new models in the power-system simulation software, e.g. wind turbine and new controller models, the initialisation problem must be solved properly (Hansen A. D. et al., 2003). Correct initialisation of a model in a power-system simulation-tool avoids fictitious electrical transients and makes it possible to evaluate correctly the real dynamic performance of the system (even in the case of a grid transient event). A transient simulation requires very small time steps and consequently very long simulation time.

Power system simulations start with a load flow calculation. Load flow calculations provide the steady state condition of the system. For these calculations certain input data has to be provided by the user. For example, the load flow input data for a squirrel-cage induction generator includes the active power, while for a doubly-fed induction generator, the required load flow data are the stator's active power, reactive power and the slip. Once the load flow calculation is performed, and thus all electrical models are initialised (e.g. mechanical turbine power at the machine and generator speed are calculated), the initialisation of non-electrical turbine component models starts.

The initialisation of the grid-connected turbine model is a successive process. The main problem is to find the sequence in which the models have to be initialised one after another. The simulation equations are solved by setting time derivatives to zero and using the load flow results and additional non-electrical input data. It is necessary to identify which inputs, outputs and states are known and which have to be initialised. Once one model is initialised, the gathered information on its signals and states is used for the initialisation of the next model. A DIgSILENT command makes it possible to check if the initial conditions are transferred correctly from one component model to another. If the initialisation is not done properly, the state variables do not stay at the value at which they were initialised, but start changing at the start of the dynamic simulation. In this case, it may take time to reach a steady state, and even numerical instability can occur before the stationary state is reached. These initialisation transients are undesirable in the dynamic simulations, especially in the case when a real grid transient event appears, just before the system achieves its steady state. A correct evaluation of the dynamic performance is then quite difficult to achieve. To overcome these difficulties, an accurate calculation of the initial conditions of the dynamic wind turbine models is required.

While Figure 16 depicts the direction of the simulation flow, Figure 17 illustrates the initialisation flow of the turbine model. The input data necessary for the initialisation are:

- electrical input data (from grid side): e.g. the initial active power of the generator and the initial capacitor status information d_c . These electrical input data are used in the load flow calculation and in the initialisation of the electrical models.
- non-electrical input data (from turbine side): the initial value of the wind speed and the initial value of the blade angle.

These input data provide information about the operating point of the turbine at the simulation start. The single-dotted lines indicate the direction of the initialisation flow, for each component model; see Figure 17. The known signals at the simulation start, indicated by the double dotted lines, are:

- electrical signals - determined in the load flow calculation: mechanical power P_t, generator speed ω_{gen}, capacitor status signal d_c, generator current I_{gen}, generator voltage U_{gen}, the "measured" active power P_{meas} and reactive power Q_{meas} in MSP (Main Switch Point).
- initially (*a priori*) known non-electrical signals: the initial wind speed u and the initial blade angle θ.

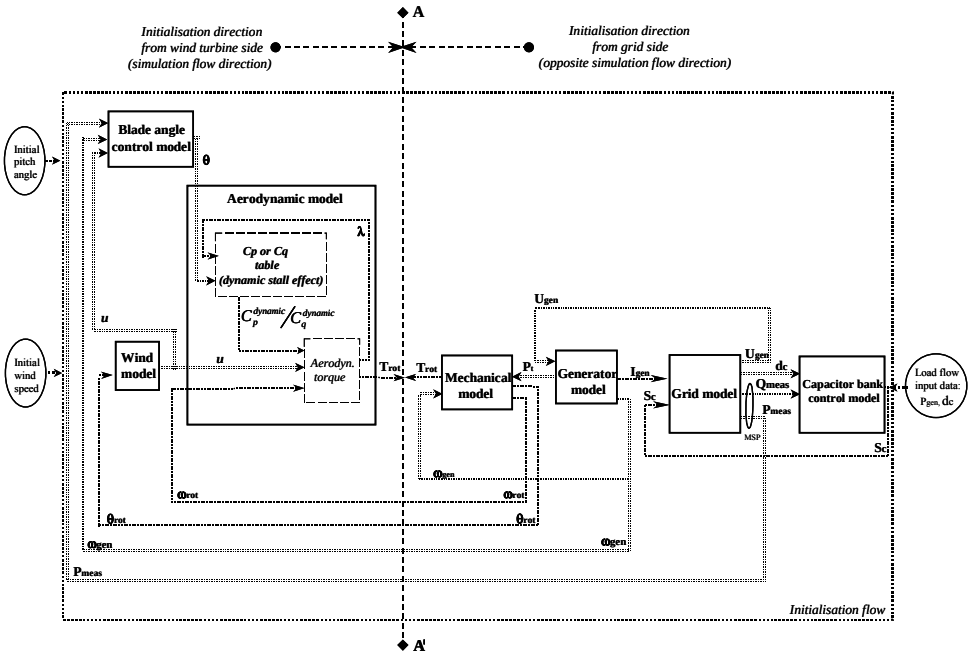

Figure 17: Initialisation flow of a blade angle controlled wind turbine with a directly connected squirrel-cage induction generator.

The non-electrical input data (from turbine side) and the load flow electrical input data (from the grid side) must correspond to each other, based on the static power curve of the wind turbine, on the generator efficiency and eventually losses in the system. The initial value of the wind speed is assumed known at the beginning of the initialisation sequence because, otherwise, its initialisation backward from the non-linear expression in wind speed of the aerodynamic torque would be quite difficult and with ambiguous solutions. The initial value of the blade angle is also assumed known (Hansen A. D. et al., 2003).

Two initialisation directions are distinguished in the initialisation procedure; see Figure 17. Some of the variables in the initialisation sequence are initialised in the opposite direction of the simulation (starting from the grid connection point towards the wind); while others are initialised in the same direction as the simulation is performed (starting from the wind to the grid). When the initialisation is performed in the opposite direction of the simulation flow, namely from the grid to the wind, the model is calculated from certain known outputs to inputs, based on load flow computations. The initial values of the inputs, outputs and state variables have thus to be calculated from the known outputs and from the model equations.

For example, in the "Mechanical model" block shown in Figure 17, the aerodynamic torque T_{rot} is initialised in the opposite direction of the simulation flow. It is based on the known outputs from the load flow calculation, i.e. the mechanical power P_t and the generator speed ω_{gen}.

When the initialisation is performed in the same direction as the simulation flow, the model initialisation is performed from certain known inputs to outputs.

The initial values of the inputs are assumed known based on the non-electrical information about the system in the starting moment, as e.g. the initial wind speed and the initial blade angle.

During the initialisation process, initial values are successively calculated in two directions approaching each other. At the point where the initialisations from the two opposite directions meet, they should match each other. If they do, a steady state is obtained. Otherwise, fictive transients in the beginning of the dynamic simulation appear. These fictive transients have been minimised by choosing a point where the transients can be absorbed, e.g. big inertia in the mechanical system. The place between the aerodynamic model and the mechanical model has been chosen as a point where the two opposite initialisation directions meet. This is illustrated in Figure 17 by the borderline AA´. The reason for this choice is that the fictive transients in the low-speed shaft torque signal, in the case of an initialisation conflict, are absorbed due to the large inertia of the rotor.

The models are initialised one after another, starting with the mechanical model, followed by the wind model, blade angle control model and the aerodynamic model. The initialisation of the capacitor-bank control model is based on the load flow data only, i.e. independent of the initialisation of the other individual component models. Once one model is initialised, all its variables are known and can be used in the initialisation of the next models in the initialisation sequence.

In the following figures, concerning the models initialisation, the known signals in the moment of initialisation are illustrated by using double-dotted lines. Single-dotted lines illustrate the signals, which must be initialised.

2.3.2 Mechanical model

In the mechanical model, Figure 18, emphasis is put only on those parts of the dynamic structure of the wind turbine that contribute to the interaction with the grid. Therefore only the drive train is considered in the first place, because this part of the wind turbine has the most significant influence on the power fluctuations. The other parts of the wind turbine structure, e.g. tower and the flap bending modes, are thus neglected.

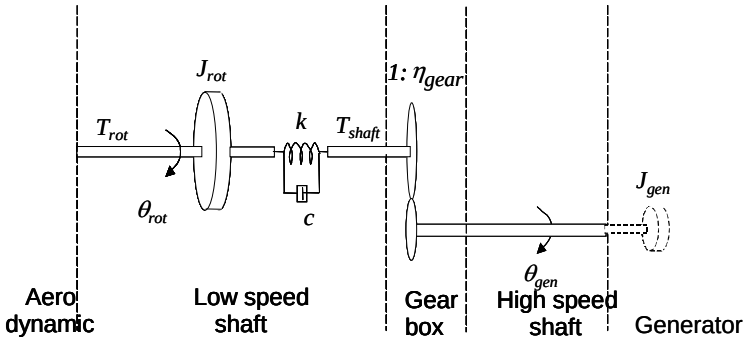

Figure 18: Drive train model in DIgSILENT.

The mechanical model is implemented as a DSL model in DIgSILENT. The drive train is essentially a two mass model (Hansen A.D. et al., 2002), (Sørensen P. et al., 2001a), namely a large mass corresponding to the rotor inertia J_{rot} and a small mass corresponding to the generator inertia J_{gen}, which is implemented as part of a DIgSILENT generator model. Thus, besides the electromagnetic description, the generator model in DIgSILENT also contains the me-

chanical inertia of the generator rotor J_{gen}. The low speed shaft is modelled by a stiffness k and a damping coefficient c, while the high-speed shaft is assumed stiff. Moreover, an ideal gear-box with a ratio ($1{:}n_{gear}$) is included.

The drive train converts the aerodynamic torque T_{rot} of the rotor into the torque on the low speed shaft T_{shaft}. The dynamical description of the mechanical model consists of three differential equations, namely:

$$\begin{aligned} \dot{\theta}_{rot} &= \omega_{rot} && [rad/s] \\ \dot{\theta}_{k} &= \omega_{rot} - \frac{\omega_{gen}}{n_{gear}} && [rad/s] \\ \dot{\omega}_{rot} &= (T_{rot} - T_{shaft})/J_{rot} && [rad/s^2] \end{aligned} \tag{22}$$

where $\theta_k = \theta_{rot} - \theta_{gen}/n_{gear}$ is the angular difference between the two ends of the flexible shaft. The mechanical torque on the low speed shaft and the mechanical power of the generator are:

$$\begin{aligned} T_{shaft} &= c\,(\omega_{rot} - \frac{\omega_{gen}}{n_{gear}}) + k\,\theta_k && [Nm] \\ P_t &= \omega_{gen}\,\frac{T_{shaft}}{n_{gear}} && [W] \end{aligned} \tag{23}$$

The damping coefficient c is given by:

$$c = 2\,\xi\,\sqrt{k\,J_{rot}} \tag{24}$$

where ξ is the damping ratio and can be expressed using the logarithmic decrement δ_s:

$$\xi = \frac{\delta_s}{\sqrt{\delta_s^2 + 4\,\pi^2}} \tag{25}$$

The logarithmic decrement is the logarithm of the ratio between the amplitude at the beginning of the period and the amplitude at the end of the next period of the oscillation:

$$\delta_s = \ln\left(\frac{a(t)}{a(t+t_p)}\right) \tag{26}$$

where a denotes the amplitude of the signal.

Figure 19 illustrates the inputs and outputs of the mechanical model, which must be initialised. These are the aerodynamic torque T_{rot}, the rotor angle θ_{rot} and the rotor speed ω_{rot}. The mechanical power P_t^{lf} and the generator speed ω_{gen}^{lf} are known (double dotted style) from the load flow calculation. The aerodynamic torque T_{rot} is initialised in the opposite direction to that of the simulation flow (i.e. *from* grid *to* wind, and not from wind to grid), while the rotor angle θ_{rot}, the rotor speed ω_{rot} and the internal states of the mechanical model are initialised in the same direction as the simulation flow.

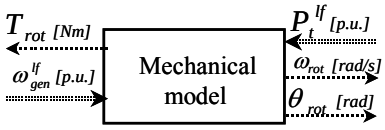

Figure 19: Known and unknown inputs/outputs in the initialisation of the mechanical model.

Notice that the electrical data available from the load flow calculation and the equations of grid components are expressed in per unit in DIgSILENT. This aspect must be taken into account in the initialisation process of the turbine model, as the turbine equations are implemented in physical units. The per unit mechanical power P_t^{lf} and the generator speed ω_{gen}^{lf}, generated by the load flow are:

$$\begin{aligned} P_t^{lf} &= \frac{P_t}{P_t^{base}} \qquad [p.u.] \\ \omega_{gen}^{lf} &= \frac{\omega_{gen}}{\omega_{gen}^{base}} \qquad [p.u.] \end{aligned} \tag{27}$$

where P_t^{base} is the rated mechanical power in *[W]* of the wind turbine, $\omega_{gen}^{base} = \frac{2\pi f}{p}$ is the synchronous speed of the generator in *[rad/s]*, with *f* as the grid frequency in *[Hz]* and p as the number of pole-pairs.

The initial steady states are determined by setting their derivatives to zero:

$$\begin{aligned} \dot{\theta}_k = 0 \quad &\Rightarrow \quad \omega_{rot}^{initial} = \frac{\omega_{gen}}{n_{gear}} \quad and \quad T_{shaft}^{initial} = k\,\theta_k^{initial} \\ \dot{\omega}_{rot} = 0 \quad &\Rightarrow \quad T_{rot}^{inital} = T_{shaft}^{inital} \quad and \quad T_{rot}^{initial} = \frac{P_t\, n_{gear}}{\omega_{gen}} \end{aligned} \tag{28}$$

Notice that since the shaft is rotating, the derivative of the rotor position θ_{rot} cannot be zero. Its value can be initialised to any appropriate value.

The mechanical model, expressed in (12) and (13), is using physical units, while the signals determined in the load flow calculation are expressed in per unit. The initialisation of the inputs and states, based on equations (18), must take the transformations (17) into account, as follows:

$$\begin{aligned} T_{rot}^{initial} &= n_{gear}\,\frac{P_t^{lf}\,P_t^{base}}{\omega_{gen}^{lf}\,\omega_{gen}^{base}} && [Nm] \\ \omega_{rot}^{initial} &= \frac{\omega_{gen}^{lf}\,\omega_{gen}^{base}}{n_{gear}} && [rad/s] \\ \theta_k^{initial} &= \frac{T_{rot}^{initial}}{k} = n_{gear}\,\frac{P_t^{lf}\,P_t^{base}}{\omega_{gen}^{lf}\,\omega_{gen}^{base}}\,\frac{1}{k} && [rad] \end{aligned} \tag{29}$$

2.3.3 Aerodynamic model

As illustrated in Figure 17, the DSL aerodynamic model block contains two sub-model blocks. One sub-model block relates to the non-linear expression of the aerodynamic torque, and the other contains the power coefficient C_p or the torque coefficient C_q look-up tables. In the later sub-model block the modelling of the dynamic stall effect can be included or not. Figure 20 depicts the known and unknown inputs/outputs of the aerodynamic model and the initialisation direction.

The rotor speed ω_{rot} is determined in the initialisation of the mechanical model. The equivalent wind speed u is known from the initialisation of the wind speed model. The initial pitch angle θ is assumed known. Based on these known non-electrical signals, the tip speed ratio λ, the output aerodynamic torque T_{rot} and the internal states are further initialised. Notice that the aerodynamic torque T_{rot} is also initialised in the "Mechanical model", based on the electrical input data (load flow data); see equations (19).

Both Figure 17 and Figure 20 illustrate the borderline AA´, where the initialisation information from two opposite directions (wind turbine side and grid side) cross each other. In this place, a conflict can appear if the initialisation information provided by the non-electrical and the electrical signals don't match.

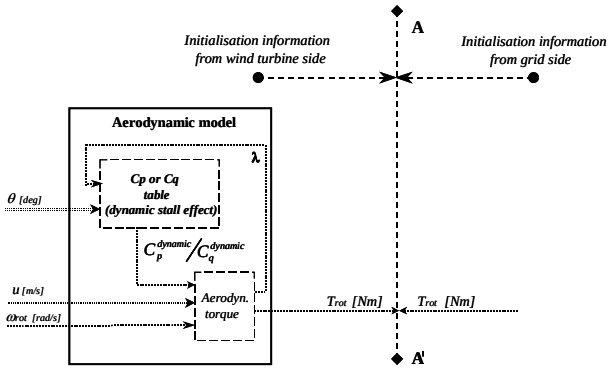

Figure 20: Known and unknown inputs/outputs in the initialisation of the aerodynamic model.

As mentioned before, this border position AA´ is chosen deliberately at the aerodynamic torque signal. The reason is that the transients in the aerodynamic torque, due to the possible discrepancy, can be absorbed by the large inertia of the rotor.

(a) Aerodynamic torque

Standard aerodynamic programs typically use blade element methods and therefore they require considerable computation time. The use of such standard aerodynamic programs to simulate wind farms with several wind turbines is therefore not attractive. A simplified aerodynamic model is preferably used instead when only the effect on the power, respectively the aerodynamic torque T_{rot} is taken into account. This simplified aerodynamic model is typically based on the aerodynamic power coefficient $C_p(\theta,\lambda)$ or on the torque coefficient $C_q(\theta, \lambda)$, provided by a standard aerodynamic program.

Thus, the aerodynamic torque developed on the main shaft of a wind turbine with rotor radius R at a wind speed u and air density ρ can be modelled by one of the following static relations:

$$T_{rot} = \frac{P_{rot}}{\omega_{rot}} = \frac{1}{2\,\omega_{rot}} \rho\, \pi\ R^2\ u^3\ C_p(\theta, \lambda), \qquad (30)$$

or

$$T_{rot} = \frac{1}{2} \rho \pi \ R^3 \ u^2 \ C_q(\theta, \lambda), \tag{31}$$

where the aerodynamic power coefficient $C_p = C_p(\theta, \lambda)$ and the torque coefficient, respectively, $C_q = C_q(\theta, \lambda)$ are tabled as matrices, depending on the pitch angle θ and on the tip speed ratio λ, which initial value is:

$$\lambda^{initial} = \frac{R \, \omega_{rot}^{initial}}{u^{initial}} \tag{32}$$

Both torque expressions (20) and (21) can be used to express the aerodynamic torque. However, the aerodynamic torque expressed in (21) with the torque coefficient has the advantage that it is determined directly and not through power and therefore it can also be used in the case of standstill ($\omega_{rot} = 0$). This is important because at standstill the aerodynamic power is zero, while the aerodynamic torque is not. Both torque expressions (20) and (21) are presently implemented and can be independently used in DIgSILENT.

Notice that both aerodynamic torque expressions (20) and (21) contain the wind speed u both in explicit and implicit form (through λ). They are non-monotone, highly non-linear and with a maximum point. This means that if the initial wind speed is not known at the beginning of the initialisation, the wind speed would have to be determined backwards from the high non-linear and non-monotone aerodynamic torque expression. This calculation would be both complicated and have ambiguous solutions.

The aerodynamic torque expressions (20) and (21) are expressed in steady state operating points, based thus on steady state power coefficient or steady state torque coefficient. This simplification underestimates the actual power fluctuations in the stall region (Sørensen P. et al., 2001a), and therefore the aerodynamic model can be improved by taking the dynamic stall effects into account. A dynamic power coefficient $C_p^{dynamic}(\theta, \lambda)$ and a dynamic torque coefficient $C_q^{dynamic}(\theta, \lambda)$, respectively, are used instead.

(b) Dynamic stall model

The dynamic stall effects, described in (Sørensen P. et al., 2001a), (Hansen A.D. et al., 2002), appear because, at strong wind speeds, the dynamic power/wind speed slope is much steeper than the static power/wind speed slope. This is the reason why, at strong wind speeds, the power fluctuations in reality are much larger than the power fluctuations estimated by using the standard power curve.

Figure 21 illustrates both the steady state power curve of a wind turbine and how large the dynamic power fluctuations are caused by wind speed fluctuations. Two situations are illustrated: low wind speed region (u < 8 m/s - case 1) and high wind speed region (u > 8 m/s - case 2). For low wind speeds (case 1) there is no significant difference between the static power P^{static} and the dynamic power $P^{dynamic}$, because the amplification factors of the fluctuations for both steady state and dynamic state are similar. This is not the case for the high wind speeds (case 2) in the stall region, where, due to the dynamic stall effects, fluctuations in wind speed, produce larger power fluctuations.

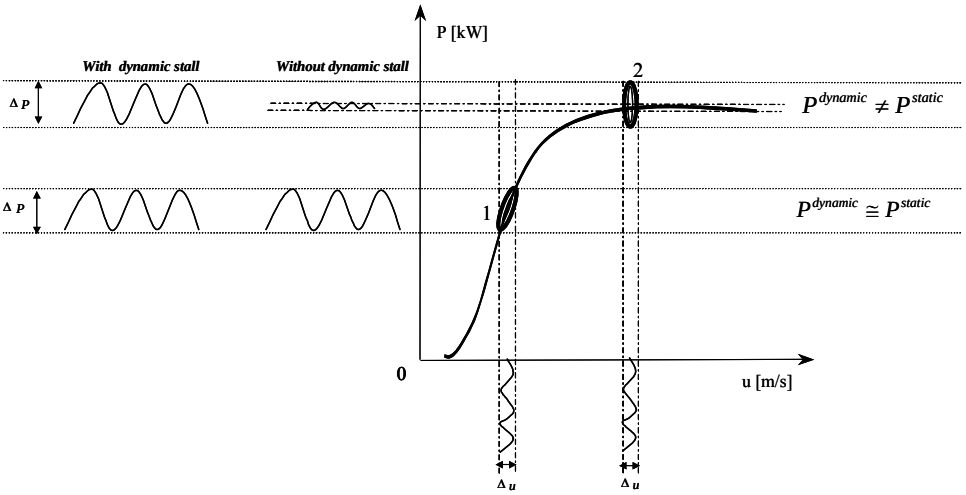

Figure 21: Power fluctuations in the stall region with and without dynamic stall.

The applied model for the dynamic stall is a slight modification of the method described by (Øye & S.,1991), where the dynamic stall is modelled as a time-lag of separation. According to this method, the lift coefficient for a blade section can be associated with different flows with different angles of attack:
(i) an attached (un-separated) flow, which corresponds to the steady state flow at low angles of attack;
(ii) a fully separated flow, which corresponds to the steady state flow at large angles of attack;
(iii) a steady state flow (static flow).

Instead of using lift coefficient C_L, as it is proposed by (Øye & S., 1991), the dynamic stall effect model can be based on the aerodynamic power coefficient C_p or on the torque coefficient C_q. In the following, only the generation of the dynamic aerodynamic power coefficient $C_p^{dynamic}$ is presented, as the generation of the dynamic aerodynamic power coefficient $C_q^{dynamic}$ is similar.

The dynamic power coefficient table, $C_p^{dynamic}$, is generated by using three other tables: one for the steady state (static) power coefficient, C_p^{static}, one for the attached power coefficient, $C_p^{attached}$ and one for the separated power coefficient, $C_p^{separated}$.

In order to illustrate these three power coefficients (static, attached and separated) and thus the influence of the dynamic stall effect over the whole wind speed range, a simulation of a single wind turbine is performed. In this example, the equivalent wind speed is designed (not modelled by the rotor wind model) to have a sinusoidal variation with a 3p frequency, amplitude of 2 m/s and a linear increasing mean value, as it is illustrated in Figure 22. The simulation is performed with a constant pitch angle, which corresponds to 2 MW power at high wind speeds.

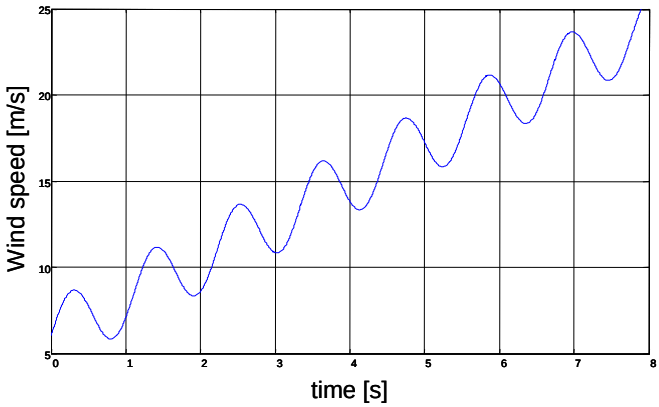

Figure 22: Designed equivalent wind speed - input for wind turbine simulation.

Figure 23 shows the profile of the dynamic power curve, modelled with and without dynamic stall. The cyclic behaviour of the sinusoidal wind speed input signal is transferred through the second order dynamic model of the transmission system to other signals, such as the aerodynamic power, the aerodynamic torque and the rotor speed ω with a corresponding phase shift. The significantly increased amplitude of the dynamic power fluctuations at high wind speeds illustrates that the dynamic stall effect is important at large wind speeds, while at small wind speeds it is not relevant. The improved aerodynamic model with the dynamic effect is thus able to simulate the larger fluctuations in the power in the stall region. It is also observed that even the power curve without dynamic stall has some cyclic behaviour. This is due to the sinusoidal wind speed input signal, which is transferred to the other state variables through the model dynamics. Beside the sinusoidal wind speed, the power coefficient without dynamic stall, expressed as a function of wind speed, $C_p(u,\theta)$, also influences the calculation of the small cycles in the power curve without dynamic stall.

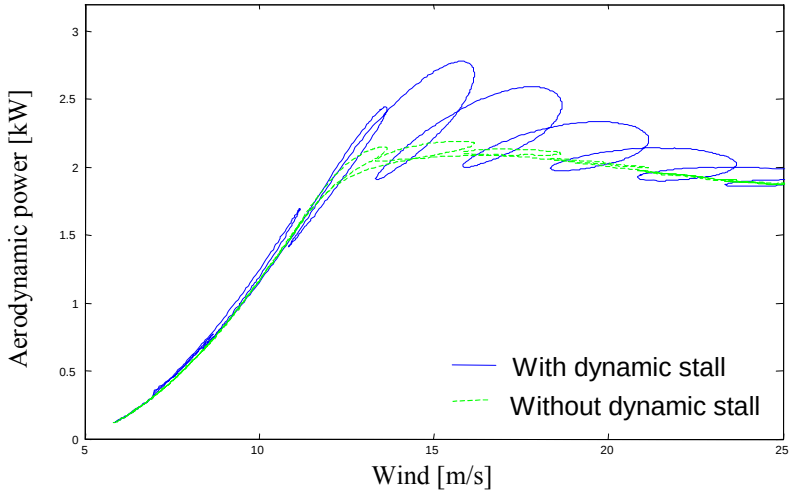

Figure 23: Power curve with and without dynamic stall effect.

Figure 24 illustrates the power coefficient as a function of tip speed ratio, $\lambda = \omega R / u$, for the steady state, attached, separated and dynamic flow, simulated with the wind speed illustrated in Figure 22. It is observed that the steady state power coefficient, C_p^{static}, illustrated this time as function of λ, does not

contain any cycles. This is because C_p^{static} is an algebraic function of rotor speed ω, wind speed u and pitch angle θ. It is also noted that the steady state C_p^{static} converges to the attached $C_p^{attached}$ power coefficient at high λ values (low wind speeds), while at small λ values (high wind speeds), the steady state C_p^{static} converges to the separated $C_p^{separated}$. Moreover, at small wind speeds, the steady state C_p^{static} power coefficient and the dynamic power coefficient $C_p^{dynamic}$ do not differ significantly, because at small wind speeds the dynamic stall effect is not relevant. At high wind speeds (small λ values) the values of the dynamic power coefficient $C_p^{dynamic}$ are delayedwith the time constant τ of the first order filter, and then moved towards the steady state power coefficient C_p^{static} on an almost "parallel" curve with the attached and separated coefficient curves. The calculated value of $C_p^{dynamic}$ is interpolated between these "parallel" curves, which correspond to different separation ratios f (Sørensen P. et al., 2001a). The dynamic value $C_p^{dynamic}$ is the result of the first order filter, which physically corresponds to the fact that it cannot change instantaneously from one value to another, remaining thus on a specific intermediary curve for a time lag. Thus, at high wind speeds, the variation of $C_p^{dynamic}$ is different from that of C_p^{static}.

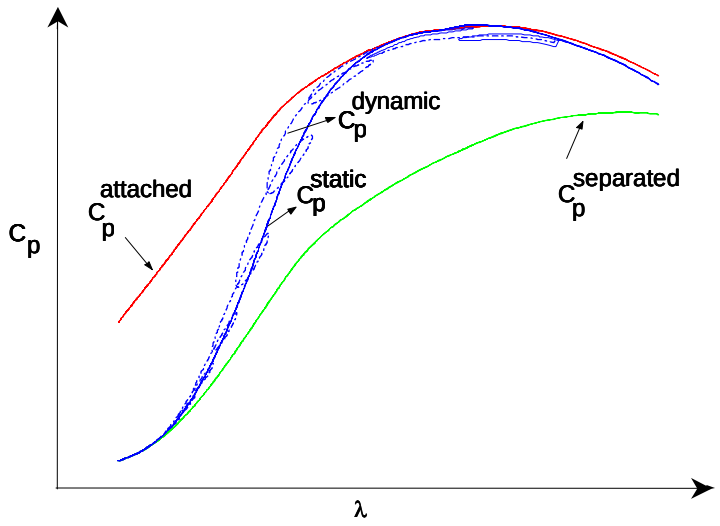

Figure 24: Steady state, attached, separated and dynamic power coefficient as a function of λ.

The three power coefficients (static, attached and separated) are determined as follows. As illustrated in Figure 25, for a certain known blade angle θ and a known tip speed ratio λ, the three power coefficient look-up tables are providing the values for $C_p^{attached}$, C_p^{static} and $C_p^{separated}$.

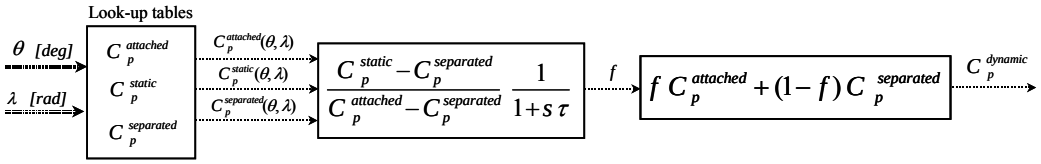

Figure 25: Known and unknown inputs/outputs in the initialisation of the dynamic stall model.

The dynamic separation factor *f* is defined as the following transfer function:

$$f = \frac{C_p^{static} - C_p^{separated}}{C_p^{attached} - C_p^{separated}} \cdot \frac{1}{1 + s\,\tau} \tag{33}$$

The dynamic power coefficient $C_p^{dynamic}$ is interpolated between the attached power coefficient, $C_p^{attached}$, and the separated coefficient $C_p^{separated}$:

$$C_p^{dynamic} = f\,C_p^{attached} + (1 - f)\,C_p^{separated} \tag{34}$$

The factor *f* is a dynamic separation ratio, obtained by using a low pass filter with a time constant (lag) τ, approximated, as in (Sørensen P. et al., 2001a), by $\tau = 4/u_0$, where u_0 is the mean wind speed.

With a known blade angle θ and an initialised tip speed ratio λ in (22), the initialisation of the dynamic power coefficient is performed in the simulation direction (see Figure 25), based on the expressions (23), (24) and on the final-value theorem (Laplace transformation):

$$C_p^{dynamic,\ initial} = C_p^{static}(\theta, \lambda) \tag{35}$$

Once the dynamic power coefficient is initialised, the aerodynamic torque T_{rot} can be also initialised:

$$T_{rot}^{initial} = \frac{1}{2\,\omega_{rot}^{initial}}\,\rho\,\pi\,R^2\,u^3\,C_p^{dynamic,\ initial} \tag{36}$$

Notice that there are two expressions, (19) and (26), which indicate the initial value of the aerodynamic torque. Nevertheless, the initial value of T_{rot} actually corresponds to (19), from which T_{rot} immediately steps to the value given by (26). In the case of mismatch between the initial input data (both from grid side and wind turbine side) in the initialisation sequence, the expressions (19) and (26) will yield different initial values of the aerodynamic torque. This produces a transient step in T_{rot}. However, due to the large inertia of the rotor, such a transient in the aerodynamic torque will be rapidly absorbed. This is why the delimitation border between the two opposite information sources (i.e. grid side or wind turbine side) is chosen deliberately to be at the aerodynamic torque signal.

2.3.4 Wind model

The wind model, implemented as DSL model in DIgSILENT, generates the equivalent wind speed *u* based on a spectral description of the turbulence and includes the rotational sampling turbulence and the tower shadow effect. The

wind model is described in details in several references, such e.g. (Sørensen P. et al., 2000), (Sørensen P. et al., 2001a), (Sørensen P. et al., 2001b).

The wind speed model is built as a two-step model – see Figure 26. The first is the hub wind model, which models the fixed point wind speed at hub height of the wind turbine. In this sub-model, possible park scale coherence can be taken into account if a whole wind farm is modelled (Sørensen P. et al., 2001a). The second step is the rotor wind model, which adds the effect of the averaging the fixed point fixed-speed over the whole rotor, the effect of the rotational turbulence and the effect of the tower shadow influence. One input of the rotor wind model block is the azimuth position of the turbine rotor θ_{rot}, which provides the frequency and the phase of the 3p fluctuation. The presence of the rotor position θ_{rot} in the model makes it directly applicable also for variable speed wind turbines.

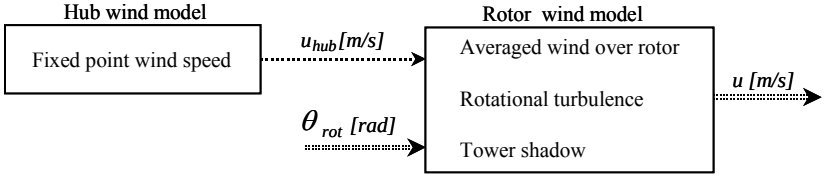

Figure 26: Simplified scheme of wind model with known and unknown inputs/outputs.

The rotational turbulence and the tower shadow are included in the model as they have a major impact on the dynamics. They cause fluctuations in the power with three times the rotational frequency (3p), which is the frequency that mainly contributes to flicker emission during continuous operation. The tower shadow is modelled as a 3p fluctuation with constant amplitude, whereas the rotational sampled turbulence is modelled as a 3p fluctuation with variable (stochastic) amplitude (Sørensen P. et al., 2000).

As indicated in Figure 26, the initialisation of the wind speed model is performed in the same direction as the simulation. The initial value of the equivalent wind speed u is the same as the initial wind speed value, inserted in the initialisation sequence in Figure 16. It corresponds to the active power of the generator, based on the static power curve of the turbine and on the generator efficiency. If a time series describing the wind speed is available, then this can directly replace the wind model. The first value in the time series is then used as the known initial wind speed value in the initialisation sequence.

The two sub-models of the wind speed model, the hub wind model and the rotor wind model, contain a cascade of second order filters (Langreder W., 1996), of the following transfer function form:

$$y_{out} = K \frac{s^2 T_4 + s T_3 + 1}{s^2 T_2 + s T_1 + 1} y_{in} \qquad (37)$$

where y_{out} and y_{in} are the output and the input, respectively, while K, T_1, T_2, T_3, T_4 are estimated parameters (Langreder W., 1996). The key in the initialisation of this cascade of second order filters is the initialisation of each second order filter, and therefore the generic initialisation of a second order filter is presented shortly in the following. The second order transfer function (27) can be expressed in terms of the following canonical state space form:

$$\begin{bmatrix}\dot{x}_1\\ \dot{x}_2\end{bmatrix}=\begin{bmatrix}0 & 1\\ -\frac{1}{T_2} & -\frac{T_1}{T_2}\end{bmatrix}\begin{bmatrix}x_1\\ x_2\end{bmatrix}+\begin{bmatrix}0\\ \frac{1}{T_2}\end{bmatrix}y_{in} \qquad (38)$$

$$y_{out} = K\begin{bmatrix}\left(1-\frac{T_4}{T_2}\right) & \left(T_3-\frac{T_4}{T_2}\right)\end{bmatrix}\begin{bmatrix}x_1\\ x_2\end{bmatrix}+\frac{T_4}{T_2}y_{in}$$

Assuming that the output y_{out} is known, the initialisation of the input y_{in} and of the two states (x_1, x_2) is:

$$\begin{aligned}\dot{x}_1 = 0 \quad &\Rightarrow \quad x_2^{initial} = 0\\ \dot{x}_2 = 0 \quad &\Rightarrow \quad x_1^{initial} = y_{in}\\ &\qquad\quad y_{in}^{initial} = y_{out}/K\end{aligned} \qquad (39)$$

2.3.5 Capacitor-bank control model

The capacitor bank (reactive power) control model is described in the following section. As illustrated in Figure 16, the capacitor-bank, with a specific number of capacitors, is controlled, at each moment, based on information about the measured reactive power. The number of capacitors to be connected or disconnected at each new step is determined by the control system.

Figure 27 illustrates the DIgSILENT block diagram for the capacitor bank controller. The diagram is general for the simulation of capacitor bank switchings, and consequently it can also be used in different wind turbine models. Only the number of capacitors, as well as the averaging time may differ from one wind turbine type to another.

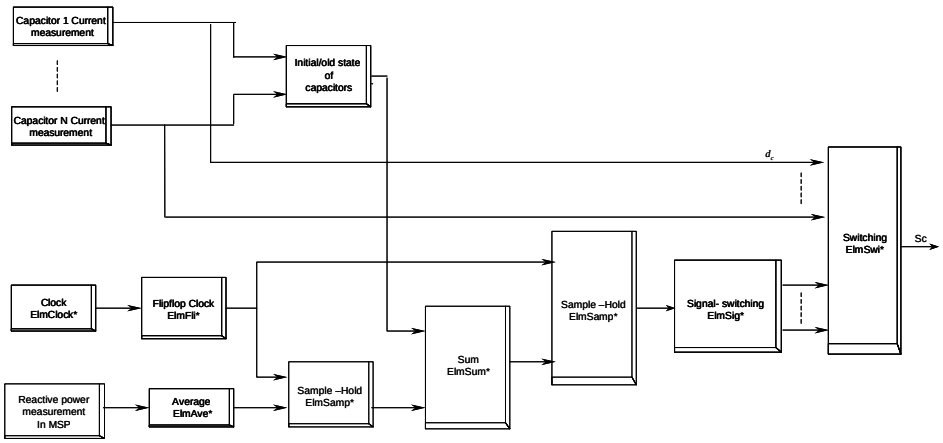

Figure 27: DIgSILENT diagram for capacitor bank controller.

The switching of capacitors is done based on the average value of the measured reactive power during a certain period of time. This average value is used to avoid rapidswitchings of the capacitors, due to the short variations in the reactive power, and thus, to reduce the switching frequency and to protect the contactors. First a moving average of the reactive power is applied, and then a sample-hold function is used to represent block averages. The sample-hold function stores its sampled input signal at the output until the next rising edge of the clock signal appears. The reactive power is measured in the Main Switch Point (MSP), where the reactive power supplied by the already connected capacitors is taken into account. Therefore the control of reactive power is a

closed loop control. Such output average includes the closed loop effect of the reactive power supply from capacitors, which are already connected at a certain moment. The total number of capacitors, which are connected at each step, is obtained by a digital integrator, implemented in the block "Sum", Figure 27. At each time step, this block has information about the closed loop reactive power and the memorised number of capacitors used previously. This information is provided by the block "Initial/old state of capacitors". The output of the digital integrator is first stored and then used to define the switching signals, which are used in the control block "Switching". Based on this process, the control block sends switching control signals S_c to the capacitor-bank contactors of the grid model, in order to operate different capacitors, and thus to supply the required number of capacitors in the grid model, at a specific moment. It is thus at each step determined how many additional capacitors should be further connected or disconnected.

A very simplified version of the control diagram of the capacitor bank is shown in Figure 28. The known and unknown inputs and outputs of the capacitor-bank control model as well as the initialisation direction are shown. The initialisation is performed in the simulation direction, based on electrical characteristics of a grid-connected turbine: the status signal of each capacitor d_c and the measured reactive power Q_{meas} of the turbine.

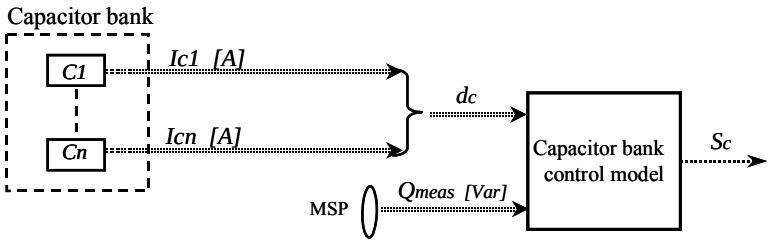

Figure 28: Known and unknown inputs/outputs in the initialisation of the capacitor bank control model.

The initialisation of the switching control signals S_c is based on the status d_c information about the capacitors. The capacitor status signal d_c indicates whether a capacitor is connected or disconnected in the starting moment of the simulation. The status initial information d_c of the capacitors (C_1, …, C_n) is indispensable for a correct initialisation of the capacitor bank control model. The capacitor k is considered connected if its current is positive, $I_{ck} > 0$. Based on how many capacitors are connected at a certain time and on the measured reactive power Q_{meas} ("required" at that moment), the number of capacitors to be further connected or disconnected at the next time step is calculated.

2.4 Combined heat and power plant

In order to obtain the characteristics of a local grid a dynamic model of a small CHP unit is implemented in DIgSILENT.

Various technologies are used in CHP plants (Jenkins N., et al. 2000) e.g. back pressure steam turbines, pass-out condensing steam turbines, gas turbine with waste heat recovery, etc.

CHP units are typically controlled, or despatched, to meet the heat demands and not to export electrical power to the utility distribution system (Jenkins N., et al. 2000). The heat output is generally controlled as a function of ambient temperature. Alternatively, a CHP unit can be controlled to meet the

electrical load demand or may be run to supply both heat and electricity in an optimal manner (Jenkins N., et al. 2000). However, the last mode of operation requires a more complex control system.

Currently, the Danish small CHP plants are mainly controlled to meet the heat demand.

Usually, the small CHP units are equipped with a self-regulated brushless synchronous generator (alternator). The rated power is in 2-10 MVA range with voltages in the 3-13.8 kV. Power generating sets are generally manufactured to meet specific requirements (A. van Kaick Neu-Isenburg, a).

The generator consists of a primary internal pole machine (G1), an external pole exciter (G2), an equal-pole type of auxiliary exciter (G3) and a voltage regulator with a thyristor control element as shown in Figure 29.

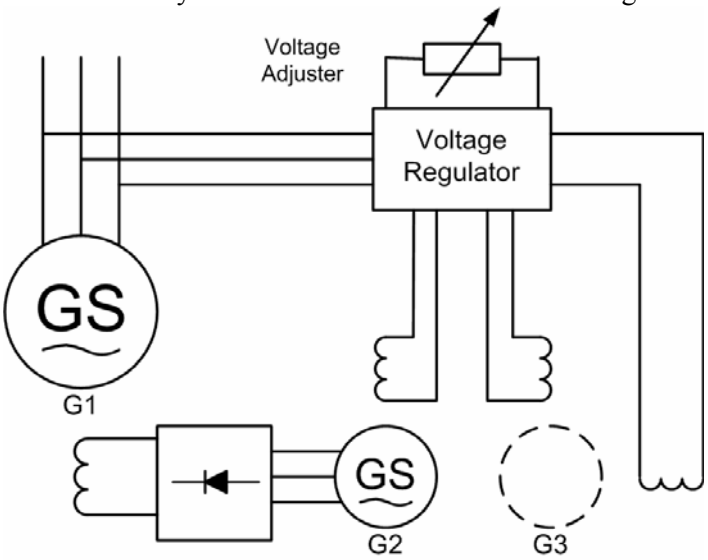

Figure 29: Block diagram of a self-regulated brushless alternator type AvK..

Some protection schemes are included such as:

- External short-circuits – in a multi branch mains system the circuit breakers should operate selectively in such a way that the switch nearest the short-circuit trips as fast as possible while all others remain in circuit. In this way the short-circuits are always isolated within the main grid and do not cause the generator switch to trip. So, the alternator short-circuit protection normally operates as a stand-by protection device.
- Overload – this is the main protection device for the generator;
- Unbalanced load – an unbalanced loading cause a temperature rise in the machine;
- Short break in the mains voltage – the generators operating in parallel with the main grid have a high risk in the case of a fault in the main grid particularly if the rating of the main grid is higher than the generator rating. The recovery voltage from the main grid may catch the generator in an asynchronous phase position and can cause high currents similar to short-circuit currents and the possibility of mechanical damage. Disconnection of the generator from the main grid should take place in less than 200 msec (A. van Kaick Neu-Isenburg, a);
- Protection against reverse power – if the prime mover fails the machine becomes an electric motor and drives the generating sets (turbine);

- Asynchronous operation – can occur as a result of a failure of the excitation system or the grid voltage collapsing during short-circuits;
- Exciter failure;
- Underspeed and overspeed protection;
- Overvoltage – this type of protection is used on medium voltage alternators. A 2-stage protection relays are used typically for 30% over voltage. Voltage monitors will not protect the alternator against external voltage peaks (switching peaks or atmospheric effects);
- Overfrequency – is used if there is a risk of dangerous over speeds caused by the prime mover.

Since the principal method of control for small CHP unit is based on active power and reactive power/power factor as shown in Figure 30 it requires a connection with an infinite bus bar.

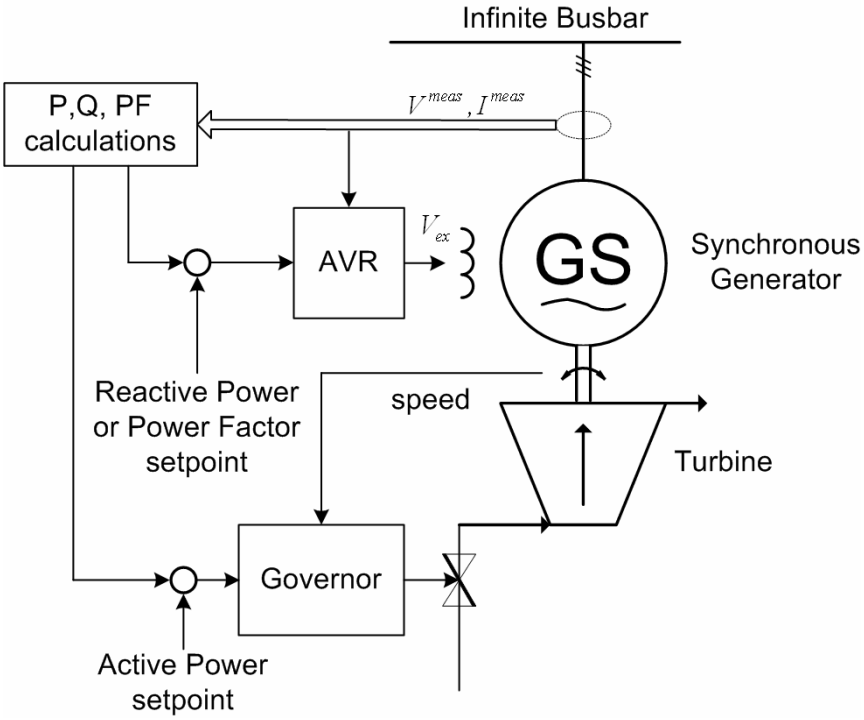

Figure 30: Typical control scheme for a small CHP unit.

A voltage measurement is supplied to the Automatic Voltage Regulator (AVR) and a speed/frequency measurement to the governor. However, in this mode of control these signals are not used.

The error between the active power set point and the measured ones fed to the governor. This governor controls the steam/gas supply to the turbine.

Similarly, the excitation of the generator is controlled based on reactive power or power factor. The error signal between the set point and the actual value is passed to the AVR and exciter. The exciter controls the field current and thus the reactive power output (power factor) of the generator.

Using this control method the operational points of the CHP are as shown in Figure 31. Usually, the CHP operates at unity power factor during the night while during the day it works at 0.8 power factor. The active power is related with the heat demand.

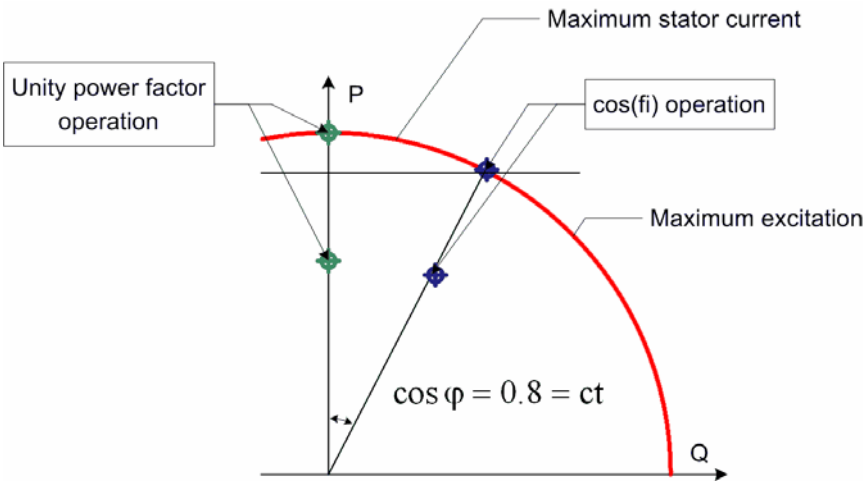

Figure 31: Operational points for a synchronous generator used in a small CHP.

It is clear that such a control scheme does not take into account the grid conditions. The active power is set to a value which does not take into account the frequency of the system whereas the reactive power set point (or power factor) does not consider the grid voltage. Moreover the operation at non-unity power factor increases the electrical losses in the generator, while changing the active power delivered to the grid according with the grid frequency will affects the prime mover if the unit operates as a CHP.

The model, which was implemented in DIgSILENT during this project has the above mentioned control characteristics. The control variables are the active power and the power factor. However, additional signals namely frequency and voltage are available. Thus, this model can be extended so that the possibilities of dispatching the unit can be explored in the future.

The block diagram of the model implemented in DIgSILENT during the project is shown in Figure 32.

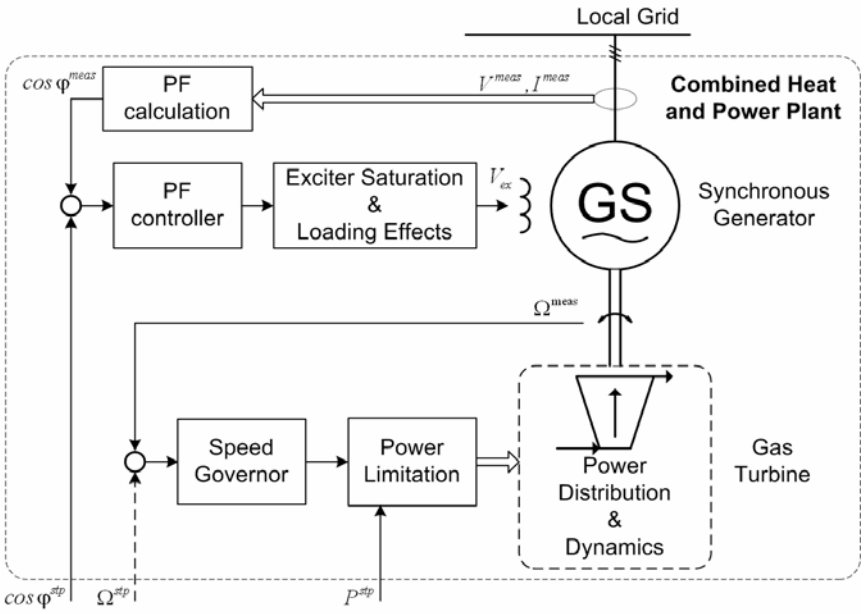

Figure 32: Block diagram of the small CHP unit implemented in DIgSILENT.

An AvK generator type DIDB 160 h/4 with 5.4 MVA rated power is used for the CHP model (A. van Kaick Neu-Isenburg, b). The prime mover model is based on a GEC Alsthom gas turbine Type GT8C2 (Cigre, 2003).

The excitation system is IEEE Type AC5A, which is a simplified model for brushless excitation systems (IEEE Std 421.5-1992). This model can be used to represent small excitation systems and has been widely implemented by the industry (IEEE Std 421.5-1992).

3 Fixed speed active stall wind turbine concept with AC connection – with traditional power controller

An active stall wind turbine is in principle a stall-controlled turbine with variable pitch angle. The generator of an active stall turbine is a simple squirrel cage induction generator directly coupled to the grid. The main difference between stall and active stall turbines is a pitch actuator system for variable pitch angles, which allows the stall effect to be controlled. In addition the power coefficient C_p can be optimised to a certain extend.

The implementation of the controller is done in a general way so that as much as possible is expressed in terms of parameters. The idea is to use this controller model to simulate different existing wind turbines with specific parameters. In-depth knowledge about manufacturer specific controller design is not necessary.

The model described in this report spans the power control during normal operation in the range from start-up wind speed to shutdown wind speed of a single speed generator turbine.

When the wind speed is between start-up wind speed and nominal wind speed the pitch angel is adjusted to optimise C_p i.e. power output.

When the wind speed is above nominal wind speed power output is limited to nominal power by utilising the stall effect. To get a flat power curve, i.e. constant nominal power in the range between nominal wind speed and shut-down wind speed, the pitch angle has to be adjusted accordingly. For comparison: In a stall-controlled turbine the pitch angle is fixed and that means that the power output cannot be held constant. Instead the stall effect leads to a drop below nominal power in the range of high wind speeds. The maximal power of a stall turbine depends on air density, grid frequency and aerodynamic influences e.g. dirt on the blades.

3.1 Active Stall Control Strategy

It is desirable to be able to control the electrical output power of wind turbines. There are different types of wind turbines, which apply different control strategies for controlling the output power of the turbine. One is the active stall controlled wind turbine.

The operation of an active stall wind turbine can be divided into two modes:

- Power limitation: power output is limited to nominal power when wind speed is between nominal wind speed and shut-down wind speed; pitch angle θ is adjusted to control the stall effect. In order to get a flat power curve, i.e. constant nominal power in the range between nominal wind

speed and shut-down wind speed, the pitch angle has to be adjusted accordingly.

- Power optimisation: power yield is maximised between start-up wind speed and nominal wind speed; pitch angle θ is adjusted to optimise the power coefficient C_p and hence the power output.

In a passive stall turbine the pitch angle is fixed and that means that the power output can neither be optimised nor controlled limited at wind speeds beyond nominal wind speeds. Instead the stall effect leads to a drop below nominal power in the range of high wind speed.

Although active stall turbines also use the stall effect like passive stall wind turbines, active stall turbines have considerable advantages. The maximum power output of passive stall turbines depends on wind speed, air density, grid frequency, and aerodynamic influences like dirt on the blades, while the maximum power output of active stall turbines can be controlled to a constant value.

3.1.1 Power Limitation

Power limitation is activated whenever the electrical power is above its nominal value, or the wind speed is above its nominal value. In the power limitation mode the power is controlled in a closed control loop, where the measured and averaged generator power is compared with its setpoint, which is the turbine's nominal power.

If the averaged power exceeds the setpoint, θ is increased in negative direction to increase the stall effect and hence to limit the power output. If the averaged power falls below the nominal power, θ is increased in positive direction to reduce the stall effect.

3.1.2 Power Optimisation

The power output of the turbine is optimised whenever the wind speed is below the nominal wind speed and the power is below the nominal power. Optimising power can only be done by finding the pitch angle that corresponds to optimal power coefficient $C_p(\theta,u)$ at a given wind speed u. Optimising power by varying the tip speed ratio λ, which in the simplest case could happen by switching between two different generator speeds, is not considered here.

The pitch angle θ can be adjusted to get optimal $C_p(\theta,u)$ at a given wind speed. In reality this means that the wind speed is averaged over a certain time and θ is adjusted so that it tracks optimal $C_p(\theta,u)$ for this averaged wind speed.

Power optimisation is an open loop control since there is no feedback from θ and power to wind speed.

By adjusting θ not only according to wind speed, but also according to power, side effects like varying air density and dirt on the blades can also be taken into account (Lehnhoff M. et al, 1998). This aspect is not considered in this project, since here focus is on the simulation of short-term operations. Dirt on the blades and varying air densities however are comparatively slow effects.
In power optimisation the controller looks up appropriate values of θ in a lookup table. This lookup table consists of wind speed values and corresponding θ values that refer to maximum C_p at the respective wind speed.

3.1.3 Transition between power limitation and power optimisation mode

The transition between the operation modes power limitation and power optimisation is a decision the controller based on the operating point of the wind turbine.

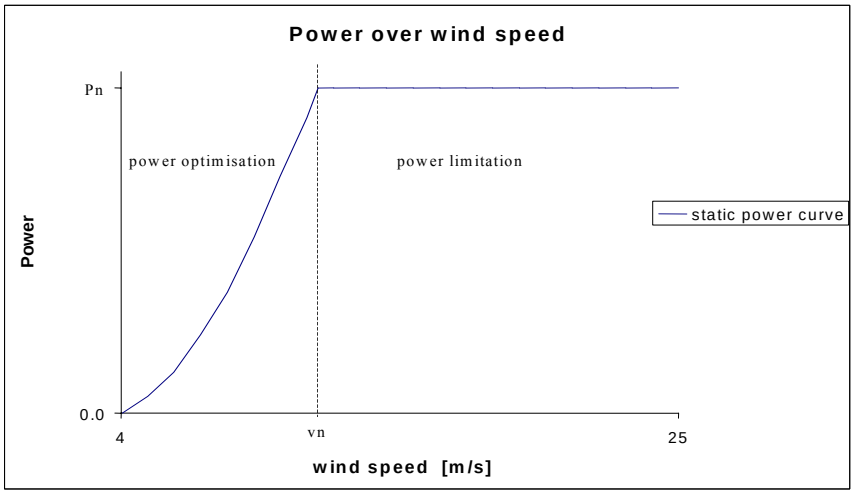

Figure 33: Static power curve with operation modes of an active stall controlled wind turbine.

The static power curve in Figure 33 shows the operation modes: power optimization and power limitation. The dashed line shows the border between the operation modes, which is where the transition takes place, considering steady state operation.

In the dynamic operation of the turbine the decision whether power optimisation or power limitation mode is to be active has to be made on the basis of averaged wind speed and averaged power values.

3.2 Traditional power controller

In the following subchapters the active stall controller is developed. For this purpose a fictive 2 MW example turbine is used.

The controllers for power optimisation, power limitation and transition are described in the following.

3.2.1 Power optimisation

In the power optimisation mode the pitch θ-values are looked up in a table. The θ-values corresponding to optimal C_p-values have to be found in the C_p table, which describes the aerodynamic properties of the blades.

In order to achieve maximum power yield for each wind speed the maximal C_p and the corresponding θ has to be found, because the aerodynamic power is calculated according to:

$$P = \frac{1}{2} \cdot \rho \cdot \pi \cdot R^2 \cdot u^3 \cdot C_p(\theta, u) \qquad (40)$$

3.2.1.1 *Generating θ lookup table*

The aerodynamic properties of the blades are applied in the simulation model, as a C_q table. In order to generate a θ lookup table that contains θ-values, which correspond to maximum C_p- and not maximum C_q-values, a C_p table has to be generated from this C_q table. This is done using the following equation:

$$C_p(\theta,u) = C_q(\theta,u) \cdot \lambda \tag{41}$$

Note that maximising C_q would not achieve maximal power output since maximum C_q and maximum C_p do not necessarily correspond to the same θ.

The lookup table needed in the controller is a θ versus u table. λ is converted to u since in a constant speed turbine the tip speed u_{tip} of the rotor does not vary. u is calculated as follows.

$$\lambda = \frac{u_{tip}}{u} \tag{42}$$

$$u = \frac{R \cdot \omega}{\lambda} \tag{43}$$

Note that rotor speed and hence tip speed u_{tip} are considered to be constant, neglecting the fact that the slip in the generator is actually a function of power. (Nominal slip is typically 1% to 2% of nominal speed.)

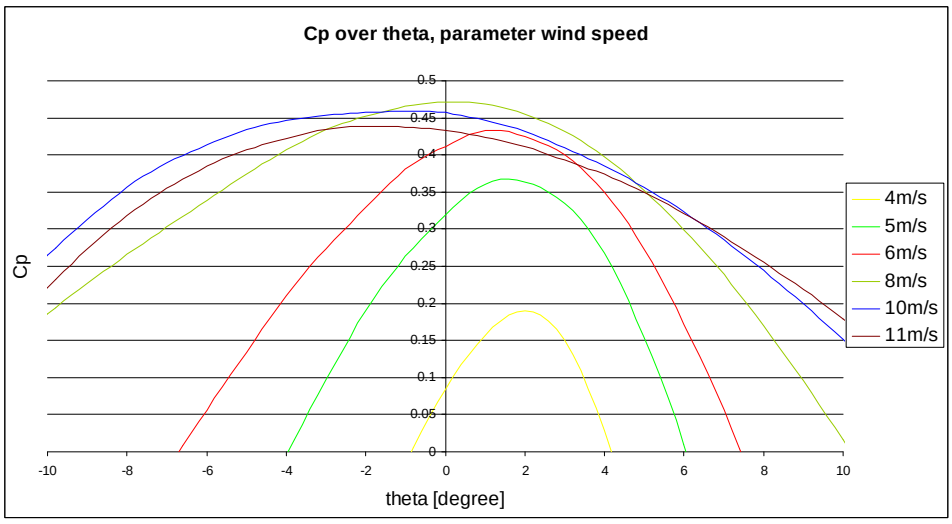

Figure 34: C_p *curve as function of the pitch angle* θ *for different wind speeds.*

To get an idea how accurately the optimal θ should be met, Figure 34 shows C_p curves for different wind speeds as a function of θ. It can be seen that at low wind speeds the C_p over θ curves have rather sharp maxima, i.e. C_p is sensitive to small deviations from optimal θ (optimal θ corresponds to maxima in C_p). At higher wind speeds the curves become flatter and the values of the

maxima lie closer to each other, i.e. deviations from optimal θ and slight variations in wind speed make no big differences in C_p.

The graph in Figure 35 shows maximum C_p, optimal θ and linearly interpolated θ over the range of relevant wind speeds (power optimisation range). Optimal θ is the pitch angle required to achieve maximum C_p under any wind speed.

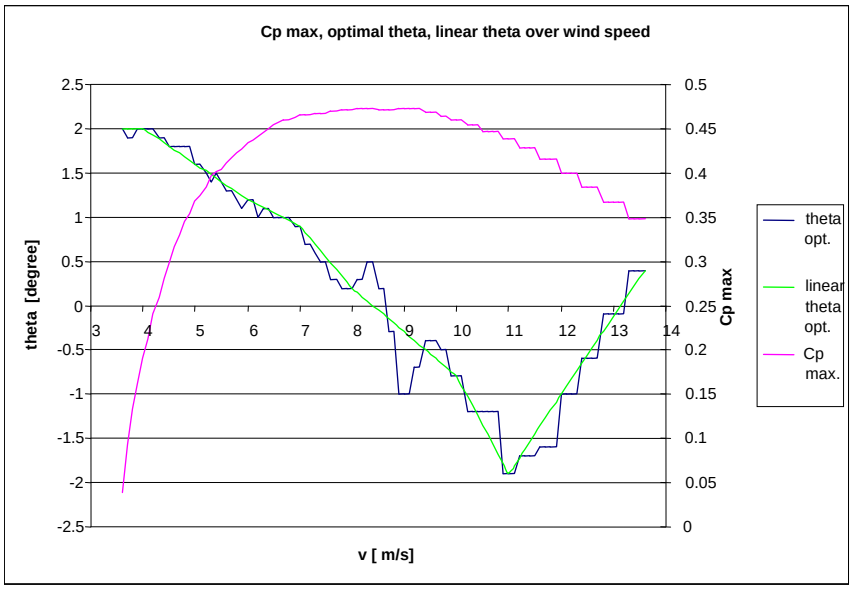

Figure 35: Maximal C_p*, optimal* θ *and linearised* θ *over wind speed.*

In Figure 35 the graph of optimal θ shows a lot of discontinuities, especially between 8 m/s and 9.5 m/s. These discontinuities stem from rounding errors and from the discrete data points in the C_p table, which have a rather low resolution (step sizes are: $\theta = 0.1$ degrees and $\lambda = 0.2$).

It is not desirable to follow the discontinuities in *theta opt* as depicted in Figure 35 in a wind turbine controller. Looking at Figure 34 it becomes clear that only a little increase in C_p can be achieved from an attempt to follow optimal θ all too accurately. Hence for control purposes a lookup table with the most relevant points and a linear interpolation between these points is used. These values can also be seen in Figure 35 where they are called *linear theta opt*.

When finding the points between which θ shall be linearly interpolated it has to be kept in mind that the optimal θ for lower wind speeds should be met precisely. As it can be seen in Figure 34 the C_p over θ curves have sharp maxima for low wind speeds.

The pitch angle θ is adjusted on the basis of averaged wind speed values instead of instantaneous wind speed values. For this purpose the method of moving average is used. Moving average is a realistic way of filtering the wind signal since this is the method often used in wind turbine controllers.

3.2.2 Power limitation

To get the power limiting stall effect the blades have to be pitched in negative direction when electrical power of the wind turbine exceeds nominal power.
Figure 36 illustrates how power over wind speed behaves for different pitch angles.

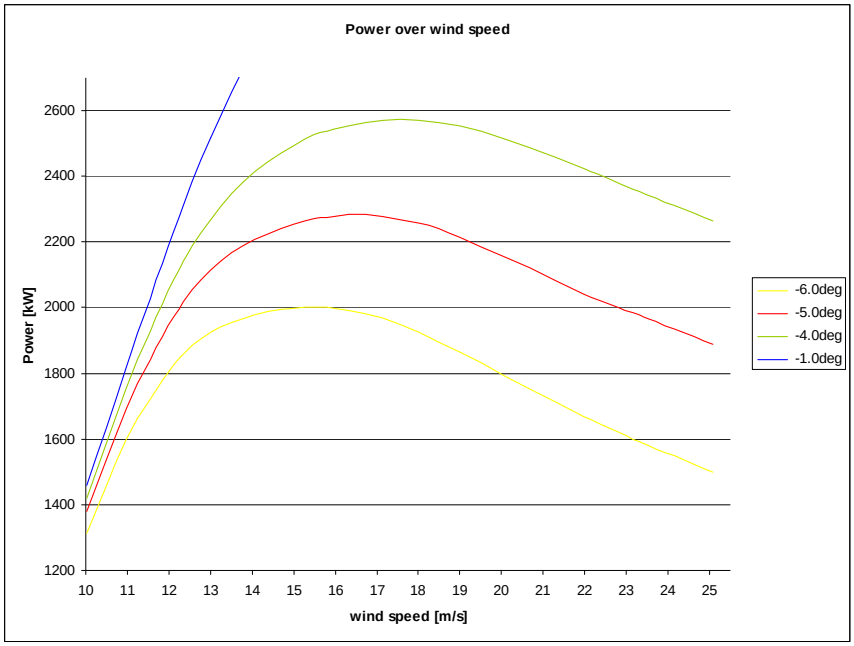

Figure 36: Power over wind speed for different pitch angles.

Figure 37 illustrates how the pitch angle has to be adjusted in order to get nominal power (which is 2 MW in this model) for all wind speed values between nominal wind speed and shut-down wind speed.

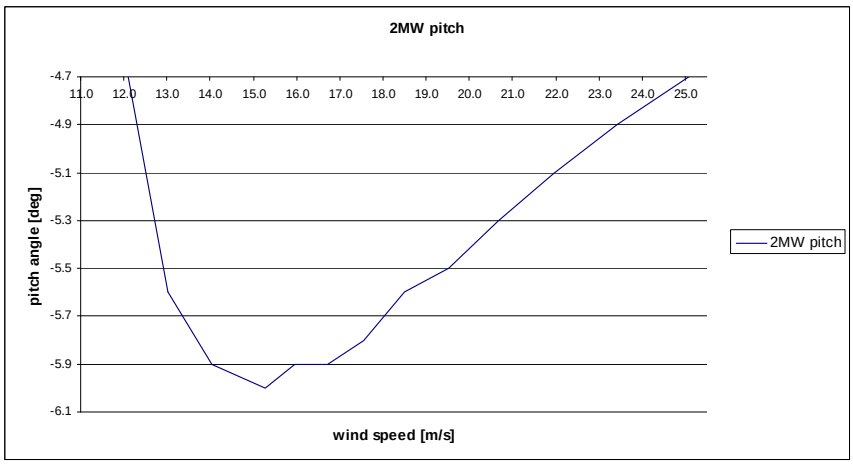

Figure 37: Pitch angle θ required for constant 2 MW power output in the power limitation wind speed range.

The pitch angle θ is controlled in a control circuit as shown in Figure 39, where the averaged electrical power from the turbine is compared with the power setpoint i.e. nominal power (2 MW).

The electrical power is filtered using moving average in the same way the wind speed signal is filtered in the power optimisation mode.

3.2.3 Transition between optimisation and limitation

Figure 35 and Figure 37 show that the pitch angle θ at the end of the optimisation range and at the beginning of the limitation range is quite different. The reason for this is that the power curves for different pitch angles in Figure 36 lie

close to each other and are very steep in the range between 10 m/s and 12 m/s. To avoid big steps in θ when moving from one operation mode to the other, the θ-values at the end of the power optimisation range have to approach the θ-values at the beginning of the power limitation range. This can be achieved by modifying the θ lookup table, so that θ falls linearly with the slope as in the linearly interpolated θ curve between 10 m/s to 11 m/s. The linearly interpolated and extrapolated θ curve, implemented as a lookup table in the simulation model, are depicted in Figure 38.

This solution is a compromise between maximal power yield in the power optimisation mode and a smooth transition between the operation modes. This compromise reduces the maximum possible power in the range between 11 m/s and 11.8 m/s (which is the nominal wind speed in this example). However, the maximal difference between the practically achieved and the theoretically possible power is only 13.5 kW at 11.8 m/s. This is not only a marginal loss in terms of power, it is also a very small loss in terms of produced energy, since it is reasonable to assume that in most wind power sites a wind speed of 11.8 m/s is a rarely occurring wind speed.

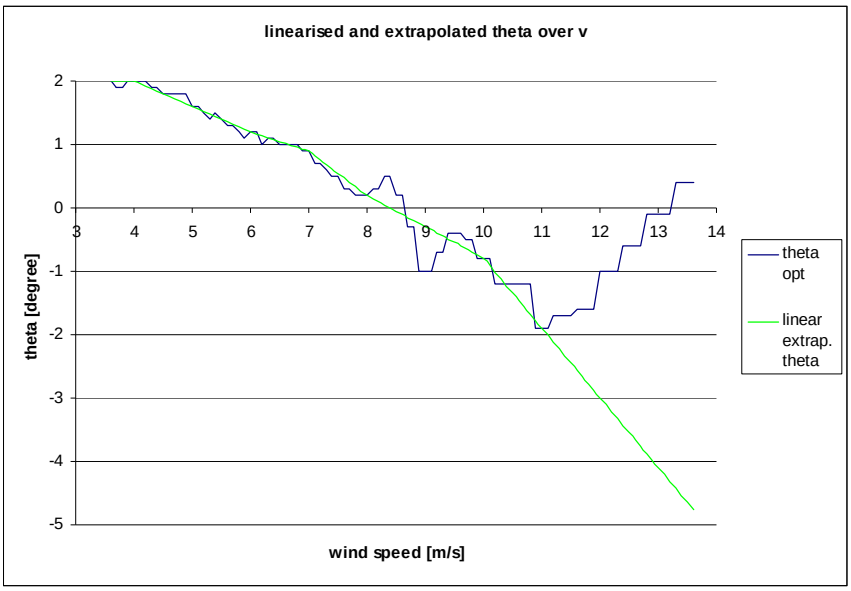

Figure 38: θ_{opt} and θ as implemented in θ-lookup table: Linearly interpolated in power optimisation range and linearly extrapolated for transition between power optimisation and power limitation.

For transition between power optimisation and power limitation the following conditions have to be fulfilled:

- Transition from power optimisation to power limitation: power output has to be greater than nominal power or wind speed has to be greater than nominal wind speed.
- Transition from power limitation to power optimisation: power output has to be less than nominal power and wind speed has to be less than nominal wind speed.

3.2.4 Pitch angle control system

In this subchapter the generation and implementation of the pitch angle setpoint in the pitch control system is described.

Figure 39 shows a diagram of the general control circuit of the pitch control system. The control circuit diagram is divided into four sections, namely "power limitation", "transition switch", "pitch logic" and "pitch system".

The PI-controller for power control (in the section "power limitation" in Figure 39) generates a pitch angle setpoint from the difference between the power setpoint and actually measured and averaged power. The I-part of the PI controller is combined with an anti-windup loop. The task of this anti-windup is to avoid that the integrator keeps integrating while the power control is not active, or while the pitch angle is held constant by the pitch logic. The gain P_{aw} in the anti-windup loop has to be tuned to the normal hold time of the sample and hold (S&H in the section "pitch logic"). When the gain P_{aw} is not tuned correctly the anti-windup either does not work properly, or effectively disables the I-controller. The first case occurs when P_{aw} is too low and the latter case occurs when P_{aw} is too high.

For safety reasons the signal from the PI-controller is limited to a reasonable range, e.g. –2deg to –90deg, which is the range in which θ can be during the power limitation mode.

Also in the section "power limitation" in Figure 39 is a block called "overpower", which detects when the averaged electrical power is excessively above nominal power.

In the section "transition switch" in Figure 39 is the switch, which selects a pitch angle setpoint, either from the power controller for power limitation mode, or from the lookup table for power optimisation mode.

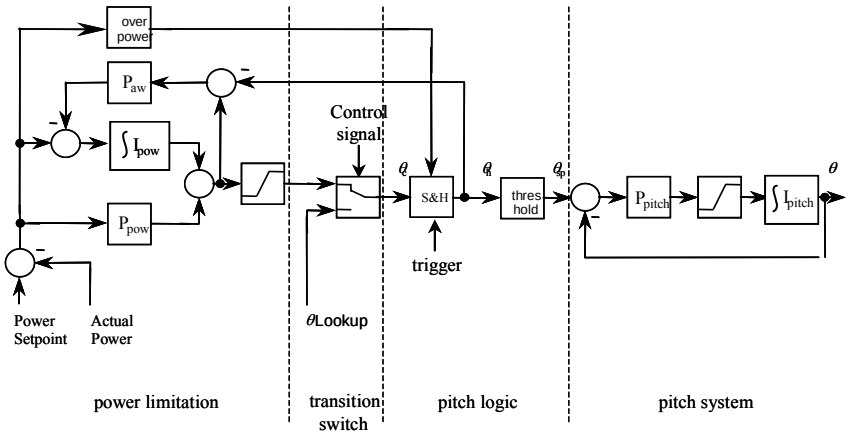

Figure 39: General control circuit of active stall pitch actuator system. PI-power controller, pitch mode selection, sample and hold with a selection of 2 hold times, threshold for pitch angle setpoint and pitch actuator system model.

To the right of the section "transition switch" in Figure 39 is the section "pitch logic". This section contains a sample and hold (S&H) and a threshold block. The desired operation of an active stall wind turbine is to pitch only when necessary. The S&H block has an input from the overpower block in section "power limitation". This input to the S&H block has impact on the hold time, which is needed for overpower protection.

In the section "pitch system" in Figure 39 is a representation of the pitch actuator system. The characteristic of the pitch actuator system is modelled by a pure limitation in the rate of change in pitch angle. The pitch angle setpoint θ_{sp} is compared with the actual pitch angle θ and the difference is multiplied with a factor P_{pitch}, which has the unit $\frac{\text{deg}/s}{\text{deg}}$. This signal is limited to a parameter that defines the maximum rate of change in the pitch angle.

The integrator in section “pitch system” integrates over the limited rate of change in the pitch angle setpoint, which leads to the actual pitch angle of the blades.

The factor P_{pitch} determines the slope of the limiter characteristic in the range between the limits. It is desirable to have the steepest possible slope in order to avoid that the simulation of the pitch actuator system shows a dynamic behaviour in the range of small rates of pitch angle changes. This would mean that the integrator would not integrate fast enough. If however P_{pitch} becomes too big, i.e. the slope becomes too steep; the limiter cannot output small rates of change. In such a case it would permanently jump from one limit to the other instead of staying at a value between the limits.

3.2.4.1 *Subsystem to avoid unnecessary pitching*

To get pitch actions only once in a specified period the pitch angle setpoint θ_c from either the power controller or from the lookup table, is held in a S&H block.

To further avoid unnecessary pitching a threshold block downstream of the S&H block (in Figure 39) allows a new setpoint θ_{sp} only when the new setpoint differs from the old setpoint by a minimum value.

The function of this combination of S&H and threshold is depicted in Figure 40 where an example θ_c with two different slopes is used to illustrate the function of the system.

The S&H block samples at each positive flank of the rectangular signal. In this example the parameters for threshold, hold time and the slopes of the input signal θ_c are chosen such that the function of the threshold block becomes clear.

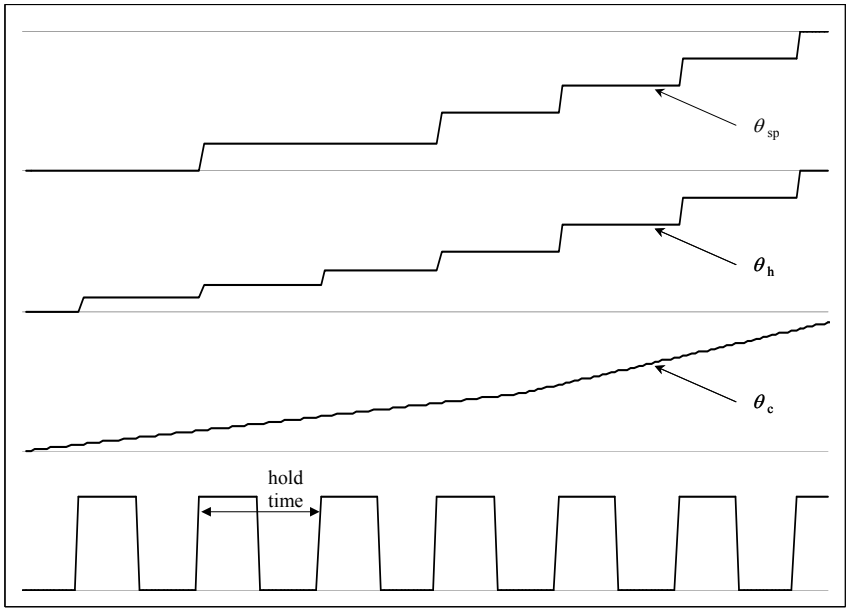

Figure 40: Function of the combination of sample and hold (S&H) and threshold. Input signal θ_c is a ramp, which leads to the output signals θ_{sp} of the S&H and the threshold block. The rectangular signal triggers the S&H at each flank.

The rectangular signal determines at which points in time the S&H block samples a new value. If however the difference between the newly sampled

value and the current output value of the threshold block is not bigger than the threshold parameter, the current output of the threshold block is held.

3.2.4.2 *Overpower protection*

Overpower protection protects the wind turbine from damages due to excessive power production. If under any circumstance the averaged power exceeds a certain level, immediate action has to be taken to limit the power output to avoid damages in mechanical and electrical components of the turbine.

The overpower block in Figure 39 compares the power error with an overpower parameter. If the power error exceeds the value of this parameter the overpower block effects that S&H uses a much shorter hold time. This means that pitching takes place much more frequently and hence the power output of the turbine can be reduced within a reasonable time.

The power signal that is used for overpower protection (and also for power control) is averaged using a moving average. The averaging time should not be too long but should only make sure that periodic fluctuations in power are filtered out. This avoids that the power controller picks up a setpoint that is not realistic to act on. If the averaging time would be too long, the implied delay would make the overpower protection ineffective.

3.3 Wind turbine controller implementation in power system simulation tool

In the following the implementation of the above-described controller, into the power system simulation tool DIgSILENT PowerFactory is described. During the implementation of the controller care has been taken, that as much as possible is expressed in terms of parameters.

The idea is to simulate different existing active stall wind turbine controllers with this simulation model. The parameters allow the model to be fitted so that it represents the existing controllers of the considered wind turbine. Furthermore the parameters make the program understandable by avoiding constants in the program that are not self-explanatory.

The controller is split up into sub-models as it can be seen in Figure 41.

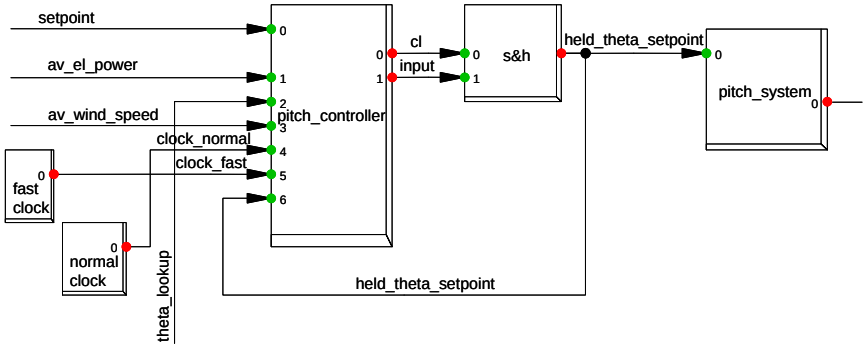

Figure 41: The part of the wind turbine composite model that contains the pitch controller, the pitch actuator system, the sample and hold (S&H) unit and the two clocks that are necessary for the two different hold times in the S&H.

The block “pitch controller” in Figure 41 contains a macro that is depicted in Figure 42. The pitch controller macro contains the PI controller for power

limitation, pitch angle setpoint selection (operation mode selection) and clock signal selection for overpower protection.

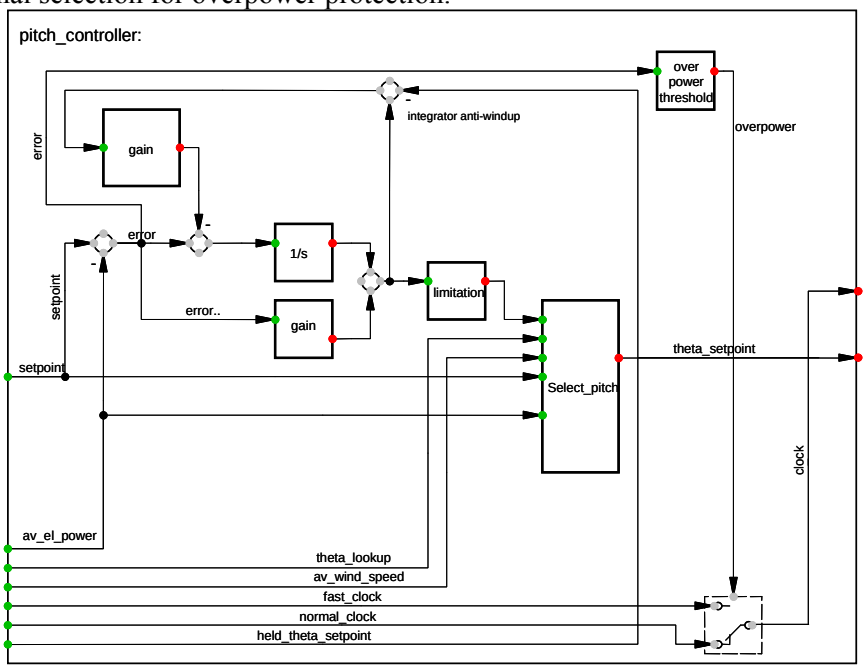

Figure 42: Pitch controller macro.

The block "pitch system" in Figure 41 contains the macro, which is depicted in Figure 43.

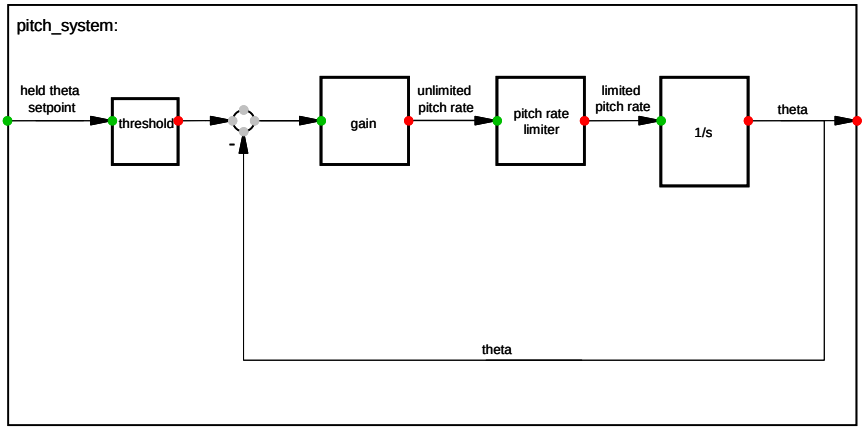

Figure 43: Pitch actuator system macro with threshold and pitch rate limiter.

As it can be seen in Figure 41 the two clocks as well as the S&H block are separate units in the composite model and not a part of the pitch actuator system macro where they would naturally belong. The reason for this is that clocks as well as S&H are built-in DIgSILENT elements and can hence only be used in composite models, but not in macros.

3.3.1 Power optimisation

For power optimisation, i.e. pitch angle from θ-lookup table, the θ versus wind speed table is implemented in the program. In Figure 42 the block select_pitch determines whether or not θ from the lookup table (in Figure 42 it is called

theta_lookup) is to be chosen. The conditions for choosing *theta_lookup* as *theta_setpoint* are:

av_el_power < setpoint OR av_wind_speed < nominal wind speed

(The variable names are as depicted in Figure 42, and "nominal wind speed" is a parameter.)

Wind speed is averaged using moving average. The averaging time is determined by setting a parameter. The averaging time should be similar to the normal hold time of the S&H block. For θ values corresponding to wind speed values, which lie between two values in the table, linear interpolation is applied.

The moving average function, used for averaging the wind speed and electrical power signal, is implemented into the program as shown in Figure 44 (here at the example of wind speed).

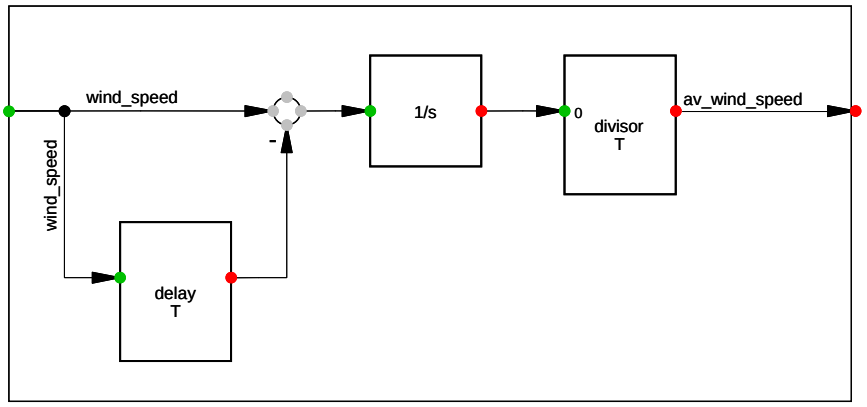

Figure 44: Moving average macro.

For initialisation of the moving average block the assumption is made that the wind speed is constantly on the initial value prior to the start of the simulation. This way a moving average with a constant averaging time can be realised, even at the beginning of the simulation i.e. before the simulation time exceeds the averaging time.

3.3.2 Power limitation

The PI-controller of the closed power control loop is split up into a P- and an I-controller.

As explained before, the I-controller is combined with an anti-windup loop. The gain in the anti-windup loop has to be tuned to the normal hold time of the S&H. When the gain is not correctly tuned the anti-windup either does not work properly, or effectively disables the I-controller. The first case occurs when the gain is too low and the latter case occurs when gain is too high.

The power that is controlled (in Figure 42 this signal is called *av_el_power*) is not the instantaneous power but a moving average of the instantaneous electrical power. The averaging time is a parameter and has to be tuned so that fast periodic fluctuations like 3p and fast transient wind speed changes are filtered out, but at the same time overpower can be detected after a tolerable time delay. Therefore it is advantageous to set the power averaging time to a value similar to the short hold time of the S&H because during overpower protection operation these two times have to match each other.

If the averaged power exceeds a certain level of overpower i.e. the condition *error < -(overpower parameter)* is fulfilled the overpower block sets its digital output to high. This effects that the switch in Figure 42 selects the fast clock signal. The clock signal is input to the S&H block where it determines the

hold time. By switching between two different clock signals the pitch controller can choose between two different hold times i.e. pitch frequencies.

3.4 Simulations

Different scenarios are simulated to assess the performance of the controller developed.

The impact of the S&H/threshold subsystem on power production is assessed, where applicable, by comparison with a reference turbine. This reference turbine is subject to the same wind speed input but has the least possible restrictions on the pitch action. In both cases i.e. the turbine to be assessed and the reference turbine, the power is averaged over 600 seconds. This allows an effective comparison of the power yields and a quantification of this difference.

3.4.1 Parameter Settings

In all simulations the parameter settings are the same and as listed in Table 2. The parameter settings are chosen such that a fictive example-turbine rated at 2 MW is simulated. By selecting other sets of parameters specific types of active stall turbines could be modelled.

The Power Averaging Time (T_{aP}) is a parameter and has to be tuned so that fast periodic fluctuations like 3p and fast transients from transient wind speed changes are filtered out, but at the same time overpower can be detected after a tolerable delay time. Therefore, it is advantageous to set $\boldsymbol{T_{aP}}$ to a value similar to T_{sh} of the S&H.

u_N	Nominal Wind Speed [m/s]	11.8
P_N	Nominal Power [kW]	2000
ρ	Air Density [kg/m^3]	1.25
R	Rotor Diameter [m]	80
T_{aP}	Power Averaging Time [s]	5
T_{aW}	Wind Averaging Time [s]	60
r	Maximum Pitch Rate [deg/s]	8
P_{pitch}	Gain Pitch System	1000
P_{pow}	Gain Power Controller	0.01
I_{pow}	I-gain Power Controller	0.0025
P_{aw}	Gain Anti-Windup	500
T_{nh}	Normal Pitch Setpoint Hold Time [s]	60
T_{sh}	Short Pitch Setpoint Hold Time [s]	5
P_{over}	Allowed Overpower [kW]	300
$\Delta\theta_{min}$	Minimum Pitch Angle Change [deg]	0.5

Table 2: Parameters of simulation model of an active controlled wind turbine.

The reference turbine, to which the power yield of the turbine described in Table 2 is compared to, has the same parameter settings as in Table 2; only the parameters listed in Table 3 are different.

T_{nh}	Normal Pitch Setpoint Hold Time [s]	5
$\Delta\theta_{min}$	Minimum Pitch Angle Change [deg]	0

Table 3: Parameters of reference turbine.

The reference turbine has the least possible restriction on the pitch actions. As it can be seen in Table 3 the pitch angle setpoint threshold is disabled and T_{nh} is set to the shortest possible value. (Continuous pitch action is not possible since the controller is not designed for that i.e. instabilities might occur under certain conditions.)

3.4.2 Power optimisation

Figure 45 illustrates the simulated operation in power optimisation mode with the mean wind speed set to 8 m/s.

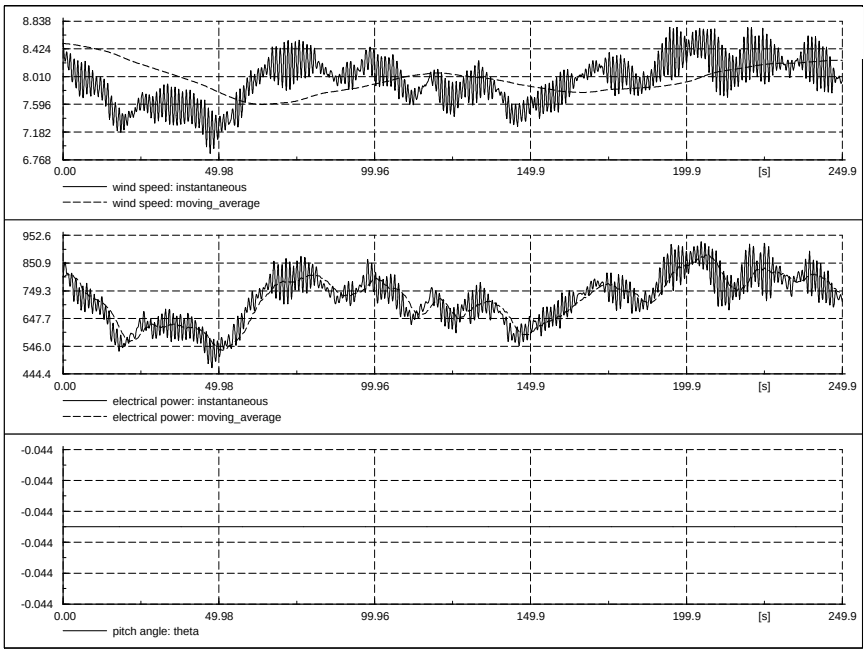

Figure 45: Normal operation in power optimisation mode at mean wind speed 8 m/s. Wind speed, electrical power and pitch angle.

In Figure 45 the pitch angle is held constant since the changes that would be due are below the threshold. The restrictions on pitching implied by the parameters $\Delta\theta_{min}$ and T_{nh} lead to losses in the 10-minute average of power production as it can be seen in Table 4. To calculate the relative difference in averaged power the power of the active stall turbine (restricted pitch action) is used as basis (100%).

600 s power average standard active stall turbine $P1$	600 s power average reference turbine $P2$	Δ averaged power $P2 - P1$	relative Δ averaged power $\frac{P2 - P1}{P1} * 100\%$
684.4 kW	691.1 kW	6.7 kW	0.98 %

Table 4: Comparison of power yield in power optimisation mode.

It can be seen that the pitch angle changes that occur maximum every 5 seconds (when no $\Delta\theta_{min}$ is used) lead to a better power yield of 0.98%. This increase in power yield however has to be paid for with many consecutive pitch actions (every 5 seconds), which means stress for the pitch actuator system.

3.4.3 Transition between optimisation and limitation

To simulate the behaviour of the controller under transition conditions the mean wind speed is set to 12 m/s.

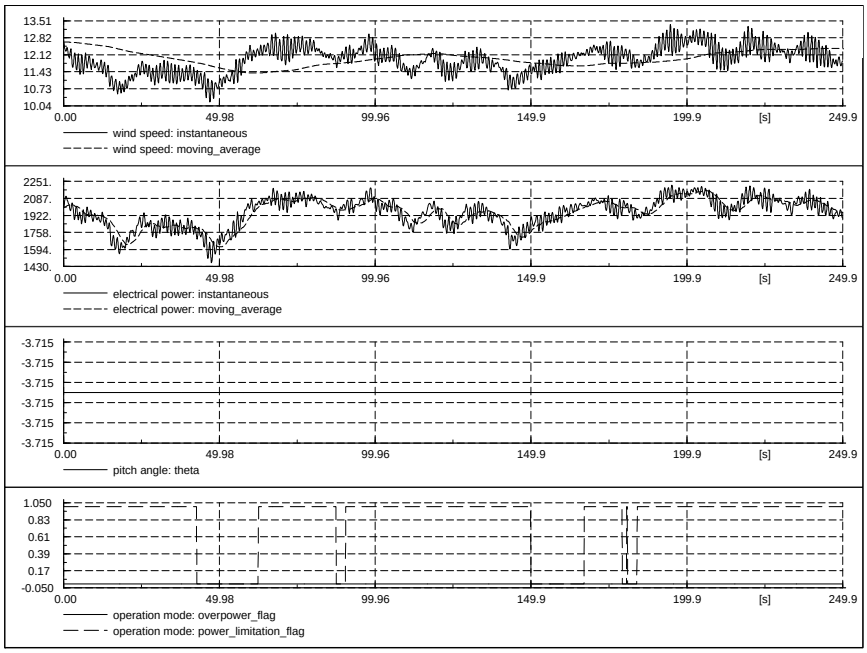

Figure 46: Operation at mean wind speed of 12 m/s. Frequent transition between operation modes. Wind speed, electrical power, pitch angle, overpower indicator and operation mode indicator.

The diagram in Figure 46 shows that transition frequently takes place. The signal "*power_limitation_flag*" is a digital indicator: If on 1 power limitation mode is active; if on 0 power optimisation mode is active.

The power is always around nominal power, intolerable overpower does not occur, nor is power below nominal power, while wind speed is above nominal wind speed. The pitch angle is held constant since the differences implied by the changes in wind speed and by the different operation modes are always be-

low 0.5 degrees. This proves that the linear extrapolation of the θ lookup table leads to a smooth transition between the two operation modes.

Unlimited pitch action leads to no increase in power yield, on the contrary averaged over 10 minutes the power yield is slightly less. Unlimited pitch action avoids not only power deviation below, but also beyond nominal power. However, damages caused by excessive overpower have not to be feared since this is cared for by the overpower protection. Hence pitching every 5 seconds leads to no improvements but to extra stress for the pitch actuator system only.

600s power average standard active stall turbine $P1$	600s power average reference turbine $P2$	Δ averaged power $P2 - P1$	relative Δ averaged power $\frac{P2 - P1}{P1} * 100\%$
1918 kW	1916.8 kW	-1.2 kW	-0.06 %

Table 5: Comparison of power yield under operation mode transition condition.

3.4.4 Power limitation

In Figure 47 the performance of the controller in power limitation mode is assessed by applying rather high wind speeds, i.e. mean wind speed is set to 23 m/s.

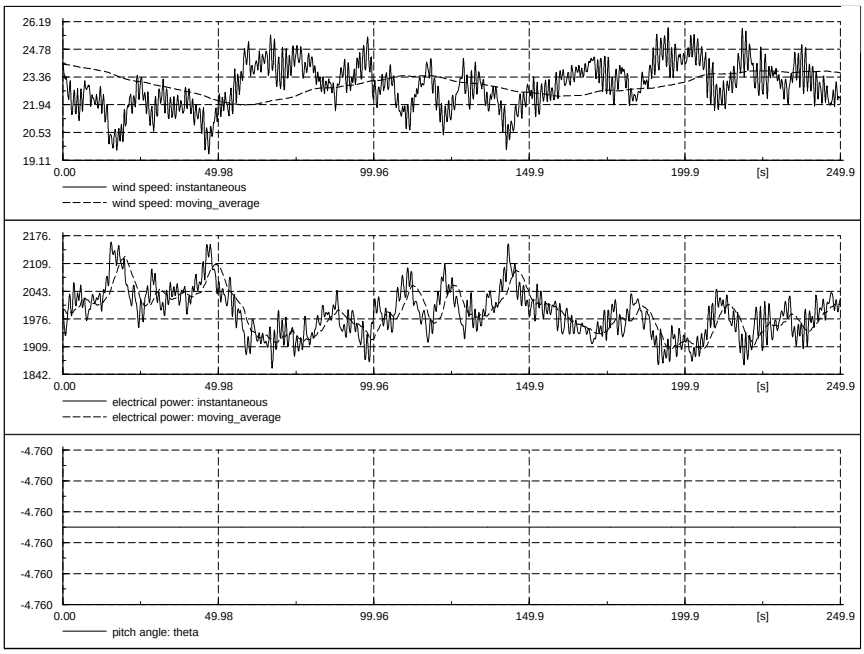

Figure 47: Operation in power limitation mode at mean wind speed 23 m/s. Wind speed, electrical power and pitch angle.

Also for such high wind speeds the controller finds the appropriate pitch angle so that power is always around nominal power. If mean wind speed is at a constant level, pitch angle changes are usually not required as can be seen in Figure 47.

Although it has to be said that the absolute power variations are rather big considering that they exceed ± 100 kW around nominal power, trying to control them out would make little sense in terms of power quality. Considering large wind farms these fluctuations anyway do not exist to such an extent at the terminals of the wind farm, since fluctuations of individual turbines partially offset each other (Rosas, P., 2003).

The operation of the reference turbine is an attempt to control out the power fluctuations. Here the power output of the turbine gets much closer to nominal power, which means less deviation from nominal power. This leads to a decrease in the 10-minute power average of negligible 0.03 % as it can be seen in Table 6.

600s power average active stall turbine $P1$	600s power average reference turbine $P2$	Δ averaged power $P2 - P1$	relative Δ averaged power $\frac{P2 - P1}{P1} * 100\%$
2000.9 kW	2000.2 kW	-0.7 kW	-0.03 %

Table 6: Comparison of power yield in power limitation mode for an active stall controlled wind turbine.

While the power limitation is a straightforward task for an active stall wind turbine in the case of moderate wind speed changes only, it becomes a more demanding task when the overall average wind speed increases considerably. To simulate such a situation in the following simulation, the mean wind speed is 11 m/s until the simulation time 60 s, between 60 s and 160 s it is ramped up from 11m/s to 16 m/s. This corresponds to a slope in mean wind speed of 3 m/s per minute. The simulation results of this scenario are depicted in Figure 48.

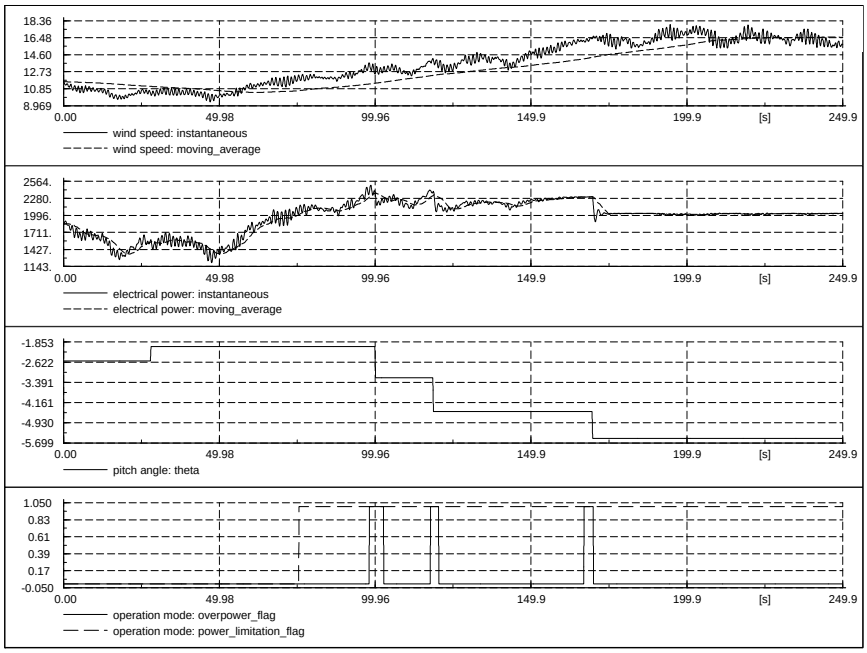

Figure 48: Operation with increasing wind speed implying overpower. Wind speed, electrical power, pitch angle, overpower indicator and operation mode indicator.

The turbine starts off in the power optimisation mode, where an increase in the pitch angle takes place. With an increasing wind speed the turbine enters into power limitation mode and a further increasing wind speed lets the average of the power exceed 2300 kW (300 kW beyond nominal power, which is the maximum allowed level of tolerable overpower). As soon as overpower is detected the pitch angle is adjusted with a maximum delay time of 5 seconds, which is T_{sh}. The signal "*overpower_flag*" is a digital indicator: If overpower is detected it is set to 1.

Due to the steadily increasing wind speed it takes three overpower protection operations to get power permanently down to nominal power.

It can be seen that the controller manages efficiently to limit power to or at least close to nominal power and at the same time does only pitch when it is effective and necessary.

4 Fixed speed active stall wind turbine concept with AC connection – with grid support power controller

Today, the wind turbines on the market mix and match a variety of innovative concepts with proven technologies for both generators and power electronics (Hansen A.D., et al., 2004), (Blaabjerg F., et al., 2004), (Hansen A.D., 2005). The survival of these wind turbine technologies is strongly conditioned by their ability to support the grid, to handle faults on the grid and to comply with the stringent requirements of the utility companies (Slootweg JG, et al., 2001), (Gjengedal T., 2003). These wind turbine technologies have to support the grid, i.e. to participate actively in the control of the active and the reactive power on the grid.

During the last years, the market interest for the fixed speed active stall wind turbine concept has decreased slightly in favour of variable speed wind turbine concepts (Hansen A.D., 2005). One reason for that is that they do not contain advanced power-electronic components and their control is typically not designed to support the grid. However, they are still attractive due to their robustness, simplicity and low cost. The market interest for wind farms with active stall turbines may therefore increase if their grid support is improved.

A grid support power controller for active stall wind turbines has been developed and presented e.g. in (Hansen A.D., et al., 2006a) and (Hansen A.D., et al., 2006b). Such designed power controller has as task of enabling better grid integration characteristics for active stall wind turbines with AC connection. It has to be as fast as possible to power reference changes, but still with physical limits on pitch activity. The active stall wind turbine model, presented in this work, is intended to cover turbines like the ones in Nysted.

Figure 49 illustrates a typical example layout of the active stall wind turbine. The induction generator, softstarter, the capacitor bank for reactive power compensation and the step-up transformer are all placed in the nacelle, and thus the transformer is considered part of the wind turbine. The control of active and reactive power is based on measured power at the Main Switch Point MSP.

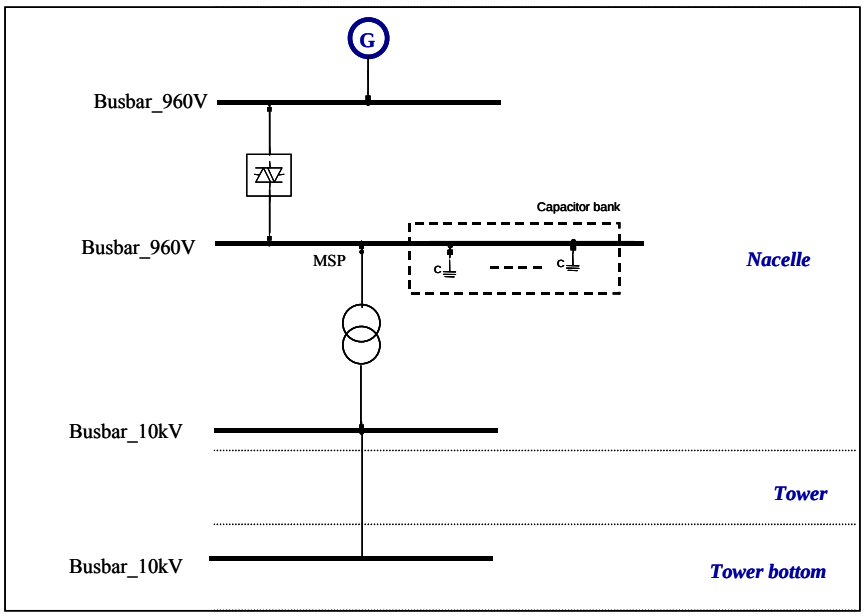

Figure 49: Active stall wind turbine layout including softstarter and capacitor bank.

4.1 Grid support active power controller

Wind turbine active power controller must be able to adjust the wind turbine production to the power reference demanded by the system operator. In case of normal operation conditions, the wind turbine has to produce maximum power. In power limitation operation mode, the wind turbine has to limit its production to the power reference received from a wind farm controller or directly from the system operator. The power reference required from the wind turbine can be equal to the rated power of the wind turbine or less than that. Figure 50 illustrates the power curve and Cp curves for a 2 MW active stall wind turbine for different imposed power setpoints.

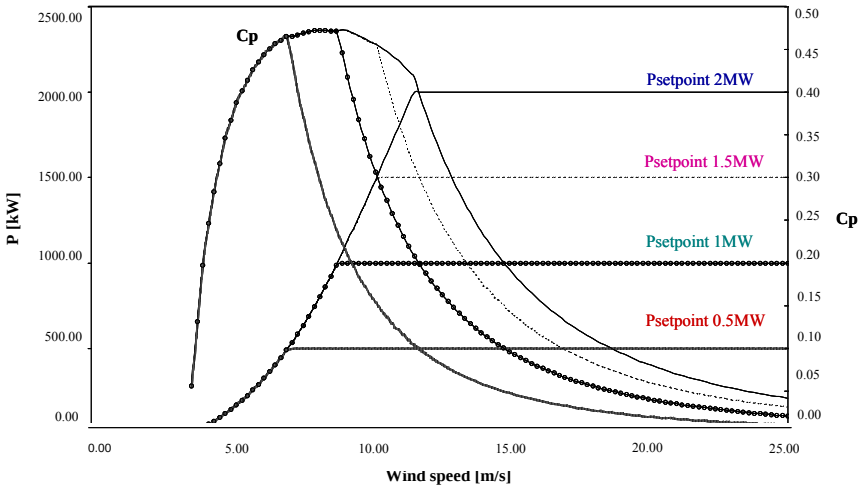

Figure 50: Power curve and Cp curve for different wind turbine power setpoints.

Notice that by imposing a power setpoint lower than the designed rated power of the wind turbine, the wind turbine range with high aerodynamic efficiency is, as expected, reduced, while the maximum aerodynamic efficiency is moving toward lower wind speeds.

In the previous chapter, i.e. Chapter 3, a traditional power controller has been presented and designed for a typical active stall wind turbine. This traditional controller is very slow because it tries to reduce the pitch activity as much as possible to limit the stress of the pitch system. Such a controller design is not optimal for grid support, since in this case the wind turbine or the wind farm is asked to act as a fast active element in the power system. To speed up the power control, a new active stall power controller is proposed and described in this chapter. To provide the best grid support, the aim is to use a simpler power controller, which enables fast control of the wind turbine power to different power setpoints imposed for example by system operator.

Figure 51 illustrates the new proposed power control scheme for an active stall wind turbine. A PI controller with antiwind-up ensures a correct active power production from the wind turbine both in power optimisation control and power limitation control modes. The input of the controller is the error signal between the measured active power at the Main Switch Point (MSP) (see Figure 49) and an imposed active power reference. The PI controller produces the pitch angle reference θ_{ref}, which is further compared to the actual pitch angle θ and then the error $\Delta\theta$ is corrected by the servomechanism. In order to get a realistic response in the pitch angle control system, the servomechanism model accounts for a servo time constant T_{servo} and the limitation of both the pitch angle and its gradient. The output of the actuator is the actual pitch angle of the blades.

The available power of the wind turbine can be monitored at each instant, based on the wind turbine's power curve and the filtered wind speed u_f, as illustrated in Figure 51. The wind speed is filtered appropriately to avoid unnecessary fluctuations.

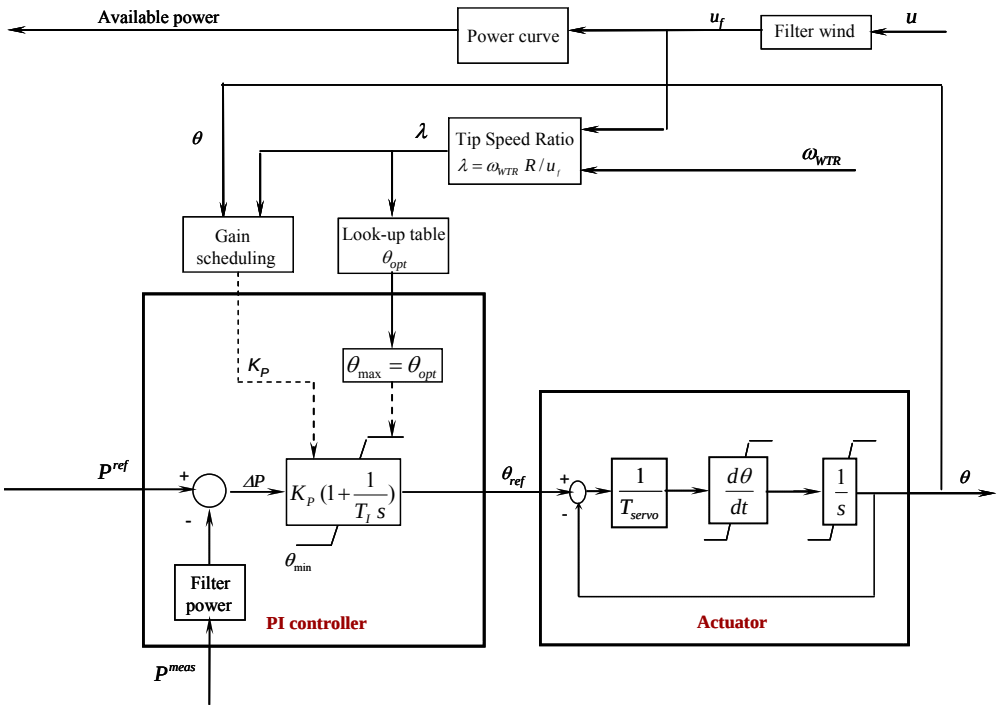

Figure 51: Grid support active power control scheme.

In the power optimisation control mode, the controller has to maximise the power production. In this case the difference between the measured power and its reference value is always positive and is integrated up until the pitch reference angle reaches the upper limit of the controller. The optimal pitch angle is thus given by the upper limitation of the controller. This upper limitation is calculated on-line based on an "optimal pitch" look-up table as a function of the estimated tip speed ratio $\lambda = \omega_{WTR} R / u_f$, where ω_{WTR} is the wind turbine rotor speed, R is the rotor radius and u_f is the filtered wind speed.

In the power limitation control mode the error signal ΔP of the controller is negative and therefore the pitch angle moves from the upper limitation and starts to actively drive the measured power to the power reference. Notice that the measured power used in the error signal is lowpass filtered in order to avoid the 3p fluctuations (three times the rotational frequency) in the power causing the pitch angle to fluctuate with the 3p frequency as well. This is because it is assumed that the pitch system is too slow to remove the 3p from the power, and thus the 3p fluctuations in the power would stress the system unnecessarily.

Compared with the controller presented in Chapter 3, the present controller contains an additional gain scheduling control of the pitch angle in order to compensate for the existing non-linear aerodynamic characteristics. The gain scheduling is necessary to ensure that the total gain of the system remains unchanged irrespective of the operational point of the wind turbine. The non-linear aerodynamic characteristics imply that the effect of pitching on the power varies depending on the operational point. The goal of the gain scheduling is therefore to change the proportional gain of the controller K_p in such a way that the total gain of the system remains unchanged irrespective of the operational point of the wind turbine. The pitch sensitivity, namely the effect of pitching, can be expressed mathematically by $\frac{dP}{d\theta}$. The total gain K_{system} of the system can be

then expressed as the proportional gain of the PI controller, K_P, times the pitch sensitivity of the system $\frac{dP}{d\theta}$, as follows:

$$K_{system} = K_P \left[\frac{dP}{d\theta}\right]^{-1} \frac{dP}{d\theta} = K_0 = const. \quad (44)$$

where K_0 is a dimensionless constant independent of the operation point.

The total gain of the system K_{system} is kept constant by changing K_P in such a way that it counteracts the variation of the pitch sensitivity $\frac{dP}{d\theta}$ by the reciprocal sensitivity function $\left[\frac{dP}{d\theta}\right]^{-1}$, hence:

$$K_P = K_0 \left[\frac{dP}{d\theta}\right]^{-1} \quad (45)$$

The pitch sensitivity $\frac{dP}{d\theta}$ of the system depends on the operational point of the wind turbine. The operation point of the wind turbine is characterised directly by the wind speed and the power setpoint and indirectly by the pitch angle and tip speed ratio. The implementation of the gain scheduling, namely the expression of the non-linear aerodynamic amplification in the system, is performed on-line based on the simulated pitch angle and tip speed ratio, according to:

$$\frac{dP}{d\theta} = \frac{1}{2} \rho \pi R^2 u_f^3 \frac{dC_p}{d\theta} \quad (46)$$

where u_f is the filtered wind speed and the power coefficient $C_p = C_p(\theta, \lambda)$ depends on the pitch angle θ and the tip speed ratio λ. Figure 52 illustrates the pitch sensitivity for different wind speeds and power setpoints.

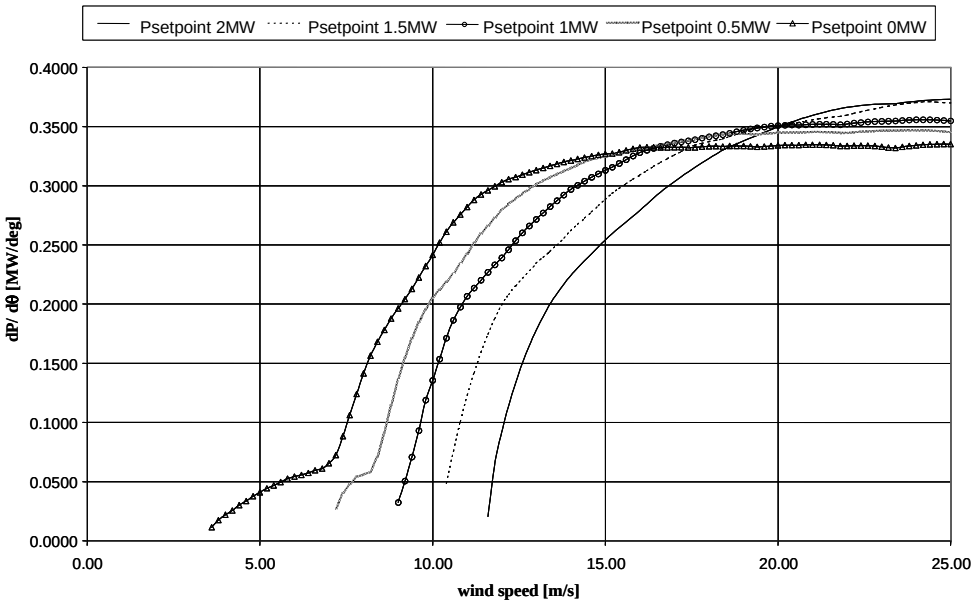

Figure 52: Pitch sensitivity function versus wind speed for different power setpoints.

Notice that the pitch sensitivity increases at higher wind speeds. This shows that the more sensitive the system is (larger pitch angles θ / higher wind speeds) the smaller the gain for the controller should be and vice versa. When the active power setpoint is decreased, the pitch sensitivity becomes significant also for lower wind speeds.

4.2 Grid support reactive power controller

Compared with the controller described in Chapter 3, the present wind turbine controller contains also an additional controller for the reactive power of the wind turbine. As illustrated in Figure 49, a capacitor bank is chosen to compensate for the reactive power absorbed by the induction generator or required by the grid operator. The reactive power consumption of an induction generator is a function of its loading and it increases as the active power increases. The power factor of the induction generator at rated load is usually in the range of 0.85-0.90, which means that the consumption of reactive power is typically about half of the active power generation. This aspect is taken into account in the design of the size of the capacitor bank. In order to be able to produce reactive power to the grid, the size of capacitor bank should thus be larger than the amount of reactive power consumed by the generator.

In the present implementation, a standard DIgSILENT SVC component is used to model the capacitor bank instead of a number of individual capacitors as used in earlier models (Sørensen P., et al, 2001a). The SVC component is a standard component in DIgSILENT and has the advantage of being an effective and easier way to simulate a capacitor bank consisting of several capacitor steps of the same size.

The standard SVC component is a combination of a shunt capacitor bank and a thyristor controlled reactance (TCR). The thyristor controlled reactance is usually used for a continuous control of reactive power. However, the compensation unit in wind turbines consists only of capacitors. Thus the TCR part of the standard SVC component is deactivated in the design of the present SVC control.

A discrete control of SVC is implemented using the dynamic simulation language DSL of DIgSILENT – see Figure 53. The capacitors in the capacitor bank can be switched on and off individually by the control system, depending on the load situation, in response to changes in the reactive power demand.

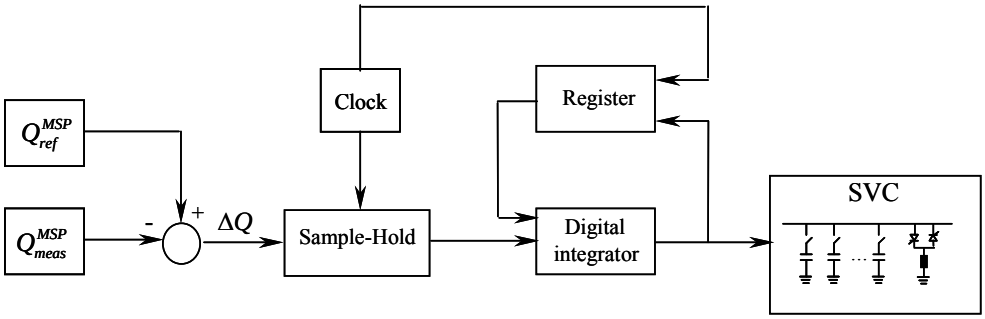

Figure 53: Designed SVC control for the active stall wind turbine.

The difference ΔQ between the measured reactive power Q_{meas}^{MSP} on the lowvoltage side of the step-up transformer at the Main Switch Point MSP (see Figure 49) and an imposed reference reactive power Q_{ref}^{MSP}, is used inside a sample-hold block. This block stores its sampled input signal at the output until the next rising edge of the clock signal appears. The clock supervises further-

more a register, which memorises the number of capacitors, which have been switched on at the previous clock period. For each clock period, based on the new updated and the old loading situation, a digital integrator determines the required number of capacitors.

The control system of SVC has to solve a dilemma: it must be able to switch the capacitors fast in order to be able to support the grid but on the other hand it should not attempt to control the 3p fluctuations in the reactive power consumption of the induction generator due to the wind fluctuations. The traditional wind turbines with directly connected induction generators are equipped with standard capacitor banks using mechanical contactors, which are typically controlled in intervals of 1-10 minutes. This control is not fast enough in the case when the turbine has to support the grid. However, if the capacitors are switched more often using mechanical contactors, the transients due to the switchings will reduce the lifetime of the capacitors and contactors too much. To provide a faster control possibility, new wind turbines are using thyristor switches instead of mechanical contactors, which can reduce the switching transients significantly and thus make it possible to switch the capacitor much more often without reducing the lifetime significantly.

As an example, the active stall controlled Bonus wind turbines in Nysted offshore wind farm in Denmark are equipped with such a dynamic phase compensation unit, using thyristor switches. Another similar dynamic phase compensation unit was tested on a wind turbine by Sørensen et.al. (Sørensen P, et al., 2004). This test concluded that the dynamic phase compensation technology should not be used to remove the 3p fluctuations in reactive power, because the transients caused by the many capacitor switchings appeared to cause more flicker than could be removed by dynamically compensating the 3p reactive power fluctuations.

The control system of the capacitor bank has thus to switch the capacitors fast in order to be able to support the grid, but on the other hand it should not attempt to control the 3p fluctuations in the reactive power consumption of the induction generator.

In the present work, the fast switching of the capacitors is ensured by the clock time 20 ms, while the insensitivity to 3p fluctuations in the wind speed is realised by implementing a hysteresis in the digital integrator. The output of the digital integrator is sent directly to the SVC component and thus the required number of capacitors is switched on or off. The hysteresis has been used instead for a lowpass filter in order to keep a very fast response to large changes in the reactive power reference. This is regarded as important for the ability of the wind turbines to support with voltage control.

4.3 Simulations

Different scenarios are simulated to illustrate the performance of the new developed grid support power controller for the active stall wind turbine. The controller's performance is assessed and discussed by means of normal operation simulations of a 2 MW active stall wind turbine.

Figure 54, Figure 55 and Figure 56 present simulation results of the proposed power control strategy of the active stall wind turbine, shown in Figure 51 and Figure 53, respectively. The active stall wind turbine is simulated at an average wind speed of 11 m/s and a turbulence intensity of 20%. This operational point for the wind turbine corresponds to a transition operational regime for the wind turbine, between power optimization and power limitation regime, where the 3p fluctuation (three times the rotational frequency) is strong.

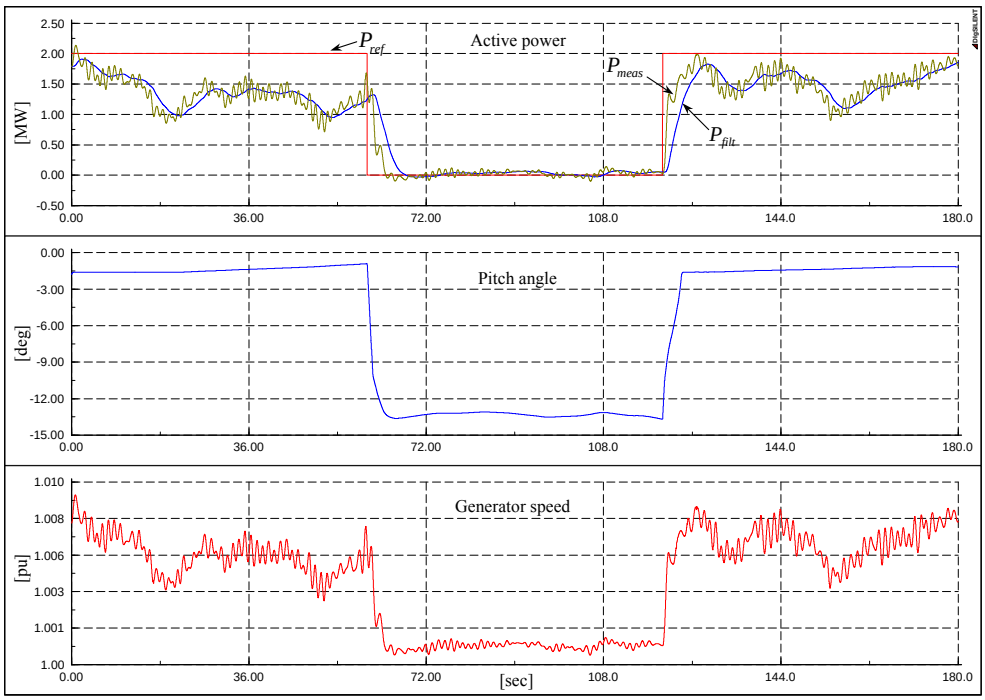

Figure 54: Power reference response of an active stall controlled wind turbine.

Figure 54 shows the reference power P_{ref}, the measured power P_{meas} at the MSP and the filtered measured power P_{filt} used in the controller, together with the pitch angle and generator speed, respectively. As expected for an active stall wind turbine, the 3p fluctuation is present in the measured electrical power P_{meas}. In order to illustrate the performance of the active stall wind turbine controller, the following sequence is assumed. The first 60 sec, the power reference is set to the rated power (i.e. 2 MW). The power reference is then stepped down to 0 MW and after 120 sec it is stepped back again to 2 MW.

In the first and last 60 sec of the simulation, by setting the power reference equal to the rated power for a wind speed less than the rated wind, the wind turbine has to produce maximum possible power. In this case the pitch angle is set by the upper limit of the controller given by the "optimal pitch" look-up table – see Figure 51. The wind turbine is then ordered to work in the power limitation mode when the power reference is set to 0 MW. In this control mode, the turbine has to produce less than it is capable of and therefore the power controller starts to actively drive the measured power to the power reference. The controller has been tuned so that the pitch angle changes smoothly from one steady state operational point to another without any overshoot. A reduction of the power production implies a more negative pitch angle and a smaller generator speed (slip). The demand of producing 0 MW is achieved while the wind turbine operates close to the border between generator and motor modes.

Figure 55 gives a more detailed view on the power and the pitch angle in the moment when the power reference is stepped down to 0 MW. The new power reference is reached in 4-5 seconds. The change in the pitch angle is limited by the pitch rate limiter ± 8 deg/s, which exists in the actuator.

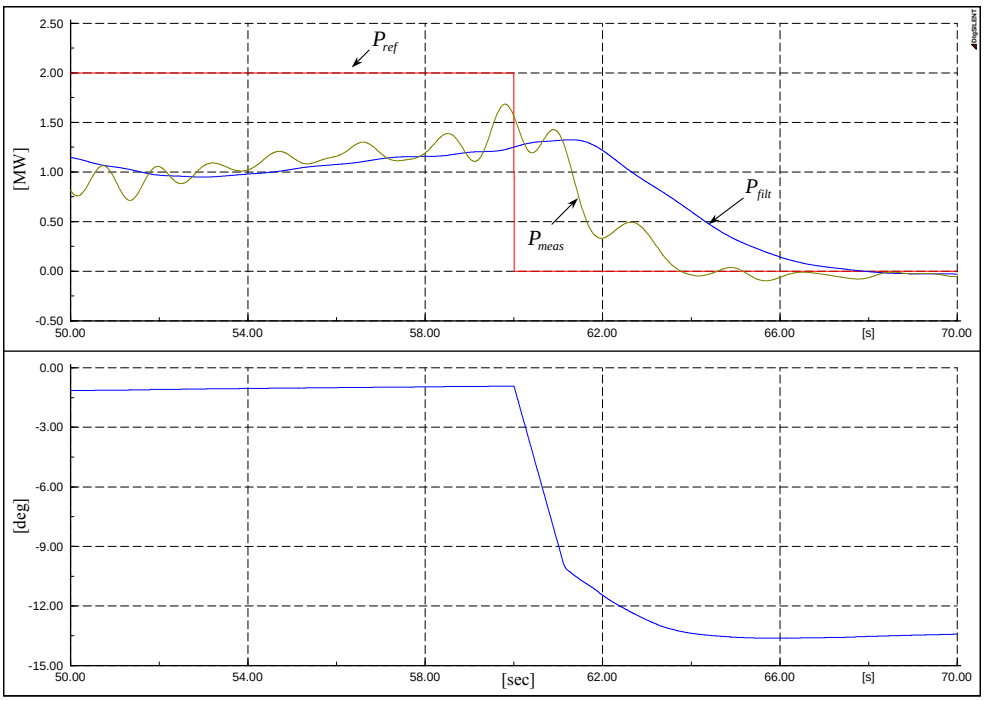

Figure 55: Detailed view of the power reference responses illustrated in Figure 54.

Figure 56 illustrates the simulation results for the reactive power control, sketched in Figure 53. The simulation case is the same as shown in Figure 54. The reactive power at the MSP is controlled to zero by switching on or off a certain number of capacitors. In the present simulation a capacitor bank consisting of 12 steps with 0.1 MVar is used. A clock with 20 ms sampling period ensures a necessary fast switch of the capacitors. With this fast sampling period, as seen in Figure 56, the reactive power is changed immediately by capacitor switchings as soon as the reactive power exceeds the hysteresis interval ±150 kVar. Figure 56 also shows the number of capacitors switched during the simulation. Notice that, as expected, a step down in the active power reference implies a reduction of the reactive power demand and, as a result, the number of connected capacitors is decreased.

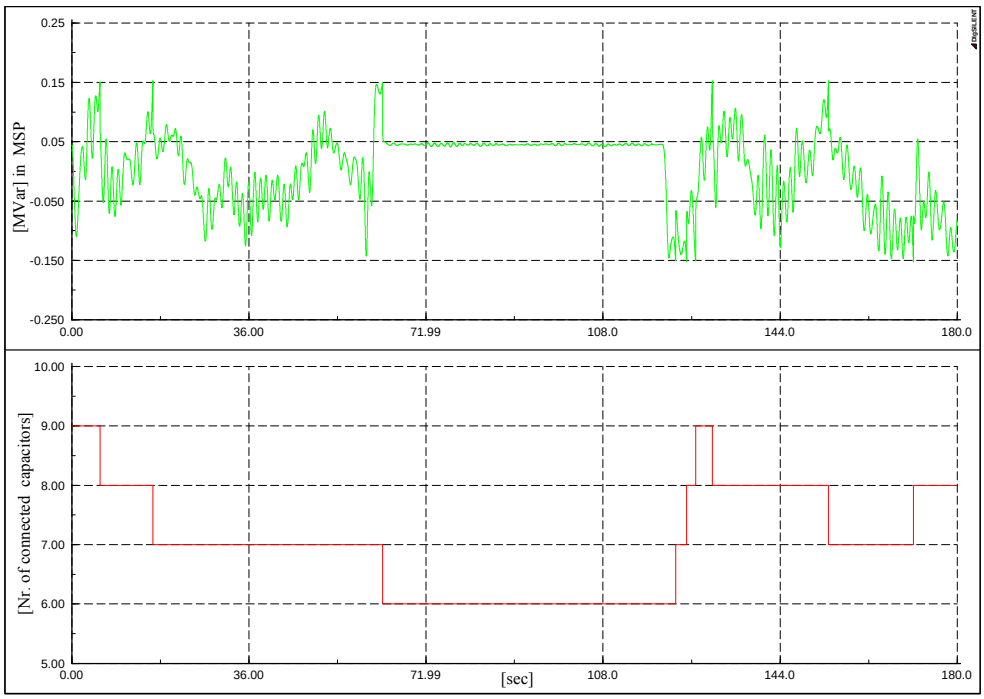

Figure 56: Reactive power control for the active stall controlled wind turbine.

5 Fixed speed active stall wind turbine concept with HVDC/VSC connection

The HVDC transmission system with Voltage Source Converter (VSC) has been developed as an alternative to the classical HVDC system due to some specific attributes such as: independent control of reactive and active power, continuous voltage and frequency regulation, black-start capability, etc (Schettler F. et al., 2000), (Bahrman M.P.et al., 2003).

Currently two main concepts exist for such a transmission system. The first concept is the HVDC Plus developed by Siemens, which use two single 6-pulse converters to form a 12-pulse bipolar group as shown in Figure 57.

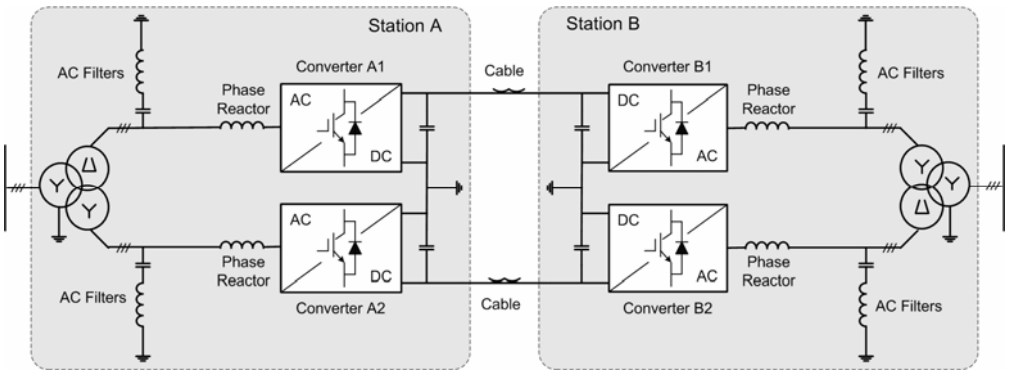

Figure 57: Main circuit diagram of a bipolar HVDC Plus transmission system.

This system is available for power ratings up to 200 MW for one bipolar unit with DC voltages up to ± 150 kV (Schettler F. et al., 2000). The second concept developed by ABB is the HVDC Light based on a 6-pulse bipolar VSC with ratings up to 330 MW/± 150 kV DC for one bipolar unit (Bahrman M.P.et al., 2003), as shown in Figure 58.

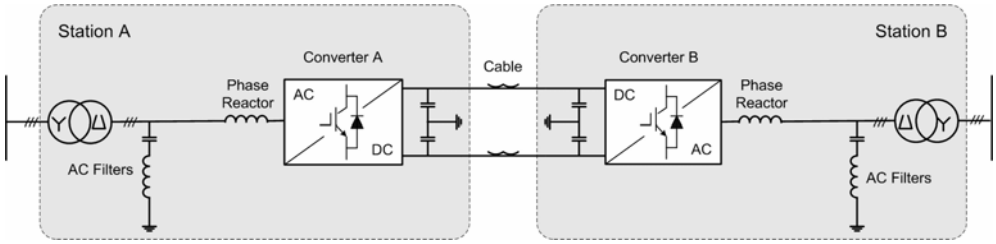

Figure 58: Circuit diagram for the HVDC Light transmission system.

Both concepts have a four-quadrant operation in the P-Q plane and decoupled control for active and reactive power. This means that each converter can operate as rectifier or inverter at variable frequency and to absorb or deliver reactive power to the AC grid.

In 1998, Eltra decided to investigate the HVDC Light technology for DC connection of wind power to transmission grid. An HVDC Light transmission system was realized on the existing wind farm at Tjæreborg (Skytt A.K. et al., 2001), (Søbrink K.H. et al., 1999).

The schematic of the Tjæreborg system including some basic data is shown in Figure 59.

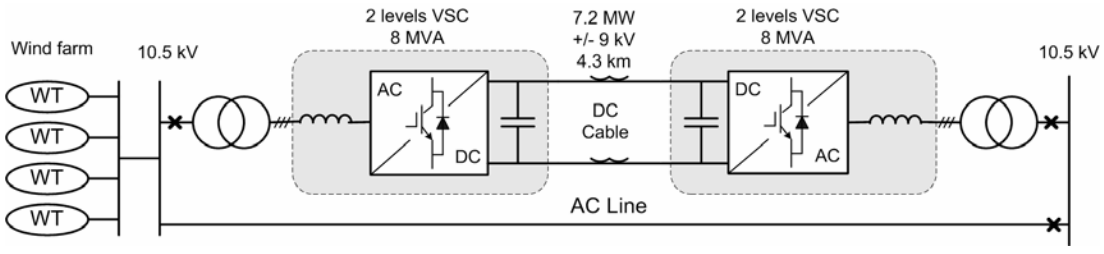

Figure 59: Schematic of the Tjæreborg transmission system.

The Tjæreborg wind farm consists of 4 different type of wind turbine with different nominal powers. Two of these turbines are pitch regulated (type B and type C) while the other two are stall controlled (type A). The rated power of the wind farm is 6.5 MW (Søbrink K.H. et al., 1999), while the HVDC system is 8 MVA rated.

The DC transmission system is in parallel with an AC line and it has a length of 4.3 km. The voltage and frequency in the wind farm can be varied continuously and independently of the transmission grid (Skytt A.K. et al., 2001), (Søbrink K.H. et al., 1999) using this DC link. In isolated operation the frequency can vary between 30 and 65 Hz (Skytt A.K. et al., 2001).

According to (Skytt A.K. et al., 2001) the control concept was implemented and tested in EMTDC program under different conditions and it has been found a "fairly good agreement between simulation and commissioning tests". However, the frequency control of the wind farm was an exception. In simulation the dynamic frequency control worked fine (Skytt A.K. et al., 2001). During the commissioning test the frequency was varied between 47 and 51 Hz. Outside this range the wind turbines are tripped by their protections (Skytt A.K. et al., 2001). In (Skytt A.K. et al., 2001) is mentioned that a reason for different result in simulation compared with the commissioning tests might be the difficulties in simulating correctly the dynamics of the wind farm. Also the following remark should be noticed "with a stiff voltage concept the interaction between the HVDC Light and the windmills is much more robust and simple".

The control schemes for the DC transmission system developed in DIgSILENT during this project take into account all the above-mentioned aspects. In the following paragraphs these schemes are presented in detail.

5.1 Control for Station A (sending end station)

The main target here was to implement a control scheme, which must have available the voltage and frequency set points for the MicroGrid Controller. Therefore, the magnitude of the PWM index and the frequency (Pm_in, f0) are used as control variables for the PMW converter model. Since each wind turbine can have different values for the wind speed in a given moment and therefore different operation points a droop control for both voltage and frequency has been adopted as shown in Figure 60.

Each wind turbine will deliver active power and will absorb reactive power according with the wind speed variations. Therefore the voltage stability is dependent on the demand for reactive power (Lasseter R. H., 2002). The voltage control loop should insure that the reactive currents, which circulate inside the wind farm, are not large. A small error in the voltage reference can generate very large reactive currents. A droop characteristic for the voltage controller will minimize the stationary error in this case. Since the induction generator will always draw reactive power from the PWM converter, the reference for voltage should be increased when the generator demand for reactive power increase as shown in Figure 61.

The voltage reference value is calculated using:

$$V^{ref} = V^{stp} + k_v Q^{meas} \tag{47}$$

where: k_v is the voltage droop coefficient.

An inner current control loop will assure a relatively fast tracking of the actual current.

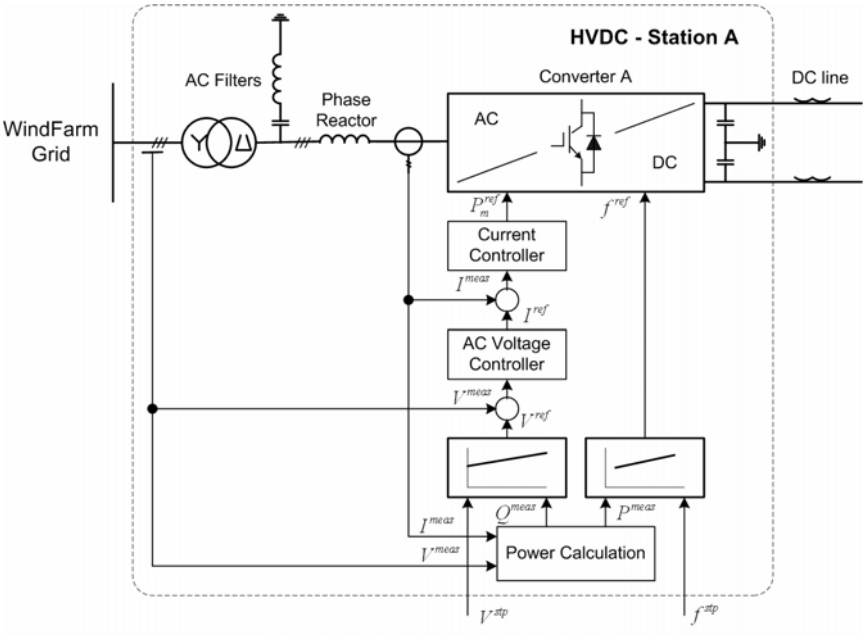

Figure 60: Structure of the control for sending end station (wind farm side).

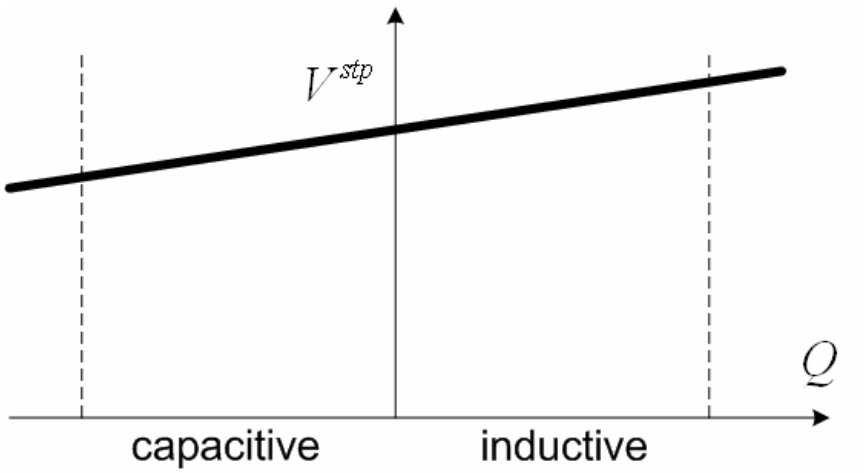

Figure 61: Voltage set point with droop characteristic.

In order to follow and to transfer the entire available power from the wind farm a frequency droop characteristic is used. The set point frequency is varied as a function of the produced power as shown in Figure 62.

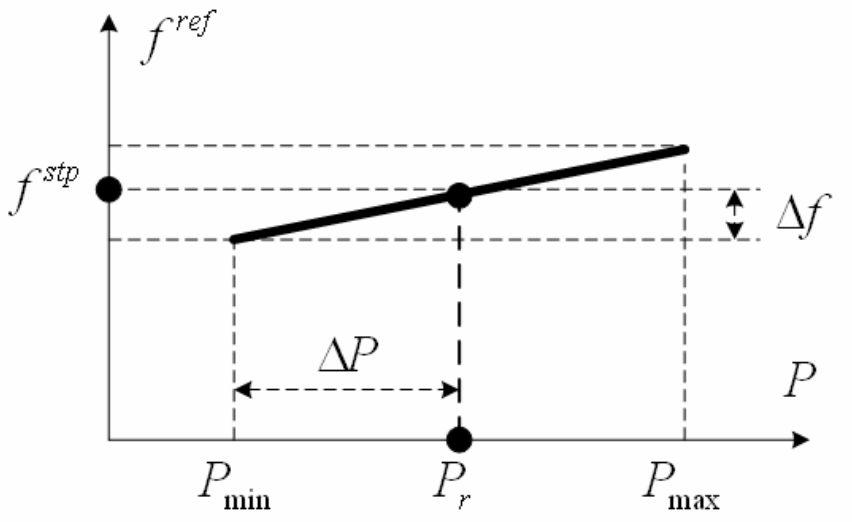

Figure 62: Frequency set point with droop characteristic.

The reference for frequency is given in per unit as:

$$f^{ref} = 1 - k_f(1 - P^{meas}) \quad (48)$$

where: k_f is the droop coefficient for frequency, $k_f = \frac{\Delta f}{\Delta P}$.

5.2 Control for Station B (receiving end station)

Usually in grid-connected applications the PWM converter from the grid side must control the DC-link voltage and the reactive power. Therefore for the receiving end station of the considered DC transmission system such a control scheme is implemented in DIgSILENT.

Several DC-link voltage control schemes exist depending on the application (Karlsson P., 2002). There are two topologies commonly used namely master/slave and droop control. The master/slave control is used for parallel operation of converters. The active load sharing is performed and the master controller distributes references for power to other converters (slave). Since this control requires communications between converters the bandwidth of the DC link voltage control can be increased if the communication bandwidth is relatively high (Karlsson P., 2002). In this way less energy needs to be stored in the DC bus and therefore the DC capacitance can be decreased. In (Karlsson P., 2002) is mentioned that the system become sensitive to interactions between the two sides when the energy storage is reduced.

In the droop control each converter delivers power to the DC bus determined by the actual DC bus voltage error at the converter (Karlsson P., 2002). This control method does not require communication between converters.

Since the PWM converter can be seen as a controlled voltage source the equivalent diagram of the receiving end station is as shown in Figure 63.

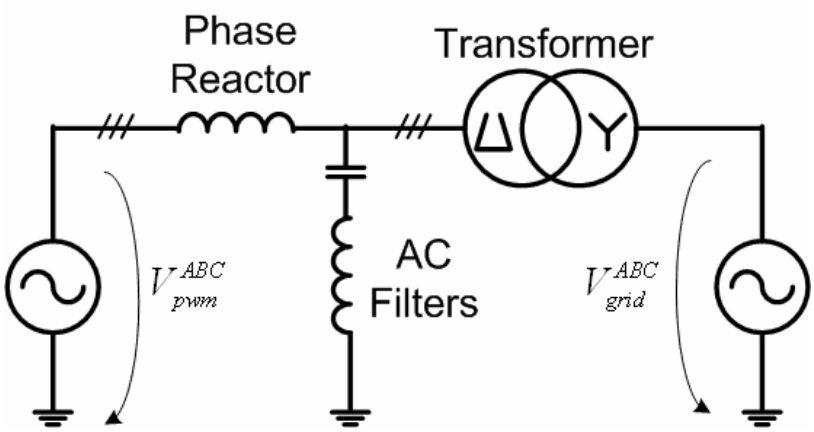

Figure 63: Equivalent diagram of the receiving end station.

As the station operates around 50 Hz grid frequency all the time the influence of the capacitors can be neglected. Therefore, the equivalent diagram of the station can be reduced as shown in Figure 64.

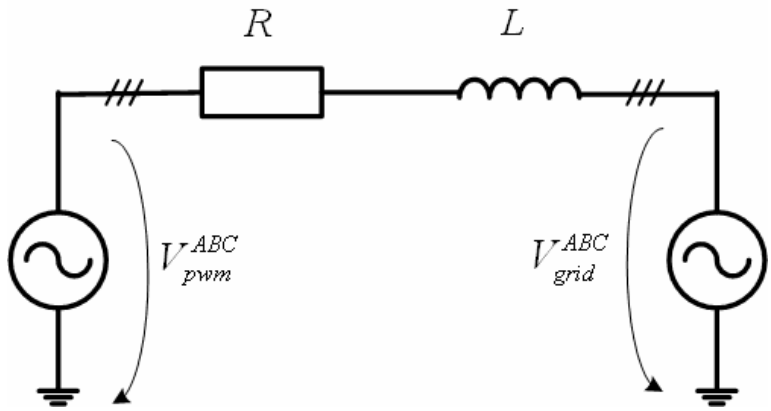

Figure 64: Simplified diagram of the receiving end station neglecting the AC filters.

The voltage equations can be written as:

$$v_{grid}^{ABC} = R \cdot i^{ABC} + L\frac{di^{ABC}}{dt} + v_{pwm}^{ABC} \tag{49}$$

Assuming that the voltage system is symmetrical and balanced the zero component can be neglected in stationary reference frame. Therefore the previous equation can be written as:

$$v_{grid}^{\alpha\beta} = R \cdot i^{\alpha\beta} + L\frac{di^{\alpha\beta}}{dt} + v_{pwm}^{\alpha\beta} \tag{50}$$

Further in synchronous reference frame it is assumed that its derivate can be neglected $\frac{d\omega_{grid}}{dt} = 0$ and therefore the previous equation can be written in matrix form as:

$$\begin{bmatrix} v_{grid}^{d} \\ v_{grid}^{q} \end{bmatrix} = L\frac{d}{dt}\begin{bmatrix} i^{d} \\ i^{q} \end{bmatrix} + \begin{bmatrix} 0 & -\omega_{grid} \cdot L \\ \omega_{grid} \cdot L & 0 \end{bmatrix} \cdot \begin{bmatrix} i^{d} \\ i^{q} \end{bmatrix} + \begin{bmatrix} v_{pwm}^{d} \\ v_{pwm}^{q} \end{bmatrix} \tag{51}$$

It can be observed that there is a cross coupling between axes with the term $\omega_{grid} L$. A change of the current e.g. in d-axis results in a change of the q-axis

current. Therefore, this cross coupling should be taken compensated in the control scheme.

In this project a droop control of the DC-link voltage is implemented for the receiving end station as shown in Figure 65. The entire control scheme is build in dq-system, therefore a PLL is used to calculate the angle for transformations between axes. The actual power from the DC-link is calculated based on the measured voltage and power. Another measurement block in the connection point delivers the signals for reactive power calculation.

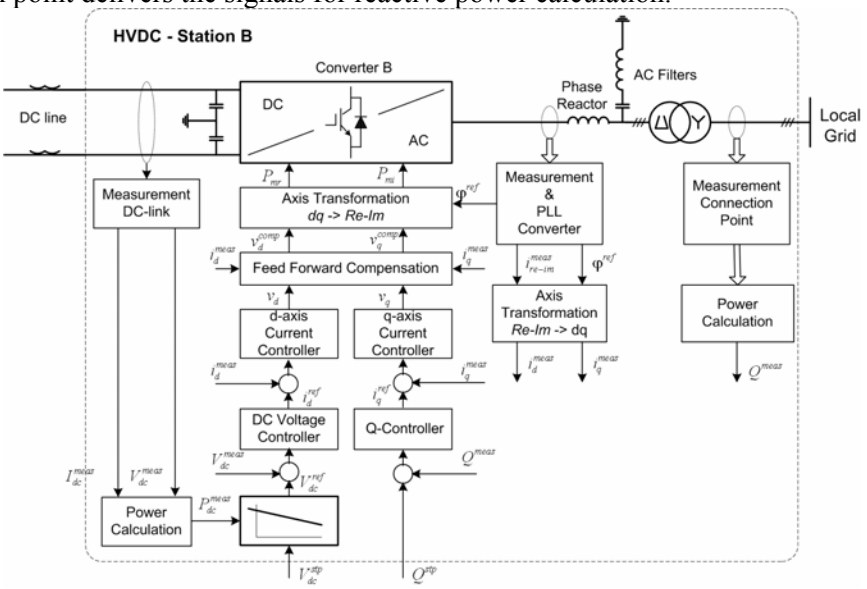

Figure 65: Control structure of the receiving end station (grid side).

The DC-link voltage set point is calculated using the actual active power from the DC-link and the droop characteristic. A 5% variation in DC-link voltage is allowed. The error signal between set point and the measured value fed the PI controller. One of the advantages of using the PI controller is the error restoration in droop control (Karlsson P., 2002). The output from DC-link voltage controller is the reference for current in d-axis. The error between the reactive power set point and the actual value is applied to a PI controller, which gives the reference for the q-axis current.

The control scheme comprises also an inner current control loop for both axis and a feed-forward compensation of the voltage references (modulation index in d and q axis). The feed-forward compensation requires the exact value of the total reactance connected between PWM converter and the connection point in the grid. This reactance is the sum of the phase reactor and transformer reactances.

The transformer reactance has been calculated based on:

$$Z_T = \frac{\Delta u_k \cdot U_n^2}{100 \cdot S_n}$$
$$R_T = \frac{\Delta P_{Cu} \cdot U_n^2}{1000 \cdot S_n} \qquad (52)$$

where:

- Δu_k - short circuit voltage [%];
- U_n - rated voltage [kV];

- S_n - rated apparent power [MVA];
- ΔP_{Cu} - copper losses [kW].

Without the feed-forward compensation the reactive power cannot be controlled accurate.

The reactive power set point is given so that the reactive power on the connection point is kept at zero. However, other values for this set point can be imposed according with the System Operator or MicroGrid Controller.

5.3 System overview

The structure of the system implemented in the power system simulation tool DIgSILENT is presented in Figure 66.

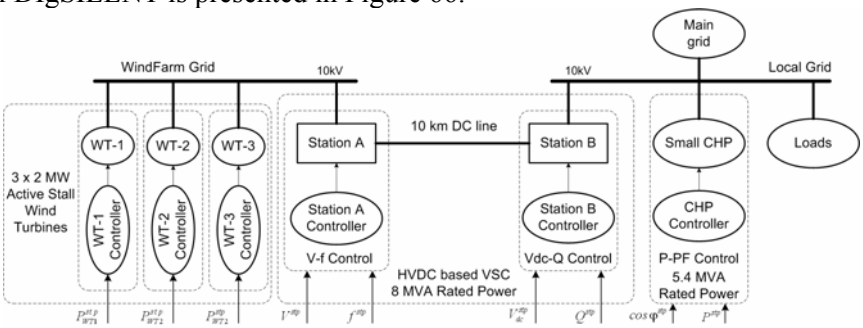

Figure 66: Structure of the system implemented in DIgSILENT.

The simulation scheme comprises an active stall wind farm, a DC transmission system, a small CHP and some loads.

Three active stall wind turbines models the wind farm, each turbine being equipped with a 2 MW squirrel-cage induction generator. The power set point from the wind turbine control is available.

The DC transmission system is based on IGBT-Voltage Source Converters. There are two stations, on the wind farm side (Station-A) and on the local grid side (Station-B) respectively. A 10 km DC cable (± 9kV) connect these two stations. The rated power of the transmission system is 8MVA.

The wind farm and the Station-A are connected at a 10 kV wind farm grid while the Station-B, a small CHP with 5.4 MVA rated power and some loads (8 MVA rated power) forms a local grid. A connection with the main grid, which is relatively stiff, (5000 MW short circuit power) is also present.

The wind farm grid has some particular characteristics as:

The wind farm delivers variable active power and draw reactive power according with the operational point of each wind turbine.

The voltage and frequency can vary in some limits. A variable frequency in this case will allow a better wind power conversion especially in the case of low wind speeds.

The voltage stability is dependent on the wind farm demand for reactive power

On the other hand the local grid has the following characteristics:

- CHP is non-despatchable , which means that the active power delivered depends on the heat demand. The reactive power produced has a fixed value. Usually, a power factor of 0.8 or 1 is used in operation.
- The voltage and frequency are controlled via the main grid. The Station B should control the voltage and frequency when this connection is not available.

In fact all these characteristics make this system to be a MicroGrid (Lasseter R. H., 2002). From the utility point of view the system should act as a single controlled cell of the power system. On the other hand from the customer point of view the system should meet some specific needs such as voltage and frequency support, island operation when the connection with the main grid is not available, etc.

A MicroGrid/Wind Farm Controller should perform the overall control for each component from this system based on the System Operator requests or based on the demand of the local loads during island operation.

5.4 Simulation results

5.4.1 Case A

There are several events in the system in this case as:

- The average wind speed is increase from 11 m/sec to 16 m/sec in the time interval 60 – 120 sec so that the wind turbines will pass through all three operating modes of the active stall controller;
- A 100% increase in the load occurs at time 50 sec. The load is 2.5 MW rated power.
- The CHP operates first at 0.7 p.u. turbine power and a power factor of 0.8. The power set point of the turbine is increased to 1 p.u. at time 300 sec.

The reactive power set point for Station B is kept to zero.

The frequency droop coefficient k_f in Station A (sending end station) is zero. Therefore a fixed reference for frequency (50 Hz) is used.

The wind time series for each wind turbine as well as the pitch angles are shown in Figure 67.

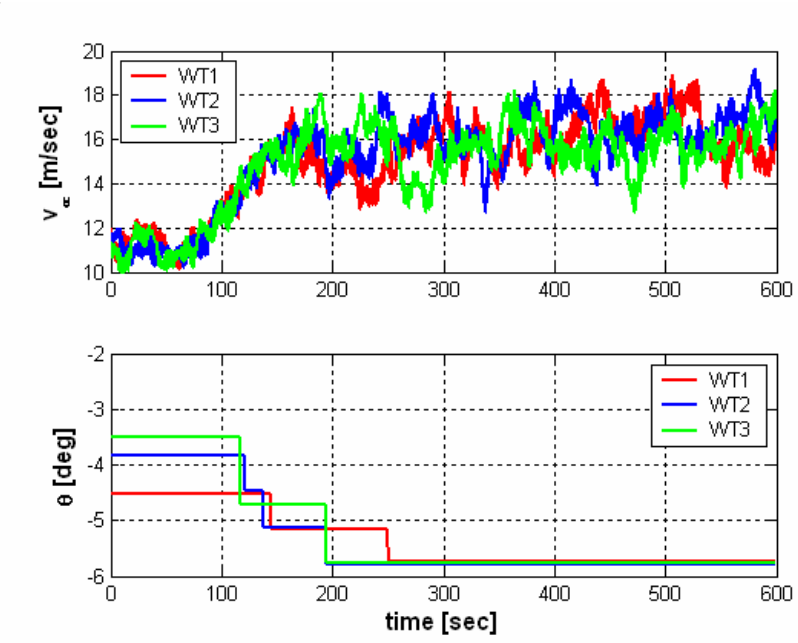

Figure 67: Wind time series and pitch angles for each wind turbine.

As the wind speed and the produced power are greater than the rated values the active stall controller take actions. In order to limit the output power the pitch angle is increase. An overpower of 300 kW is allowed. The active and reactive powers for each wind turbine are shown in Figure 68.

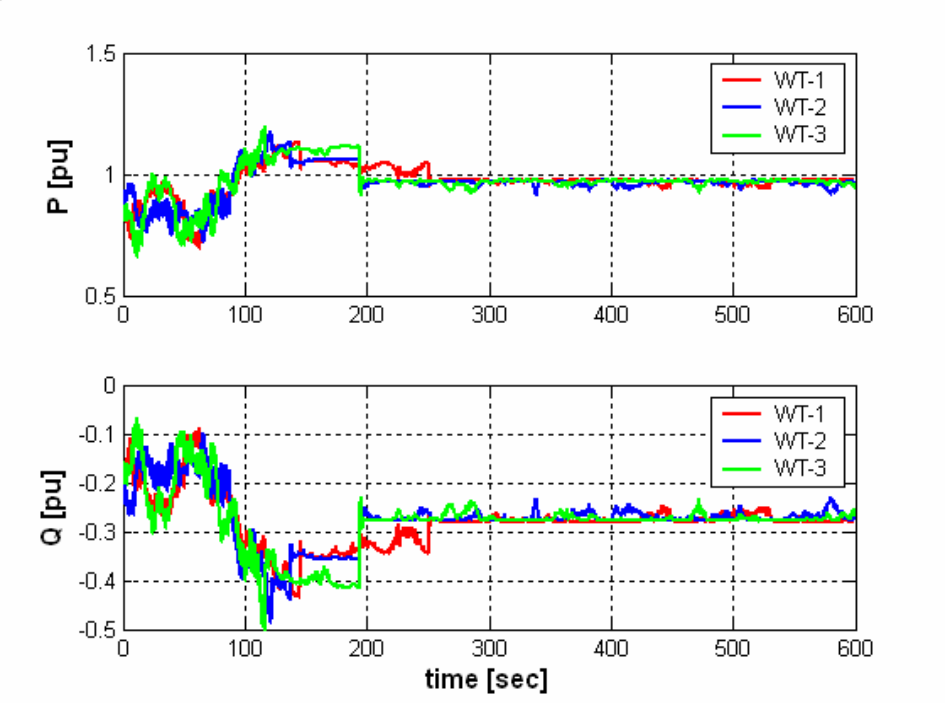

Figure 68: Active and reactive power for each wind turbine.

The power balance in the connection point is shown in Figure 69.

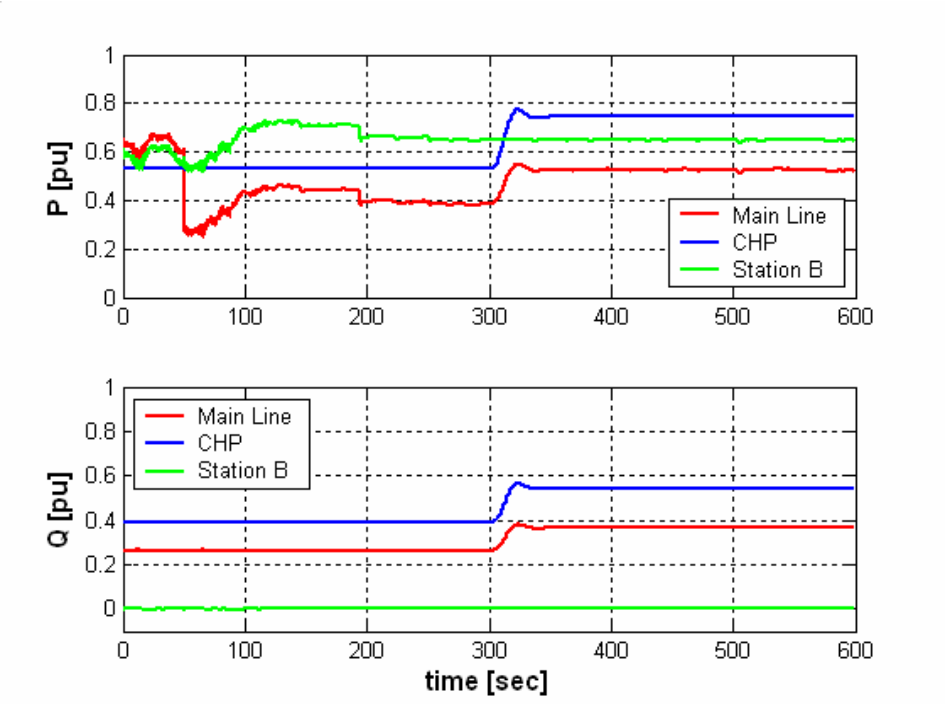

Figure 69: Power balance in the connection point.

It can be observed that the receiving end station operates at zero reactive power.

The voltage and frequency profile for each Station are shown in Figure 70.

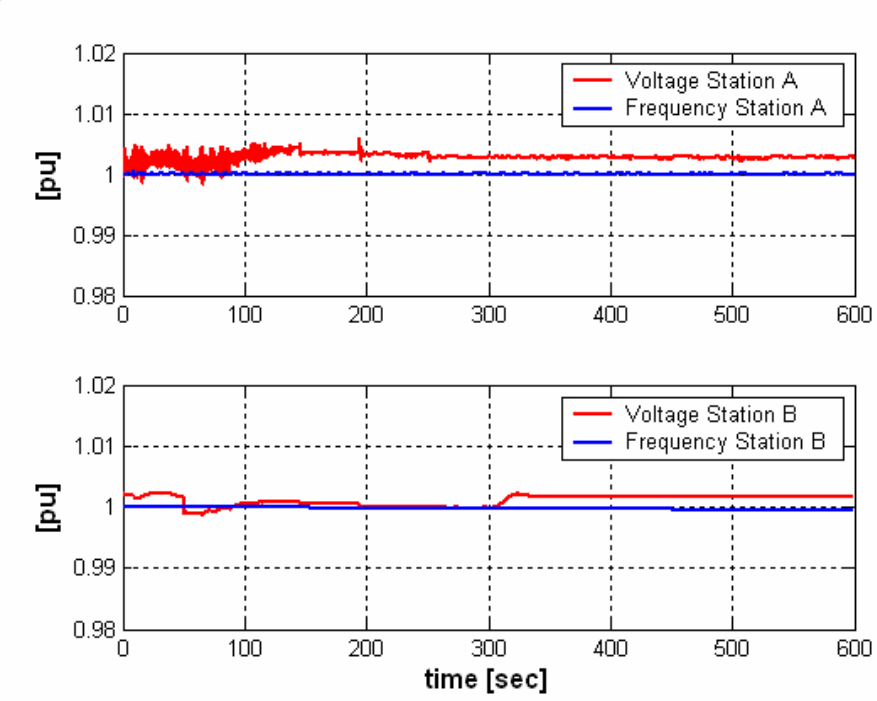

Figure 70: Voltage and frequency for both terminals of the DC transmission system.

The DC-link voltage is shown in Figure 71. There is an overshot of 1.5% for the DC-link voltage when the wind farm starts to deliver the rated power. Since the control scheme allows a 5% variation in the DC-link voltage, this result shows that the DC-link voltage control works properly.

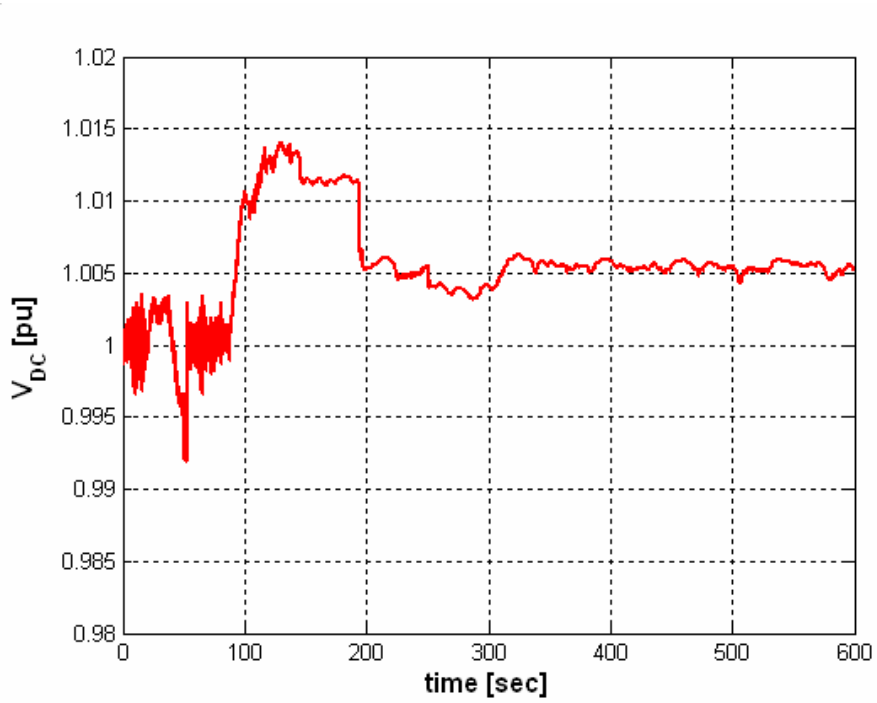

Figure 71: DC-link voltage.

Finally, the output of the CHP in terms of power and power factor is shown in Figure 72.

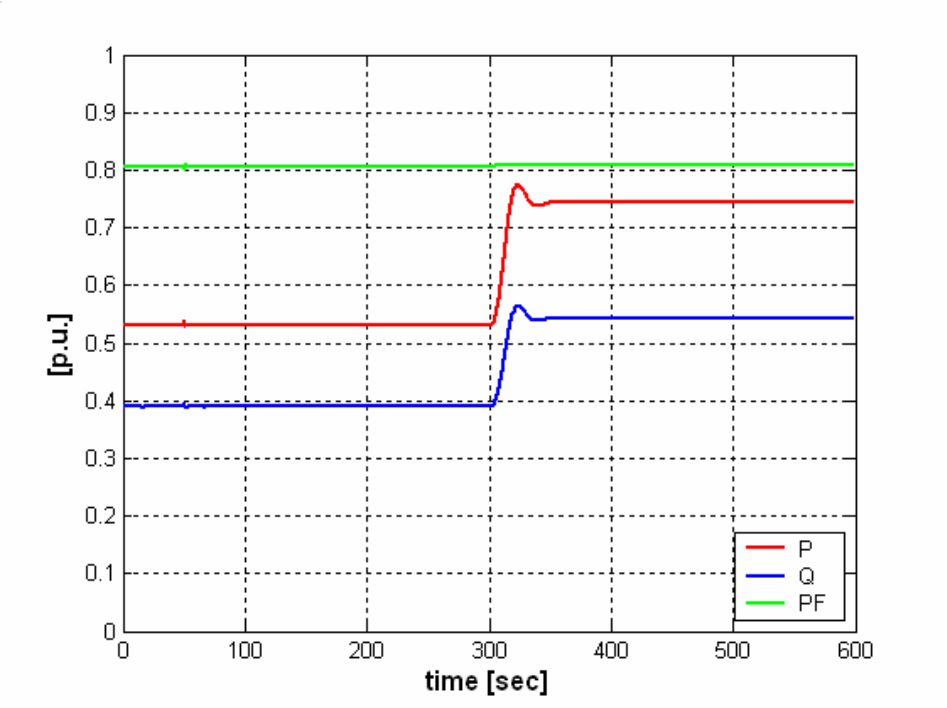

Figure 72: The output of the CHP.

Even if the power set point of the turbine varies, it can be observed that the CHP operates at constant power factor. The output power factor of the plant is not exactly 0.8 because of the parameters for the excitation system and the rated voltage of the generator. The rated voltage of the generator is 11.5 kV whilst the bus bar voltage of the local grid in Dig Silent is 10.5 kV. Changing the bus bar voltage or using another generator will correct this problem.

5.4.2 Case B

In this case the frequency droop coefficient for Station A (sending end station) is 0.02 that correspond with ca. 50.2 Hz for the maximum output power of the wind farm. The frequency at the wind farm bus bar will vary according with the produced active power.

The wind time series for each wind turbine as well as the pitch angles are shown in Figure 73.

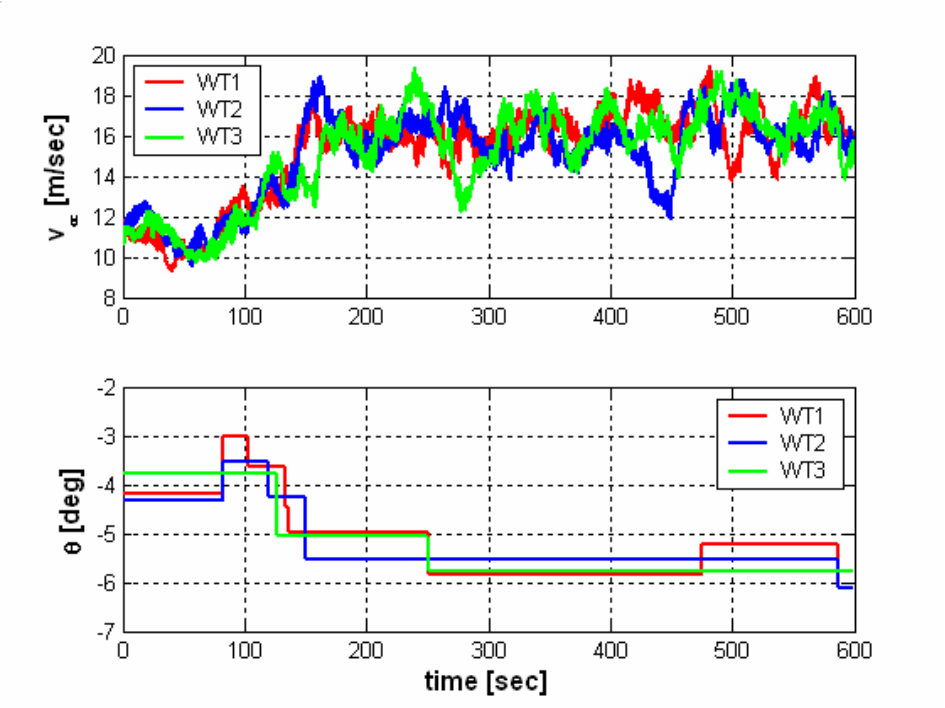

Figure 73: Wind time series and pitch angles for each wind turbine.

The active and reactive power for each wind turbine, as well as the power balance in the connection point are shown in Figure 74 and Figure 75.

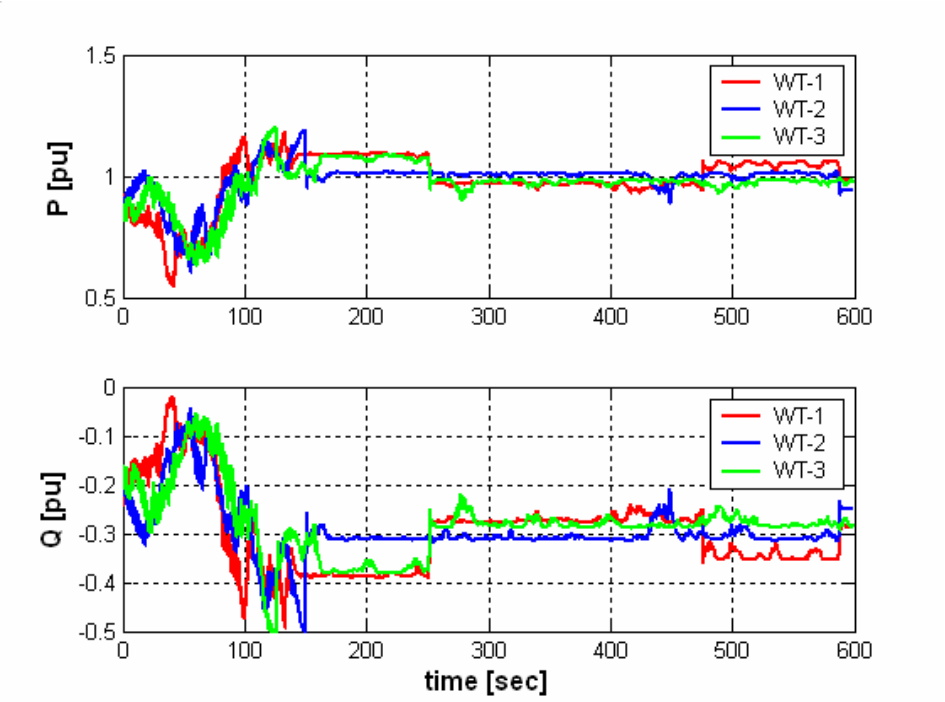

Figure 74: Active and reactive power for wind farm.

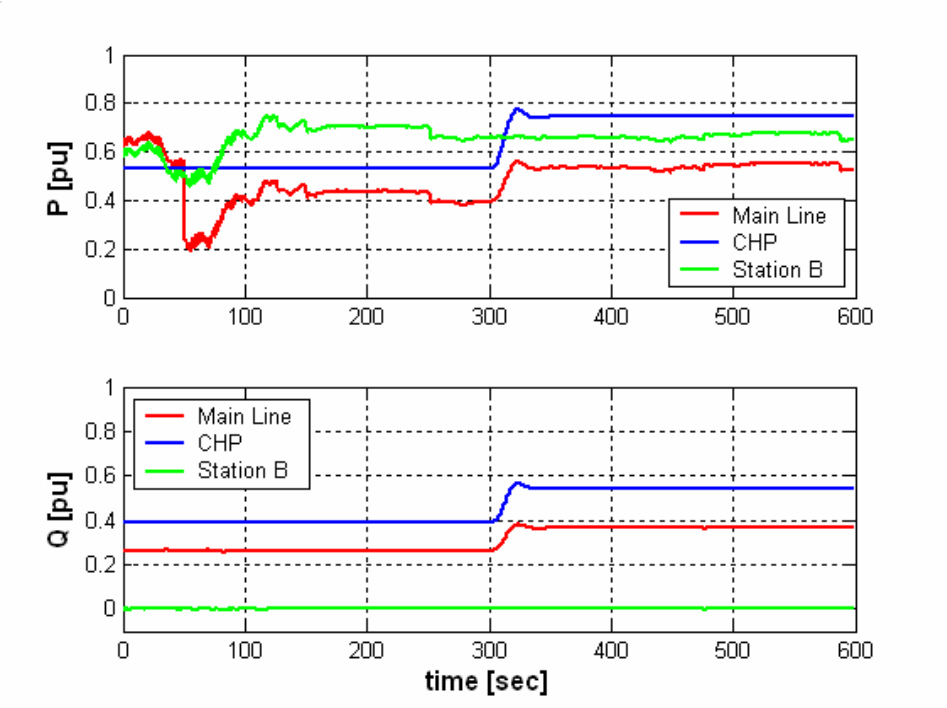

Figure 75: Active and reactive power in the connection point.

The voltage and frequency profile for each Station are shown in Figure 76.

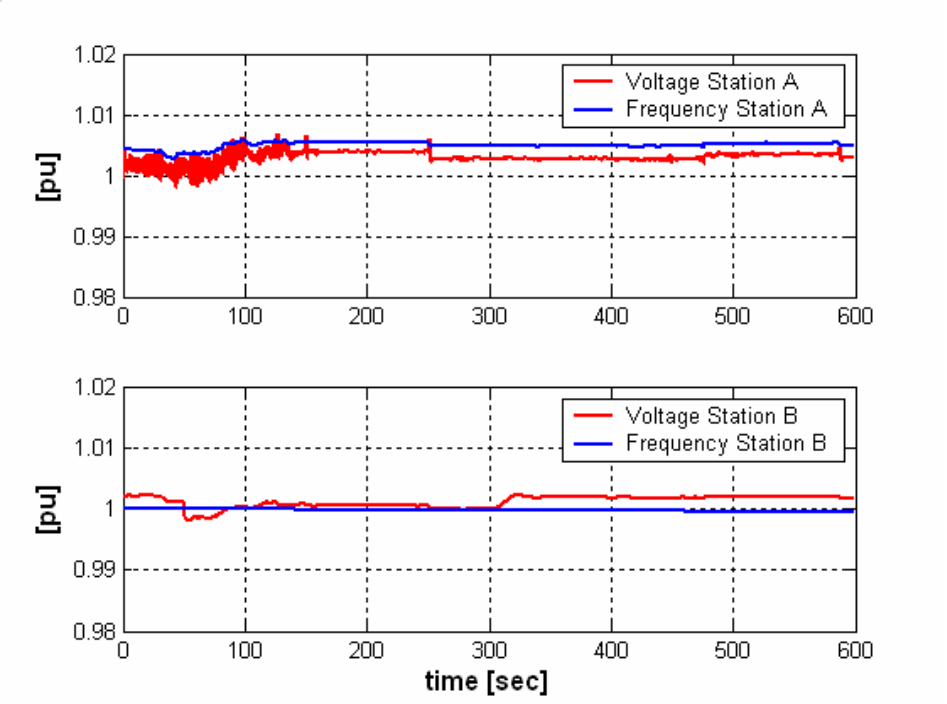

Figure 76: Voltage and frequency for DC transmission system.

It can be observed that the deviations from the rated values for both frequency and voltage are less than 0.5%

The DC link voltage is shown in Figure 77.

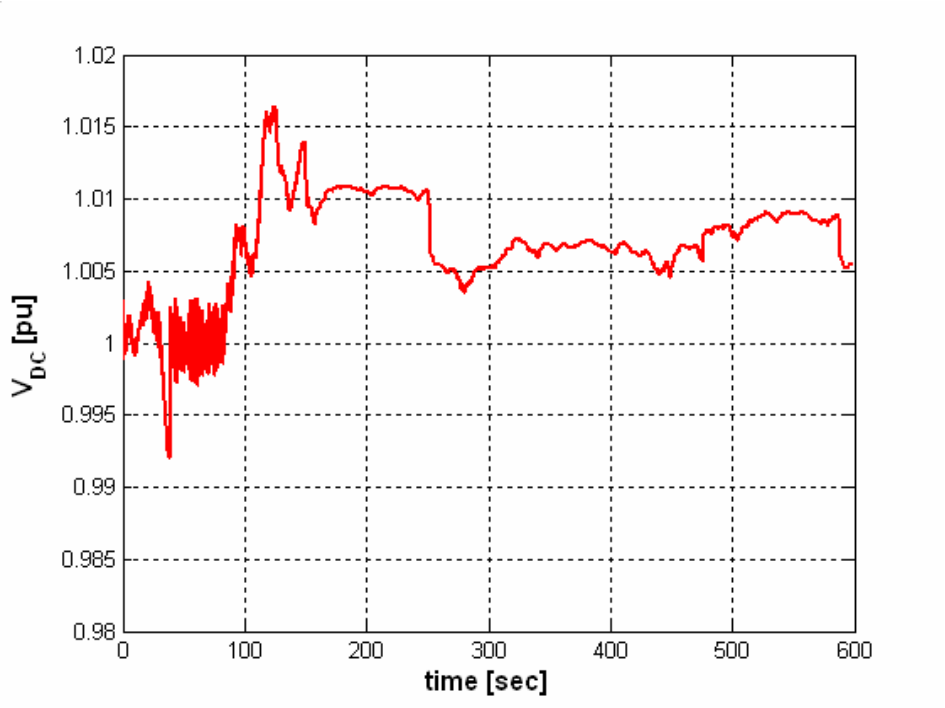

Figure 77: DC-link voltage.

Again there is an overshot of 1.5% when the wind farm operates in power limitation mode.

The output of the CHP is shown in Figure 78.

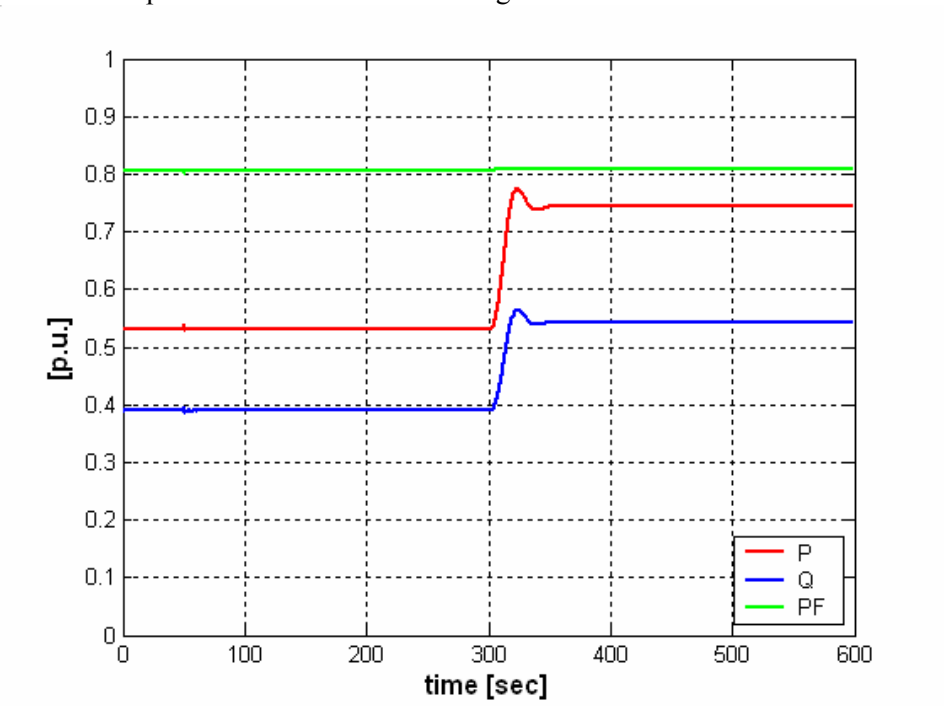

Figure 78: Output of the small CHP.

Based on these results it can be concluded that the control of the DC connection works properly.

5.4.3 Different frequency drop coefficients

Some comparisons for different frequency droop coefficients are made. During the calculation of initial condition different pitch angles are calculated for each wind turbine, even if the initial conditions are identically (see Figure 67 and Figure 73). Therefore, in order to evaluate the droop control for sending end station a fixed pitch angle is used for all wind turbines. This pitch angle is the optimal value (ca. -1.5 deg) for an average wind speed of 11 m/sec. The system has been simulated for 120 sec with a fixed value for the pitch angle and an average wind speed of 11 m/sec. For the sake of simplicity only the relevant waveforms are shown.

First the frequency for the wind farm bus bar is shown in Figure 79.

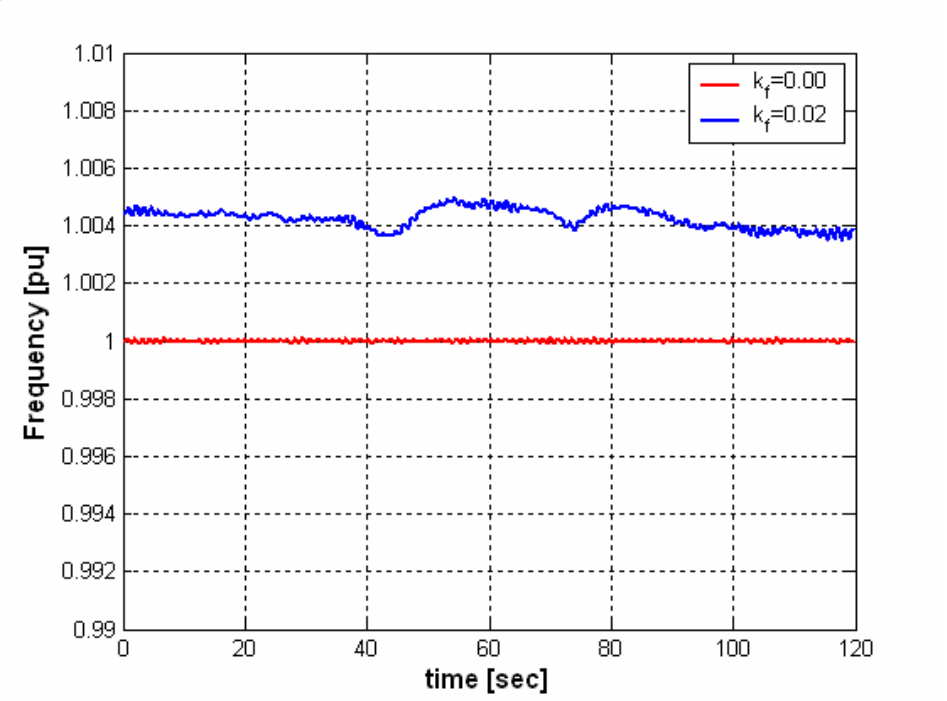

Figure 79: Wind farm frequency for different droop coefficients.

The average frequency increases with 0.4%, which corresponds to a frequency of 50.2 Hz.

The shaft speed of the generator for “Wind Turbine 1”, when different coefficients for the droop characteristics are used, is shown in Figure 80.

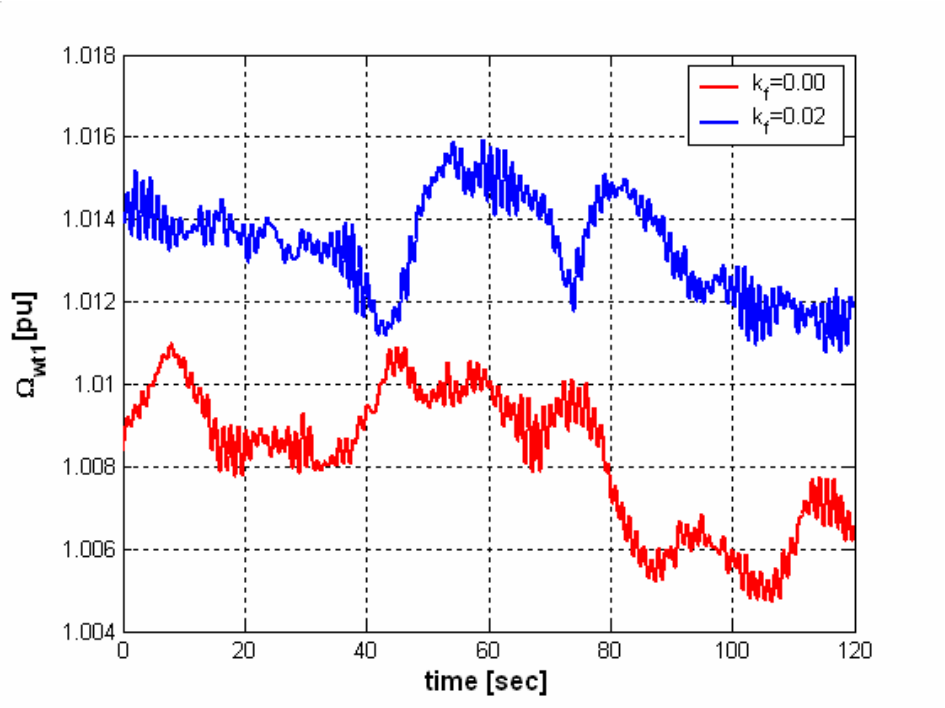

Figure 80: Shaft speed for on wind turbine using different droop coefficients.

Some simple calculations shows that the average speed increase with only 0.5% while the increase in the energy capture is around 7% for the considered time frame.

The power spectra density of the shaft speed in the considered cases is shown in Figure 81.

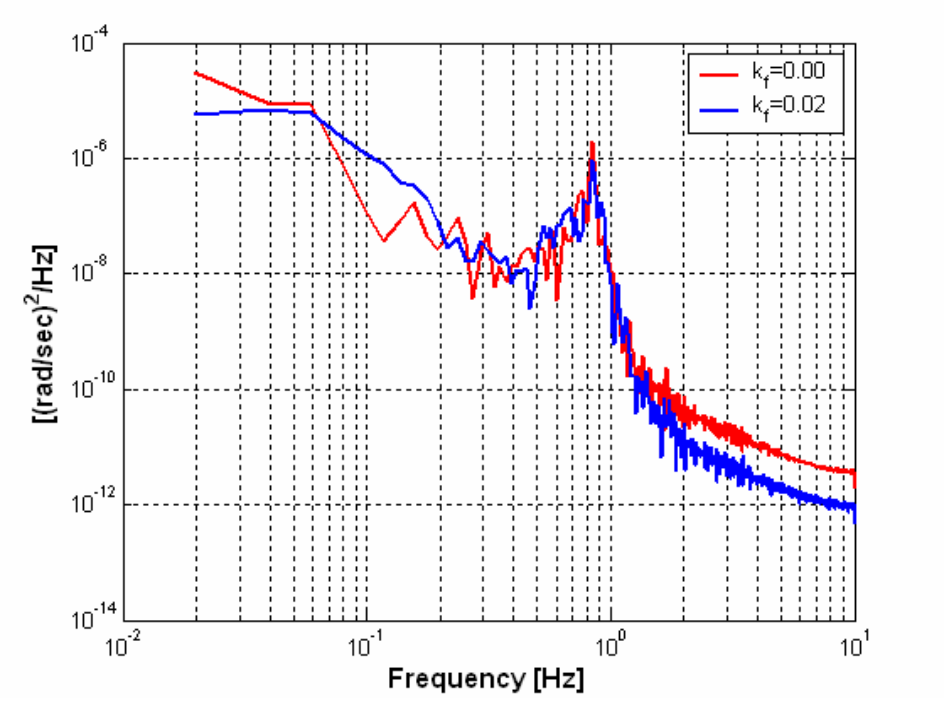

Figure 81: Power spectra density of the shaft speed for Wind Turbine 1.

It can be observed that the power spectra density of the shaft speed is reduced when the frequency droop coefficient is not equal with zero. This means that the shaft speed is smoother in this case than in the previous case and the mechanical stress is also reduced.

In order to evaluate this control strategy for a wide range of wind speeds further investigations are necessary. Moreover an optimal value for the frequency droop coefficient should be found.

5.4.4 Island operation

The entire system is analysed when the connection with the main grid is lost. There are several events in the system in this case as:

- The average wind speed is kept constant to 8 m/sec so that the wind turbines controller will operate in optimization mode;
- A 100% increase in the load occurs at time 50 sec. The load is 2.5 MW rated power.
- The CHP operates first at 0.7 p.u. turbine power and a power factor of 0.8. The power setpoint of the turbine is increased to 1 p.u. at time 200 sec;
- The circuit breaker for connection to the main grid is opened at time 300 sec. The system will operate in island mode.

The reactive power set point for Station B is kept to zero as well as the frequency droop coefficient k_f in Station A (sending end station). Therefore a fixed reference for frequency (50 Hz) is used.

The wind time series for each wind turbine as well as the pitch angles are shown in Figure 82.

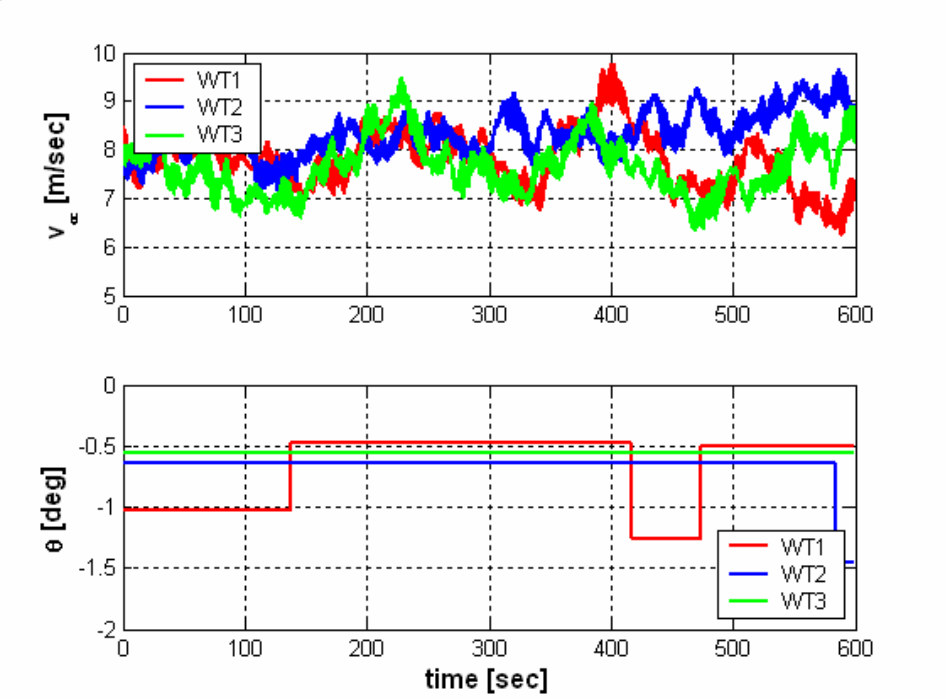

Figure 82: Wind speeds and pitch angle for each wind turbine.

The active and reactive powers for wind turbines are shown in Figure 83.

The power balance in the connection point is shown in Figure 84.

The voltages and frequencies for each terminal of the DC connection are shown in Figure 85.

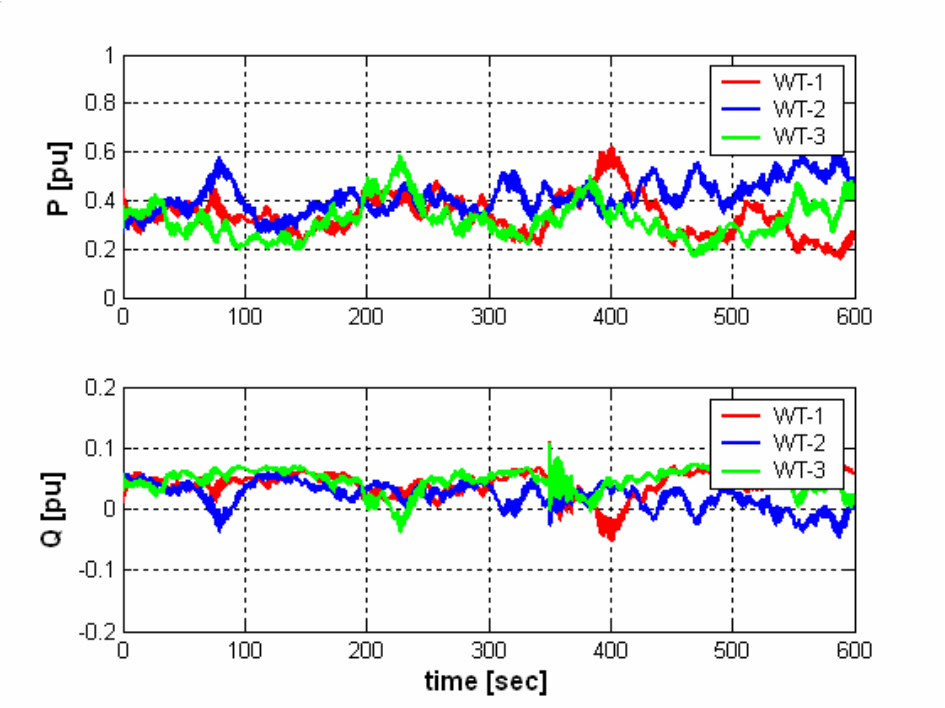

Figure 83: Active and reactive power for wind turbines.

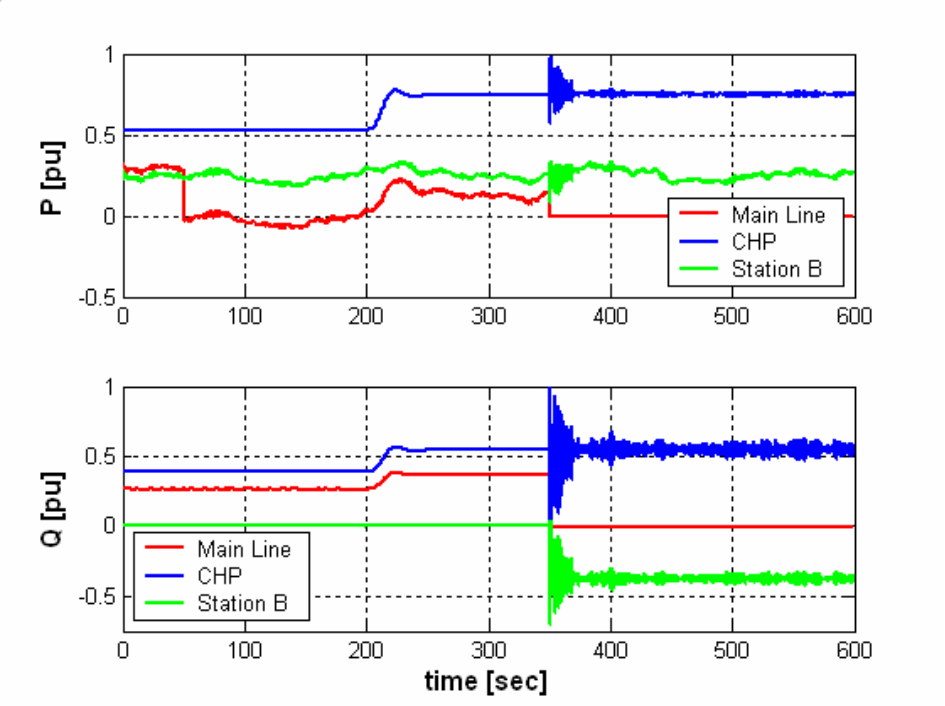

Figure 84: Active and reactive power on the connection point.

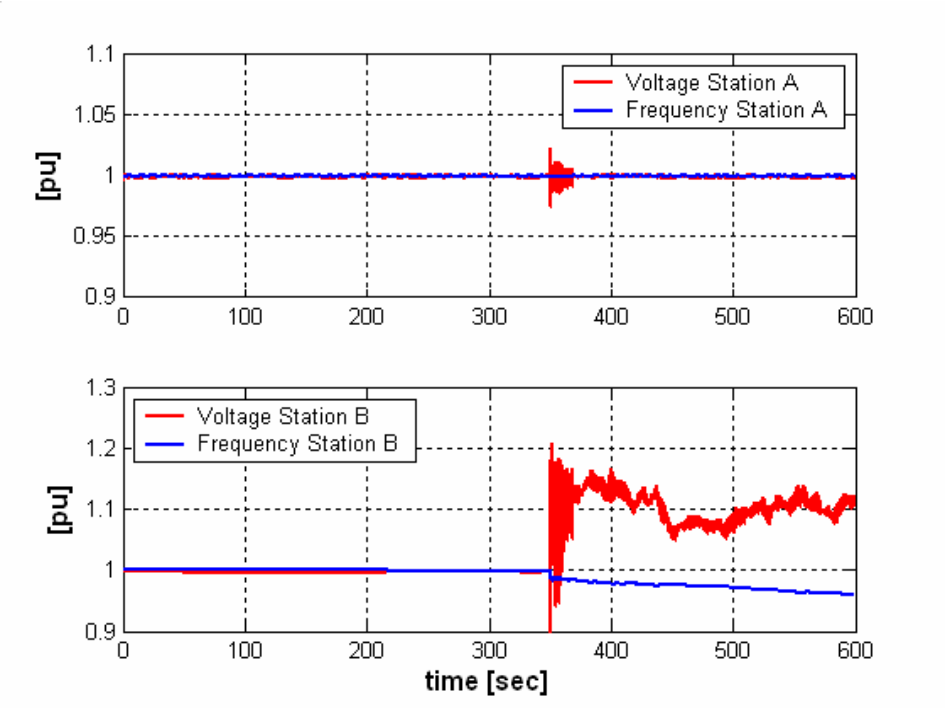

Figure 85: Voltages and frequencies in each terminal.

The DC-link voltage is shown in Figure 86 while the CHP output in Figure 87, respectively.

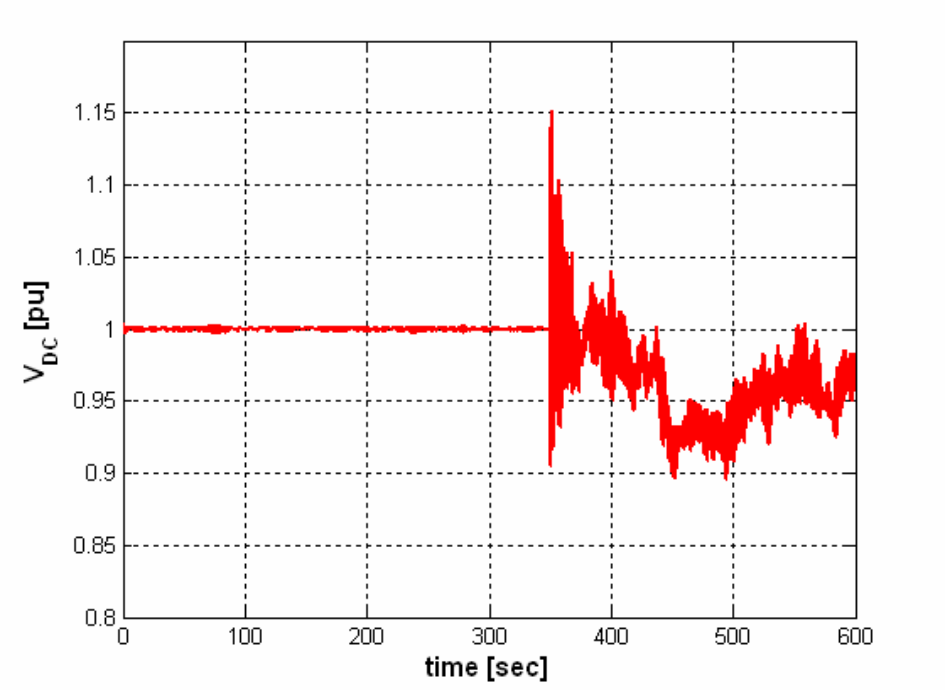

Figure 86: DC-link voltage.

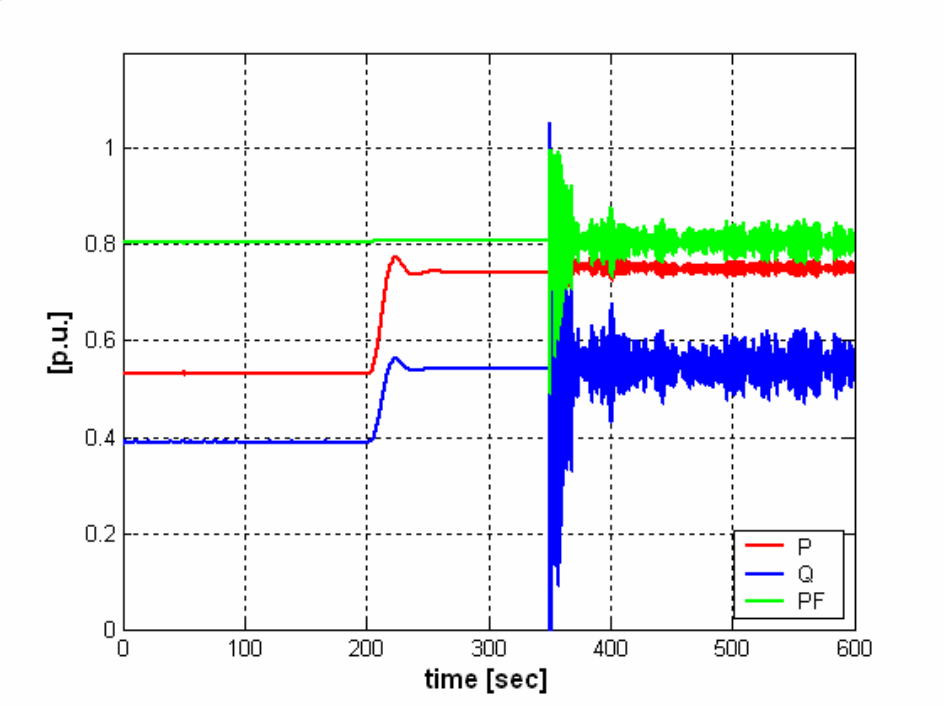

Figure 87: CHP output.

From the above figures it can be concluded that the control scheme for the receiving end station (Station B) is not able to regulate the voltage and the frequency of the local grid because of the following reasons:

- There is no active power balance in the local grid. Since the wind farm is not controlled, the production of the wind farm and the CHP output does not match the load demand.
- The reactive power set point for station B is kept at zero whilst the CHP operate at constant power factor. Therefore there is no reactive power balance in the local grid.

Using a MicroGrid/WindFarm controller the set points for each wind turbine can be given according with the load demand as well as the set point for the reactive power in station B. However, the station B controls the DC-link voltage and an AC voltage control might be necessary.

6 Variable speed wind turbine concepts

During the last few years, variable speed wind turbines have become the most dominating type of yearly installed wind turbines (Hansen, A.D., 2004), (Hansen, L.H., et al., 2001). The increased interest in the variable speed wind turbines is due to their very attractive features, given by the presence of the power converter, with respect to both the wind turbine itself as well as to more onerous grid requirements.

The variable speed wind turbines have a more complicated electrical system than the fixed speed wind turbines. They are typically equipped with an induction or synchronous generator and a power converter. If the wind turbine

operates with variable rotational speed, it implies that the electric frequency of the generator varies and therefore it is decoupled from the grid frequency through a power electronic. The presence of the power converter makes the variable speed operation itself possible. By introducing the variable speed operation, it is possible to continuously adapt (accelerate or decelerate) the rotational speed of the wind turbine to the wind speed, in such a way that the turbine operates continuously at its highest level of aerodynamic efficiency. Contrary to fixed speed wind turbines, which are designed to obtain maximum efficiency at one wind speed only, the variable speed wind turbines are designed to achieve maximum aerodynamic efficiency over a wide range of wind speeds.

The power converter controls the generator speed in such a way that the power fluctuations caused by wind variations are more or less absorbed by changing the generator speed and implicitly the wind turbine rotor speed. Seen from the wind turbine point of view, the most important advantages of the variable speed operation compared to the conventional fixed speed operation are:

- *reduced mechanical stress on the mechanical components such as shaft and gearbox* – the large inertia of the wind turbine is used as a flywheel during gusts, i.e. the power fluctuations are absorbed in the mechanical inertia of the wind turbine.
- *increased power capture* – due to the variable speed feature, it is possible to continuously adapt (accelerate or decelerate) the rotational speed of the wind turbine to the wind speed, so that the power coefficient is kept at its maximum value.
- *reduced acoustical noise* – low speed operation is possible at low power conditions (lower wind speeds).

Additionally, the presence of power converters in wind turbines also provide high potential control capabilities for both large modern wind turbines and wind farms to fulfil the high technical demands imposed by the grid operators (Eltra, 2000), (Sørensen,P., et al.,2000), such as:

- *controllable active and reactive power (frequency and voltage control)*
- *quick response under transient and dynamic power system situations*
- *influence on network stability*
- *improved power quality (reduced flicker level, low harmonics filtered out and limited in-rush and short circuit currents)*

Due to these advantages, the variable speed operation offers the possibility of increased "grid friendliness". Its direct drawbacks are the additional losses due to power electronics, more components, thereby reliability issues, and an increased capital cost due to the power electronics. As power electronic is a rapidly developing technology today, it is clear that variable speed wind turbines will continue to be the norm and not the exception.

As well known, a wind turbine is characterised by its power speed characteristics. For a horizontal axis wind turbine, the amount of mechanical power P_{mec} that a turbine produces in steady state is given by:

$$P_{mec} = \frac{1}{2} \rho \pi R^2 u^3 C_p(\theta, \lambda) \tag{53}$$

where ρ is the air density, R the turbine radius, u the wind speed and $C_p(\theta, \lambda)$ is the power coefficient, which for pitch controlled wind turbines depends on both the pitch angle θ and the tip speed ratio λ. The tip speed ratio λ is given by:

$$\lambda = \frac{\omega_{rot} R}{u} \tag{54}$$

where ω_{rot} denotes the rotor turbine speed.

The prime motivation for variable speed wind turbines at lower wind speeds is to adjust the rotor speed at changing wind speeds so that $C_p(\theta, \lambda)$ always is maintained at its maximum value. The power coefficient $C_p(\theta, \lambda)$ has a maximum for a particular tip-speed ratio λ_{opt} and pitch angle θ_{opt}. This means that for extracting maximum power from a particular wind speed, the control strategy has to change the turbine rotor speed in such a way that the optimum tip speed ratio λ_{opt} is always obtained. The maximum power a particular wind turbine can extract from the wind is a cubic function of the turbine optimum speed, as follows:

$$P_{mec}^{\max} = K_{opt} \left[\omega_{rot}^{opt} \right]^3 \tag{55}$$

where:

$$K_{opt} = \frac{1}{2} \rho \pi R^5 \frac{C_p^{\max}}{\lambda_{opt}^3} \tag{56}$$

K_{opt} depends on the turbine characteristics and the air density. Tracking the maximum power is the goal as long as the generated power is less than the rated power. At wind speeds higher than rated wind speed, the control strategy has to be changed so that the wind turbine no longer produces maximum power but only rated power. The blades are thus pitched to reduce the power coefficient $C_p(\theta, \lambda)$ and thereby to maintain the power at its rated value. Wind gusts are absorbed by rotor speed changes, the wind turbine's rotor behaving as energy storage.

The mechanical power is transformed in the generator into electrical power, the relation between them being given by:

$$P_{el} = \eta_{gen} P_{mec} \tag{57}$$

where η_{gen} is the generator efficiency.

Currently, for units above 1MW, there are two dominating groups of variable speed wind turbine concepts with a fast growing market demand (Hansen, A.D., 2004):

- *Variable speed concept with partial scale frequency converter* – known as doubly-fed induction generator (DFIG) concept. The generator is a wound rotor induction generator (WRIG), where the stator is directly connected to the grid, while the rotor is controlled by a partial scale power converter. The rotor frequency and thus the rotor speed are controlled by the partial-scale frequency converter, whose size defines the range of the variable speed (typically +/- 30% around synchronous speed).
- *Variable speed concept with full-scale frequency converter* – where the generator stator is interconnected to the grid through a full-scale power converter. The generator can be synchronous (wound rotor synchronous generator WRSG or permanent magnet synchronous generator PMSG) or induction generator (wound rotor induction generator WRIG).

The attention in the following chapters is thus focused on a detailed model and control strategies description of variable speed DFIG wind turbine concept and variable speed multi-pole PMSG wind turbine concept, respectively.

7 Variable speed DFIG wind turbine concept – normal operation

In this chapter, the attention is drawn to the control strategies and performance evaluation of the variable speed pitch controlled wind turbine with DFIG. The chapter is organised as follows. First, the characteristics of the variable speed wind turbine and of the doubly-fed induction generator (DFIG) are summarized. Then, the overall control system of the variable speed wind turbine with DFIG is described, with focus on the control strategies at the different control levels: DFIG control and wind turbine control.

The fundamental feature of the DFIG is that the power processed by the power converter is only a fraction of the total wind turbine power, and therefore its size, cost and losses are much smaller compared to a full-scale power converter used in the full variable speed concept.

The typical DFIG configuration, illustrated in Figure 88 consists of a wound rotor induction generator (WRIG) with the stator windings directly connected to the three-phase grid and with the rotor windings connected to a back-to-back partial scale power converter. The back-to-back converter is a bi-directional power converter. It consists of two independent controlled voltage source converters connected to a common DC-bus. These converters are illustrated in Figure 88, as rotor-side converter and grid-side converter. The behaviour of the generator is governed by these converters and their controllers both in normal and fault conditions. The converters control the rotor voltage in magnitude and phase angle and are therefore used for active and reactive power control.

Because the optimal voltage of the rotor is typically less than the optimal stator voltage, the transformer connecting the system to the grid has two secondaries: one winding connecting the stator and the other connecting the rotor.

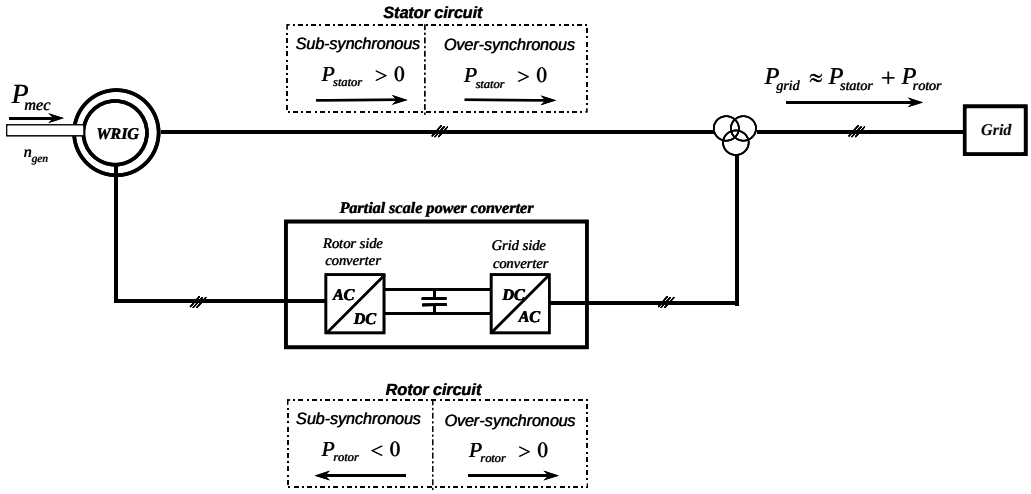

Figure 88: Principle diagram of the power flow in doubly-fed induction generator.

DFIG system allows variable speed operation over a large but restricted range. The smaller the operational speed range the less power has to be handled

by the bi-directional power converter connected to the rotor. For example if the speed should be controllable between +/- 30%, the converter must have a rating of approximate 30% of the generator. Thus the size of the converter does not relate to the total generator power but instead to the selected speed range and hence the slip power (Heier, S., 1998), (Leonhard, W., 2001). Therefore, the cost of the power converter increases when the allowed dynamic speed range around synchronous speed increases.

Notice that, since the speed range is restricted, the slip-induced voltage is only a fraction of the grid voltage, depending on the turn-ratio between the stator and rotor. The DC bus voltage is thus relatively low. The operation at a lower DC bus voltage is possible because of the voltage reduction on the rotor side realised by the three winding transformer.

In order to cover a wide operating range from sub-synchronous to over-synchronous speed, i.e. the DFIG is able to work as a generator in both sub-synchronous (positive slip $s>0$) and over-synchronous (negative slip $s<0$) operating area, the power converter has to be able to operate with power flow in both directions. This is the reason why a back-to-back PWM (bi-directional) converter configuration is used. The slip is defined as:

$$s = \frac{n_{syn} - n_{gen}}{n_{syn}} \tag{58}$$

where n_{syn} and n_{gen} are the synchronous speed and generator speed in rpm, respectively. For a doubly-fed induction machine, it is the sign of the electrical torque, independent of the slip, which indicates if the machine is working as motor or generator.

Assuming that all the losses in the stator and rotor circuit can be neglected, the power through the power converter (through the rotor circuit), known as the slip power, can be expressed as the slip s multiplied with the stator power, P_{stator}. Furthermore, the delivered stator power can be expressed based on the grid power P_{grid} or on the mechanical power:

$$\begin{aligned} P_{rotor} &\approx -s\, P_{stator} \\ P_{stator} &\approx P_{grid} / (1-s) = \eta_{gen}\, P_{mec} / (1-s) \end{aligned} \tag{59}$$

where η_{gen} is the generator efficiency. Depending on the operating condition of the drive, the power is fed in or out of the rotor: it is flowing from the grid via the converter to the rotor ($P_{rotor} < 0$) in sub-synchronous mode or vice versa ($P_{rotor} > 0$) in over-synchronous mode, as it is indicated in Figure 88. In both cases (sub-synchronous and over-synchronous) the stator is feeding energy to the grid ($P_{stator} > 0$) (Leonhard, W., 2001).

The presence of the power converter allows DFIG a more versatile and flexible operation compared with a squirrel-cage induction machine. The power converter compensates for the difference between the mechanical and electrical frequency by injecting a rotor current with a variable frequency according to the shaft speed. Through collector rings, the power converter supplies thus the rotor windings with a voltage with variable magnitude and frequency. It improves the controllable capabilities of such generator, as for example:

- it provides DFIG the ability of reactive power control. DFIG is therefore capable of producing or absorbing reactive power to or from the

grid, with the purpose of voltage control (i.e. in the case of weak grid, where the voltage may fluctuate).
- it can magnetize the DFIG through the rotor circuit, independently of the grid voltage.
- it decouples active and reactive power control by independent control of the rotor excitation current.

7.1 The overall control system of a variable speed wind turbine with DFIG

The control system of a variable speed wind turbine with DFIG has as goals to control the reactive power interchanged between the generator and the grid and the active power drawn from the wind turbine in order to track the wind turbine optimum operation point or to limit the power in the case of high wind speeds.

Each wind turbine system contains subsystems (aerodynamical, mechanical, electrical) with different ranges of time constants, i.e. the electrical dynamics are typically much faster than the mechanical. This difference in time constants becomes even bigger in the case of a variable speed wind turbine, due to the presence of the power electronics. Such more complicated electrical system requires a more sophisticated control system too.

The overall control system of a variable speed DFIG wind turbine is built up with a hierarchical structure. It consists of two control levels with different bandwidths, strongly connected to each other, i.e. it contains a slow dynamic control level and a fast dynamic control level.:

- **Wind turbine control (slow control)**
- **DFIG control (fast control)**

The fast dynamic control level, i.e. DFIG control, encompasses the electrical control of the power converters and of the doubly-fed induction generator. Since this controller is an electric one, it works very fast. It addresses the electrical control of the frequency converter. The DFIG control level has as goal to control the active and reactive power of the wind turbine independently. The DFIG control contains two controllers:

- *Rotor-side converter controller* - controls independently the active and reactive power on the grid point M – see Figure 89.
- *Grid-side converter controller* - controls the DC link voltage U_{DC} and guarantees unity power factor in the rotor branch. The transmission of the reactive power from DFIG to the grid is thus only through the stator.

As the pulse-width modulation factor *PWM* is the control variable of the converter, each of these control channels generates a pulse-width modulation factor *PWM*, for the respective converter. This control variable is a complex number and therefore can control simultaneously two variables, such as the magnitude and phase angle of the rotor induced voltage. For example, for a predefined DC voltage and a control variable (pulse-width modulation factor *PWM*), the line-to-line AC-voltage is determined as follows:

$$\left|U_{AC}\right| = \frac{\sqrt{3}}{2\sqrt{2}} \cdot \left|PWM\right| \cdot U_{DC} \qquad (60)$$

On the other hand, the wind turbine control is a control with slow dynamic responses. The wind turbine control contains two cross-coupled controllers: a speed controller and a power limitation controller. It supervises both the pitch

angle actuator system of the wind turbine and the active power setpoint of the DFIG control level. It thus provides both a reference pitch angle θ_{ref} directly to the pitch actuator and a converter reference power signal $P_{grid}^{conv,ref}$ for the measurement grid point M to the DFIG control.

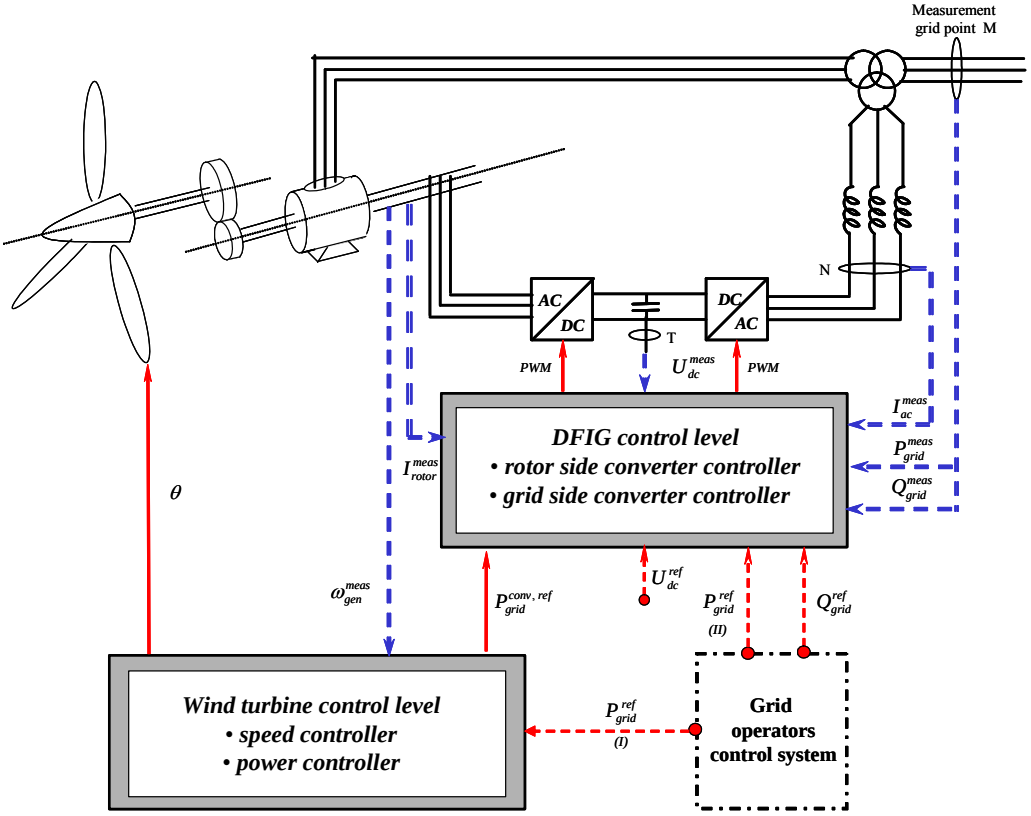

Figure 89: Overall control system of variable speed wind turbine with doubly-fed induction generator.

Figure 89 sketches the overall control system of the variable speed DFIG wind turbine. Different line styles are used to provide a quick overview of the signals of the overall control system in Figure 89:

- double-dotted lines mark the measured signals.
- single dotted-lines reveal reference (setpoint) signals
- solid lines reveal the output signals from the controllers

Notice that the overall control system requires information on different measured electrical signals: the active P_{grid}^{meas} and reactive Q_{grid}^{meas} power (measured in the measurement grid point M), the voltage U_{dc}^{meas} on the DC – busbar, the AC- converter current I_{ac}^{meas} (measured in point N), the generator speed ω_{gen}^{meas} and the rotor current I_{rotor}^{meas}.

The DFIG control level has three reference input signals:

- The converter reference active power $P_{grid}^{conv,ref}$ in the measurement grid point *M*. This information is delivered by the wind turbine control level.
- The converter reference reactive power Q_{grid}^{ref} in the measurement grid point *M*. This reference can be extraordinarily imposed by the grid operators (based for example on a certain dispatch control). For example in the case of a weak grid or a grid fault situation, the DFIG can have the extra task to generate reactive power to support the grid voltage.

- The reference DC- voltage U_{dc}^{ref} is a value strictly connected to the size of the converter, the stator-rotor voltage ratio and the modulation factor of the power converter.

The wind turbine control level has a slower dynamic response than the DFIG control. It controls the pitch angle of the wind turbine and the reference active power to the DFIG control level.

Different control strategies of variable speed wind turbine are widely presented in the literature (Novak P., et al., 1995), (Bossany E.A., 2000), (Bindner H., et al., 1997), (Hansen A. D., et al., 1999), (Wortmann B., et.al, 2000).

In this work two of the most frequent control strategies for variable speed wind turbines, see Figure 90, have been implemented and described:

- **Control strategy I** - where the power converter is used to control the generator speed, while the pitch system limits the power. In this control strategy, as long as the power limit P_{grid}^{ref} is not reached (i.e. wind speeds less than the rated wind speed), the wind turbine control keeps the pitch angle to its optimal value and it generates the optimal active power reference $P_{grid}^{conv,ref}$ to the DFIG control level. The DFIG control has then to adjust continuously the generator speed in order to keep the power reference provided by the wind turbine control level.
- **Control strategy II** - where the power converter controls the power, while the pitch system prevents the overspeeding of the generator, i.e. the pitch angle limits the generator speed to its rated value in case of high wind speeds. It provides a fast power control.

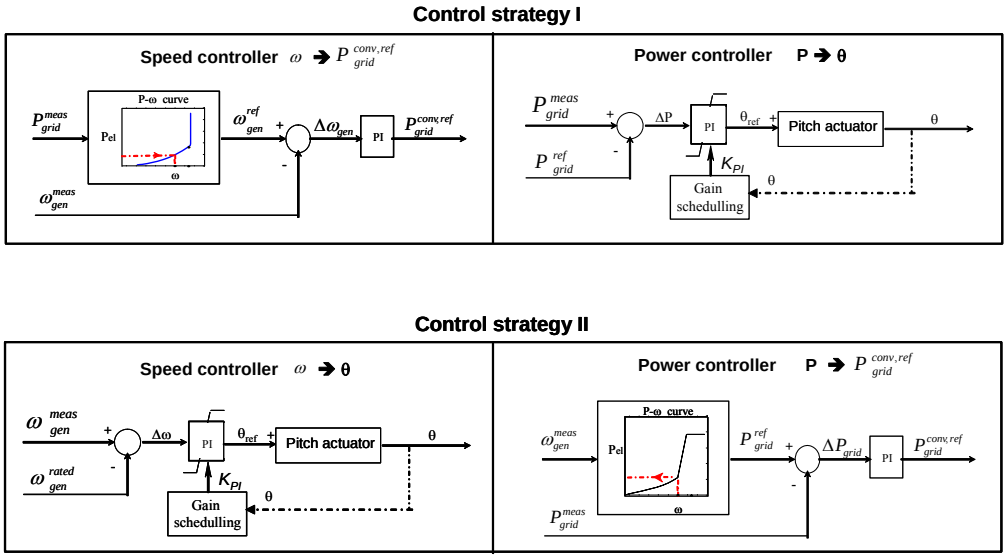

Figure 90: Variable speed wind turbine control strategies

No matter which control strategy is used, the wind turbine control generates two control signals:

- The converter reference active power $P_{grid}^{conv,ref}$ - is the setpoint for the active power signal for the DFIG control level. For example in control strategy (I), when the wind speed is less than the rated wind speed, the wind turbine control level generates the converter reference active power $P_{grid}^{conv,ref}$ by adjusting the generator speed in such a way that the turbine captures the maximum power.

- The pitch angle θ - is delivered directly to the wind turbine blades. The pitch angle actuator system is implemented as a part of the controller.

The active power reference signal $P_{grid}^{ref}(I)$ or $P_{grid}^{ref}(II)$, depending on the used control strategy, is normally equal to the nominal power of the wind turbine. Similarly to Q_{grid}^{ref}, the active power reference signal can be imposed in special situations by the grid operators control system to a power value less then the nominal (rated) power of the wind turbine. The present work considers the case when P_{grid}^{ref} is the nominal (rated) power of the wind turbine.

In the following sections, the two control levels, i.e. DFIG control level and wind turbine control level with their individual controller, are described.

7.2 DFIG control

The DFIG control contains the fast electrical control of the doubly-fed induction generator. Control strategies and performance evaluation of doubly-fed induction generators have been widely discussed in the literature (Leonhard W., 2001), (Mohan N., et al., 1989), (Novotny D.W. et al., 1996), (Pena, R., et al., 1996), and it is therefore briefly presented in this report.

Power converters are usually controlled utilizing vector control techniques. Briefly, vector control allows decoupled control of both active and reactive power. The idea is to use a rotating reference frame based on an AC flux or voltage and then to project currents on this a rotating frame. Such projections are usually referred to as the d and q components of their respective currents. With a suitable choice of reference frames the AC currents appear as DC quantities in the steady state. For flux-based rotating frames, changes in the q component will lead to active power changes, while changes in the d component will lead to reactive power changes. In voltage-based rotating frames (and thus 90 degrees ahead of flux-based frames) the effect is the opposite.

7.2.1 System reference frames

Briefly, the vector control techniques allow de-coupled control of active and reactive power. These techniques are based on the concept of d-q controlling in different reference frames, where the current and the voltage are discomposed into distinct components related to the active and reactive power. Each specific reference frame is defined by two orthogonal axes, namely d-axis (direct axis) and q-axis (orthogonal axis). In this report the stator flux oriented rotor current control with decoupled control of active power and reactive power is adopted (Novotny D.W. et al., 1996).

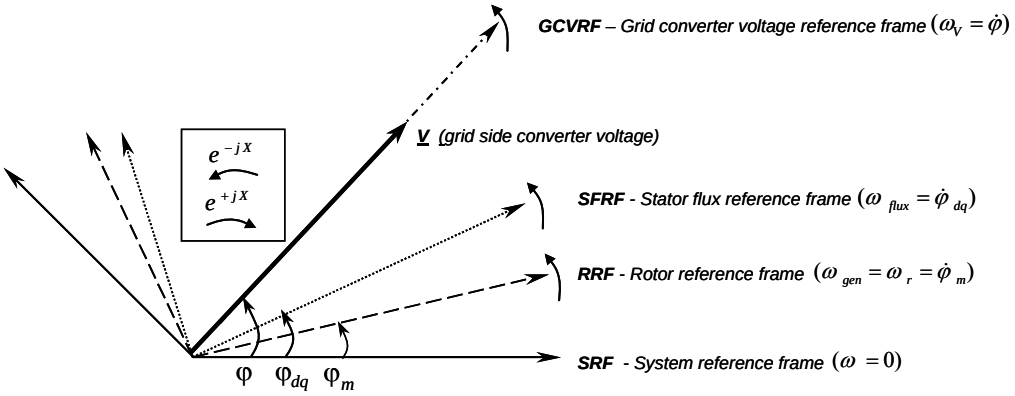

Figure 91: Reference frames used in doubly-fed induction generator control.

The doubly-fed induction generator DFIG and its control in DIgSILENT is using the following reference frames, illustrated in Figure 91:

- System reference frame *(SRF)*– is the reference frame fixed to the grid, and it is rotating with the grid reference voltage. Therefore its relative speed to the grid is considered zero.
- Rotor reference frame *(RRF)* - is the reference frame fixed to the rotor. The d-axis in the rotor reference frame is chosen collinear to the rotor phase winding. The position of the rotor reference frame is the actual position of the rotor φ_m.
- Stator flux reference frame *(SFRF)* – is the reference frame, which rotates synchronously with respect to the stator flux, namely its d-axis is chosen collinear to the stator flux vector. The position of stator flux reference frame is the instantaneous position φ_{dq} of the stator flux vector. This is calculated as $\tan(\varphi_{dq}) = \frac{\psi^{SRF}_{q,stator}}{\psi^{SRF}_{d,stator}}$ where $\psi^{SRF}_{d,stator}$ and $\psi^{SRF}_{q,stator}$ are its stationary components on *d*- and *q*- axis, respectively in the system reference frame *SRF*. Since the d-axis of this reference frame is chosen to be the instantaneous axis of the stator field, the phase angle φ_{dq} of the stator voltage is generally not a constant, although its frequency and magnitude are constants constrained by the power system. This reference frame is defined with respect to the stator flux and not to the stator voltage because the stator flux basically represents the integral of the stator voltage and is therefore much smoother.
- Grid converter voltage – oriented reference frame *(GCVRF)*– is the reference frame which d-axis is chosen collinear to the voltage grid converter $\underline{V}$. This reference frame is positioned by the voltage angle φ, which is measured with a PLL (phase-locked loop) block.

Once, a reference frame is defined, a vector can be discomposed into distinct components on the axes. For example, the grid converter voltage vector $\underline{V}$, shown in Figure 91, can be expressed in system reference frame *SRF* as:

$$\underline{V} = |\underline{V}| \, e^{\,j\varphi} = V_d^{SRF} + j\, V_q^{SRF} \qquad (61)$$

where V_d^{SRF} and V_q^{SRF} are the components on *d* (real) and *q* (imaginary) axis, respectively, in the system reference frame *SRF*. $|\underline{V}| = \sqrt{\left(V_d^{SRF}\right)^2 + \left(V_q^{SRF}\right)^2}$ is the absolute value of the voltage vector, while φ is the angle of voltage vector $\underline{V}$ in the system reference frame *SRF*.

In the vector control, the signals are typically transformed from one reference frame to another. Such coordinate transformations have as scope to simplify the modelling and the control algorithms. For example, the voltage grid converter vector $\underline{V}^{SFRF}$ expressed in *SFRF* can be transformed in *RRF* by:

$$\underline{V}^{RRF} = \underline{V}^{SFRF} e^{jX} \tag{62}$$

where $X = \varphi_{dq} - \varphi_m$ is the angle between the two reference frames, $\underline{V}^{RRF}$ and $\underline{V}^{SFRF}$ are the voltage vectors expressed in coordinates of *RRF* and *SFRF*, respectively. The angle sign convention for the coordinate transformation is also shown in Figure 91.

7.2.2 Control configuration of DFIG in DIgSILENT

The power converter is a standard built-in model in the *PowerFactory* library. Its control is not a standard model in the *PowerFactory* library and therefore it has to be implemented as a user-written model in the dynamic simulation language of the *PowerFactory*. In this report, the converter control is modelled on a generic level, without focusing on any particular design of a manufacturer.

Figure 92 shows the overall control configuration of DFIG in DIgSILENT. Notice that the DFIG model and the control of the converters in DIgSILENT are not using the same reference frame, and therefore different coordinate transformations are performed in order to be able to make possible the interconnection between these different blocks.

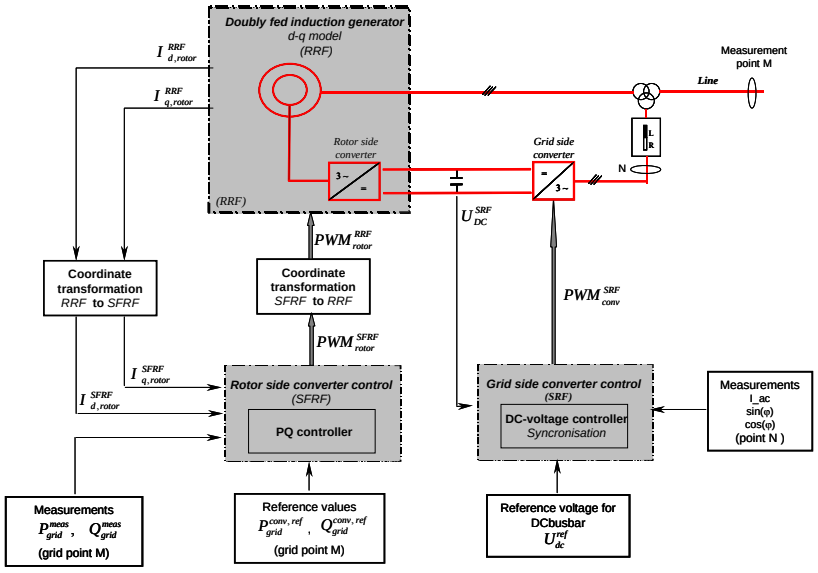

Figure 92: Control scheme of DFIG in DIgSILENT.

As illustrated both in Figure 88 and Figure 92, the configuration of the doubly-fed induction generator contains two converters with a DC link:

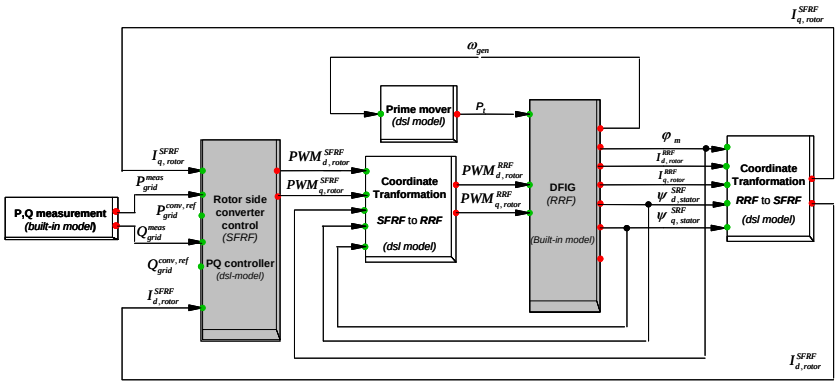

Figure 93: Inputs and outputs of the rotor-side converter control.

1. *Rotor-side converter*: is an integrated part of the DFIG model in DIgSILENT together with the usual induction machine d-q model. The DFIG model in DIgSILENT is expressed in the rotor reference frame *RRF* and it is a d-q built-in model with predefined inputs and outputs. The rotor-side converter (RSC) operates in a stator flux reference frame *SFRF*. The q-axis current of the RSC is used to control the active power, while the d-axis current is used for reactive power control.
2. *Grid-side converter* - is an independent component in DIgSILENT's library, which can be added to the machine model to form the DFIG with back-to-back converter. The grid-side converter (GSC) operates in the stator voltage reference frame *SRF*. The d-axis current of the GSC is used to control the DC link voltage to a constant level, while the q-axis current is used for reactive power control.

In the following, it is focus on the control of the two converters existing in the DFIG configuration. Both the rotor- and grid- side controllers are explained only to the necessary extent.

7.2.3 Rotor-side converter control

As mentioned before, the rotor windings are connected to the main grid by a power converter allowing controlling the slip ring voltage of the generator in magnitude and phase angle. Figure 93 illustrates the blocks, which are connected with the rotor-side converter control block. Notice that some of the block models are built-in type while others are dsl type. The diagram contains the following blocks:

<u>*P, Q measurement block*</u> *(built-in model)* – delivers the measured active P_{grid}^{meas} and reactive power Q_{grid}^{meas} in a predefined grid point *M* – see Figure 89.

<u>*Coordinate transformation blocks*</u> *(dsl model)* –perform different coordinate transformations, as for example:

- from *SFRF* to *RRF*:
  The induced controlled rotor voltage is modulated with the pulse-width amplification factor PWM. This modulation factor is the output of the rotor-side converter controller and it is expressed in *SFRF*. As the DFIG model is expressed in *RRF*, the output of the rotor-side converter's controller has therefore to be transformed to *RRF*:
  $$PWM_{rotor}^{RRF} = PWM_{rotor}^{SFRF} \, e^{+j(\varphi_{dq} - \varphi_m)} \qquad (63)$$
- from *RRF* to *SFRF*

The output of the generator model is expressed in *RRF* and therefore it has to be transformed back to *SFRF* in order to be used by the rotor-side converter's controller:

$$I_{rotor}^{SRFR} = I_{rotor}^{RRF} e^{-j(\varphi_{dq} - \varphi_m)} \quad (64)$$

<u>*DFIG block*</u> *(built-in model)* – comprises the model of the doubly-fed induction generator and of the rotor-side converter. Notice that its inputs, outputs and equations are expressed in rotor reference frame *RRF*. This block can have as output the rotor current I_{rotor}^{RRF}, the rotor position φ_m and the stator flux ψ_{stator}^{SRF}.

<u>*Prime mover block*</u> *(dsl model)* – gets as input the generator speed ω_{gen} and it delivers as output the mechanical power P_t to the generator. In wind turbine applications, the prime mover of the generator is the turbine itself, where the mechanical component model provides the mechanical power to the generator.

<u>*Rotor-side converter control block*</u> *(dsl model)* – contains the rotor-side converter control, which is illustrated in Figure 94. As mentioned before, the aim of the rotor-side converter is to control independently the active and reactive power in the measurement grid point M (see Figure 89), and therefore the stator flux oriented rotor current control approach is used. The active and reactive powers are not controlled directly. The impressed rotor current is controlled instead.

The rotor-side converter control consists of two PI- control loops in cascade – see Figure 94:

- a slower (outer) power control loop
- a very fast (inner) rotor current control loop.

The power control loop controls the active and reactive power, while the very fast current control loop regulates the machine's rotor currents to the reference values that are specified by the slower power controller.

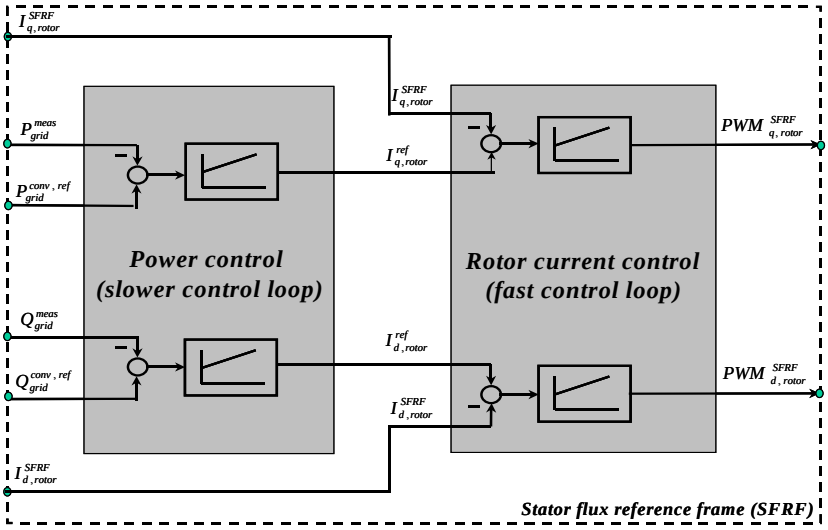

Figure 94: Rotor-side converter control scheme using a cascade control structure.

Such cascade control structure is advantageous as the electrical and mechanical dynamics are in different time scales, i.e. the electrical dynamics are much faster than the mechanical dynamics. Since the electrical dynamics are the fastest, the rotor current control loop is the inner loop.

The rotor current is thus split into a parallel and orthogonal component to the stator flux, respectively. In the stator flux reference frame *SFRF*, the d-axis is equivalent to the reactive component and the q-axis is equivalent to the active component. In such a reference frame, the active power (the electromagnetic torque, respectively) is only a function of the q- component of the rotor current, while the reactive power is expressed as function of the *d*- component of the rotor current (Novotny D.W. et.al., 1998):

$$\begin{aligned} P &= func(\ I_{q,rotor}^{SFRF}\ ) \\ Q &= func(\ I_{d,rotor}^{SFRF}\ ) \end{aligned} \tag{65}$$

This means that the active power *P* control is therefore achieved by controlling the *q*- component of the rotor current $I_{q,rotor}^{SFRF}$ orthogonal on the stator flux, while the reactive power *Q* control is achieved by controlling the *d*- component of the rotor current (the magnetising current) $I_{d,rotor}^{SFRF}$ collinear with the stator flux. Expression (46) illustrates that in *SFRF* the control of active and reactive power is decoupled.

The power control loop generates the reference rotor current components $I_{q,rotor}^{ref}$ and $I_{d,rotor}^{ref}$, respectively, for the rotor current control loop. The rotor current control loop generates the reference rotor voltage components. As the pulse-width modulation factor *PWM* is the control variable of converter, the output of the rotor-side converter's controller is expressed in terms of pulse-width modulation factor components $PWM_{d,rotor}^{SFRF}$ and $PWM_{q,rotor}^{SFRF}$, respectively.

Notice that the outputs of the controller are expressed in *SFRF*. As the model of the rotor-side converter is comprised in the DFIG model and expressed in the rotor reference frame (*RRF*), the outputs of the rotor-side converter controller have to be transformed from stator flux reference frame (*SFRF*) to the rotor reference frame (*RRF*), according to equation (44) and to Figure 93.

Notice that the converter active and reactive power references $P_{grid}^{conv,ref}$ and $Q_{grid}^{conv,ref}$ for the measurement grid point *M*, respectively, used as inputs by the rotor-side converter controller (see Figure 89, Figure 94), can be dynamically varied depending on each specific application.

The protection of the rotor-side converter against over-currents is an integral part of the doubly-fed induction machine model in DIgSILENT and it is discussed in (Pöller, M., 2003).

7.2.4 Grid-side converter control

The aim of the control of the grid-side converter is to maintain the DC-link capacitor voltage in a set value regardless of the magnitude and the direction of the rotor power and to guarantee a converter operation with unity power factor (zero reactive power). This means that the grid-side converter exchanges only active power with the grid, and therefore the transmission of reactive power from DFIG to the grid is done only through the stator.

Figure 95 illustrates the blocks, which are connected with the grid-side converter control block. Similar to Figure 93, the types of model blocks are also specified. The scheme contains the following blocks:

DC - voltage measurement block (built-in model) – measures the DC-voltage in the common DC-busbar of the back-to-back converter.

AC-current measurement block (built-in model) – measures the ac- current of the grid-side converter (measurement point *N* in Figure 89).

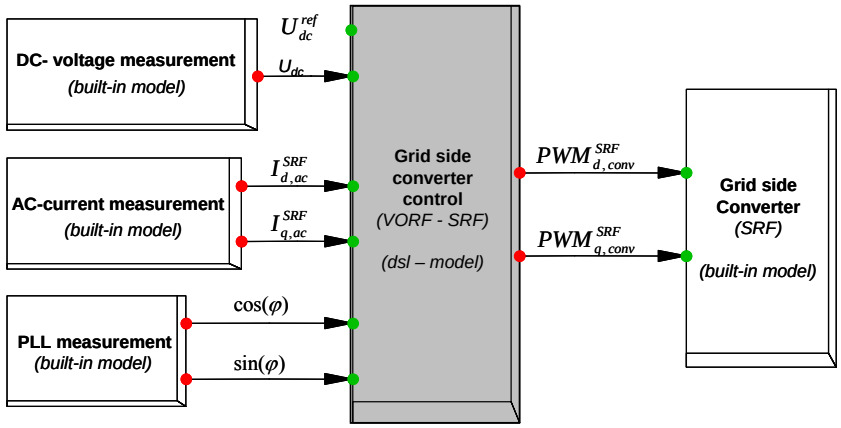

Figure 95: Inputs and outputs for the grid-side converter control in DIgSILENT.

PLL measurement block (built-in model) – measures the phase angle φ of the AC-voltage generated by the grid-side converter. The voltage phase angle is measured in order to synchronize the AC-converter voltage to the AC-grid voltage.

Grid side converter block (built-in model) –is an independent IGBT converter component in DIgSILENT's library. As mentioned before, DIgSILENT provides several control modes for the control of the converters. The typical control mode used for the grid-side converter of the DFIG is U_{DC}-*Q mode*, as its function is to regulate the DC-voltage and the reactive power.

Grid-side converter control block (dsl model) – contains the grid-side converter control, illustrated in Figure 96. Similarly to the rotor-side converter, the grid-side converter is current regulated. The DC-voltage and the reactive power are controlled indirectly by controlling the grid-side converter current.

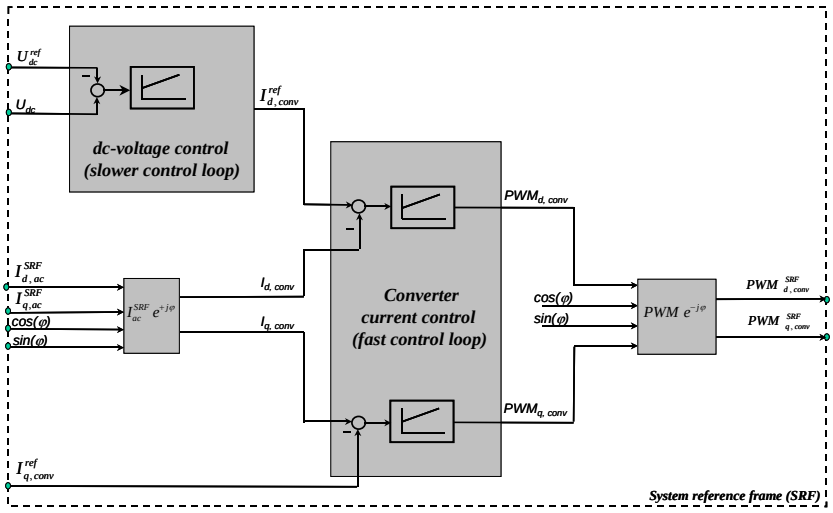

Figure 96: Grid-side converter control in DIgSILENT.

The grid-side converter control contains two PI control loops in cascade:

- a slower (outer) DC-voltage control loop
- a very fast (inner) converter current control.

The DC- voltage control loop regulates the DC-link voltage to a predefined value U_{dc}^{ref} , while the very fast current control loop regulates the converter current to the reference value specified by the slower DC-voltage controller.

The outputs of the grid-side converter controller define the magnitude and phase angle of the AC-voltage terminal of the converter. The converter current control operates in the grid converter voltage oriented reference frame *GCVRF*. The converter current is discomposed into a parallel and an orthogonal component on the grid-side converter voltage. In such reference frame the d-axis is equivalent to the active component, while the q-axis is equivalent to the reactive component. The converter current component parallel to the converter voltage (direct phase) $I_{d,conv}$ is used to control the DC-voltage (active power), while the component orthogonal to the converter voltage (quadrature phase) $I_{q,conv}$ is used to control the reactive power.

The DC-link voltage is controlled in the outer slower control loop to its setpoint value U_{dc}^{ref} by the d-converter current component. It generates the reference of the direct phase component of the converter current $I_{d,conv}^{ref}$. The reference of the quadrature component of the converter current $I_{q,conv}^{ref}$ is constant, almost proportional to the reactive power. To operate the converter with unity power factor $(Q_{conv} = 0)$ implies a zero q- current reference $I_{q,conv}^{ref} = 0$.

Notice that the converter current control loop generates the direct $PWM_{d,conv}$ and the orthogonal $PWM_{q,conv}$ component of the pulse-width modulation factor in the grid converter voltage oriented reference frame (*GCVRF)*. These components are then transformed into the system reference system *SRF*, as the grid converter requires controlling signals in *SRF*.

Notice in Figure 89 that the grid-side converter is connected in series with inductors to the line in order to smooth the converter currents. These inductors may also be integrated into the transformer.

7.3 DFIG wind turbine control strategy I

As described in Section 7.1, in the wind turbine control strategy (I) the power converter is used to control the generator speed, while the pitch system limits the power.

This control strategy is close to that described in (Wortmann B., et.al, 2000). The strongest feature of the implemented control method is that it allows the turbine to operate with the optimum power efficiency over a wider range of wind speeds. Moreover, due to the design of this control method, the transition between power optimisation mode and power limitation mode is not dominated by large power fluctuations due to small changes in generator speed.

The control strategy I are fundamentally based on the two static optimal curves, illustrated in Figure 97:

(a) Mechanical power of turbine versus wind speed
(b) Electrical power versus generator speed.

These characteristics are determined based on predefined aerodynamically data of the turbine. A parallel presentation of them, as shown in Figure 97 for a 2 MW wind turbine, provides a graphical illustration of the relation between the generated power, the wind speed and the generator speed for each operational

stage of the wind turbine. Notice in Figure 97(b) that, as long as the speed can be varied, the maximum power extracted from the wind is a cubic function of the turbine optimum speed, as expressed in (37).

Each wind turbine has some physical operational restrictions, related to the acceptable noise emission, the mechanical loads and the size and the efficiency of the generator and of the frequency converter. It is therefore necessary to limit the stationary wind turbine rotational speed, to a range given by a minimum and a rated (nominal) value $\left[\omega_{rot}^{\min}, \omega_{rot}^{nom}\right]$. Notice that, the graph Figure 97 (b) in also indicates the operational speed range $[n_{gen}^{\min}, n_{gen}^{dyn,\max}]$ for the generator speed. The generator speed can be expressed in [rad/s] or in [rpm] as follows:

$$\begin{aligned} \omega_{gen}(u) &= \eta_{gear}\,\omega_{rot}(u) && [rad/s] \\ n_{gen}(u) &= \frac{60}{2\pi}\,\omega_{gen}(u) = \frac{60}{2\pi}\,\eta_{gear}\,\omega_{rot}(u) && [rpm] \end{aligned} \qquad (66)$$

where η_{gear} is the gear-box ratio. The operational speed range $[n_{gen}^{\min}, n_{gen}^{dyn,\max}]$ covers both the stationary generator speed range as well as the dynamical generator overspeed range, which is allowed by the doubly-fed induction generator DFIG's control.

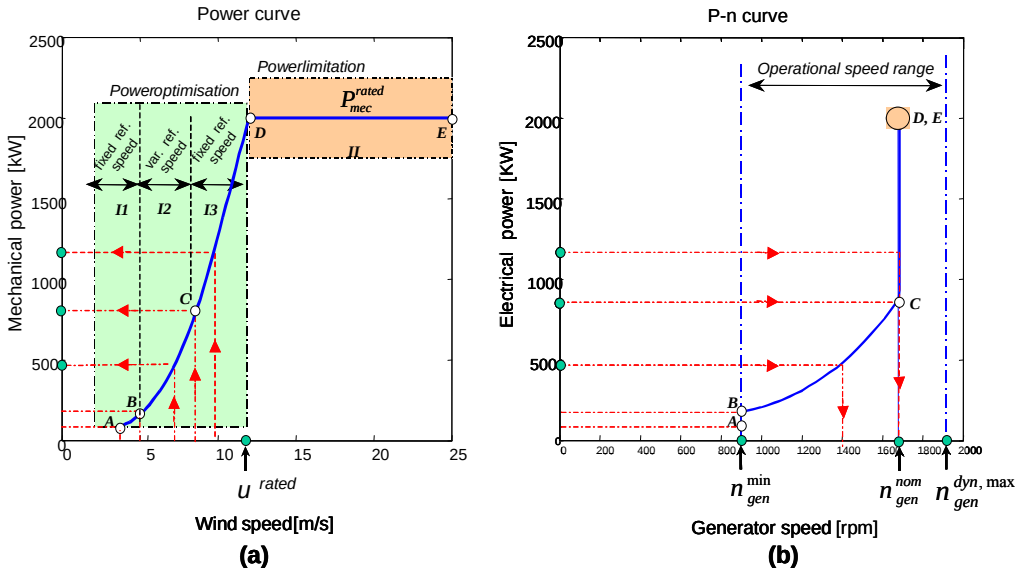

Figure 97: Two static curves used in the design of the control strategies for a doubly-fed induction generator:
(a) mechanical power versus wind speed and (b) electrical power versus wind speed.

Two control strategies for the variable speed wind turbine are indicated in Figure 97:

I. ***Power optimisation strategy*** (below rated wind speed u^{rated})– where the energy capture is optimised. It is depicted by the range *A-B-C-D*, both in Figure 97(a) and in Figure 97(b).

II. ***Power limitation strategy*** (above rated wind speed u^{rated}) – where the goal of the controller is to track the nominal (rated) power reference $P_{grid}^{rated,ref}$ of the wind turbine. It is depicted by the range *D-E* both in Figure 97(a) and in Figure 97(b).

Figure 97 points out four different control algorithms for the control of the variable speed wind turbine:

Algorithm I1. *Partial load operation with fixed reference speed at the lower limit* (power optimisation strategy zone *A-B*)

This case corresponds to the situation when the wind speeds are so small that the rotational speed is less than the lower limit $\omega_{rot} \le \omega_{rot}^{\min}$ (the generator speed $n_{gen} \le n_{gen}^{\min}$). The turbine's reference speed is therefore set to the minimal value $\omega_{rot}^{ref} = \omega_{rot}^{\min}$ and the tip speed ratio *λ(u)* is calculated by:

$$\lambda(u) = \frac{\omega_{rot}^{\min} \; R}{u} \tag{67}$$

For each determined tip speed ratio *λ(u)*, the optimal power coefficient value $C_p^{opt}(\lambda)$ and then the corresponding pitch angle θ is found in the look-up table $C_p(\theta, \lambda)$. The optimum power is therefore achieved by keeping the turbine speed at the lower limit $\omega_{rot}^{\min}$:

$$P_{mec}^{opt}(u) = \frac{1}{2} \rho \, \pi \, R^5 \, \frac{C_p^{opt}(u)}{\lambda^3(u)} \left[\omega_{rot}^{\min}\right]^3 \qquad [W] \tag{68}$$

Algorithm I2. *Partial load operation with variable reference speed* (power optimisation strategy zone *B-C*)

This case corresponds to the situation when the rotational speed is higher than the lower limit and less than the nominal rotational speed $\omega_{rot}^{\min} < \omega_{rot} \le \omega_{rot}^{nom}$ (the generator speed $n_{gen}^{\min} < n_{gen} \le n_{gen}^{nom}$). The goal here is to maximise the energy capture by tracking the maximum power coefficient $C_p^{\max}$ curve. The maximum power coefficient value $C_p^{\max}$ corresponds to one pitch angle θ_{opt} and one tip speed ratio λ_{opt}. The pitch angle is therefore kept constant to the optimal value θ_{opt}, while the tip speed ratio is tuned to the optimal value λ_{opt} over different wind speeds by adapting the rotor speed ω_{rot} to its reference, expressed by:

$$\omega_{rot}^{ref}(u) = \frac{\lambda_{opt} \; u}{R} \qquad [rad/s] \tag{69}$$

The maximal mechanical power is therefore achieved by tracking the reference rotational speed:

$$P_{mec}^{\max}(u) = \frac{1}{2} \rho \, \pi \, R^5 \, \frac{C_p^{\max}}{\lambda_{opt}^3} \left[\omega_{rot}^{ref}(u)\right]^3 \qquad [W] \tag{70}$$

Algorithm I3. *Partial load operation with fixed reference speed at the higher limit* (power optimisation strategy zone *C-D*)

This case corresponds to the situation when the turbine speed is restricted to the nominal value $\omega_{rot}^{ref} = \omega_{rot}^{nom}$ and when the generated power is less than the rated value ($P_{mec} < P_{mec}^{rated}$). The control algorithm is similar to ***Algorithm I1*** (presented for zone *A-B*), with the only difference that the tip speed ratio, the optimal power coefficient value $C_p^{opt}(\lambda)$, the optimal pitch angle θ and the op-

timal power are determined based on ω_{rot}^{nom} instead for $\omega_{rot}^{\min}$. In this case, the highest efficiency is obtained by operating the turbine at nominal speed ω_{rot}^{nom}.

Algorithm II. *Full load operation* (power limitation strategy zone *D-E*)

This case corresponds to the situation of wind speeds higher than the rated wind speed. The reference output power is the rated mechanical power $P_{mec}^{ref} = P_{mec}^{rated}$ while the reference rotor speed is the nominal rotor speed $\omega_{rot}^{ref} = \omega_{rot}^{nom}$. Thus, for each wind speed *u*, the power coefficient is calculated as:

$$C_p(\lambda) = \frac{2\, P_{mec}^{rated}\, \lambda^3(u)}{\rho\, \pi\, R^5 \left[\omega_{rot}^{nom}\right]^3} \tag{71}$$

Once the power coefficient value $C_p(\lambda)$ is calculated and the tip speed ratio $\lambda(u) = \omega_{rot}^{nom} R/u$ is known, the static pitch angle θ can then be determined by interpolation in the power coefficient table $C_p(\theta,\lambda)$.

An example of the pitch angle and rotor speed versus wind speed, determined based on the presented control strategies for a variable speed 2 MW wind turbine, is shown in Figure 98. Similar to Figure 97, Figure 98 also points out the wind turbine operation ranges (*A-B*, *B-C*, *C-D*, *D-E*). The pitch angle values in the power optimisation strategy are all found close to zero for the given wind turbine, while at higher wind speeds in order to limit the power, the pitch angle is increasing by a non-linear function. The static reference values of the rotor speed are, as expected, varying in zone *B-C* and otherwise are kept constant. However, as the DFIG control design allows overspeed in the case of a wind gust, the rotor speed can vary dynamically in zone C-D-E. Therefore, the ability to vary the rotor speed ω_{rot} is used in both strategies (power optimisation and power limitation), but it is mostly exploited below rated wind speed (in the power optimisation strategy). The ability to vary the pitch angle θ with wind speed is mostly used above rated wind speed to prevent over rated power production.

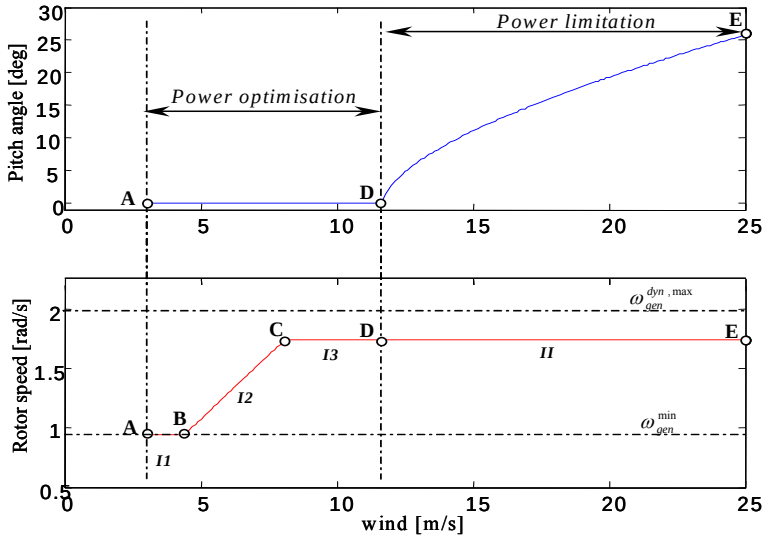

Figure 98: Generic static pitch angle and rotor speed versus wind speed - result of the control strategies.

As illustrated in Figure 89, this wind turbine control strategy contains two controllers, which are cross-coupled to each other:

1. Speed controller
2. Power limitation controller

The design of these two controllers is based on the previous described control strategies. The speed controller is the main controller in the power optimisation strategy, while in the power limitation strategy both controllers are active and cross-coupled to each other. This interconnection can be exemplified as follows.

If the wind speed is less than the rated wind speed u^{rated}, the pitch angle is kept constant to the optimal value θ_{opt}, while the generator speed ω_{gen} is adjusted by the wind turbine control in such a way that the maximum power is captured out of the wind. If a wind gust appears, the rotor speed ω_{rot} and thus also the generator speed ω_{gen} will increase due to the increased aerodynamic torque. In this moment, the speed control loop reacts by increasing the power reference $P_{grid}^{conv,ref}$ to the DFIG control, see Figure 99. If the wind speed increases further beyond the rated wind speed, then the power limitation control loop, see Figure 100, reacts by increasing the pitch angle to prevent the power generation becoming too large. Meanwhile, the speed control loop controls the rotor speed to its nominal value, but allows rotor speed dynamic variations in a predefined speed range. The changes in the aerodynamic power are thus absorbed as changes in the rotational speed instead of as changes in torque and therefore the impact of the wind speed variations on the drive train loads is reduced.

7.3.1 Speed controller (I)

The *speed controller* has as main tasks:

1. to achieve the optimum power by keeping the generator speed at the lower limit $\omega_{gen}^{\min}$ (***Algorithm I1***) in power optimisation *A*-*B* zone with fixed low reference speed limit.

2. to keep the optimal tip speed ratio λ_{opt} over different wind speeds *u*, by adapting the steady state generator speed to its reference ω_{gen}^{ref} (***Algorithm I2***) in power optimisation *B*-*C* zone with variable reference speed.

3. to control the generator speed to its nominal value, allowing however dynamic variations in the predefined speed range indicated in Figure 97(b). For wind speeds above rated wind speed u^{rated} (in power limitation), the speed control loop prevents the rotor/generator speed becoming too large.

Figure 99 shows the implemented speed control loop. It has as input the difference between the reference generator speed and the measured generator speed. The reference generator speed ω_{gen}^{ref} is obtained from the predefined static characteristic (see Figure 97(b)), and it corresponds to the generator speed at which the measured active power P_{grid}^{meas} on the grid is optimal. The error $\Delta\omega_{gen} = \omega_{gen}^{ref} - \omega_{gen}^{meas}$ is sent to a PI controller and then further to a power gradient limitation block. Unbalance between turbine torque and generator torque will result in an accelerating torque until the desired speed is reached. The output of the speed controller is the reference power value on the grid $P_{grid}^{conv,ref}$ to the DFIG control.

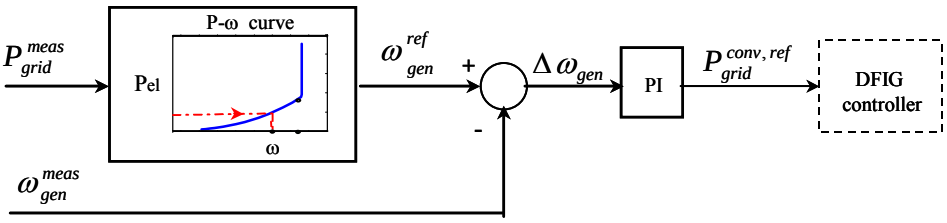

Figure 99: Speed controller of the wind turbine control.

Notice that the speed controller is active both in the power optimisation and power limitation operating modes. The parameters of the speed controller are changed depending on the wind turbine-operating mode (power optimisation or power limitation).

7.3.2 Power controller (I)

The *power limitation controller* has as task to increase or decrease the pitch angle in the power limitation strategy, i.e. in order to limit the generated power to the rated power.

Figure 100 shows the power limitation control loop. The error signal $\Delta P = P_{grid}^{meas} - P_{grid}^{rated,ref}$ based on the measured power in the grid point M, is sent to a PI-controller. The PI controller produces the reference pitch angle θ_{ref}. This reference is further compared to the actual pitch angle θ and then the error $\Delta\theta$ is corrected by the servomechanism. In order to get a realistic response in the pitch angle control system, the servomechanism model accounts for a servo time constant T_{servo} and the limitation of both the pitch angle and its gradient. The output of the power limitation controller is the pitch angle of the blades.

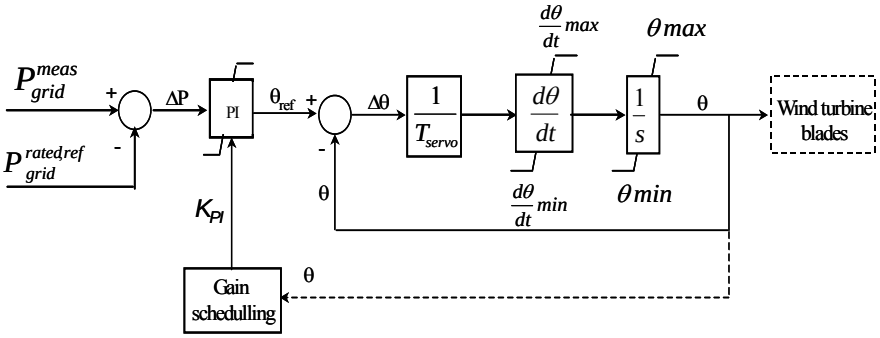

Figure 100: Power limitation controller of the wind turbine control, which controls the pitch.

Notice that both speed and power limitation controllers do not need a wind speed measurement. Only the generator speed and the generator active power are required. Ideally, the control parameters would be chosen as a function of the wind speed, but this is not an appropriate procedure due to the fact that it is not possible to measure the wind speed precisely. Assuming that the wind turbine system is well controlled, then the pitch angle and the active power can be used as gain-scheduling parameters instead of wind speed. Therefore, the implementation of the gain scheduling is performed based on knowledge of the pitch angle, which can be thus used to express the non-linear aerodynamic amplification in the system.

The non-linear variation of the pitch angle versus wind speed for high wind speeds, illustrated in Figure 98, implies the necessity of a non-linear control (gain scheduling) – as indicated in Figure 100. A linear control would result in instabilities at high wind speeds.

The total gain of the system in the power control loop K_{system}, can be expressed as a proportional gain K_{PI} in the PI controller times aerodynamic sensitivity of the system $\frac{dP}{d\theta}$:

$$K_{system} = K_{PI} \frac{dP}{d\theta} \tag{72}$$

The aerodynamic sensitivity $\frac{dP}{d\theta}$ of the system depends on the operating conditions (the setpoint power value, the wind speed or the pitch angle). Therefore, in order to maintain the total gain of the system K_{system} constant, the proportional gain of the PI controller K_{PI} is changed in such a way that it counteracts the variation of the aerodynamic sensitivity $\frac{dP}{d\theta}$. The gain of the controller K_{PI} must therefore incorporate information on the dependency of the variation of the power with the pitch angle. The variation of the aerodynamic sensitivity with the pitch angle for a 2 MW wind turbine is illustrated in Figure 101(a). It increases numerically (absolute value) with the pitch angle and it can vary with a factor up to 10.

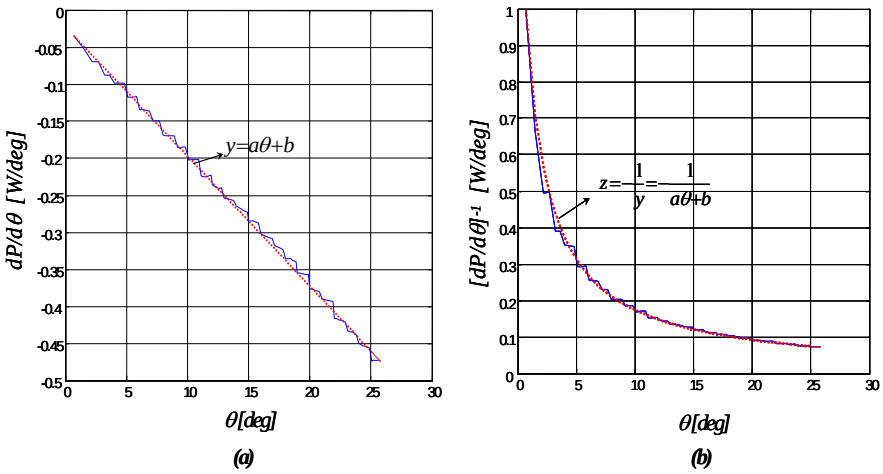

Figure 101: Sensitivity function and the inverse sensitivity function of the wind turbine. (a) sensitivity function dP/dθ *versus pitch angle* θ *. (b) inverse sensitivity function* $[\mathrm{dP/d\theta}]^{-1}$ *versus pitch angle* θ.

Observe that the variation of the aerodynamic sensitivity is almost linear in the pitch angle θ and therefore a linear expression with the parameters a and b can be estimated:

$$\frac{dP}{d\theta} = a\theta + b \tag{73}$$

This linear description makes it possible to determine the reciprocal of the aerodynamic sensitivity, defined as follows:

$$\left[\frac{dP}{d\theta}\right]^{-1} = -\frac{1}{a\theta + b} \tag{74}$$

where the negative sign compensates for the negative ramp of the aerodynamic sensitivity and thus assures that the sign of the total gain of the system does not change. Notice that the reciprocal sensitivity function $\left[\frac{dP}{d\theta}\right]^{-1}$, illustrated in Figure 101(b), is non-linear with the pitch angle. It is used in the definition of the controller gain K_{PI} to counteract the mentioned variation, as follows:

$$K_{PI} = K_{basis} \left[\frac{dP}{d\theta}\right]^{-1} \tag{75}$$

where K_{basis} is the constant designed proportional gain of the PI- controller, determined to be appropriate for one arbitrary wind speed. Notice that the more sensitive the system is (larger pitch angles θ / higher wind speeds) the smaller the gain for the controller should be and vice versa. The introduction of the gain scheduling enables the PI- controller to perform an adequate control over the whole wind speed range.

7.3.3 Cross-coupled control

Both the speed control loop and the power control loop are cross-coupled in the power limitation strategy. Notice that these two strategies do not need a wind speed measurement. Only the generator speed and active power are required.

The interconnection between speed control loop and power control loop can be exemplified as follows. If the wind speed is less than the rated wind speed u^{rated}, the pitch angle is kept constant to the optimal value θ_{opt}, while the generator speed ω_{gen} is adjusted by the frequency converter control in such a way that the maximum power is obtained. If now a wind gust appears, the rotor speed ω_{rot} and thus also the generator speed ω_{gen} are increasing due to the increased aerodynamic torque, and the speed control loop reacts by increasing the power reference $P_{grid}^{conv,\,ref}$ (in Figure 99). If the wind speed increases further over the rated wind speed, then the power control loop reacts by increasing the pitch angle to prevent the power generation becoming too large. Meanwhile, the rotor speed is also prevented to become too large by the speed control loop, which tries to keep the rotor speed to its nominal value. DFIG control has the advantage to permit a dynamical variation range of the generator/rotor speed around the nominal value. Thus the impact of the wind speed variations on the drive train loads is reduced. The changes in the aerodynamic power are absorbed as changes in the rotational speed instead of as changes in torque.

7.3.4 Simulation results (I)

Different scenarios are simulated to asses the performance of both the DFIG controller and of the overall control of the variable speed /variable pitch wind turbine.

A. **DFIG control**

Using the stator flux control approach, the active power control is decoupled from reactive power control. As mentioned before the active and reactive power can be controlled using the impressed rotor currents in the stator flux reference frame. Thus, the active power control is achieved by controlling the rotor cur-

rent q- component $I_{q,rotor}^{meas}$ orthogonal to the stator flux, while the reactive power control is achieved by controlling the *d*- component of the rotor current referred to the stator flux $I_{d,rotor}^{meas}$. Figure 102 illustrates the control of the active power on the grid when a step in the reference active power signal $P_{grid}^{conv,ref}$ on the grid is imposed and when the reference reactive power signal $Q_{grid}^{conv,ref}$ remains unchanged.

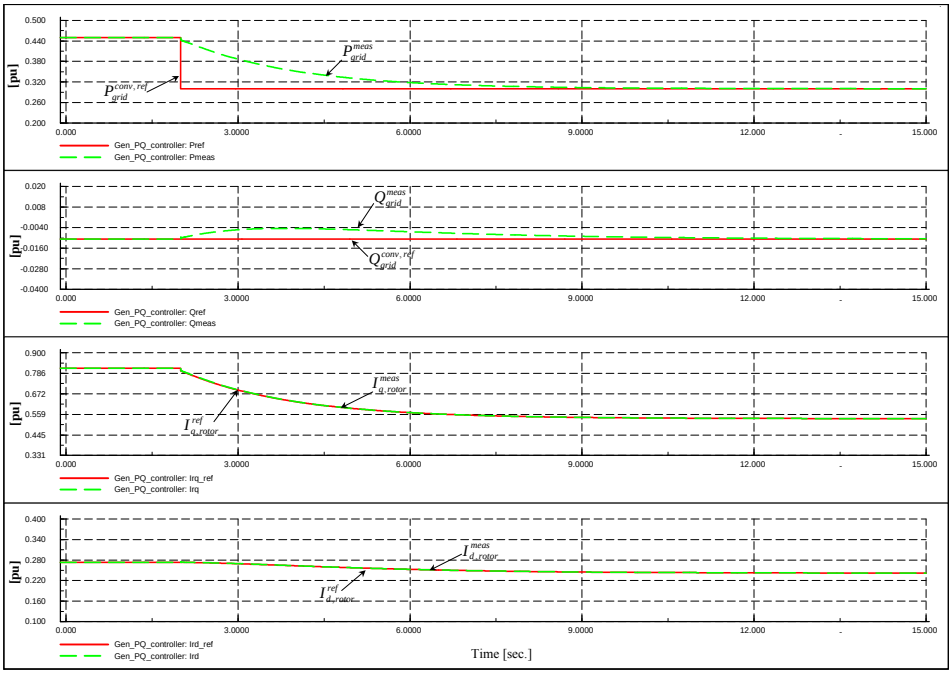

Figure 102: Decoupled control of active and reactive power of DFIG.

The active power step response, measured on the grid (30 kV), exhibits good dynamic performance. A little coupling with the reactive power control is observed in the transient phase. However, in steady state the reactive power is not affected by the active power step, as it is back to its reference value. As expected, the step in the reference of the active power is reflected only in the q-component and not in the d- component of the rotor current, as the reactive power is controlled by the d- component.

B. **Power flow inside DFIG**

Both Figure 103 and Figure 104 illustrate the results of a simulation, where a fictive non-turbulent wind speed with fixed mean value and a sinusoidal variation with a 3p frequency is used. A variable speed DFIG wind turbine with 2 MW rated power is considered. A step in the mean speed value from 7 m/s to 9 m/s is performed to force the system from sub-synchronous to over-synchronous operation. The purpose of this simulation is to illustrate:

- the power flow through the grid, stator and rotor when the DFIG changes between sub-synchronous and over-synchronous operations, due to a step in the wind speed.
- the filter effect of the mechanical 3p fluctuations in the electrical power.

Notice in Figure 103 that during sub-synchronous operation the power delivered to the grid is less than that delivered by the stator P_{stator}, as in the rotor circuit the power is flowing from the grid to the rotor via power converter ($P_{rotor}<0$). Meanwhile in over-synchronous operation, the power delivered to the grid is higher than that from the stator because of the power contribution from

the rotor. The rotor power flows from the rotor to the grid in over-synchronous operation ($P_{rotor} > 0$).

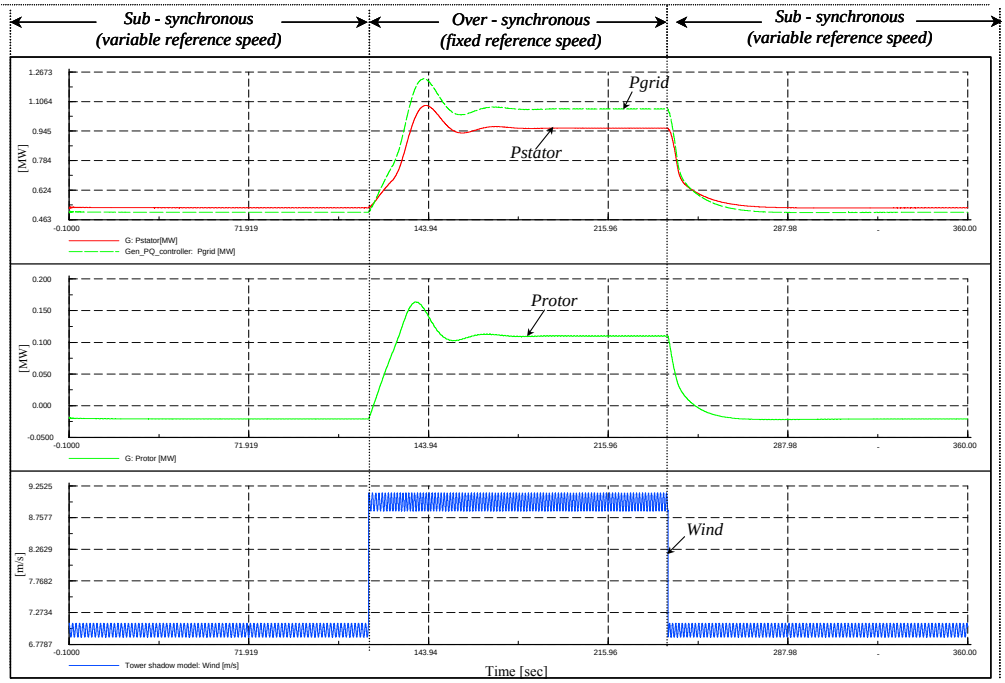

Figure 103: Simulated power through the grid, stator and rotor in sub-synchronous and over-synchronous operations.

The 3p fluctuations of the wind speed are present in the mechanical part of the system, i.e. in the aerodynamic torque, but not on the electrical part, i.e. in the electrical torque – see Figure 104. The 3p fluctuations in the wind are thus not visible in the electrical power. They are reduced substantially by the control of the DFIG. For this wind speed range (7 m/s to 9 m/s), the wind turbine operates in the power optimisation mode (zone B-C-D), where the speed controller seeks to maximise the power captured from the wind according to Figure 97(b). It thus adjusts the generator speed to its predefined reference (variable or fixed) to be able to capture as much energy from the wind as possible. The power limitation controller is not active here, as the rated power is not reached. The pitch angle is kept constant to its optimal value determined with the control ***Algorithm I2*** and ***I3***.

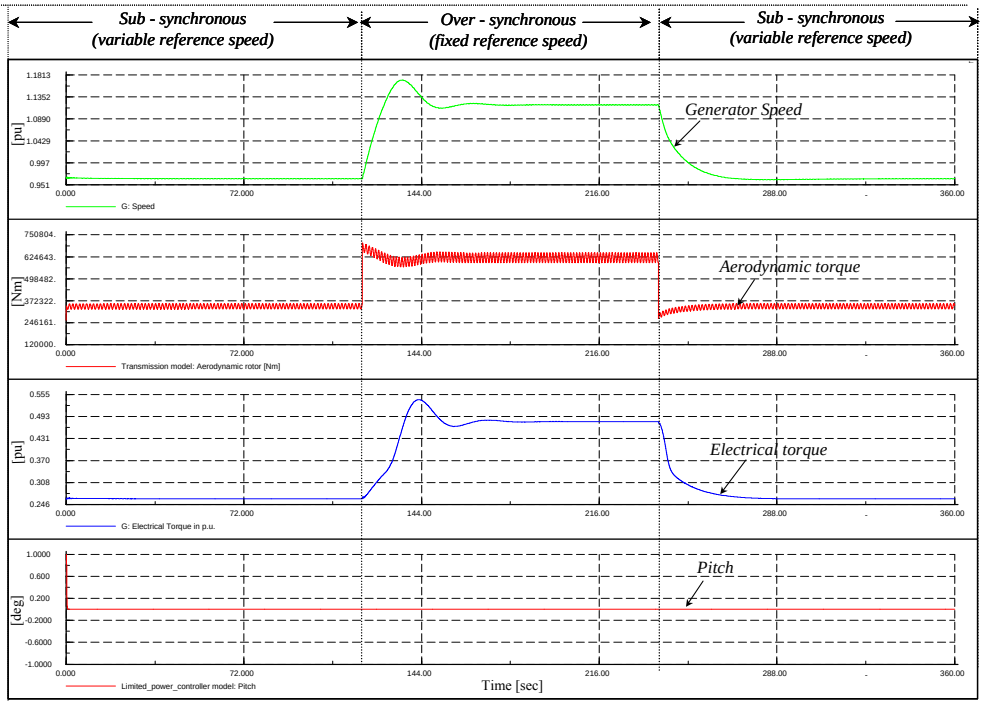

Figure 104: Simulated generator speed, aerodynamic torque, electrical torque and pitch angle.

C. **Overall control of the wind turbine**

Both Figure 105 and Figure 106 illustrate how the control algorithms are working at different operating conditions. Again a variable speed wind turbine with a rated power of 2 MW is used. The rated wind speed is 11.5 m/s and the rated generator speed ω_{gen}^{nom} is 1686 rpm. Typical quantities are shown: wind speed, generator speed and reference generator speed, the pitch angle and the generator power on the grid.

Figure 105 illustrates the simulation operation at 7 m/s mean value turbulent wind speed with turbulence intensity of 10%. This operation corresponds to the power optimisation with variable generator speed reference (zone B-C in Figure 97).

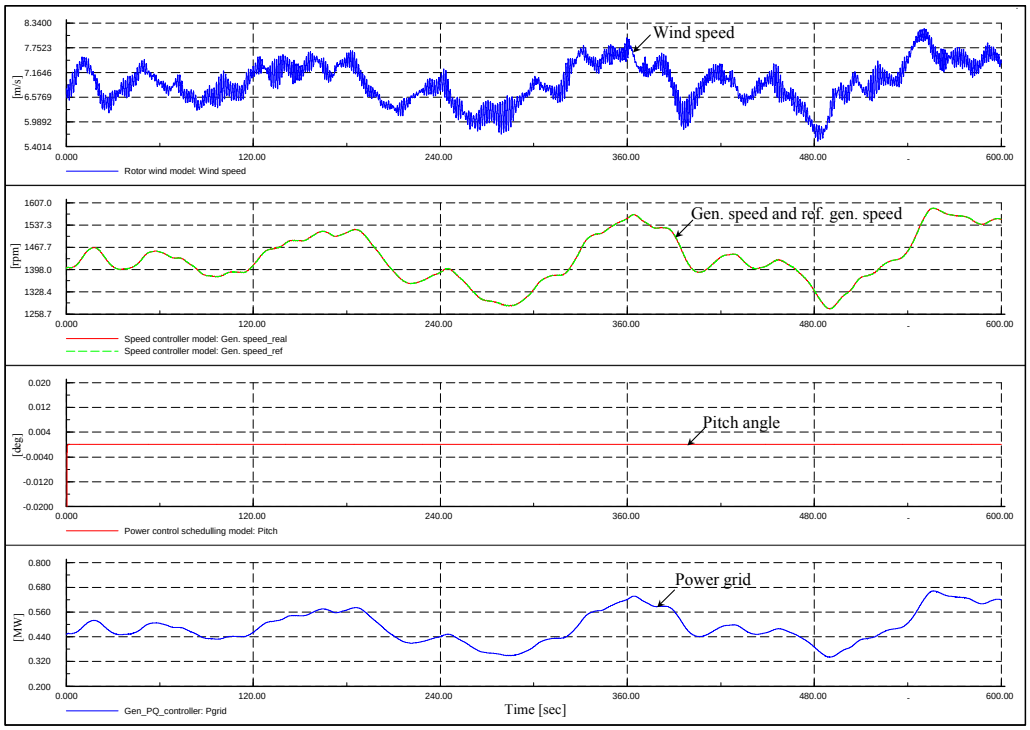

Figure 105: Simulation with turbulent wind speed, with mean 7m/s and turbulence intensity of 10%.

In power optimisation, the main turbine controller is the speed controller. As the rated power is not reached, the power limitation controller is not active. The speed controller has here to be strong and fast in order to seek to the maximum power. It has to assure that the generator speed follows very well the variable generator speed reference in order to be able to absorb the maximum energy from the wind. The speed reference is generated based on the static curve illustrated in graph (b) of Figure 97 and it corresponds to the generator speed for which the measured power is optimal. As expected for this wind speed range (7 m/s mean value), the pitch angle is not active, being kept constant to its optimal value (i.e. zero for the considered wind turbine). Notice that the fast oscillations in the wind speed are completely filtered out from the electrical power.

Figure 106 shows the simulation results when a turbulent wind speed with a mean value of 18 m/s and a turbulence intensity of 10% is used. In order to illustrate the elasticity of the variable speed DFIG wind turbine, some gusts about 5 m/s up and down, respectively, are introduced in the wind speed at each 150s.

This simulation case corresponds to the power limitation strategy, where both the speed controller and the power limitation controller are active. The power limitation control loop is strong and fast, while the speed control loop is deliberately much slower, allowing dynamic variations of the generator speed in the speed range permitted by the size of the power converter.

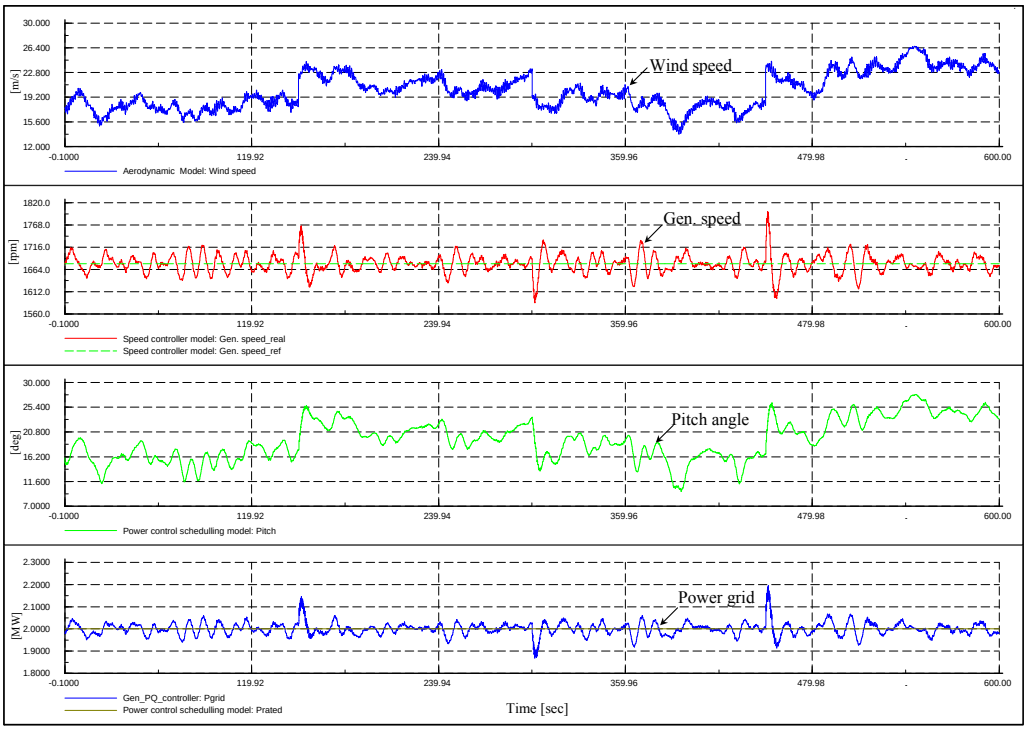

Figure 106: Simulation with turbulence wind speed, with mean speed 18 m/s, turbulence intensity 10% and gusts.

The power limitation controller changes the pitch angle to keep the rated power, while the speed controller prevents the generator speed from becoming too high. Contrary to the power optimisation, illustrated in the previous simulation, the speed controller allows here deviations of the generator speed from its reference (rated) value. For example, at the time instant t=150 s, the wind speed rapidly reaches 22 m/s. The generator speed increases quickly due to the increased aerodynamic torque. The electrical power increases too, until the pitch controller reacts modifying the pitch angle. The pitch controller is not fully capable of capturing this fast wind speed change. The pitch angle follows the slow variation in the wind speed, while fast gusts in the wind speed are absorbed as variation (peaks) in generator speed. The rotational speed of the turbine rotor is thus allowed to increase storing energy into the turbine's inertia.

7.4 DFIG wind turbine control strategy II

As described in Section 7.1, in the wind turbine control strategy (II) the power converter controls the power, while the pitch system prevents the overspeeding of the generator.

This second control strategy is expected to be closer to the real controllers in DFIG wind turbines, although this is not easy to clear up because the actual control algorithm is kept confidential by the wind turbine industry.

The two controllers of the control strategy (II), sketched in Figure 90, are as follows:

- **Speed controller** – controls the generator speed to its reference value by acting on the pitch angle. It has as task to control the generator speed at high wind speeds i.e. to change the pitch angle in order to prevent the overspeeding of the generator. At low wind speeds, the pitch angle is kept constant to a optimal value.

- **Power controller** – assures the power reference by acting on the reference to the DFIG control level. It generates the active power reference signal for the active power control loop, performed by the rotor-side converter controller in DFIG control level. This reference signal is determined from the predefined characteristic P-ω look-up table, illustrated in Figure 107, based on filtered measured generator speed. This characteristic is based on aerodynamical data of the wind turbine's rotor and its points correspond to the maximum aerodynamic efficiency. As illustrated in **Figure 107**, this characteristic is truncated at rated speed, so no speed reference over rated speed is provided.

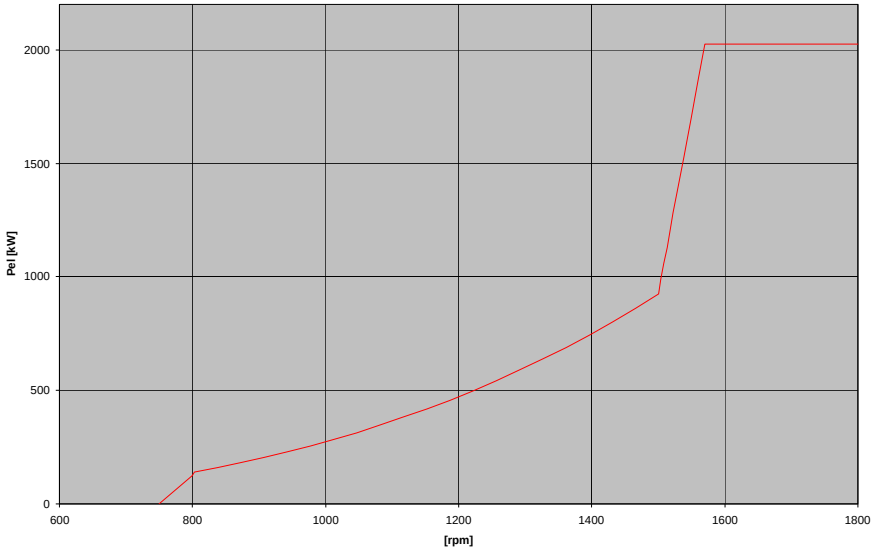

Figure 107: Maximum power tracking (MPT) characteristic used for DFIG wind turbine.

Both the speed controller and the maximum power-tracking controller are active in the power limitation strategy, while only maximum power tracking controller is active in the optimization power strategy. In the case of high wind speeds there is a cross-coupling between these two controllers.

Figure 108 illustrates explicitly the speed controller, the maximum power tracking controller and the rotor-side converter controller. The grid-side converter controller is out of interest in the present study and therefore it is shown as a "black box".

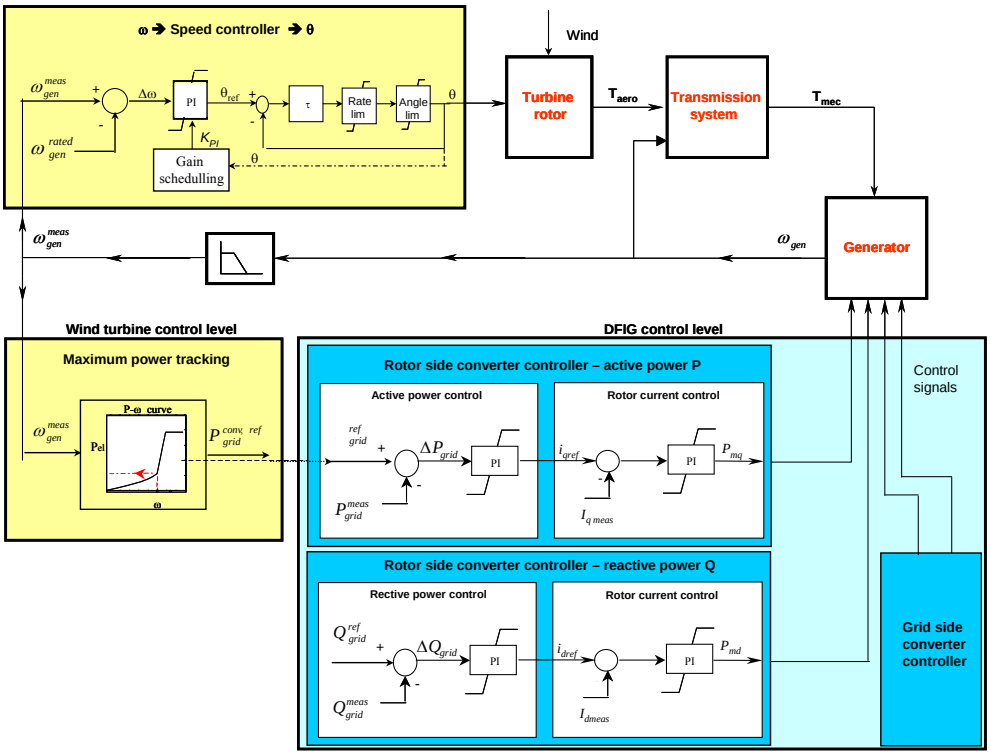

Figure 108: Wind turbine control level.

In the rotor-side converter control, there are two independent control braches, one for the active power control and the other for reactive power control. Each branch consists of 2 controllers in cascade. Only the active power control loops are relevant in the present study.

Notice that all these controllers, except maximum power tracking controller, are basically PI controllers. Both the speed controller and the maximum power tracking have as input the filtered measured generator speed. The generator speed is measured and a low-pass filter is used to avoid that the free-free frequency in the transmission system is amplified through the control system.

7.4.1 Speed controller (II)

The error between the filtered measured generator speed and the rated generator speed is thus sent to the PI speed controller. The output of this PI-controller is used as reference pitch signal θ_{ref} to the pitch system. In order to get a realistic response in the pitch angle control system, the servomechanism model accounts for a servo time constant T_{servo} and the limitation of both the pitch angle (0 to 30 deg) and its gradient (± 10 deg/s). Thus the reference pitch angle θ_{ref} is compared to the actual pitch angle θ and then the error $\Delta\theta$ is corrected by the servomechanism.

A gain scheduling control of the pitch angle, as described in Section 7.3.2, is implemented in order to compensate for the existing non-linear aerodynamic characteristics.

Assuming that the dynamic behavior of the system can be approximated with a second order system behavior, then the parameter design of the PI speed controller can be based on the transient response analysis for a second order system:

$$\frac{K}{I s^2 + D s + K} = \frac{\omega_0^2}{s^2 + 2\xi\omega_0 s + \omega_0^2} \qquad (76)$$

where *I, K* and *D* denote the system inertia, stiffness and damping, respectively. Hence the natural frequency and the damping ration can be expressed as: $\omega_0 = \sqrt{\frac{K}{I}}$ and $\xi = \frac{1}{2}\frac{D}{I\omega_0} = \frac{D}{2K}\omega_0$, respectively.

In the literature, two main parameterizations of the PI controller are applied:

♦ *PI controller - parameterization 1:*

$$y = (K_p + \frac{K_i}{s})\, u \tag{77}$$

where the proportional and integral gain can be expressed (see Stig Øje's calculations) as:

$$K_i = \frac{K\Omega_0}{N_{gear}\frac{30}{\pi}}\left[-\frac{dP}{d\theta}\right]^{-1} \tag{78}$$

$$K_p \cong 2\xi\ \frac{K_i}{\omega_0}$$

In this PI controller parameterization form, the integral gain K_i is proportional to the stiffness *K* of the system, while the proportional gain K_p is proportional with the damping of the system $D = 2\xi K/\omega_0$. Notice that when this parameterization is used, both controller parameters contain gain scheduling, i.e. they vary with the reciprocal sensitivity function $\left[-\frac{dP}{d\theta}\right]^{-1}$.

♦ *PI controller - parameterization 2:*

$$y = K_p\ (1 + \frac{1}{sT_i})\, u \tag{79}$$

where the integral time and the proportional gain are expressed as:

$$T_i = \frac{K_p}{K_i} = \frac{2\xi}{\omega_0} \tag{80}$$

$$K_p \cong \frac{2\xi}{\omega_0}\ \frac{K\Omega_0}{N_{gear}\frac{30}{\pi}}\left[-\frac{dP}{d\theta}\right]^{-1}$$

This parameterization of the PI controller is typically used in control systems. Notice that here only one parameter, i.e. the proportional gain K_p, has a proportional variation with the reciprocal sensitivity function $\left[-\frac{dP}{d\theta}\right]^{-1}$, while the integral time T_i can be directly determined based on design parameters (damping ration ξ and natural frequency ω_0).

The implementation in DIgSILENT of the PI controllers is using the *parameterization 2*. As design parameters in the controllers, there are used the damping ratio $\xi = 0.66$ and the natural frequency about 0.1 Hz (i.e. $\omega_0 = 0.6$). Using the expressions (6) and (12), the proportional gain K_{basis} of the PI- controller can be expressed as:

$$K_{basis} = \frac{2\xi}{\omega_0} \frac{K\Omega_0}{N_{gear}\frac{30}{\pi}} \quad (81)$$

Based on design data (ξ and ω_0) and on the equations (11) and (13), the parameters of the PI speed controller (SC) become: $K_p^{SC} = 850$ (normalized) and $T_i^{SC} = 2.2$.

7.4.2 Power controller (II)

The active power reference $P_{grid}^{conv,\,ref}$ signal, determined from the maximum power tracking look-up table, is further used in the active power control on the grid, performed by the rotor-side converter controller.

The aim of the rotor-side converter is to control independently the active and reactive power. As mentioned before, the attention, in this report, is mainly drawn to the active power control. The active power is controlled indirectly by controlling the impressed rotor current. As illustrated in Figure 108, the active power control, in DIgSILENT, contains two control loops in cascade: a slower (outer) power control loop and a fast (inner) rotor current control loop. The slower power control loop has thus as output the reference rotor current signal, which is used further by the fast current control loop. The parameters of the PI controllers in the rotor-side converter are the following:

- for the power controller (PC): $K_p^{PC} = 0.1$ and $T_i^{PC} = 0.1$
- for the current controller (CC): $K_p^{CC} = 1$ and $T_i^{CC} = 0.01$

Notice that these two control loops existing in the rotor-side converter controller and taking care of the active power on the grid, are not implemented in HAWC and Flex5.

7.4.3 Simulation results (II)

In order to evaluate the performance of variable speed wind turbine controller implemented in power system simulation DIgSILENT a set of step response simulations with deterministic wind speed (no turbulence, no tower shadow) are performed. Typical quantities versus of time are shown: wind speed in [m/s], pitch angle in [deg], generator speed in [rpm] and the generator power in [MW]. For comparison purpose, the scales of the figures have been kept similar to those used in the FLEX5 simulations. Unless it is specified, the simulations are performed using the parameters of the PI controllers, mentioned before.

In Figure 109, Figure 110 and Figure 111, the wind speed is stepped-up with 1m/s every each 20 seconds.

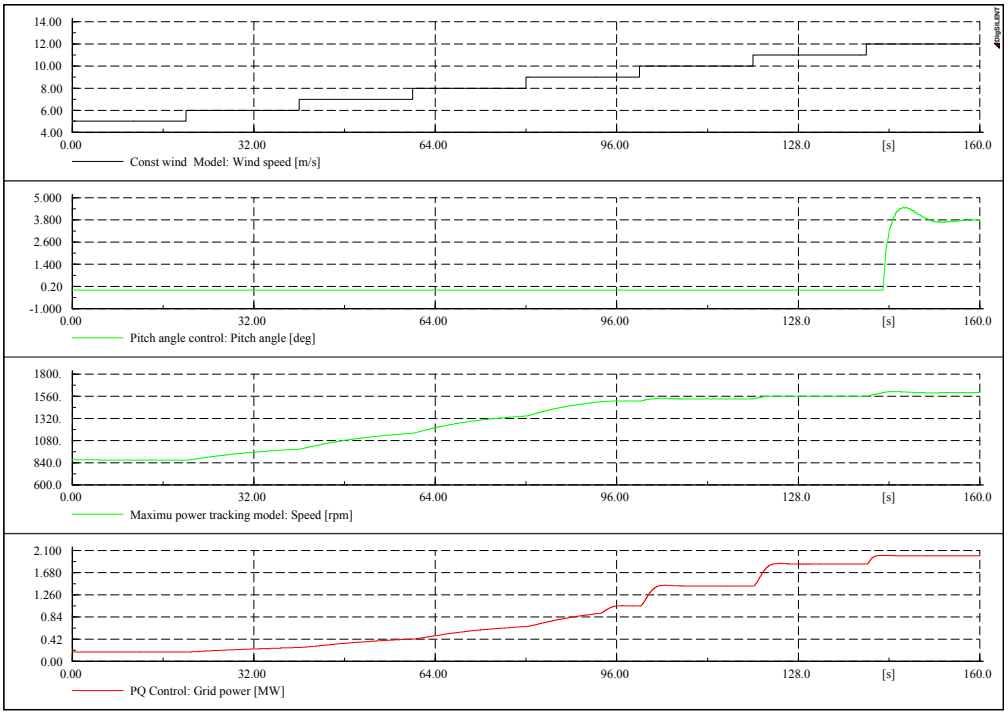

Figure 109: Step in wind from 5m/s to 12m/s.

In the power optimization strategy (at low wind speeds less than 12m/s), as illustrated in Figure 109, the speed controller is passive, keeping the pitch angle constant to the optimal value (i.e. zero for the considered wind turbine). Meanwhile, the power controller controls the active power to the active power reference signal provided by the maximum power tracking look-up table. The generator speed is thus continuously adapted to the wind speed, in such a way that it is extracted maximum power out of wind. Notice that the response time in the steps is bigger at lower wind speeds then at higher wind speeds.

At higher wind speeds than 12 m/s, illustrated in Figure 110, both the speed controller and the active power controller are active.

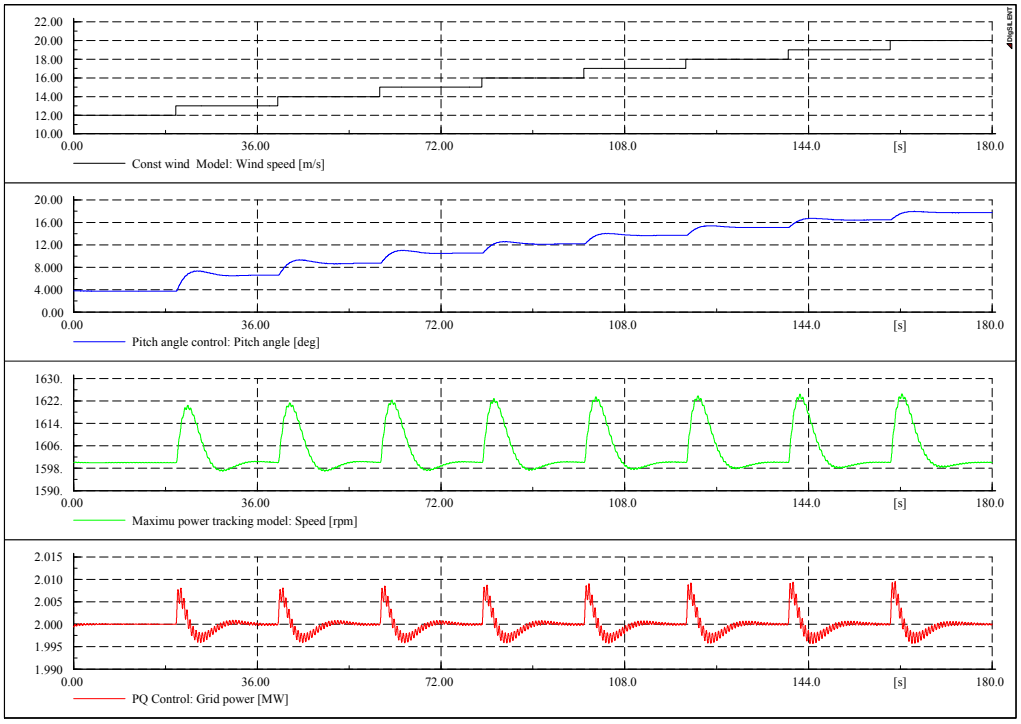

Figure 110: Step in wind from 12 m/s to 20 m/s.

The steps in the wind speed yield changes in both the pitch angle and the generator speed. The step response of the pitch angle and generator speed does not present big overshoots and oscillations (fast in steady state). Remark also that the response of the generator speed is almost identical over the whole wind range between 12m/s and 20m/s, a fact that indicates that the gain scheduling in the speed controller is working properly. The power controller keeps the active power to 2MW with a small deviation about 1%.

By changing the parameters of the frequency converter controller, the performance of the system can be improved. Figure 111 illustrates the influence of the parameter tuning in the frequency converter controller. A similar simulation to that shown in Figure 110 is shown in Figure 111, but with a stronger integral action of the controllers in the frequency converter, i.e. $T_i^{PC} = 0.01$ and $T_i^{CC} = 0.001$. This action has as result an error in the control of the power less than 1 per thousand, while the other signals are unchanged.

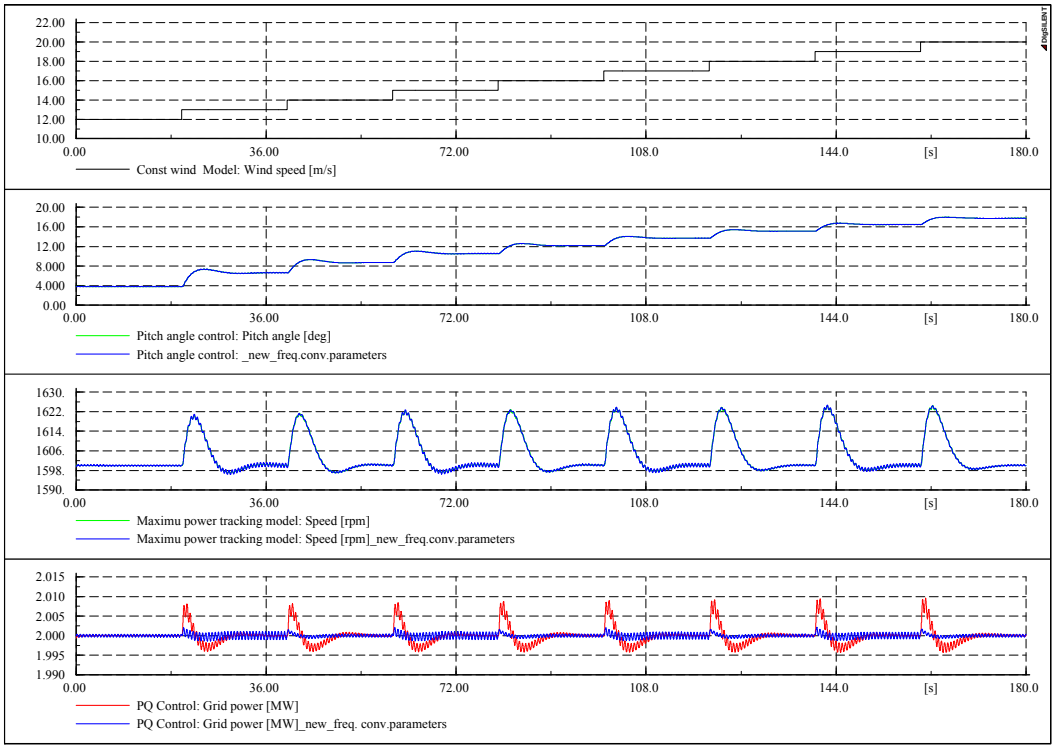

Figure 111: Influence of control parameters of the frequency converter.

Figure 112 and Figure 113 illustrate the simulations where the wind speed is stepped-down from 20 m/s to 4 m/s with 1 m/s step and 2m/s step, respectively.

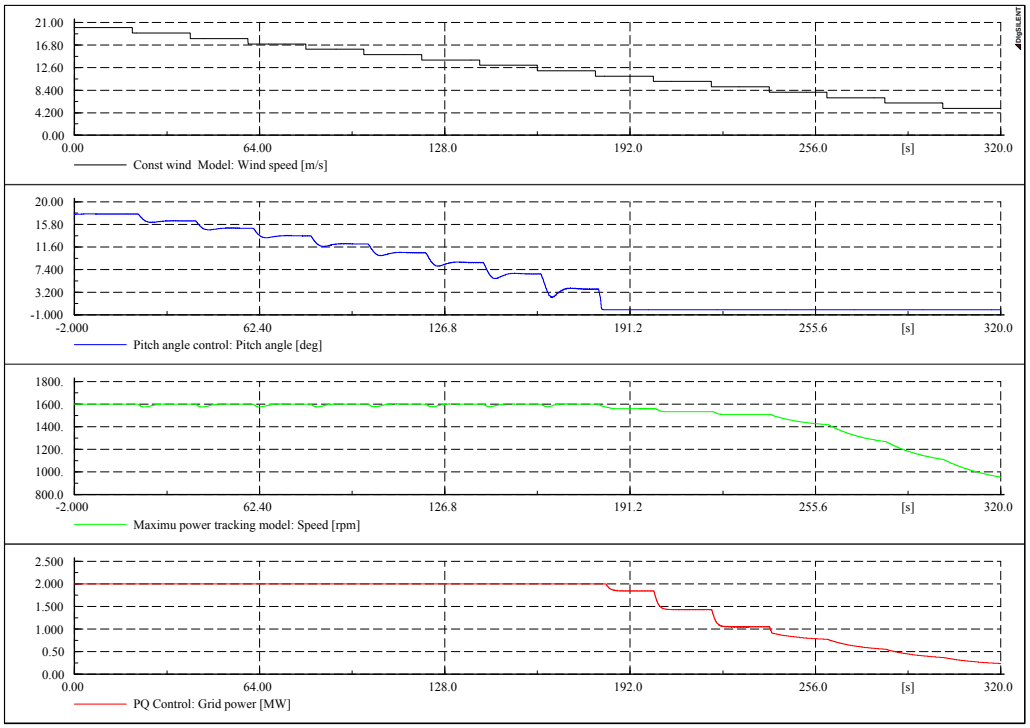

Figure 112: 1m/s step-down in wind from 20 m/s to 5 m/s.

Figure 112 shows that as long as the wind speed is higher than 12m/s, the power is kept constant to 2MW. The generator speed is slightly varying around

its rated value, while the pitch angle is changed at each 1m/s step to another appropriate steady state value. As desired, the power is stepped out of the rated power (i.e. 2MW) when the wind speed becomes less than 12m/s. The pitch angle is then kept constant to zero, while the generator speed varies according to the P-ω characteristic, shown in Figure 107.

However, as it is illustrated in Figure 113, keeping the same control parameters (i.e. $T_i^{SC} = 2.2$) also for the case when there is 2m/s step in wind, reveals that the speed controller is too lazy/slow. Due to the cross-coupling between the controllers at high wind speeds, the power control is then not able to keep the power to the rated power. Figure 113 also illustrates the simulation when the integral action of the speed controller is increased ($T_i^{SC} = 0.5$). A reduced integral time of the speed controller is corresponding to a lower damping ration or a higher natural frequency for the second order system. It means that in order to keep the power to the rated power, it is necessary to be able to force the generator speed to react faster to changes in the wind.

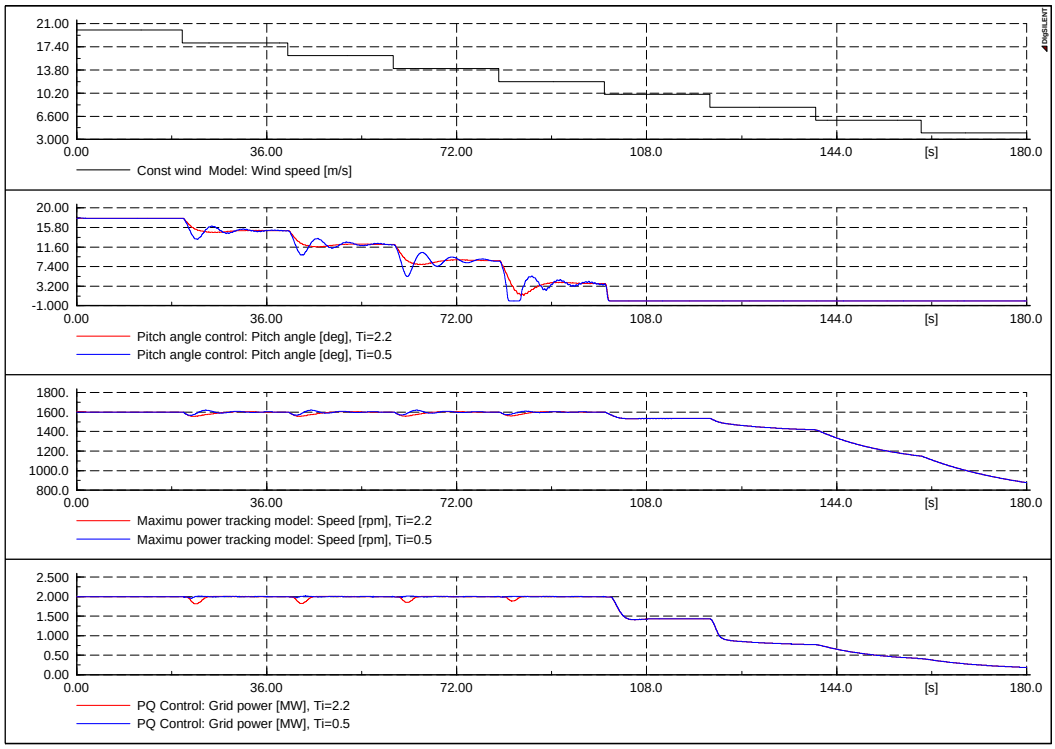

Figure 113: 2m/s step down in wind from 20 m/s to 5 m/s and influence of the speed controller.

Notice that such changing of the integral time of the speed controller yields to an increased rate of the pitch angle. This can off course imply both higher requirements to the pitch system and higher aerodynamical loads. As always, the choice of control parameters is and has to be a trade-off between different aspects. It seems that in the case of higher wind steps, as it is the case of gusts, the parameters designed through the transient response has to be slightly changed in order to be able to handle gusts in a satisfying way.

Figure 114 reflects the same aspects as Figure 113, but for the case of a turbulent wind with mean speed 20m/s and turbulence 10%. By making the speed controller faster, the power control manages to keep the power to the rated value, and to avoid thus the drops in the power.

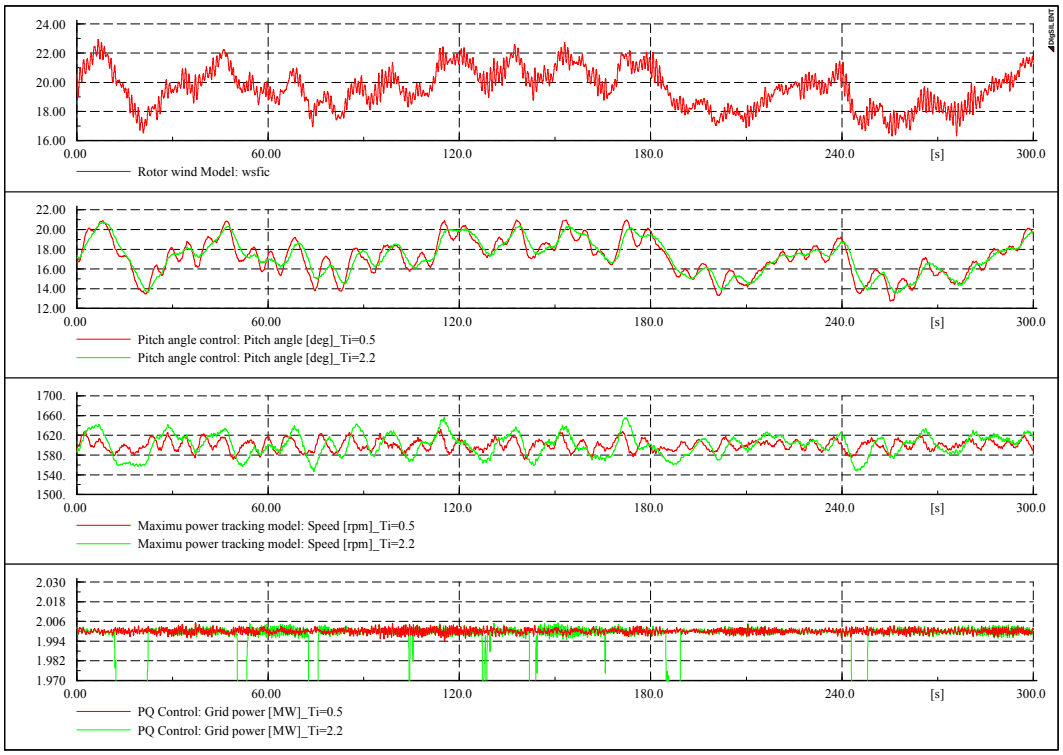

Figure 114: Turbulent wind. Influence of integral time of the speed controller.

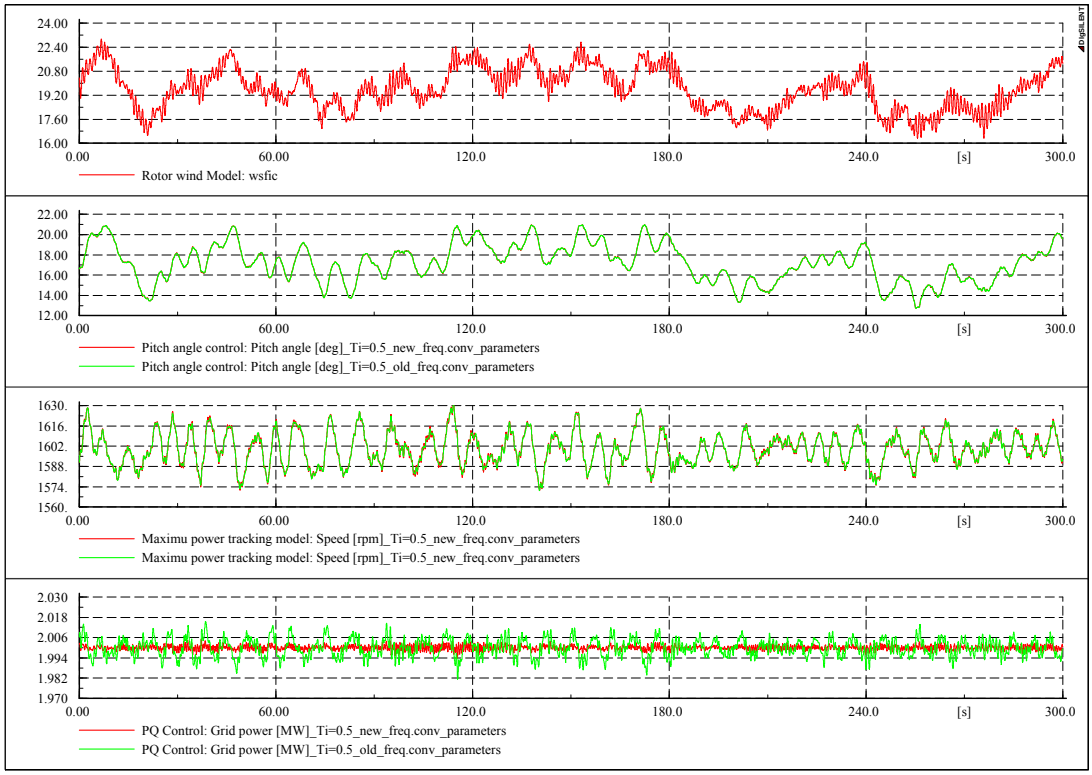

Figure 115: Turbulent wind. Influence of frequency converter.

Figure 115 illustrates the influence of better tuning of the parameters in the frequency converter controller. Notice that the frequency converter alone can improve the control of the power, without affecting the behavior of the other signal, as i.e. the pitch angle and the generator speed.

Figure 116 illustrates a simulation of variable speed wind turbine with turbulent wind, where the mean is 8 m/s and the turbulence intensity of 10%.

The generator speed is tracking the slow variation in the wind speed. As expected for this wind speed range, the pitch angle is passive, being kept constant to its optimal value (i.e. zero for the considered wind turbine). The active power delivered to the grid does reflect the variation in the wind speed. Notice that the fast oscillations in the wind speed are completely filtered out from the electrical power.

Figure 117 illustrates the simulation with turbulent wind, where the mean

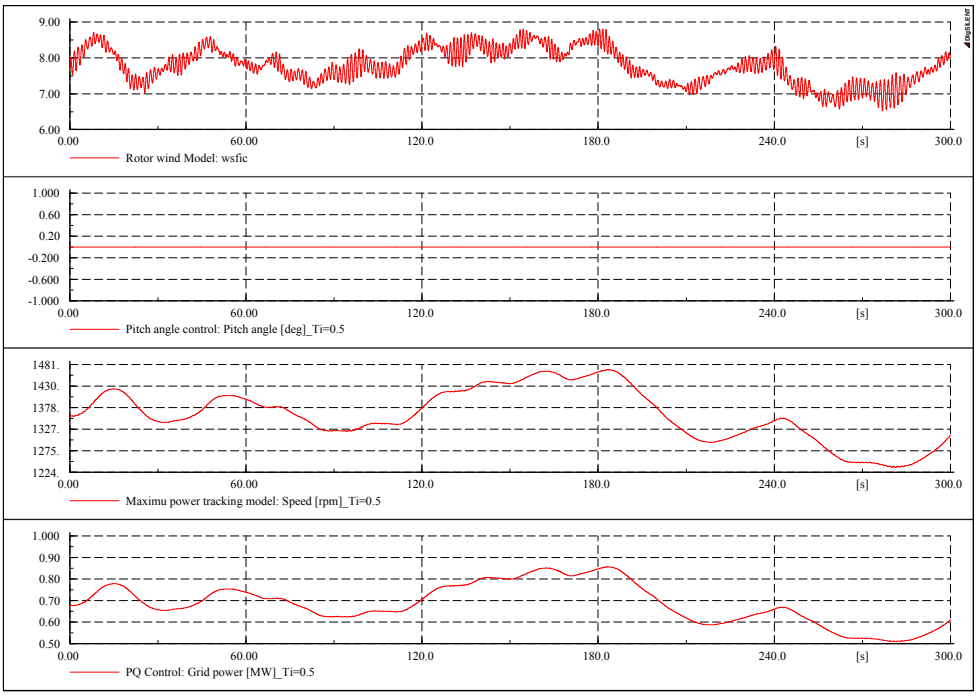

Figure 116: 8 m/s turbulent wind (turbulence 10%).

speed is 12 m/s and the turbulence intensity of 10%. The power is kept to the rated power as long as the energy in the wind permits that.

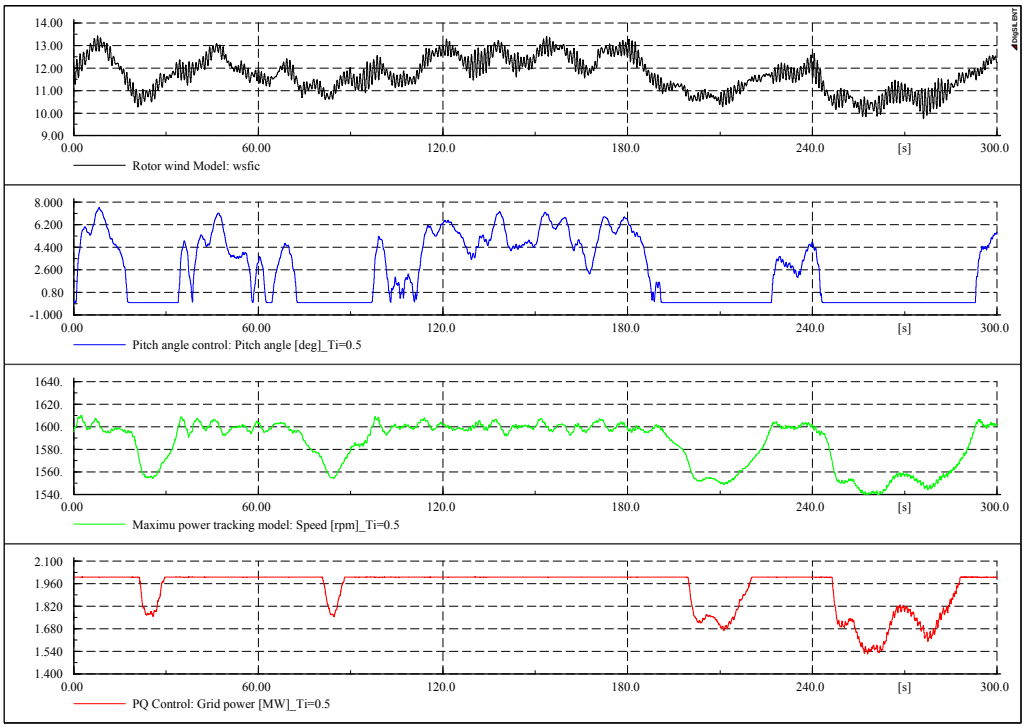

Figure 117: 12m/s turbulent wind (turbulence 10%).

8 Variable speed DFIG wind turbine concept – grid fault operation

This chapter address the fault ride-through and voltage grid support capability of a DFIG wind turbine under a grid fault operation.

Up to 5-6 years ago, most grid codes did not require wind turbines to support the power system during a grid disturbance – wind turbines were only required to be disconnected from the grid when an abnormal grid voltage was detected. With the increased capacity of wind power in the power system over the years, a sudden high loss of power during grid faults, due to wind turbines disconnection, could generate control problems of frequency and voltage in the system, and as worst case a system collapse.

The increased penetration of wind energy into the power system over the last decade has therefore led to serious concern about its influence on the dynamic behaviour of the power system. It has resulted in the power system operators revising the grid codes in several countries, such as in Denmark and Germany (Energinet.dk, 2004), (E.ON., 2006). Basically, for wind power, these grid codes require an operational behaviour more similar to that of conventional generation capacity, and more responsibility in network operation. An overview of existing grid connection codes is given in (Bolik S.M., 2003) and (Jauch C. et al., 2004). The attention in these requirements is drawn to both the wind turbine fault ride-through capability and the wind turbine grid support capability, i.e. their capability to assist the power system by supplying ancillary services. The ancillary services represent a number of services required by the power system operators, such as voltage control, in order to secure safe and reliable grid

operation. Fault ride-through capability addresses primarily the design of the wind turbine controller in such a way that the wind turbine is able to remain connected to the network during grid faults (e.g. short circuit faults).

The effect of wind farm integration in the power system depends on both the power system design to which the wind farms are connected and the wind farm control ability to fulfill the grid requirements. This ability depends of course on the wind turbine/wind farm technology. This fact has challenged different wind turbine manufactures and initiated important research activity regarding the ability of different wind turbine concepts to comply with high-power system operator requirements. There is presently much research activity worldwide, involving model simulation studies to understand the impact of system disturbances on wind turbines and consequently on the power system itself (Akhmatov V., 2003), (Sørensen, P. et al., 2003).

8.1 DFIG wind turbine modelling and control issues – in case of grid fault

As a mainstream configuration for large wind turbines (Hansen A.D. et al., 2007), DFIG wind turbines are also required to remain grid connected during grid faults so that they can contribute to the stability of the power transmission system. This raises problems in terms of generator/converter protection and control. In the case of grid faults the controllability of DFIG variable speed wind turbines embraces both the wind turbine control for preventing over-speeding of the wind turbine and the control and protection of the power converter during and after grid faults.

Figure 118 provides an overview on the control and protection of DFIG wind turbine system configuration under grid faults:

- Wind turbine itself with the drive train, the aerodynamics and the pitch angle control system
- DFIG protection and control system during grid faults

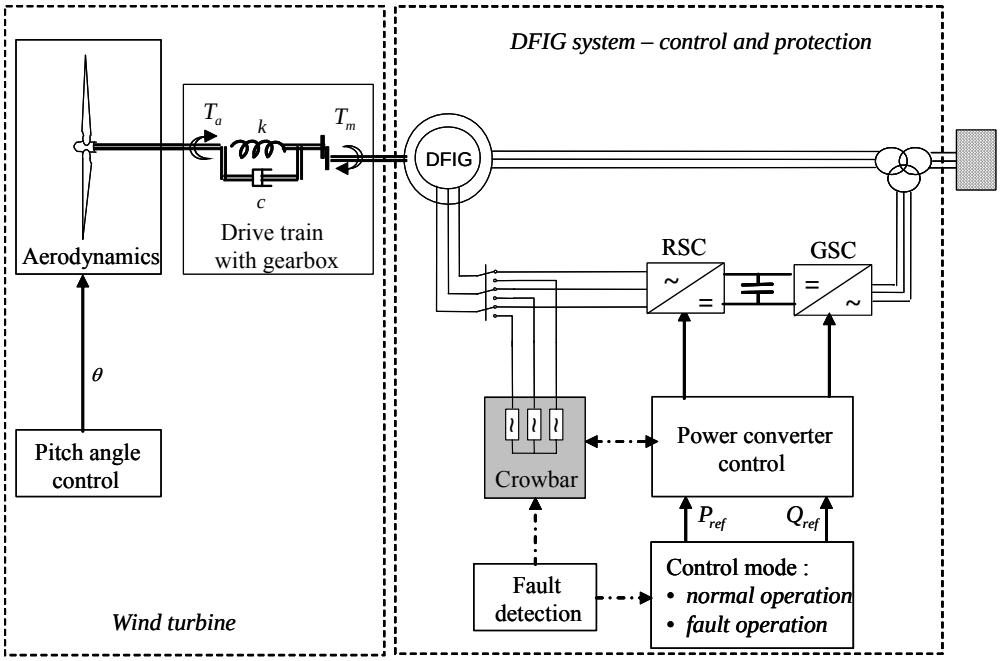

Figure 118: DFIG wind turbine protection and control block diagram during grid faults.

The level of detail required for the stability model of a DFIG, used in case of grid fault, is still subject to discussions (Akhmatov V., 2003), (Poeller M., et al., 2003). It is generally accepted that stator flux derivatives can be neglected. As mentioned in Chapter 2, the DFIG model in *PowerFactory* DIgSILENT is a standard built-in model whose detailing level can be chosen depending on the study propose.

8.1.1 Drive train, aerodynamics and pitch angle control system

In stability analysis, when the system response to heavy disturbances is analysed, the drive train system must be approximated by at least a two-mass model (Akhmatov V., 2003). The idea of using a two-mass mechanical model is to get a more accurate response from the wind turbine during grid faults and to have a more accurate prediction of the impact on the power system.

The mechanical model used in the present context is therefore a two-mass mechanical model, connected by a flexible shaft characterized by a stiffness *k* and a damping *c*, as described in Section 2.3.2. The stiffness and damping components are modelled on the low-speed shaft, while the high-speed shaft is assumed stiff. Moreover, an ideal gear with the exchange ratio *1:* n_{gear} is included. One mass represents the turbine inertia J_{rot}, while the other mass is equivalent to the generator inertia J_{gen}. The motion equations on the low and high speed shaft of the turbine are:

$$J_{rot}\ \dot{\omega}_{rot} = T_{aero} - T_{shaft}$$

$$J_{gen}\ \dot{\omega}_{gen} = T_{mec} - T_{el}$$

where $T_{mec} = T_{shaft} / n_{gear}$. The aerodynamic torque from the rotor acts on one end of the drive train, while the mechanical torque from the generator side acts on the other end of the drive train. The result of this is torsion of the shaft. In steady state, all torques are in equilibrium, i.e. $T_{aero} = T_{shaft}$ and $T_{mec} = T_{el}$.

During grid faults the electrical torque is significantly reduced and therefore the drive train system acts like a torsion spring that gets untwisted. Owing to the torsion spring characteristic of the drive train, both the mechanical torque, aerodynamical torque, and thus the generator speed, start to oscillate with the so-called free-free frequency:

$$f_{osc} = \frac{1}{2\pi} \cdot \sqrt{\frac{k}{J_{eq}}}$$

where J_{eq} is the equivalent inertia of the drive train model determined by:

$$J_{eq} = \frac{J_{rot} \cdot n_{gear}^2 \cdot J_{gen}}{J_{rot} + n_{gear}^2 \cdot J_{gen}}$$

As these torsional oscillations may influence the converter operation during the grid disturbance and also a short while after the disturbance, their modelling by using at least a two-mass model for the drive train system is essential. Furthermore, these torsional oscillations can even be excited and become undamped at a fast converter control (Akhmatov V., 2003).

A simplified aerodynamic model is sufficient to illustrate the effect of the speed and pitch angle changes on the aerodynamic power during a grid fault. The simplified aerodynamic model, described in Section 2.3.3, is typically based on a two dimensional aerodynamic torque coefficient C_q table provided by a standard aerodynamic program.

In dynamic impact studies, the wind speed can be assumed constant during the observed time frames, as the fault operation is small compared to the wind speed fluctuations.

The pitch angle control is realised by a PI controller. In order to get a realistic response in the pitch angle control system, the servomechanism model accounts for a servo time constant, T_{servo} and a limitation of both the pitch angle and its rate-of-change, as illustrated in Figure 119. A gain-scheduling control of the pitch angle, as described in Section 7.3.2, is implemented in order to compensate for the non-linear aerodynamic characteristics.

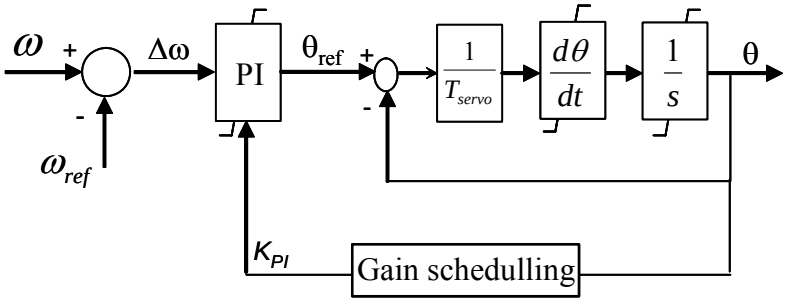

Figure 119: Pitch angle control.

Note that the pitch angle control is implemented in such a way that the pitch angle controls the generator speed, i.e. the input in the controller is the error signal between the measured generator speed and the reference generator speed. In case of overspeeding, the speed is controlled to its rated value, while the aerodynamic power is automatically reduced by increasing the pitch angle. The dynamic stability of the generator is thus increased by the pitch angle control.

This control is able to prevent overspeeding both in normal operations and during grid faults, owing to the fact that the pitch angle controls the generator speed directly. This means that there is no any need to design another pitch control solution additional to the existing one, sketched in Figure 119, in order to improve the dynamic stability during grid faults. This is, for example, the case in (Holdsworth L. et al., 2004) and (Sun T. et al., 2005), where the reduction of the aerodynamic power and the prevention of the overspeeding during grid faults are realised by implementation of an additional pitch control solution.

The rate-of-change limitation is very important during grid faults, because it decides how fast the aerodynamic power can be reduced in order to prevent overspeeding during faults. In this work, the pitch rate limit is set to the typical value of 10 deg/s.

8.1.2 DFIG protection system during grid faults

The use of the partial-scale converter to the generator rotor makes this concept on one hand attractive from an economical point of view. On the other hand, this converter arrangement requires an advanced protection system, as it is very sensitive to disturbances on the grid. Without such protection, high transient currents induced in the rotor can damage the power converter device.

As illustrated in Chapter 7, the control performance of the DFIG is very good in normal grid conditions allowing active and reactive power changes in the range of a few line periods. DFIG control can, within limits, hold the electrical power constant in spite of fluctuating wind, storing thus temporarily the rapid fluctuations in power as kinetic energy.

The concern with DFIG is usually the fact that large disturbances lead to large fault currents in the stator due to the stator's direct connection to the grid.

Because of the magnetic coupling between the stator and the rotor and the laws of flux conservation, the stator disturbance is further transmitted to the rotor. High voltages are thus induced in the rotor windings that in turn cause excessive currents in the rotor as well.

High stator currents may be advantageous for the co-ordination of the protection in the grid. They guarantee that the fault current level is high enough to trip circuit breakers in the faulty part of the grid and thus disconnect the turbine. Since the stator-rotor ratio of the DFIG is designed according to the desired variable speed range, in case of grid faults it might not be possible to achieve the desired rotor voltage in order to control the high rotor currents. The converter has thus only partial control over the generator during grid faults. It reaches its limits quickly and as a consequence loses the control of the generator. The results are both high rotor currents and voltages during the grid faults. Furthermore, the surge following the fault includes a "rush" of power from the rotor terminals towards the converter. As the grid voltage drops in the fault moment, the grid-side converter (GSC) is not able to transfer the power from the rotor-side converter (RSC) further to the grid and therefore the additional energy goes into charging the DC bus capacitor, i.e. the DC bus voltage rises rapidly.

A suitable protection system for the DFIG converter is therefore necessary to break the high currents and the uncontrollable energy flow through the RSC to the DC link and thus to minimize the effects of possible abnormal operating conditions. The protection system monitors different signals such as the rotor current and the DC link voltage; when at least one of the monitored signals exceeds its respective relay settings, the protection is activated.

A simple protection method is to short circuit the rotor through a device called crowbar. The crowbar protection, specific to DFIG, is an external rotor impedance, coupled via the slip rings to the generator rotor instead of the converter, as illustrated in Figure 118. The function of the crowbar is to limit the rotor current.

The crowbar protection is an integral part of the DFIG model in *PowerFactory* DIgSILENT, while its control can be implemented as a user-written model in the dynamic simulation language of the *Power Factory*.

When the crowbar is triggered, the rotor is short circuited over the crowbar impedance, the RSC control is disabled and therefore DFIG behaves as a squirrel cage induction generator (SCIG) with an increased rotor resistance. The disabling of RSC control yields to the fact that the independent controllability of active and reactive power gets lost during fault detection. This implies that the magnetization of the generator, which in normal operation is done over the rotor circuit by the RSC, must in the case of a fault be done over the stator, from the grid.

Since the GSC is not directly coupled to the generator windings, where the high transient currents occur, there is no need to disable this converter, too. The GSC can therefore be used as a STATCOM to produce reactive power (limited however, by its rating) during faults. The crowbar protection can be removed after a predefined time or according to additional criteria, such as the magnitude of the grid voltage. When the crowbar is removed, the RSC is enabled again to control independently the active and reactive power.

Figure 120 illustrates the static curves for the torque and reactive power as function of speed for different crowbar resistances, applied for one 2MW DFIG.

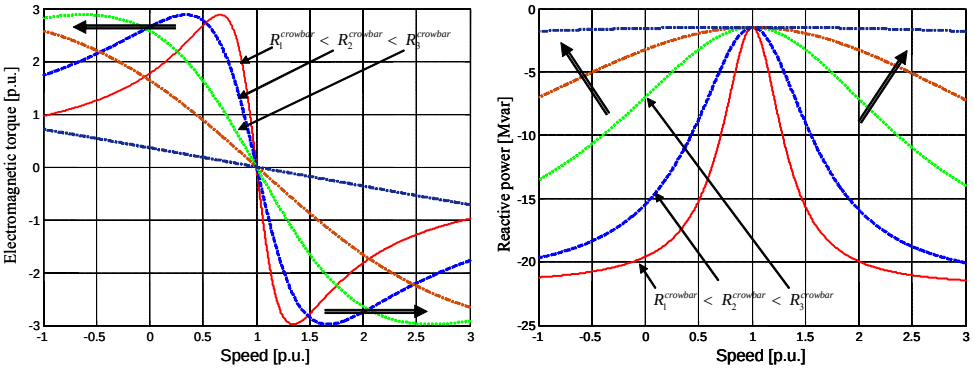

Figure 120: Static curves for torque and reactive power as function of speed for different crowbar resistances.

Note that an increased crowbar resistance improves the torque characteristic and reduces the reactive power demand of the generator at a certain speed. By the addition of the external resistance (crowbar resistance) in the rotor circuit during grid faults, the pull-out torque of the SCIG generator is moved into the range of higher speeds. The dynamic stability of the SCIG generator is thus improved by increasing the external resistance (Akhmatov V., 2003).

Several EMT (electromagnetic transient) dynamic simulations have been also carried out in the following for different crowbar resistance values in case of a 100ms three-phase fault at the high voltage terminal of the 3-windings transformer of the DFIG wind turbine. The simulations are performed for a 160MW wind farm model, which is an aggregation of 80 equal 2MW DFIG wind turbines, e.g. one turbine model with re-scaled power capacity (Poeller M., et al., 2003), (Akhmatov V., et al., 2006).

Figure 121 illustrates the simulation results: the rotor current, the electromagnetic torque and the reactive power of the generator. As these electrical signals are generated by EMT simulations, they are determined using the full-order transient generator model. In the moment of the short circuit fault, the rotor current starts increasing until the over current protection triggers the crowbar and inhibits the RSC control. In the simulation, the time delay due to the switching of shunt resistance is neglected.

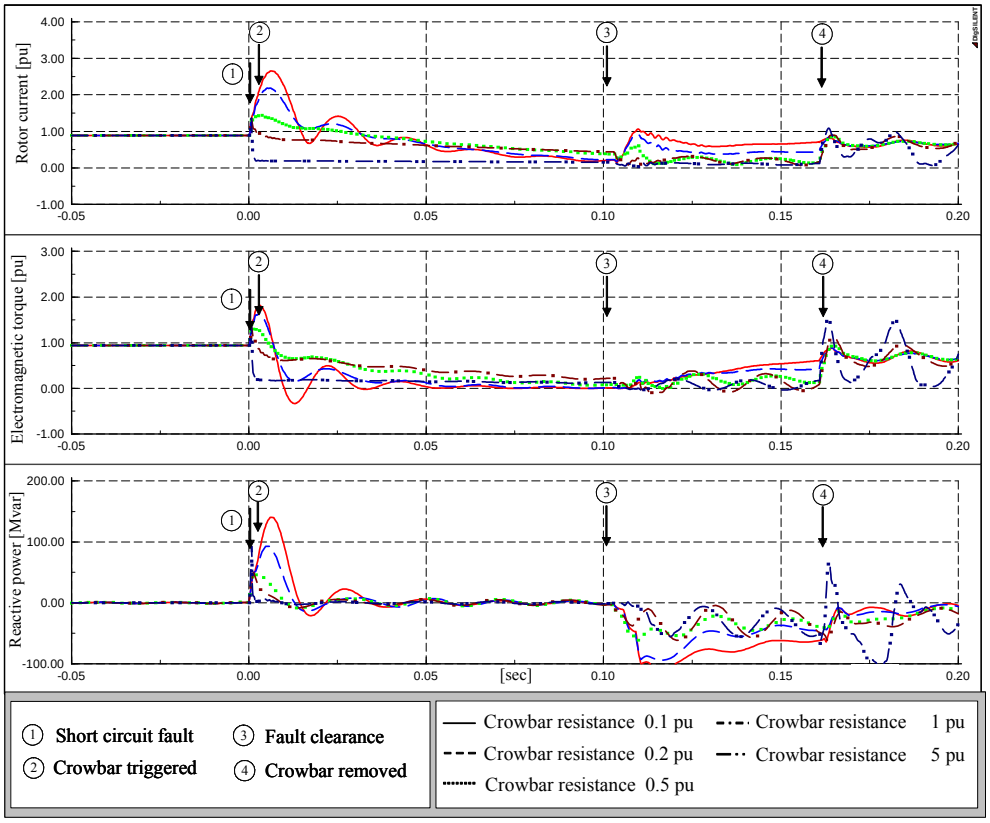

Figure 121: Dynamic performance of DFIG for different values of the crowbar resistance.

Figure 121 depicts both the crowbar's function to limit the rotor current and the crowbar's influence on the reactive power demands of the generator. Small resistance values cause higher current and torque transient peaks in the fault moment. A higher crowbar resistance has an efficient damping effect on both the rotor current and the electromagnetic torque. In accordance with Figure 120, an increased crowbar resistance has also a positive effect on the dynamic stability of the power system, as it implies a reduced reactive power consumption in the fault clearance moment.

However, as illustrated in Figure 121, a too high crowbar resistance can imply a risk of excessive torque and reactive power transients when the crowbar is removed.

A correct choice of the crowbar resistance must therefore take into account the previous considerations. For the present study case, a crowbar resistance value of 0.5 p.u. has been found to be an appropriate trade-off.

8.1.3 DFIG control system during grid faults (fault ride-through control)

DFIG control during grid faults is in the following built on as an extension of the normal operation control structure of DFIG. Before moving on to the DFIG control during grid faults, the DFIG control structure in normal operation, described in Chapter 7, is therefore shortly reviewed and illustrated in Figure 122.

Note that, the DFIG control structure contains the electrical control of the power converters, which is essential for the DFIG wind turbine behavior both in normal operation and during fault conditions. The aim of the RSC is to control independently the active and reactive power on the grid, while the GSC has to keep the DC-link capacitor voltage at a set value regardless of the magnitude

and the direction of the rotor power and to guarantee a converter operation with unity power factor (zero reactive power). As illustrated in Figure 122, both RSC and GSC are controlled by a two stage controller. The first stage consists of very fast current controllers regulating the rotor currents to reference values that are specified by a slower power controller (second stage).

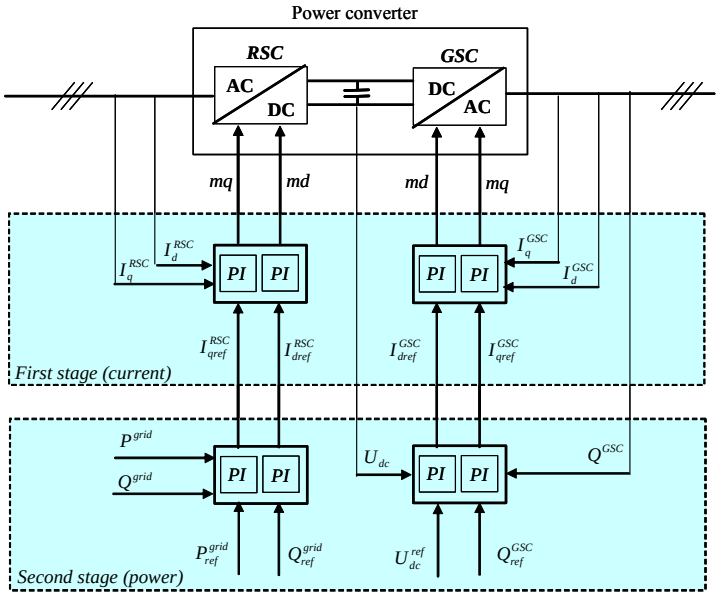

Figure 122: DFIG control structure – normal operation.

In the following, the attention is drawn on the active and reactive power set-point signals for the second stage controllers of the converters in Figure 122. Their definition is strongly depending on which operational mode the wind turbine is working, i.e. in normal or in grid fault operation. For example, in normal operation, as described in Section 7.1:

- the active power set-point P_{ref}^{grid} for the RSC is defined by the maximum power tracking point (MPT) look-up table, as function of the optimal generator speed – see Figure 123, i.e. for each wind speed there is only one generator speed resulting in maximum aerodynamic coefficient C_p.
- the reactive power set-point Q_{ref}^{grid} for the RSC can be set to a certain value or to zero according to whether or not the DFIG is required to contribute with reactive power.
- the GSC is in normal operation reactive neutral, i.e. $Q_{ref}^{GSC} = 0$. This means that, in normal operation, the GSC exchanges with the grid only active power, and therefore the transmission of reactive power from DFIG to the grid is done only through the stator.
- the DC-voltage set-point signal U_{dc} is set to a constant value, independent on the wind turbine operation mode.

In case of grid faults, the generator speed variation is not due to the wind speed change but due to electrical torque reduction, as described in Section 8.1.1. This means that the active power set-point P_{ref}^{grid} has to be defined differently in case of grid faults, i.e. as the output of a damping controller. Such a controller has as task to damp the torsional excitations that are excited in the drive train owing to the grid fault. When a fault is detected, the definition of the

active power set-point P_{ref}^{grid} is switched between the normal operation definition (i.e. MPT) and the fault operation definition (damping controller).

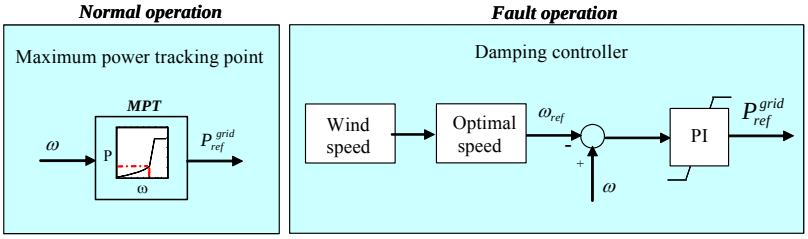

Figure 123: Definition of active power set-point for normal and fault operation, using MPT and damping controller respectively.

Different control schemes can be applied to damp these oscillations. In this work the damping controller of (Akhmatov V., 2003) is adopted. As illustrated in Figure 123, in case of grid faults, the PI damping controller produces the active power reference signal P_{ref}^{grid} for the RSC control based on the deviation between the actual generator speed and its reference. The speed reference is defined by the optimal speed curve at the incoming wind. The damping controller is tuned to actively damp the torsional oscillations excited at a grid fault in the drive train system. (Akhmatov V., 2002) shows that absence or insufficient tuning of this PI controller may lead to self-excitation of the drive train system and to a risk of tripping as protection against vibrations in the mechanical construction.

Note that, the pitch control is not able to damp the torsional oscillations, because of several delay mechanisms in the pitch (Akhmatov V., 2003a). The pitch control damps the slow frequency variations in the generator speed, while a damping controller has to damp the fast oscillations in the generator speed.

Figure 124 illustrates the effect of the damping controller in case of a 100ms three phase fault at the high voltage terminal of the 3-windings transformer of a 2MW DFIG wind turbine. It is assumed that the wind turbine works at its rated power at the fault instant. The generator speed and the mechanical torque of the equivalent DFIG wind turbine are illustrated for the situations with and without damping controller respectively.

Note that without damping controller the torsional oscillations excited by the grid fault are only slightly damped still 10 s after the grid fault incident. It is clearly visible that the oscillations are quickly damped over a few seconds when the damping controller is used. Furthermore the amplitude of the mechanical torque oscillations is much smaller when using the damping controller. Moreover, in contrast to the case when no damping controller is used, the mechanical torque crosses only once through zero when the damping controller is used, and therefore the mechanical stress of the drive train is substantially reduced in this case. The damping controller is thus minimizing the grid fault effect on both the mechanical and the electrical side of the turbine. The protection system together with the damping controller enhances thus the DFIG fault ride-through capability.

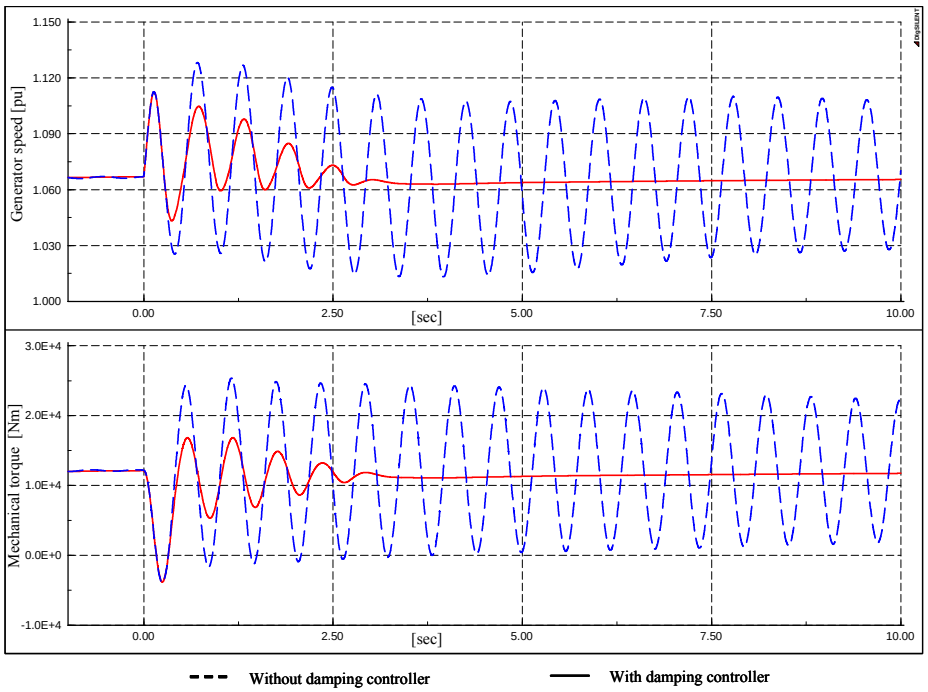

Figure 124: Damping controller effect.

During a grid fault, the tasks of RSC and GSC can be changed, depending on whether the protection system (i.e. crowbar) is triggered or not. In the case of less severe grid faults (i.e. not triggered crowbar) or reactive power unbalance in the system, the RSC and the GSC have the same tasks as in the normal operation. In case of severe fault (i.e. triggered crowbar), a specific grid support strategy, according to the grid codes defined by the power system operators, has to be designed and developed.

8.2 Voltage grid support of DFIG wind turbine

The technical specifications defined by the power system operator require that the wind turbines remain connected to the grid during a grid fault and to support the grid during the faults, i.e. with voltage grid support. The voltage grid support capacity of a DFIG depends on the quantity of reactive power injection but also on the line characteristic from the generator to the connection point with the power system.

In general, different possible voltage control strategies exist for regulating voltage at the terminals of the DFIG. The voltage can in principle be controlled by either the rotor-side converter (Eping C. et al., 2005) or the grid-side converter (Kayikci M. et al., 2005) or by both of them (Akhmatov V., 2003). The solution addressed in this work, to enhance the DFIG grid support capability during grid faults, is based on the voltage control strategy, similar to that presented in (Akhmatov V., 2003). The design of the control strategy is based on the idea that the reactive power contribution is performed by both converters in a co-ordinated manner. The RSC is used as the default reactive power source, while the GSC is used as a supplementary reactive power source during the blocking of the RSC.

In the case of less severe grid faults (i.e. not triggered crowbar) or reactive power unbalance in the system, the RSC is not blocked and therefore can still independently supply active and reactive power to the grid. On the other hand, at a severe grid fault, if the generator is not tripped, the DFIG wind turbine has

to continue its operation and to try to sustain grid connection. The RSC is blocked at the moment when the crowbar is triggered by either an overcurrent in the rotor circuit or an overvoltage in the DC link. In such a situation the DFIG grid support capability is strongly reduced. Its capability to control independently the active and reactive power is lost when it is actually most needed, namely during and shortly after the fault. The idea of the control strategy is that the grid voltage (reactive power) control is taken over by the GSC when RSC is blocked. The GSC does not block at a grid fault, but it can continue its operation as STATCOM as long as the RSC is blocked. When the crowbar is removed, the RSC starts to operate and the GSC is set again to be reactive neutral. The remove of the crowbar protection, and thus the re-start of the RSC can be performed according different criteria, such as the magnitude of the grid voltage or of the rotor currents. A too soon RSC restarting may cause tripping of the converter again at the fault clearance.

The voltage grid support strategy for DFIG wind turbine, considered in this work, is illustrated in Figure 125. It is implemented as an extension of the DFIG control structure for normal operation, sketched in Figure 122.

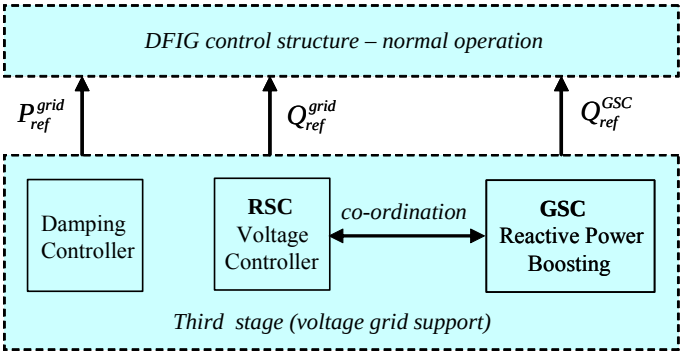

Figure 125: Extended DFIG control structure for voltage grid support during grid faults.

An additional third control stage, having as task to improve the DFIG voltage grid support capability during grid faults, is thus added to DFIG control structure used in normal operation. This third (voltage) control stage, as illustrated in Figure 125, provides the reference signals for the second stage controllers in the case of fault operation. This control stage contains three controllers, such as a damping controller (described already in Section 8.1.3), a RSC voltage controller and a GSC reactive power boosting. Similar to the first and second control stages, the third control stage is also implemented as a user-written model in the dynamic simulation language of the *PowerFactory*.

The RSC voltage controller provides the reactive power reference signal Q_{ref}^{grid} for the RSC, when the crowbar protection is not triggered. The RSC controller is realised by a PI controller, as illustrated in Figure 126. The RSC controller adjusts the reactive power reference signal Q_{ref}^{grid} for the second stage controller of the RSC, based on the deviation of the actual grid voltage U_{ac}^{grid} at the point of common coupling from its reference value $U_{ac,ref}^{grid}$. The RSC voltage controller controls the grid voltage as long as the RSC is not blocked, i.e. if there is a lack of reactive power in the grid and as result a decay in the grid voltage.

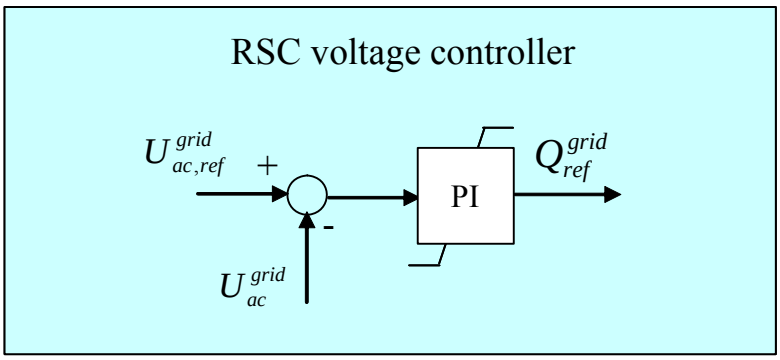

Figure 126: RSC voltage controller.

To asses the performance of the RSC controller, a simulation is performed with a reactive power sink connected at the high voltage terminal of the DFIG wind turbine and disconnected after 1 second. The idea is to simulate a voltage dip, which is not too large to trigger the crowbar and thus to block the RSC.

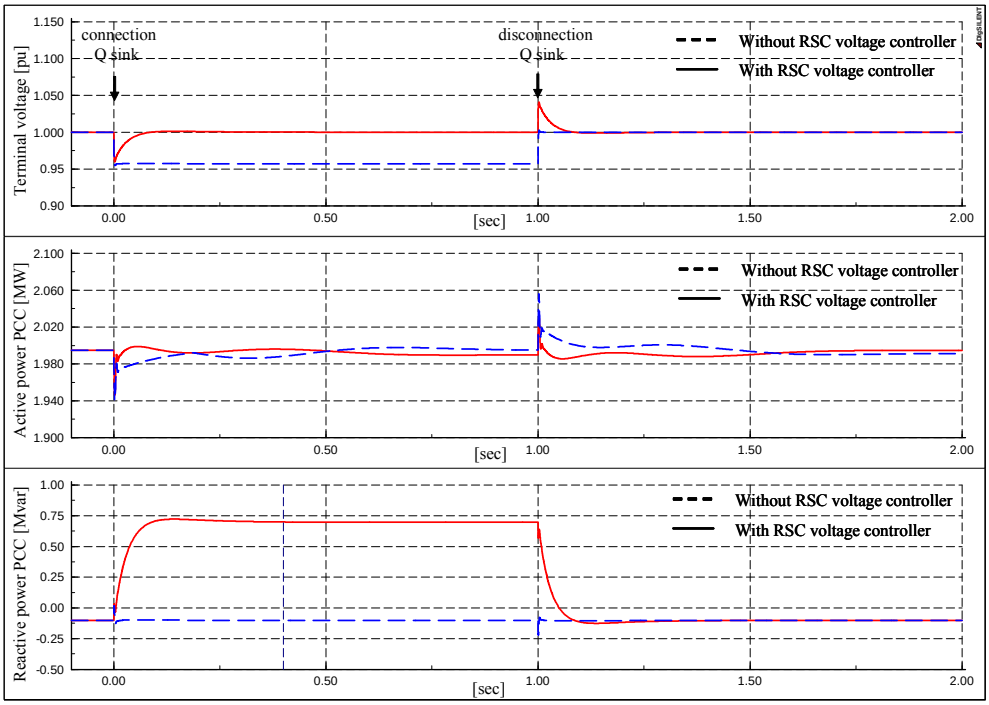

Figure 127: RSC voltage controller performance.

Figure 127 illustrates the voltage, the active and the reactive power in the point of common coupling of the DFIG wind turbine for the situations with and without RSC voltage controller, respectively. The voltage drops about 4% in the moment of reactive power sink connection. The RSC voltage controller notices the deviation in voltage and commands more reactive power. The increased reactive power supplied by the DFIG pushes the voltage back to its nominal value (1pu) in less than 100ms. At the moment when the reactive power sink is disconnected, the voltage increases suddenly, but the RSC voltage controller controls again quickly the voltage to its nominal value by absorbing reactive power. Note that the active power has small drop/peak in the connection/disconnection respectively, otherwise being unchanged. In the case of no RSC voltage control, the voltage drop is not compensated by reactive power and the voltage recovers to its nominal value only when the reactive power sink is disconnected.

The GSC reactive power boosting (a supplementary reactive power controller) generates a reactive power reference signal Q_{ref}^{GSC} for the GSC control, in case when RSC is blocked – see Figure 122, Figure 125. GSC is set to work as a STATCOM. The implemented reactive power boosting provides a zero reactive power reference when the RSC is active, and a maximum reactive power of the GSC (1p.u.) as reference value in case when the RSC is blocked. This means that the GSC contributes with its maximum reactive power capacity for grid support under severe grid faults. Beside its STATCOM function during grid faults, the GSC control has still to keep the DC link capacitor voltage at a set predefined value. The control capacity of the GSC during grid fault, namely when the voltage at its terminal is also reduced, is less than the control capacity of the RSC during normal operation.

Figure 128 illustrates the effect of the GSC reactive power boosting in case of 100ms three phase fault at the high voltage terminal of the DFIG wind turbine. The crowbar protection is removed after a predefined time, i.e. 200 ms after the crowbar was triggered. In this simulation a voltage drop of 50% is chosen in order to illustrate better how the GSC can improve the voltage level during the crowbar connection. The high voltage terminal of the turbine and the GSC reactive power production are illustrated.

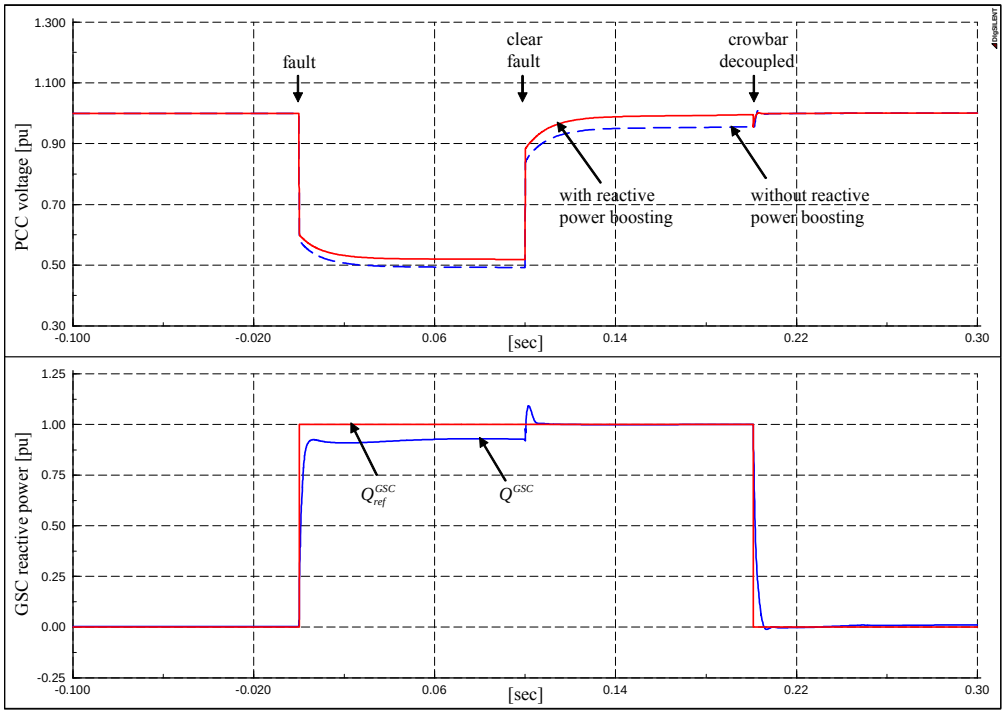

Figure 128: GSC reactive power boosting effect.

During the grid fault, the GSC reactive power boosting is active, while the RSC control is disabled. The GSC reactive power boosting improves the voltage level during the grid fault: both between fault and fault clearing and also between fault clearing and crowbar decoupling. The crowbar connection causes the reactive power boosting to set the reference value to 1pu. Between fault and fault clearing moment, the reactive power reference is not achieved, the reason being the fact that the current limits of the reactive power controller are reached. However, in the moment of fault clearing, the terminal voltage starts to recover and this increases the possibility of the GSC to produce more reactive power. When the crowbar is decoupled, the GSC is set to be reactive neutral

($Q_{ref}^{GSC} = 0$), GSC reactive power boosting is disabled and replaced by the RSC voltage control.

As illustrated in Figure 125, a co-ordination control between the RSC and GSC voltage control is implemented. During the grid fault, some of the controllers have to be disabled, while others are enabled. Controller start-up must be treated with some care to avoid discontinuities and to minimize the loads on the wind turbine. Such discontinuities could eventually lead to prolonged transients and, implicitly, to subsequent operations of the crowbar protection. The controller start-up of the RSC is, for example, realized in this work by introducing a minor feedback loop, which prevents the integrator action of the controller from adopting an inappropriate state during blocking of the controller.

8.3 Case studies

Different case studies are carried out in the following in order to illustrate and evaluate the dynamic interaction during grid faults between large DFIG wind farm and power transmission system model.

The attention is drawn to studies regarding the fault ride-through capability, the voltage grid support features of large DFIG wind farms and the influence of the DFIG voltage control on the performance of a nearby active stall wind farm during the grid fault. Such studies require a realistic enhanced power transmission system model, which is characterised by a voltage and a frequency, which are not fixed to their respective rated values but may be subject to fluctuations when the transmission system is subjected to disturbances.

8.3.1 Aggregation method

Aggregated modelling of large wind farms is commonly used to facilitate the investigation of the impact of a large wind farm on the dynamics of the power system to which it is connected. This type of modelling is often used in system studies where the concern is not the individual wind turbines but the impact of the entire farm on the power system. The advantage of an aggregated model is that it eliminates the need to develop a detailed model of the wind farm with tens or hundreds of wind turbines and their interconnections. It reduces both the complexity of the system and the computation time substantially.

This work is using the aggregation approach presented in (Poeller M., et al., 2003). The accuracy of this approach is demonstrated and validated with the help of some simulations, where an aggregated wind farm model and a detailed wind farm model consisting of many single turbines are compared, showing good accordance in power system studies.

The idea of the aggregation is to represent an entire large wind farm in voltage stability investigations by one equivalent lumped wind turbine with rescaled power capacity. According to (Akhmatov V., 2004), the mutual interaction between converter control systems of the wind turbines equipped with the DFIG can be neglected.

PowerFactory DIgSILENT offers a built-in directly aggregation technique for the electrical system (i.e. generator, power converter, transformer, capacitor, inductance) of the wind turbine (Poeller M., et al., 2003): for example, the generator and the transformers, can be modelled directly by a certain number of parallel machines or transformers, respectively, while the other electrical components (power converter, capacitance, inductance) and control can be upscaled accordingly to the increased power flow. The mechanical part of the wind farm aggregated model, namely the shaft model, the aerodynamics and the pitch system, is modelled as for one individual wind turbine. The mechanical power used

as input to the aggregated generator is then the mechanical output from one turbine multiplied by the number of turbines in the wind farm.

8.3.2 Power system test model

A realistic model for the power transmission system is usually not easily disposable, and if it is, it contains a large amount of detailed confidential data, which makes it inappropriate for publication of the studies.

The Danish Transmission System Operator Energienet.dk has fortunately noted this aspect and therefore developed a small test model for the power transmission system (Akhmatov V. et al., 2006), especially for educational and research purposes. This small test model is a generic simplified model of a power transmission grid, but it is still a fairly realistic model to investigate the response of a power transmission system with grid-connected wind turbines to grid faults. It is implemented in the simulation tool *PowerFactory* DIgSILENT and produces a realistic output when the response of a whole wind farm has to be evaluated. The test model for the power transmission system in its original form, as described in (Akhmatov V. et al., 2006), is used in this work as a basis for extension. The outline of the extended test model is presented in Figure 129.

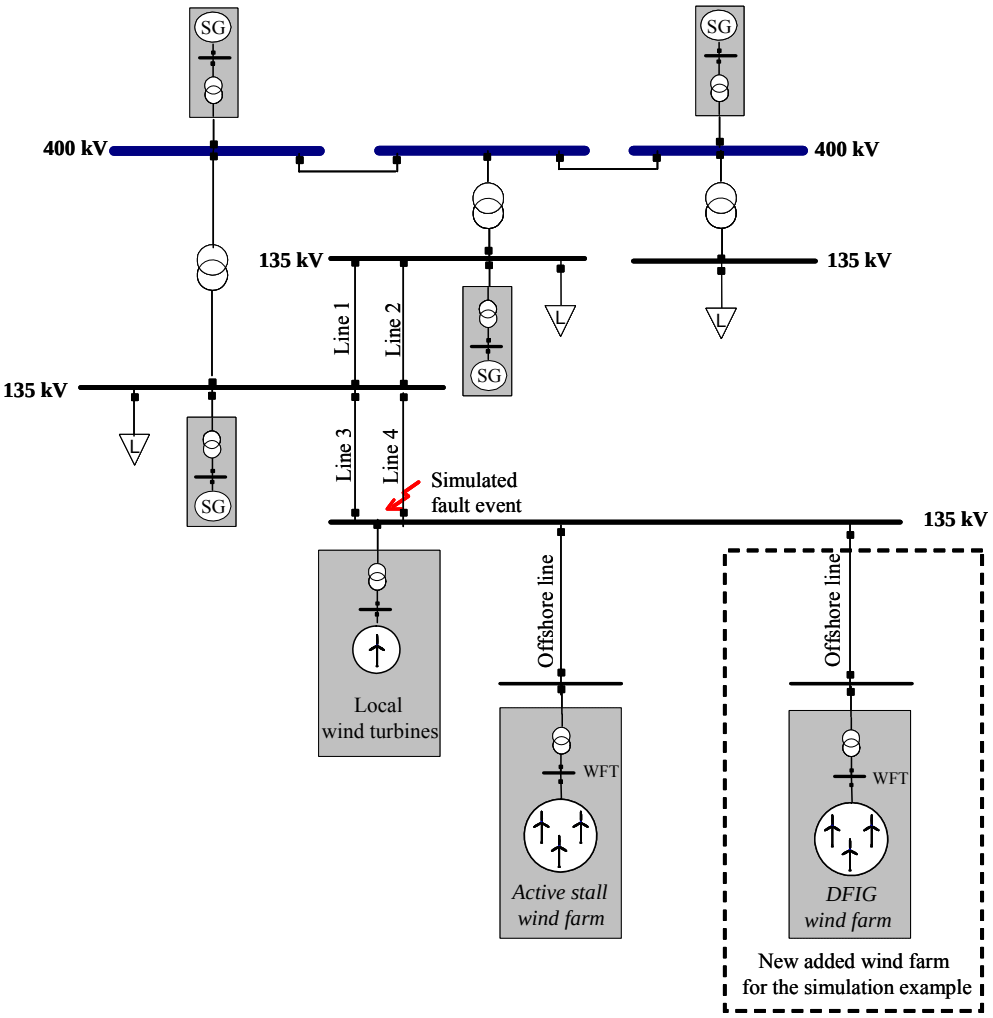

Figure 129: Simplified grid structure of the transmission network model.

The grid model contains busbars with voltages from 0.7kV to 400kV, four conventional power plants with their control, several consumption centres, a

lumped equivalent for local wind turbines and a model for a 165 MW offshore wind farm connected through a sea cable to the transmission grid of 135kV. The conventional power plants are synchronous generators with primary voltage control. The model can be easily extended with frequency controllers, but as the focus in the present work is on the voltage stability issues, the frequency stability in the system is assured only by large generator inertia. The on-land local wind turbines are fixed-speed, stall controlled wind turbines equipped with no-load compensated induction generators. The 165 MW offshore wind farm is modelled as active stall-controlled wind turbines with induction generators, similar to the Danish offshore wind farm at Nysted. The offshore wind farm is modelled with a one-machine approach based on aggregation technique. The wind turbine symbol in Figure 129 denotes the wind turbine model, containing models for the drive train system with constant mechanical torque, generator, transformer and the control respectively, as described in details in (Akhmatov V. et al., 2006).

The local wind turbines illustrated in Figure 129 are old land-based wind turbines without any ride-through control implemented and are therefore disconnected from the system by the protection system to avoid overspeeding, in the case of a grid fault. As required in (Energinet.dk, 2004), large wind farms connected to the transmission system have to be able to withstand grid faults without being disconnected in cases where the clearance of the fault does not isolate the wind farm. This is normally the case when the grid fault happens in the transmission system. In contrast to the local wind turbines, the active stall offshore wind farm illustrated in Figure 129 is equipped with a fault ride-through capability control. In the case of a severe voltage drop the active power production is reduced to avoid uncontrolled overspeeding. The mechanical power of the rotor is directly ramped down to 20% of the rated mechanical power to comply with the Danish grid code. The reduction of the active power production implies that the reactive power absorption is reduced too. Such power reduction control has a positive effect, contributing to a better stabilisation of the wind farm. It is a kind of passive reactive power control, as it does not participate actively in the voltage control of the system.

The test model for the power transmission system in its original form, described in (Akhmatov V. et al., 2006), is extended in this work by adding a new offshore wind farm made up exclusively of DFIG wind turbines. As illustrated in Figure 129, the new added wind farm consists of 80 identical 2MW DFIG wind turbines. It is connected to the transmission system at a 135 kV busbar through an offshore line similarly to the active stall offshore wind farm. The new wind farm is modelled based on the mentioned aggregation technique, namely by one equivalent lumped wind turbine with rescaled power capacity. It is also equipped with the co-ordinated voltage control, as described in the chapter.

8.3.3 Simulation Examples

In this section, a set of simulations are carried out in order to investigate the dynamic interaction during grid faults between DFIG wind turbines and power transmission system. It is assumed that, during the grid fault, the DFIG wind farm operates at its rated capacity, as this is worst for the voltage stability.

In each simulation a severe three-phase short circuit grid fault is considered to occur in the transmission grid at the end of line 4 close to the wind farms – see Figure 129. The grid fault lasts for 100ms and gets cleared by permanent isolation (tripping the relays) of the faulty line (line 4 in Figure 129). Note that, by tripping line 4, the power system becomes weaker (higher impendance) and some components (e.g. line 3) are fully loaded. At the moment of the grid fault

it is assumed that the on-land wind turbines are disconnected from the system by their protection system. The frequency stability in the grid at the moment of on-land wind turbines disconnections is assured by large generator inertia.

Two sets of application studies are illustrated. The first set has as focus the dynamic interaction between DFIG wind turbines and the power system during the grid faults. The second set illustrates how the DFIG wind farm provides voltage grid support and how the DFIG voltage control affects the performance of the active stall wind farm located in the vicinity.

8.3.3.1 **Dynamic interaction of DFIG wind turbines and power system**

In this study, the attention is drawn to the dynamic interaction between the DFIG wind turbines and the power system model, during and shortly after the short circuit fault. It is therefore assumed that in this simulation DFIG wind turbines are only equipped with fault ride-through capability, without any voltage grid support capability. The simulation results are presented in *Figure 130* and Figure 131.

A grid fault affects both the mechanical and electrical components of the wind turbine. The mechanical time constants are much larger than the electrical, and therefore the mechanical and the electrical effects cannot be illustrate in the same time frame. As the mechanical aspects of a DFIG wind turbine during a grid fault has already been discussed and illustrated in Figure 124, the focus in the following is on the electrical signals of the DFIG wind turbine, in a time frame about 500 ms.

Behavior immediately after the fault

In the fault instant, the voltage at the DFIG generator terminal drops and it leads to a corresponding decrease of the stator and rotor flux in the generator. This result in a reduction in the electromagnetic torque and active power – see *Figure 130*. As the stator flux decreases, the magnetization that has been stored in the magnetic fields has to be released. The generator starts thus its demagnetization over the stator, which is illustrated in *Figure 130* by the reactive power peak in the moment of the fault. As the electromagnetic torque of the generator drops according to the voltage drop too, the torsion spring in the drive train gets untwisted and therefore the mechanical torque drops too. However the drop of the mechanical torque is slower than of the electromagnetic torque and therefore the generator starts to accelerate. The dynamic relation between the electrical torque, mechanical torque and the generator speed is reflected in *Figure 130*. The overspeeding of the generator during the fault is counteracted by the pitch control system.

In the fault moment, as the stator voltage decreases significantly, high current transients appear in the stator and rotor windings – see Figure 131. Note that the rotor current resembles the stator current. In order to compensate for the increasing rotor current, the RSC increases the rotor voltage reference, which implies a “rush” of power from the rotor terminals through the converter. On the other side, as the grid voltage has dropped immediately after the fault, the GSC is not able to transfer the whole power from the rotor through the converter further to the grid. The GSC’s control of the DC-voltage reaches thus quickly its limitation. As a result, the additional energy goes into charging the DC-bus capacitor and the DC-voltage rises rapidly – see Figure 131.

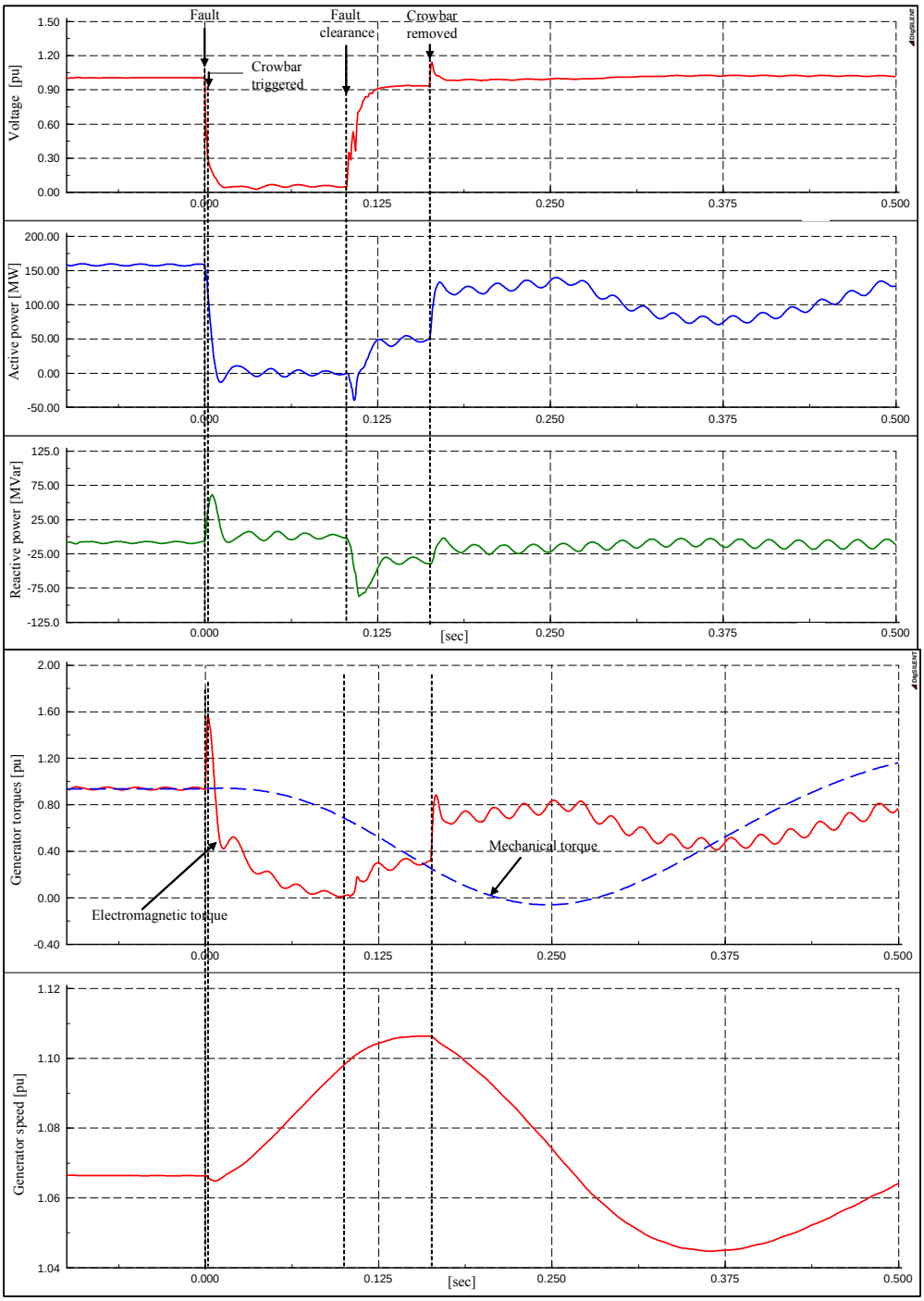

Figure 130: Generator's terminal (WFT) voltage, active power, reactive power, electrical torque, mechanical torque and speed.

When at least one of the monitored signals, i.e. the rotor current or the DC-voltage, exceeds its respective limits, the protection system is activated. This short circuits the generator rotor by triggering the crowbar. The RSC is blocked and therefore its control of the rotor currents is disabled. In the moment the crowbar is triggered, the DC-bus capacitor starts discharging; the GSC begins to control the DC-link voltage back to its reference. Note that, as long as the crowbar is triggered, the generator behaves as a conventional squirrel cage induction generator (SCIG), namely the converter rotor voltage output is zero – as illustrated in Figure 131.

Behavior after fault clearance

Immediately after the fault is cleared, the stator voltage start to recover, the electromagnetic torque and active power start to increase – see *Figure 130*. As the grid voltage and the flux increases, the demagnetised stator and rotor oppose this change in flux leading thus to an increase in the rotor and stator currents – see Figure 131. Note that when the fault is cleared, the voltage does not recover completely immediately. Just after fault clearance, it reaches a voltage level lower than its nominal value, while it reaches completely its nominal voltage level after the removing of the crowbar. The reason for that is that just after fault clearance the generator continues to behave as squirrel cage induction generator and therefore it starts to absorb reactive power for its magnetization – see *Figure 130*. The RSC is disabled until the crowbar is removed, and therefore it is not able to provide the reactive power necessary for the magnetization of the generator. The generator absorbs thus reactive power from the grid and this action delays the recovering process of the grid voltage.

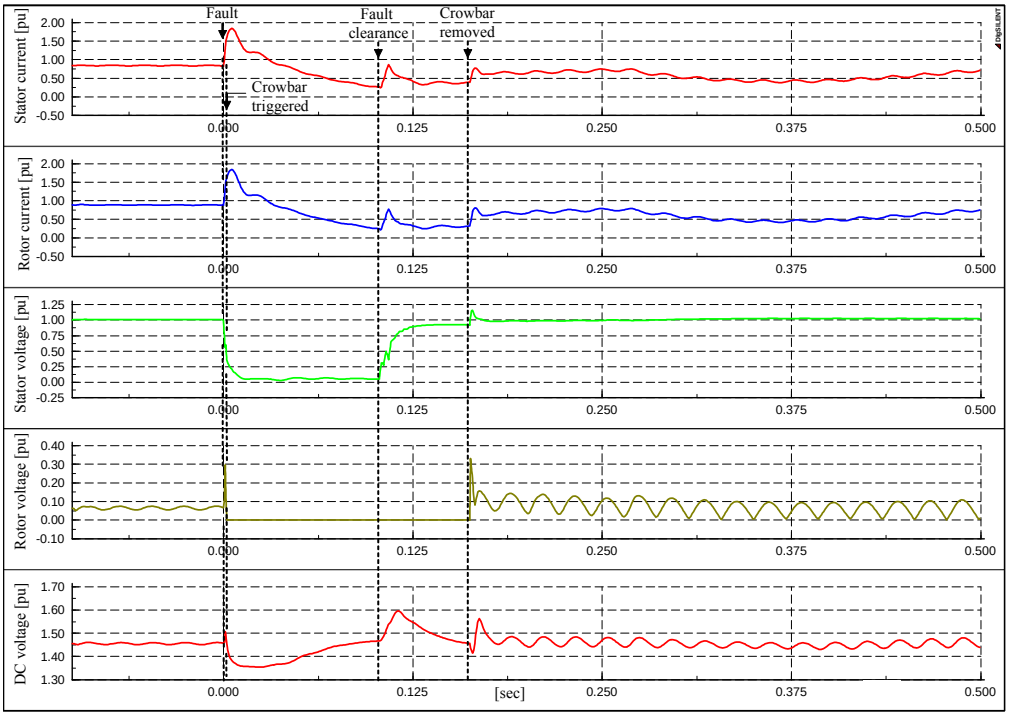

Figure 131 : Generator currents and voltages.

When the grid voltage recovers over a certain value, the crowbar is removed. From this moment, the RSC starts actively to control the active and reactive power, the voltage recovers completely due to the activation of the RSC voltage controller, the generator currents and voltages start to converge to their pre-fault values and.

The detailed simulations illustrated in *Figure 130* and Figure 131 provides a quick overview and a better understanding of the functionality of the DFIG wind turbine control and protection during grid fault.

8.3.3.2 **Voltage grid support of DFIG wind turbines**

In this study, the attention is drawn to the voltage grid support capability of DFIG wind turbines. The effect of the DFIG wind turbines equipped with the presented co-ordinated voltage control both on the power system voltage stability and the performance of a nearby active stall wind farm during the grid fault is illustrated.

In the moment of the grid fault, a voltage drop occurs. Immediately after the fault, when the rotor current magnitude is above the current protection limitation, the crowbar protection system of the DFIG is triggered, the rotor is short circuited, the RSC is blocked and the GSC operates as STATCOM. The damping controller starts to damp the drive train oscillations caused by the fault. When the fault is cleared and the DFIG wind farm terminal voltage recovers to a certain value, the crowbar protection is disabled, the RSC starts to control the grid voltage and the GSC is again set to be reactive neutral.

Figure 132 illustrates the voltage, active and reactive power of the wind farm at the wind farm terminal (WFT) for two situations:

1. The DFIG is not equipped with voltage control capability - the turbine maintains a power factor of 1.
2. The DFIG is equipped with voltage control capability.

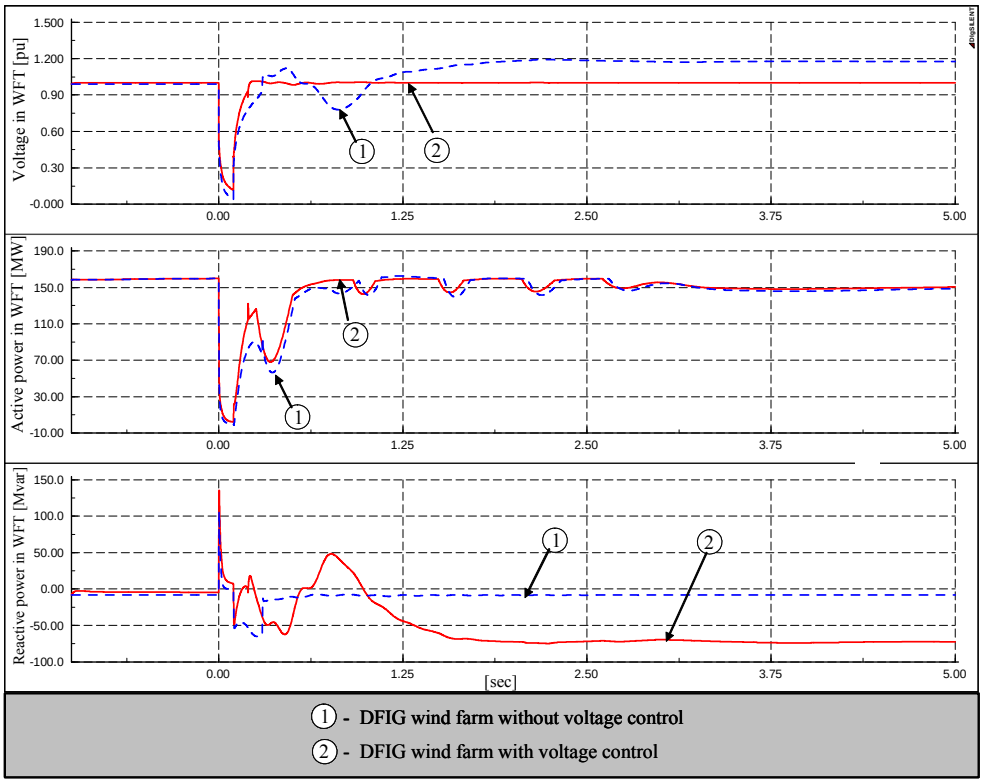

Figure 132: DFIG wind farm terminal (WFT) - with or without co-ordinated voltage control.

As expected, the influence of voltage control is visible both during the fault, when the GSC operates as STATCOM and supplies reactive power, and after disconnection of the crowbar, when the RSC controls the voltage. When no voltage control is enabled, the grid voltage oscillates and stabilizes to a higher voltage level after the fault is cleared. This can be explained both by the reactive power surplus existent in the system as a result of the on-land wind turbines disconnections and by the fact that, as a result of the fault clearance (tripping line 4), the transport of active power from the wind farms to the grid is done through a higher resistance transmission line. Figure 132 shows that the existing reactive power surplus in the system is absorbed by the DFIG when the voltage control is enabled. Note that the DFIG voltage control reestablishes the grid voltage to 1p.u. very quickly without any fluctuations. No significant effect of the voltage control appears on the active power production. However, there it is a slight improvement in active power when voltage control is used. The small

"drops" in the power, visible in both cases just after the fault is cleared, correspond to the damped torsional oscillations in the generator speed. The damping controller damps the torsional oscillations appearing in the drive train and in the generator speed, due to the grid fault within a few seconds. The initial level of the active power is reached after a few more seconds.

The next simulation is basically the same as that illustrated in Figure 132, but this time the active stall wind farm is not equipped with the fault ride-through control, i.e. its power reduction control is disabled. The simulation results are shown in Figure 133.

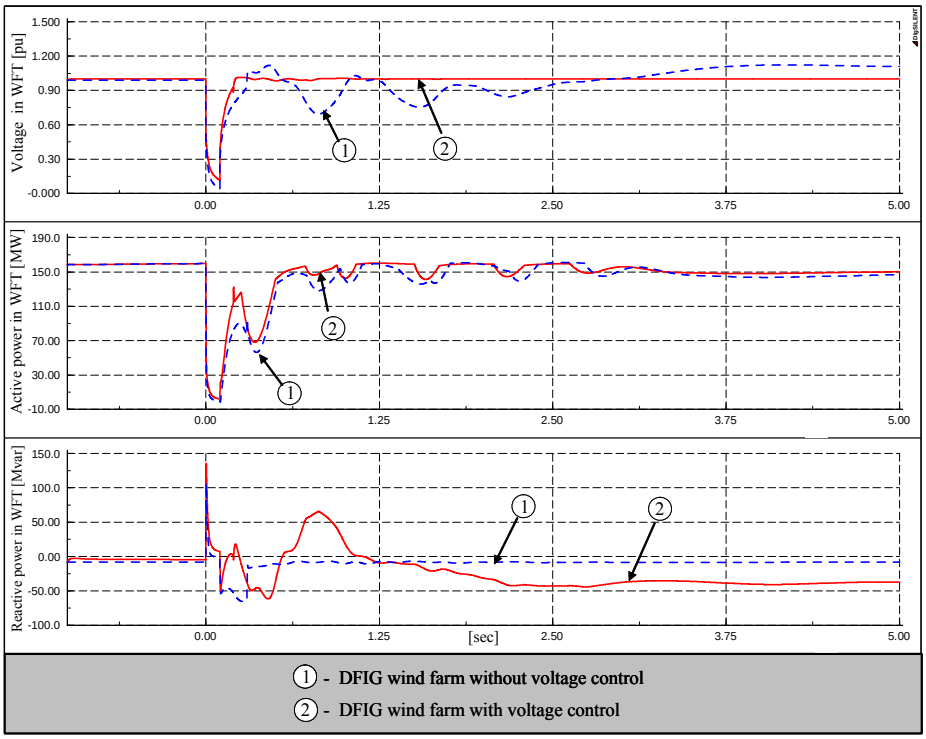

Figure 133: DFIG wind farm terminal (WFT) - with or without co-ordinated voltage control when the power reduction control of the active stall wind farm is disabled.

The fact that the active stall wind farm, located in the vicinity of the DFIG wind farm, has no fault ride-through control enabled this time has, as expected, a negative influence on the voltage stability in the grid. In the case of no voltage control for the DFIG wind farm, the grid voltage oscillates longer time than in the previous example before stabilizing again to a higher voltage level. This behavior reflects that the active stall wind farm does not have any power reduction control during the fault. The oscillations in the drive train of the active stall wind turbine due to the grid fault are transferred uncontrolled to the generator speed and the grid voltage. However, the DFIG wind farm equipped with voltage control manages again to reestablish the voltage rapidly, by controlling the reactive power supply.

In Figure 132 and Figure 133, attention was focused on the performance of the DFIG wind farm during a grid fault when it is or is not equipped with voltage control. One question in mind is now how the DFIG wind farm voltage control influences the performance of a nearby active stall wind farm during a grid fault, located as illustrated in Figure 129. The next two figures therefore contain only information concerning the active stall wind farm during the grid fault, namely the active and the reactive power at the wind farm terminal (Figure 134)

and the generator speed and the mechanical power of the active stall wind turbines (Figure 135).

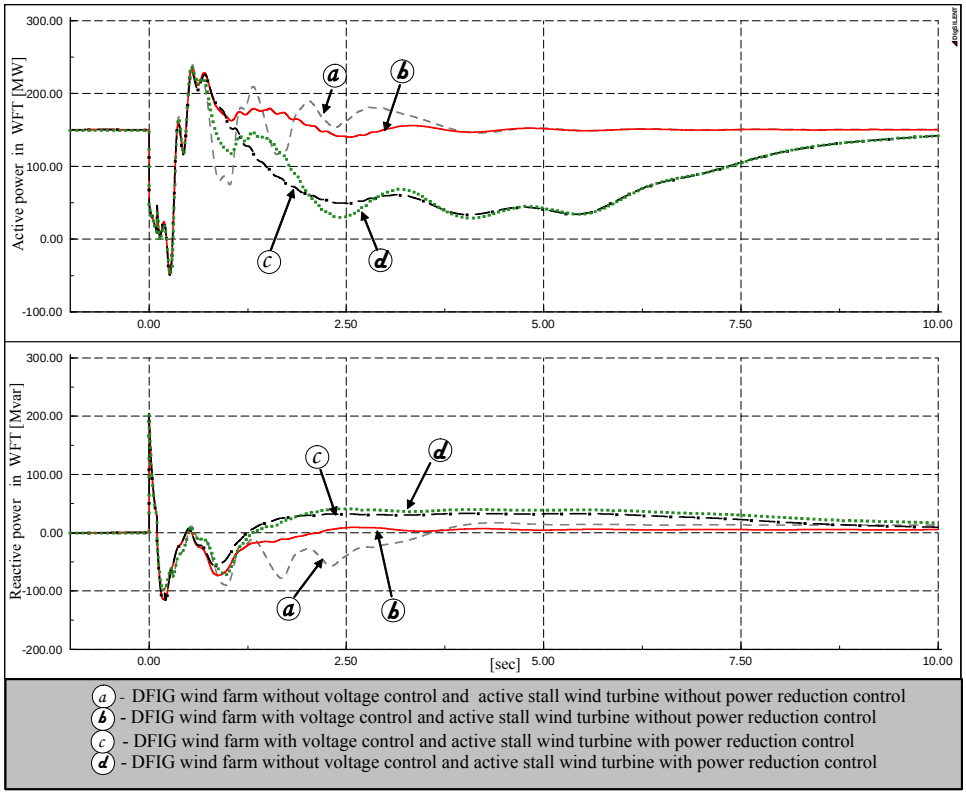

Figure 134: The active and the reactive power of the active stall wind farm in different 4 situations.

Both Figure 134 and Figure 135 illustrate the simulation results for the active stall wind farm from the following four different control scenerios:

a. DFIG wind farm ***without*** voltage control and active stall wind farm ***without*** power reduction control.

b. DFIG wind farm ***with*** voltage control and active stall wind farm ***without*** power reduction control.

c. DFIG wind farm ***with*** voltage control and active stall wind farm ***with*** power reduction control.

d. DFIG wind farm ***without*** voltage control and active stall wind farm ***with*** power reduction control.

The following observations can be made:

- The voltage control of the DFIG wind farm (case *b* and *c*) has a damping effect on the active stall wind farm, no matter whether this has or does not have power reduction control.
- The active power, the generator speed and the mechanical power are almost identical during the grid fault, no matter which case is simulated. The fact that the mechanical power is unchanged in this period means that the drive train system is equally stressed in all four cases.
- The worst case for the active stall wind farm is clearly case *a*, when the DFIG wind farm has no voltage control and the active stall wind farm has no power reduction control.
- The best case for the active stall wind farm is clearly case *b*, when the DFIG wind farm is equipped with voltage control and the power reduction con-

trol of the active stall wind farm is not enabled. Note that the wind farm is not subjected to torsional oscillations and there is no loss in the active power production. The influence of the DFIG voltage control on the active stall wind farm is thus even better when the latter does not have any special control implemented to ride-through a grid fault.

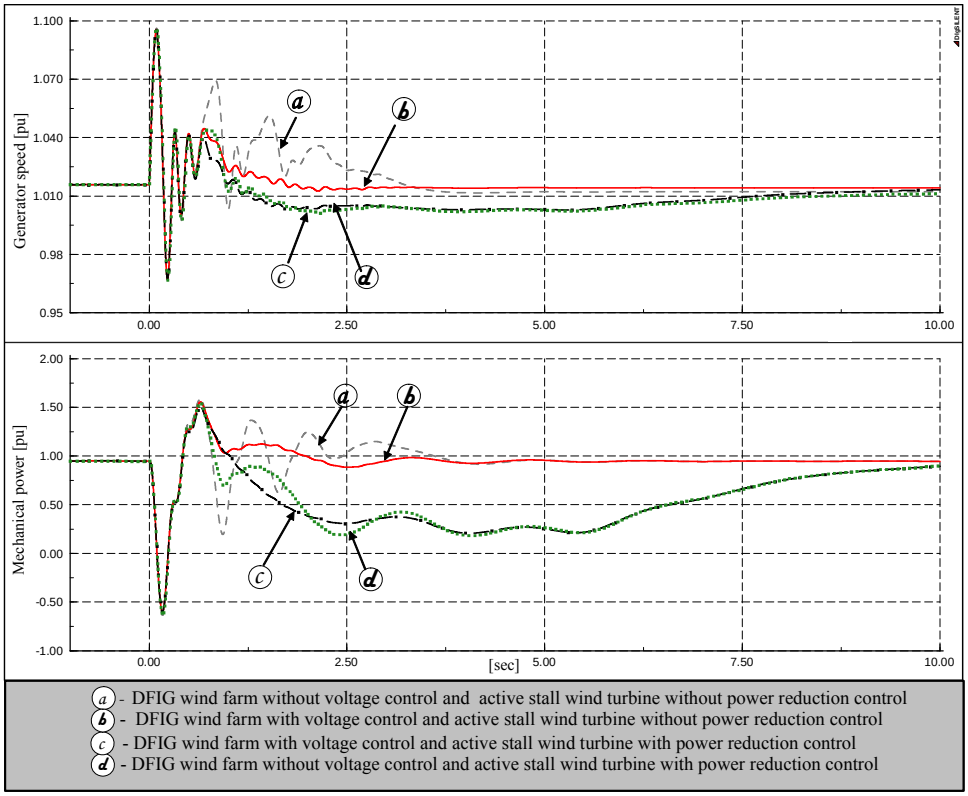

Figure 135: Generator speed and mechanical power of the active stall wind farm in different situations.

The overall conclusion from Figure 134 and Figure 135 is that the DFIG wind farm equipped with voltage control can help a nearby active stall wind farm through a grid fault, without any need to implement additional ride-through control strategy in the active stall wind farm.

9 Variable speed multi-pole PMSG wind turbine concept – normal operation

In this chapter, a dynamic model for a variable speed wind turbine with multi-pole permanent magnet synchronous generator (PMSG) and its control during normal operation conditions is described. The multi-pole PMSG wind turbine concept performance during grid faults is out of the scope of the present report.

9.1 Multi-pole (direct-driven) wind turbine generators

Traditionally wind turbine generators are operating best at high speeds and require step-up gearboxes. However, the gearbox of the wind turbine is expensive, subjected to vibration, noise and fatigue, needs lubrication as well as maintenance. In recent years the idea of gearless, i.e. direct-driven wind energy systems have gained interest, especially for offshore applications, where no gear maintenance is an attractive option.

In a direct-driven wind turbine concept the rotor and the generator shafts are mounted directly to the same shaft. The generator is running at very low speeds, typically 10 to 25rpm for wind turbines in the MW range. Low shaft speed operation is in generally a drawback for electric generators, owing to the fact that the torque needed to produce the required power has to be increased. Standard generators can therefore not be used and generators have to be developed specifically for this application. Because of the high rated torque, the direct-driven generators are usually heavier and less efficient than conventional generators. To increase the efficiency and reduce the weight of the active parts, direct-driven generators are usually designed with a large rotor diameter and a high number of poles to get suitable frequency at low speed. The size and the losses of the generator are to a large extent determined by the required torque.

Asynchronous generators with large number of poles and thus small pole pitch have a very low magnetizing reactance. This means that multi-pole asynchronous generators require even larger magnetizing current (i.e. poorer power factor) than conventional asynchronous generators. It is therefore recommended to use multi-pole synchronous generators (Grauers A.,1996).

A multi-pole synchronous generator can either be electrically excited or with permanent magnets. Almost all large generators are electrically excited.

However, for low-speed gearless wind turbine generators, the permanent magnet generator is more competitive because it can have higher pole number than a conventional synchronous generator. The use of the permanent magnet generators is beginning to become more attractive, due to their higher efficiency and the absence of the DC excitation system, compared to the conventional synchronous generators. The permanent magnets eliminate thus the need of a field winding, the copper losses in the rotor due to the field current and the use of slip rings. Their disadvantages are the fact that their excitation can not be controlled and that they are more expensive. However, since midding'90 the permanent magnets generators have become more attractive due to the decreasing magnet prices. For example, the radial flux permanent magnet synchronous generator is now cheaper and more efficient than the electrically excited SG.

The multi-pole generators can be either:

- Fixed-speed and connected directly to the ac grid
- Variable speed and connected to the ac grid through a frequency converter

The multi-pole fixed speed generators are frequently used in hydropower applications (Binder A. et al., 2005). They are directly connected to the ac grid and they have therefore their terminal voltage and electrical frequency fixed to the grid.

In this chapter, the attention is drawn to the multi-pole variable speed generators as they look more attractive for wind turbine industry. In variable speed wind turbine concepts, the generator is controlled by a power electronic equipment. The electric frequency of the generator is decoupled from the electric frequency of the power system because the generator is grid connected via a frequency converter.

In the following, the modelling and control features of a variable speed multi-pole PMSG wind turbine concept are described. A comprehensive dynamic simulation model of this concept is implemented in the power system simulation software DIgSILENT PowerFactory and a control strategy for the entire turbine system is developed.

9.2 System configuration of variable speed multi-pole PMSG wind turbine

As mentioned in Chapter 6, variable speed operation of a wind turbine is possible when the electric frequency of its generator varies and it is thus decoupled from the grid frequency through a power electronic.

Till now, the most commonly used electrical system for a variable speed multi-pole synchronous generator wind turbine has consisted of a synchronous generator connected to the grid over a diode rectifier, an intermediary DC circuit and a thyristor inverter. However, due to the fast development in the last years of rapid switching valves with high power ratings, the use of self-commutated converters (IGBT) is increasing in wind power applications. This is especially common for permanent magnet synchronous generators (PMSG), where both generator-side converter and grid-side converter are realised by IGBT converters (i.e. back-to-back converter). A diode rectifier is usually chosen for its low price and low losses, while an IGBT converter is used because it produces high quality power to the grid, i.e. current harmonics from the inverter are decreased and any desired power factor can be obtained and the energy can flow in both directions. An advantage of IGBT converter is that contrarily a diode rectifier solution, is that it can produce a constant dc-voltage regardless of generator speed. It has the potential of utilizing the generator best. However, it is more expensive and has higher rectifier losses.

A typical configuration of variable speed multi-pole PMSG wind turbine is depicted in Figure 136. It consists of:

- Wind turbine mechanical level:
  - Aerodynamics
  - Gearless drive train
  - Pitch angle control
- Wind turbine electrical level:
  - Multi-pole permanent magnet synchronous generator (PMSG)
  - Frequency converter and its control

In this configuration, the synchronous generator is connected to the power network through a frequency converter system that controls the speed of the

generator and the power flow to the grid. The full-scale frequency converter system consists of two back-to-back voltage source converters (generator-side converter and the grid-side converter), controlled by IGBT switches and connected via a DC link, which behaves as an energy storage device. The use of such converter enables the PMSG to define its terminal voltage and its electric frequency according to the desirable optimal rotational speed of the wind turbine, independently of the fixed electric frequency and the voltage of the ac grid.

Notice that the aerodynamic rotor of the wind turbine is directly coupled to the generator without any gearbox, i.e. through a gearless drive train. The permanent magnets are mounted on the generator rotor shaft, while the stator consists of several windings and feeds into a full- scale frequency converter. As the converter system decouples the generator from the power network, the electrical frequency of the generator may vary as the wind speed changes, while the network frequency remains unchanged. Contrarily fixed speed wind turbines where the power flow to the grid is dependent on the mechanical power that drives the wind turbine, in variable speed wind the power flow is set by the power converter. The rating of the converter system in this topology corresponds to the rated power of the generator plus losses.

The whole system is equipped with the wind turbine itself controller, i.e. pitch angle controller, and the frequency converter controller. Both controllers are using information about the generator speed. The converter's controller controls the generator speed by controlling the grid power according to a speed versus power control characteristic of the wind turbine. The pitch controller controls the rotor speed as well, but it is operational only at high wind speeds, when the power is reduced by pitching the blades in order to avoid the overloading of the converter and generators.

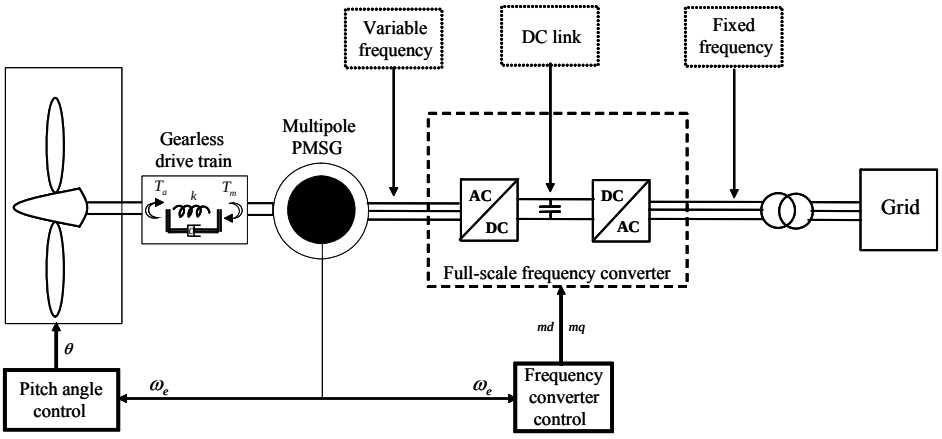

Figure 136: Variable speed multi-pole PMSG wind turbine configuration.

Note that the total turbine power goes through the converter that converts the varying generator frequency to the constant grid frequency. Since the PMSG is connected to the grid through the back-to-back converter, only the active power of the PMSG is transferred to the grid. The reactive power cannot be exchanged through the DC link in the converter system. However, the grid-side converter, whose electric frequency and voltage are fixed to the grid, can be set to control the reactive power/voltage on the grid. Like the variable speed wind turbine with doubly-fed induction generator, this concept enables full active and reactive power control.

The electric frequency at the PMSG terminals, f_e, is the product of the mechanical frequency of the wind turbine rotor, f_m, and the number of generator pole-pairs *p:*

$$f_e = f_m \; p \tag{82}$$

where the mechanical frequency of the generator rotor is related to the turbine rotor speed ω_m.

$$\omega_m = 60 \; f_m \qquad [rpm] \tag{83}$$

The common target of the control is to adjust the electrical frequency of the generator to the optimized mechanical frequency of the aerodynamic rotor and to keep the voltage at the PMSG terminals on a desired level.

In the present investigation, it is assumed a number of pole-pairs of 38 and that the rotational speed of the rotor ω_m varies between 9 and 21 rpm, depending on the incoming wind. This means that the mechanical frequency f_m is between 0.15 and 0.35Hz, while the electric frequency f_e at the terminals of PMSG varies in the range from 5.7Hz at small winds to 13.3Hz in strong winds. The losses from the converters are neglected and the grid is supposed to be stiff.

In Table 7, the main characteristic data of a fictive typical 2MW variable speed multi-pole wind turbine with PMSG are given.

Rated power	2 [MW]
Dynamic speed range	9-21 [rpm]
Rated speed	16.7 [rpm]
Generator type	Multi-pole PMSG
Number of pole pairs	38
Electrical frequency	5.7-13.3 [Hz]
Rated grid voltage	3.3 [V]
Converter type	IGBT
Rated converter power	2.2 [MVar]
Rated DC link voltage	5.4 [V]
DC link capacitor	2400 [F]

Table 7: Data example of multi-pole PMSG wind turbine.

9.3 Gearless drive train, aerodynamics and pitch angle control system

Wind turbines have relatively soft shafts (Akhmatov V., 2003), the eigen-frequency of the drive train being rather low and within the bandwidth that is normally taken into account in power system dynamics simulations (0.1-10Hz). A two-mass model representation of the drive train is therefore essential in order to illustrate properly the dynamic impact of wind turbines on the grid. A lumped mass representation is usually sufficient for example in the case of load flow analyses, where the impact of wind fluctuations on the electrical power balance is in focus.

A two-mass mechanical model, as described in Section 2.3.2, is also used in this chapter to model the gearless drive train of a direct-driven multi-pole PMSG wind turbine.

One mass represents the turbine inertia J_{rot}, while the other mass is equivalent to the generator inertia J_{gen}. These two masses are connected by a flexible low speed shaft characterised by a stiffness k and a damping c, as described in Section 2.3.2. The high speed shaft is assumed stiff. No gearbox is used in this concept, i.e. $n_{gear}=1$.

The aerodynamic torque T_a from the rotor acts on one end of the drive train while the mechanical torque T_m from the generator side acts on the other end of the drive train, as illustrated in Figure 136. The result of this is the torsion of the shaft. As the drive train of a wind turbine behaves as a torsional spring characteristic, the generator speed of the turbine is usually prone to oscillations whenever the system gets excited by changes in the wind speed, pitch angle or grid faults. The frequency of these oscillations is the so-called free-free frequency:

$$f_{osc} = \frac{1}{2\pi} \cdot \sqrt{\frac{k}{J_{eq}}} \tag{84}$$

where J_{eq} is the equivalent inertia of the drive train model, determined by:

$$J_{eq} = \frac{J_{rot} \cdot J_{gen}}{J_{rot} + J_{gen}} \tag{85}$$

Figure 137 illustrates how a two-mass model representation of a drive train is indispensable in order to achieve correctly the wind turbine impact on the power system during external disturbances (as for example load changes). For exemplification, a sudden change in the wind speed from 12m/s to 11 m/s is performed with both one-mass model and two-mass model representation of the drive train, in a simulation of a 2MW variable speed multi-pole PMSG wind turbine.

Figure 137 shows how, contrarily one-mass model, a two-mass model representation of the drive train reflects the presence of the torsional oscillations. The change in wind speed excites the drive train oscillations, and this is obviously reflected only when the two-mass model for the drive train is used. These oscillations, illustrated in Figure 137 as appearing in the generator speed and the grid power, are clearly amplified and insufficiently damped by the multi-pole PMSG wind turbine configuration when no any specific external damping system (mechanical or electrical) is used. The wind speed change causes a drop in generator speed and active power. Note that, the active power drop is delayed compared to the generator speed, this owing to the specific design around rated speed of the MPP tracking characteristic, in order to avoid unnecessary power fluctuations.

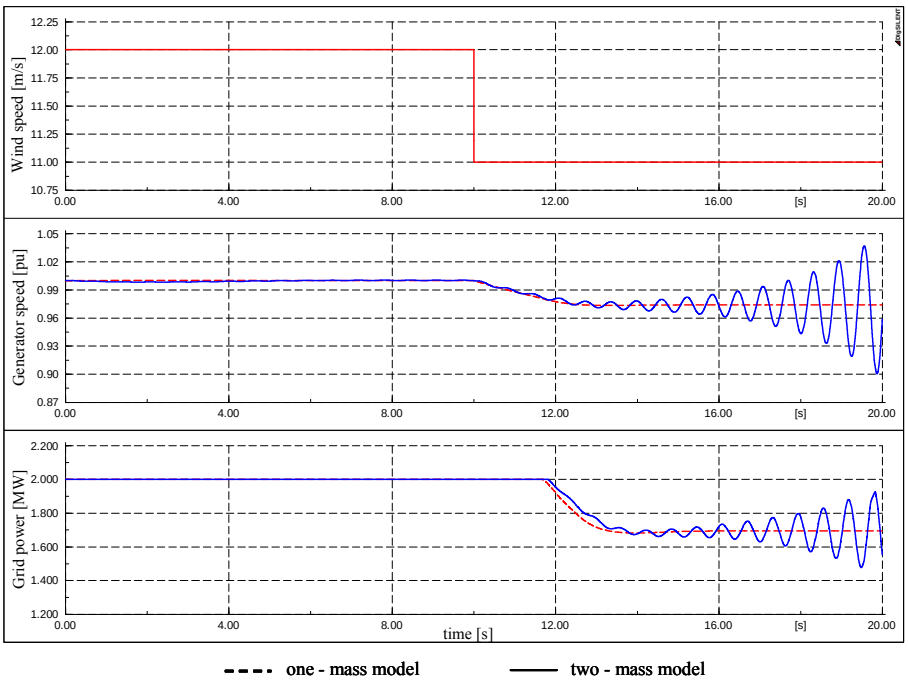

Figure 137: Torsional oscillations reflected by using one-mass model or two-mass model representation of the drive train.

The use of a two-mass model is very important especially in the case of a multi-pole generator wind turbine concept. According to (Akhmatov V., 2003), larger number of pole-pairs is, "softer" the drive train shaft becomes. The effective stiffness of the shaft is reduced by increasing the number of pole-pairs p according to:

$$K_s = \frac{k}{S_n} \cdot \frac{\omega_m}{p} \tag{86}$$

where K_s is the effective shaft stiffness, k is the shaft stiffness in Nm/rad, S_n denotes the rated MVA-base of the generator and ω_m is the rated mechanical speed. This implies that a mechanical shaft twist results in larger dynamic change of the electrical rotor angle for generators with a large number of poles. In multi-pole generators the same electrical angle corresponds to a much smaller mechanical angle than in generators with small pole numbers. The torsional twist of the shaft for a multi-pole generator wind turbine affects the operation of the generator itself more significantly.

The simplified aerodynamic model, described in Section 2.3.3, can also be used for the variable speed multi-pole PMSG wind turbine concept. As mentioned, this simplified aerodynamic model is typically based on a two dimensional aerodynamic torque coefficient C_q table, provided by a standard aerodynamic program.

The pitch angle control in Figure 136, is the same as that described for variable speed DFIG wind turbine concept in Chapter 7. It is realised by a PI controller with antiwind-up, using a servomechanism model with limitation of both the pitch angle and its rate-of-change. The pitch angle controls the generator speed, i.e. the input in the controller is the error signal between the measured generator speed and the reference generator speed. The pitch angle controller limits the rotor speed when the nominal generator power has been reached, by limiting the mechanical power extracted from the wind and thus restoring the balance between electrical and mechanical power.

9.4 Permanent magnet synchronous generator (PMSG) model

The equations describing a synchronous generator can be found in (Kundur P., 1994). It is beyond the scope of this text to present a detailed treatment of the synchronous generator. A brief overview is however provided, in order to present the most important features of the permanent magnet synchronous generator (PMSG) used in wind turbines.

The equivalent circuit for one phase of synchronous generator is shown in Figure 138.

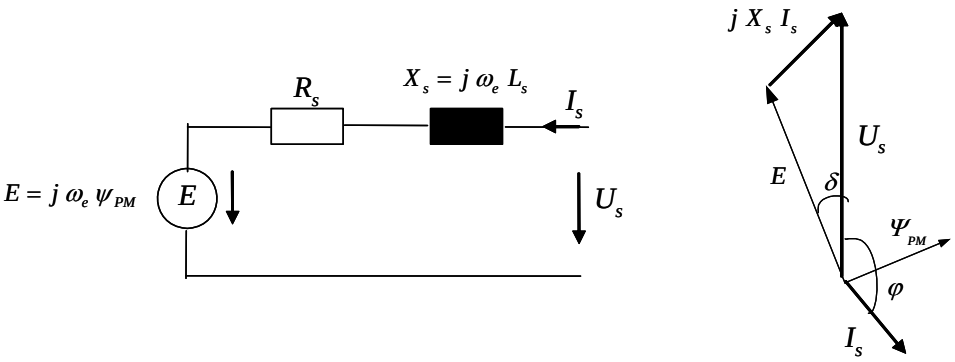

Figure 138: Equivalent circuit and phasor diagram of a PMSG.

Synchronous machine models for power system analysis are usually based on the assumption that the magnetic flux distribution in the rotor is sinusoidal. With this assumption the flux can entirely be described by a vector and in the case of PMSG, the magnetic fields from the permanent magnets induces a voltage E in the stator winding, expressed as:

$$|E| = \omega_e\,\psi_{PM} = 2\,\pi\,f_e\,\psi_{PM} \tag{87}$$

where ω_e is the electrical speed, ψ_{PM} is the magnitude of the flux induced in the stator by the permanent magnets of the rotor, and f_e, is the electrical frequency. A current I_s in the stator winding causes losses and voltage drop, both phenomena are represented in the model by the resistance R_s. Apart from causing resistive voltage drop, the stator current also produces a magnetic field of its own, which is added to the field generated by the permanent magnets. Thus, the voltage U_s at the stator terminal of PMSG corresponds to the voltage induced by the total magnetic field. Depending on the phase delay of the stator current, the total magnetic field in the generator either increases or decreases as the current increases. This effect is represented by the synchronous reactance X_s in the model. The resistance R_s is normally much smaller than X_s, and therefore it is normally neglected except in efficiency calculations. It can be found in (Grauers A. et al., 1999) and (Akhmatov V. et al., 2003) that multi-pole synchronous generators are characterized with a relatively high stator reactance.

The load angle δ between the internal voltage E and the stator voltage U_s drives the stator current I_s. The relationship among E, U_s and I_s is shown in the phasor diagram of Figure 138. Note that the induced voltage E is proportional with the electrical speed of the generator. When $E < U_s$ it is said that the machine is underexcitated, otherwise it is overexcitated. The electrical excited machines are typically controlled to be reactive neutral, i.e. the converter rating is reduced to the active power value. The permanent magnet generators due to their fixed excitation, work typically underexcited, i.e. the converter provides

reactive power to the generator and therefore the converter must be oversized (Jöckel S., 2006). Based on this, the expressions of the active and reactive power of the generator in terms of E, U_s and the load angle δ can be derived:

$$P_{gen} = \frac{|U_s||E|}{X_s}\sin\delta$$
$$Q_{gen} = \frac{|U_s||E|}{X_s}\cos\delta - \frac{|U_s|^2}{X_s} \quad (88)$$

If the mechanical power input increases, i.e. the load angle (the phase shift between U_s and E) increases, the electrical power output increases also, reaching a maximum at $\delta = 90^o$. The converter is able to generate or absorb active and reactive power, if both the load angle and voltage magnitude are controllable.

The equations of a PMSG can be expressed directly from the equations of a DC excited synchronous generator SG, with the simplification that PMSG does not have damper winding (Kundur P., 1994). The steady state voltage equations of the generator, expressed in the rotor-oriented dq-reference frame RRF (defined as in Section 9.6.1), can be expressed as follows:

$$u_{sd} = R_s\, i_{sd} - \omega_e\, \psi_{sq} + \dot{\psi}_{sd}$$
$$u_{sq} = R_s\, i_{sq} + \omega_e\, \psi_{sd} + \dot{\psi}_{sq} \quad (89)$$

With the stator flux components:

$$\psi_{sd} = L_d\, i_{sd} + \psi_{PM}$$
$$\psi_{sq} = L_q\, i_{sq} \quad (90)$$

Where u_{ds} and u_{qs} are the terminal stator voltages, i_{ds} and i_{qs} are the stator currents, L_d and L_q are the stator inductances in the dq reference frame. In stability studies, where the stator transients can be neglected, the stator voltage equations can be reduced to:

$$u_{sd} = R_s\, i_{sd} - \omega_e\, \psi_{sq}$$
$$u_{sq} = R_s\, i_{sq} + \omega_e\, \psi_{sd} \quad (91)$$

The electrical torque of the generator is:

$$T_e = \frac{3}{2}\, p\, \mathrm{Im}\left[\overline{\psi}_s^*\, \bar{i}_s\right] = \frac{3}{2}\, p\, \left[\psi_{sd}\, i_{sq} - \psi_{sq}\, i_{sd}\right] \quad (92)$$

Expressing further the stator flux components, the electrical torque can be calculated by:

$$T_e = \frac{3}{2}\, p\, \left[(L_d - L_q)\, i_{sd}\, i_{sq} + \psi_{PM}\, i_{sq}\right] \quad (93)$$

If the generator is a round rotor machine, where L_d=L_q, the equation for the electrical torque results only from the permanent magnet flux and the q-component of the stator current:

$$T_e = \frac{3}{2}\, p\, \psi_{PM}\, i_{sq} \quad (94)$$

The active and reactive power of the synchronous generator can be then expressed as:

$$P_{gen} = T_e\ \omega_m = \frac{3}{2}\left[u_{sd}\ i_{sd} + u_{sq}\ i_{sq}\right] \qquad (95)$$

$$Q_{gen} = \frac{3}{2}\left[u_{sq}\ i_{sd} - u_{sd}\ i_{sq}\right]$$

In the case of variable speed wind turbines, the active and reactive powers of the generator are controlled by the converter, which acts on the generator stator voltage and current. As the generator is fully decoupled from the grid by the converter, the reactive power expressed previously is exchanged with the generator-side converter and not with the grid.

The PMSG has no damper windings. As a PMSG is connected to the grid through a converter, which provides a variable stator frequency according to the actual rotor speed, there is never any relative movement between stator and rotor field, which could induce a voltage in the damper winding (Jauch C., 2006). Furthermore, due to the permanent excitation, a PMSG has no field windings, in which transient currents could be induced or damped, respectively. Hence, in case of transients the field windings do not contribute to damping either. The PMSG connected to a converter is thus a system without inherent damping. Nevertheless, an external damping of the system must then be applied by means of the converter control.

9.5 Full-scale frequency converter configuration

The full-scale frequency converter in a direct-driven wind turbine consists of a generator-side converter, a dc-link and the grid-side converter.

9.5.1 Generator-side converter

Two converter topologies are typically used for the generator-side converter, for instance a diode rectifier with a boost converter and an IGBT voltage source converter.

The diode rectifier represents a cheap and simple solution with low losses. However, it cannot control the current phase and it is unable to feed the generator with the needed reactive power. This means that the stator current and the stator voltage are always in phase, which leads to large voltage drops and to a decreasing DC-link voltage when the stator current increases (Grauers A. et al., 1999). The generator feeds power to the network as long as the DC-link has a constant voltage higher than the peak voltage of the network. The generator is not capable of generating a constant high voltage at low speed, as it is the case of direct-drive wind turbines, and therefore in case of a diode rectifier configuration a boost converter (known also as DC-DC step-up converter), must be used to raise the voltage of the diode rectifier – see Figure 139.

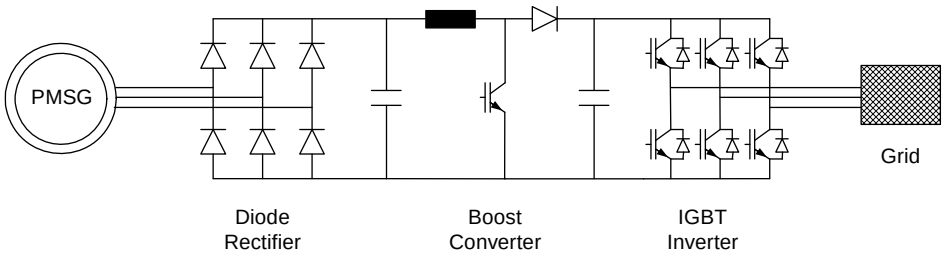

Figure 139: PMSG connected via diode rectifier with boost converter.

The diode rectifier is not the best solution for a PMSG wind turbine configuration. In such topology a PMSG would be insufficiently utilized because as a PMSG has a fixed excitation, it is only optimal for one operational point. It follows, that a PMSG is insufficiently utilized, if a diode rectifier is used (Jöckel S., 2002). The best performance of direct-driven PMSG wind turbine concept is achieved with fully controllable active inverters, i.e. the PWM controlled IGBT voltage source converters existing in the structure of back-to-back converter, as illustrated in Figure 140. Such IGBT converter is able to feed the generator with the needed reactive power and to provide a very high efficiency of the system. However, an IGBT converter is more expensive and it must be protected against overcurrents and overvoltages.

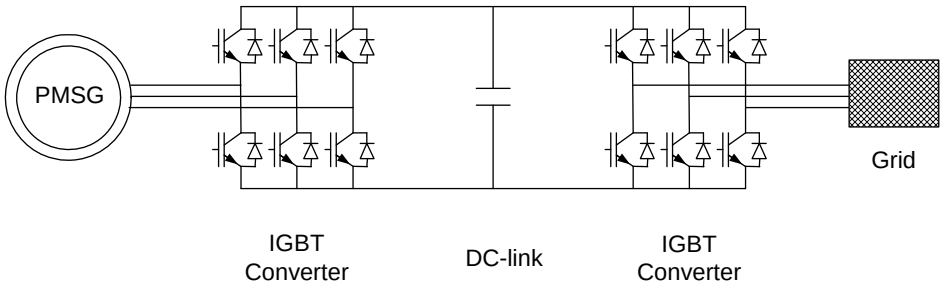

Figure 140: PMSG connected via IGBT voltage source converter.

In the applications with focus on control behaviour of IGBT converters (e.g. power system stability), a fundamental frequency model of the converter can be used. This technique is widely used in variable speed wind turbine stability research and is accepted as the standard approach in this topic. Assuming an ideal DC voltage and an ideal PWM modulation, the level of the DC-link voltage U_{DC} can be expressed based on the AC voltage level of the generator (Pöller, M., 2003), as follows:

$$U_{DC} = |U_{AC}| \frac{2\sqrt{2}}{m\sqrt{3}} \qquad (96)$$

where m ($0 \le m < 1$) denotes the pulse-width-modulation index. The DC-link voltage must be higher than the peak voltage of the network and is regulated by controlling the power flow to the AC grid.

An important property of the back-to-back converter is the possibility of fast control of the power flow. By controlling the power flow to the grid, the DC-link voltage can be held constant. The presence of a fast control loop for the DC-link voltage makes it possible to reduce the size of the DC-link capacitor, without affecting inverter performance.

9.5.2 DC-link

The DC-link capacitor provides an intermediate energy storage, which decouples the generator-side converter and the grid-side converter.

The transfer of the active power from the generator into the grid can be realised via the DC-link, only whether the DC-link voltage is kept constant. If a lossless converter is assumed, the AC power is equal to the DC power.

$$P_{AC} = P_{DC} = U_{DC} \cdot I_{DC} \tag{97}$$

In steady state operation and with no losses in the DC-link, the instantaneous power on the DC side must equal the instantaneous power on the AC side. In the moment that this power balance is broken, the instantaneous difference in power is stored in the DC-link capacitor and this leads to fluctuations in the DC-link voltage. An instantaneous current in the DC-link capacitor is then derived to complete the power balance:

$$i_C = C_{DC} \frac{dU_{DC}}{dt} \tag{98}$$

The DC-link capacitor current is discontinuous, as it is switched on and off with the switching frequency of the converter. This process induces voltage ripples in the DC-link. This voltage ripple must be made small enough for the voltage to be virtually constant during a switch period. This sets a lower limit on the capacitor size.

Small voltage ripples requires larger capacitor, which on one side has a slow response to voltage changes, but on the other side has a smaller current and thus an increased lifetime. On the other hand, a small capacitor makes fast changes in the DC voltage possible, but results in higher voltage ripples and reduced lifetime. Selecting the size of the DC-link has thus to be a trade-off between voltage ripples, lifetime and the fast control of the DC-link. The trade-off relation for the design of the DC-link capacitor in the back-to-back converter is described in (Lindholm M. (2004), as follows:

$$C_{DC} = \frac{S_n}{\overline{U}_{DC} \cdot \Delta U_{DC} \cdot 2 \cdot \omega_e} \tag{99}$$

C_{DC}	DC-link capacitance	S_n	apparent converter power
$\overline{U}_{DC}$	average DC-link voltage	ω_e	electrical frequency
ΔU_{DC}	allowed voltage ripple (peak-peak)		

9.5.3 Grid-side converter

Grid-side converters are usually realised by self commutated PWM circuits, i.e. IGBTs or GTOs. They convert the DC-link voltage to the AC grid voltage with fixed frequency of the power system. It may thus be operated to give sinusoidal grid currents. A grid-side converter can thus generate or consume reactive power by injecting or lagging current to the grid. Since the back-to-back converter decouples the reactive power of grid-side converter and generator-side converter, the reactive power supply to the grid can be determined by the grid-side converter only, independent of the reactive power set-point of the generator. The reactive power supply of the grid-side converter is however limited by the converter rating and the active power flow from the turbine. Under normal operating conditions the grid-side converter is operated with unity power factor.

In case of grid faults the converter can serve as a reactive power source in order to contribute to voltage stability.

9.6 Full-scale frequency converter control

Similar to the control of DFIG, the PMSG behaviour is strongly dependent by the control of the frequency converter both in normal operation and during fault conditions.

As mentioned in Section 7.2, frequency converters are usually controlled utilizing vector control techniques (Heier S., 1998). Briefly, vector control allows decoupled control of both active and reactive power. The idea is to use a rotating reference frame based on an AC flux or voltage and then to project currents on this rotating frame. Such projections are usually referred to as the d and q components of their respective currents. With a suitable choice of reference frames the AC currents appear as DC quantities in the steady state. For flux-based rotating frames, changes in the q component will lead to active power changes, while changes in the d component will lead to reactive power changes. In voltage-based rotating frames (and thus 90^0 ahead of flux-based frames) the effect is the opposite.

9.6.1 System reference frames

The system reference frames relevant in the control of PMSG together with a phasor diagram of PMSG are sketched in Figure 141, in order to illustrate the alignment of the machine vectors to the reference frames:

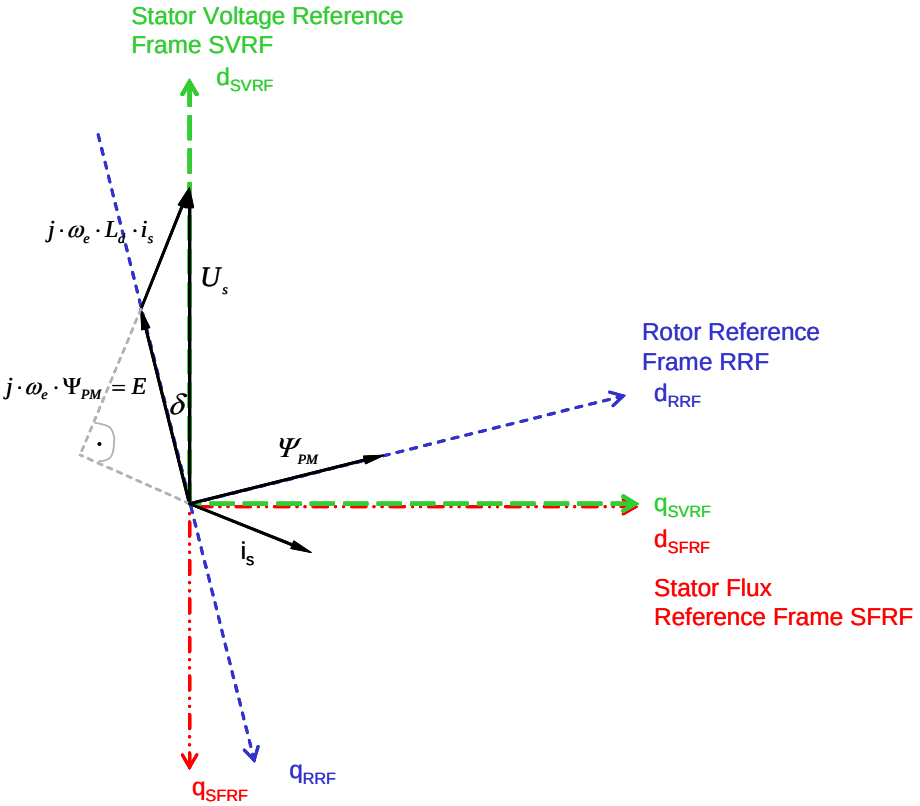

Figure 141: System reference frames used in the control of a PMSG connected via IGBT voltage source converter.

- Rotor oriented reference frame (RRF) is aligned with its d-axis to the permanent magnet flux vector Ψ_{PM}. The rotor reference frame rotates with the rotational speed ω_e of the rotor flux, which is equal to mechanical rotor speed ω_m times the pole pairs *p*:

$$\omega_e = \omega_m \; p = 2\,\pi \; f_m \tag{100}$$

  Note that the vector of the electromotive force *E* is perpendicular to the rotor flux vector.
- Stator voltage oriented reference frame (SVRF) is aligned with its d-axis to the stator voltage vector U_s. This means that the voltage U_s has only a d-component in the SVRF. This simplifies e.g. the equations for active and reactive power of the generator to:

$$\begin{aligned} P_{gen} &= \frac{3}{2}\, u_{sd} \; i_{sd} \\ Q_{gen} &= -\frac{3}{2}\, u_{sd} \; i_{sq} \end{aligned} \quad \text{(in SVRF)} \tag{101}$$

  In SVRF, the active power of the generator is thus determined by the d-component of the stator current, while the reactive power of the generator is determined by the q-component of the stator current. The SVRF rotates with the angular frequency of the stator voltage, which is the same rotational speed as for the RRF.
- Stator flux oriented reference frame (SFRF) is perpendicular to the stator voltage reference frame and rotates as well with the frequency of the stator voltage. The stator flux of the generator is perpendicular to the stator voltage vector U_s and represents the total flux linkage of the machine, namely the permanent magnet flux ψ_{PM} superposed to the flux generated by the stator current.
- System reference frame (SRF) is a reference frame in DIgSILENT aligned with one reference machine (a synchronous generator) in the power system and rotates with a frequency of 50 Hz. However, if the only generator in the power system is a PMSG behind a full-scale converter, i.e. it has a variable stator frequency, the definition of a system reference frame is more problematic. In this case it must be distinguished between global (50 Hz) and local reference frame (variable generator frequency).

9.6.2 Overall control strategy of PMSG with full-scale converter

As mentioned in the previous chapter, the frequency converter is a standard built-in model in the DIgSILENT library. However ts control is not a standard model in the DIgSILENT library and therefore it has to be implemented as a user-written model in the dynamic simulation language of DIgSILENT.

In the present research, the converter control is modelled on a generic level, as illustrated in Figure 142, without focusing on any particular design of a manufacturer. Similar to the DFIG, the presence of the frequency converter makes possible to control independently the active and reactive power of the wind turbine. As illustrated in Figure 142, the converter control is exercised by means of two controllers:

- Generator-side converter controller (controller 1)
- Grid-side converter controller (controller 2)

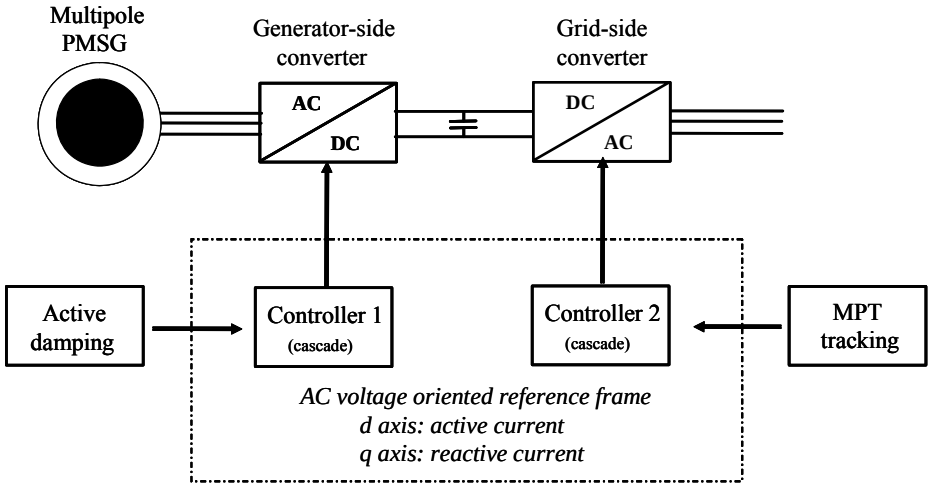

Figure 142: Power converter control in the variable speed multi-pole PMSG wind turbine.

The control of the converter can be realised by using different strategies. In this work, the control concept of the converter is using an AC voltage oriented reference frame, i.e. d-axis is used to control the active current, while q-axis is used for reactive current:

- Controller 1 is using the stator voltage reference frame
- Controller 2 is using the grid voltage reference frame

In the present control strategy, the oscillations existing in the drive train of a variable speed multi-pole PMSG wind turbine are actively damped by the control of the converter. Such strategy is able to ensure a stable operation of the whole wind turbine. As illustrated in Figure 142, an active damping block system is generating a reference signal in the generator-side converter controller (controller 1).

9.6.3 Damping system

It was illustrated in Figure 137 that due to the torsional characteristic of the drive train, the generator speed of a variable speed wind turbine is prone to oscillations whenever the system gets excited by changes i.e. in the wind speed or in the terminal voltage.

Such speed oscillations subside very quickly in the case of a fixed speed wind turbine. The reason is that the generator of a fixed speed wind turbine (i.e. squirrel cage induction generator SCIG) is characterised by a steep torque versus slip characteristic, as it is directly connected to the stiff grid.

All variable speed wind turbines are able to vary their rotor speed because their generator is either partially or fully decoupled from the fixed grid frequency. As described in Chapter 7, in the DFIG partially variable speed wind turbine concept, the stator windings are directly connected to the grid, while the

rotor windings are connected to the grid via a frequency converter. In this configuration the torque versus slip characteristic of the generator, controlled by the frequency converter accordingly, can still be used to damp the drive train oscillations as in the case of fixed speed wind turbines. However this is possible only for normal operation conditions. As it is shown in Chapter 8, in case of grid faults, the DFIG control system needs also an additional damping controller to stabilise the torsional oscillations and thus to enhance the fault ride-through capability of the DFIG wind turbine.

As sketched in Figure 136, a variable speed direct-driven SG wind turbine is completely disconnected from the grid via a full-scale converter. The frequency of the generator in such a configuration is thus decoupled from the stiff grid frequency. According to (Jauch C., 2006), an electrical excited synchronous generator behind a full-scale converter has no inherent damping, being practically an unstable system. The full-scale converter, to which the generator stator is connected, decides the rotor frequency according to how much power should be extracted from the wind. There is thus no relative movement between the rotor field and the stator field and it can therefore not be induced a current in the damper winding. The damper winding has thus no influence. There does not exist any torque to counteract the speed oscillations. This is also the case of a PMSG with full-scale converter wind turbine, which does not even have a damper winding. Moreover, the unstable speed oscillation is even worst for a multi-pole PMSG wind turbine, because a multi-pole generator wind turbine configuration has an extremely soft drive train shaft, as underlined in Section 9.2.

Figure 143 illustrates how the speed of a multi-pole PMSG with full-scale converter wind turbine concept oscillates with gradually increasing oscillation amplitude, causing the system to break down eventually even in case of a simple normal operation.

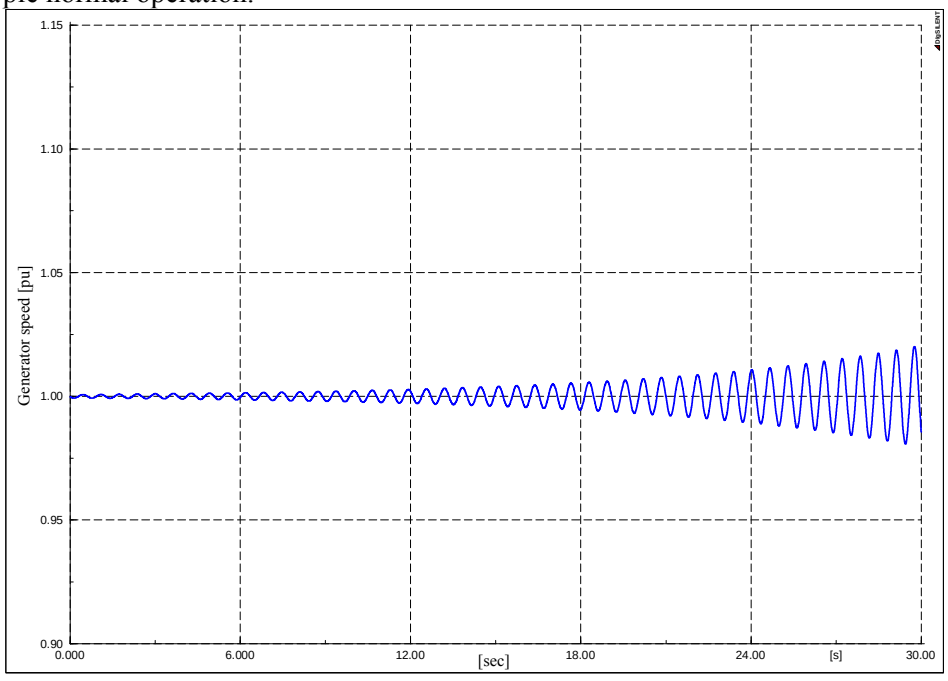

Figure 143: Unstable speed of the multi-pole PMSG wind turbine with full-scale converter, in normal operation at 12m/s and without any damping system.

Such a wind turbine configuration has thus no inherent damping and therefore an external additional damping system is necessary. Otherwise any small speed oscillation is quickly amplified causing instability.

The unstable speed oscillation can be counteracted either by controlling the mechanical power input in the generator or the electrical power produced by the generator into the grid. Different mechanical control schemes can be applied to damp these oscillations, e.g. damping by means of blade pitching (Jöckel S. et al., 2001) or damping by means of a compliant mounting of the generator (Westlake A. J. G. et al., 1996).

A straight forward way for damping the speed oscillations by controlling the electrical power sent to the grid is described in Chapter 8. The drive train oscillations of a DFIG wind turbine configuration during grid faults have been for example damped by controlling the power that the converter sends into the grid. However, this damping method has the disadvantage that it has a negative impact on the power that the wind turbine injects into the grid, namely the speed oscillations become visible as oscillations in the power on the grid.

The another solution which is adopted in this work to damp the speed oscillations, is known from large synchronous generators in power systems, where a power system stabilizer (PSS) provides damping for speed and rotor angle oscillations by controlling generator excitation. The synchronous generator voltage is controlled by changing the excitation of the generator. PSS counteracts the speed oscillations by producing thus an electrical torque in phase with the generator speed. A similar method, presented in (Jauch C., 2006), is applied for wind turbines with DC excited synchronous generator. The speed oscillations are damped by controlling the DC-link voltage by changing the excitation of the generator. The idea is to use temporarily the capacitor in the DC circuit as energy storage (buffer) between the generator and the grid. Small variation of the DC voltage is allowed in order to absorb torque oscillations. By periodically short term charging and discharging the capacitor, energy is stored in the capacitor and the load current varies. This in turn influences the torque in such a way that counteracts the speed oscillations and provides effective damping.

In this work, the damping method presented in (Jauch C., 2006), is adopted for the case of multi-pole PMSG wind turbine. This method is slightly modified, since a PMSG has a fixed excitation. In this case, the speed oscillations can not be damped by controlling the electrical excitation, but through the power converter.

As the power flowing through the full-scale converter into the grid is independent of the DC voltage, the damping of drive train oscillations by using the converter can be achieved without impacting on the power that is sent into the grid.

Similar to the case of a PSS, the damping of the drive train oscillations in a multi-pole PMSG wind turbine can also be realised when it is provided a component of the electrical torque of the generator in phase with the speed oscillation. The idea of the damping method using the DC capacitor as a short-term energy storage is thus to translate the speed oscillations into the definition of a DC voltage reference U_{DC}^{ref} oscillating with the same frequency and phase angle as the speed.

The frequency and the phase angle of the drive train oscillations, reflected in the generator speed, are very important to be known in order to design the damping system.

The frequency of the oscillations, which have to be damped, is, as mentioned before, the so-called free-free frequency:

$$f_{osc} = \frac{1}{2\pi} \cdot \sqrt{\frac{k}{J_{eq}}} \tag{102}$$

where J_{eq} is the equivalent inertia of the drive train model, determined in case of gearless system by:

$$J_{eq} = \frac{J_{rot} \cdot J_{gen}}{J_{rot} + J_{gen}} \tag{103}$$

Once the frequency to be damped is known, the phase angle to be compensated, has to be identified. In order to do that, the DC voltage reference signal U_{DC}^{ref} is defined as follows:

$$U_{DC}^{ref} = U_{DC}^{setpoint} + \Delta u_{osc} \tag{104}$$

where Δu_{osc} is a sinusoidal disturbance signal that has the frequency f_{osc}, and it is superimposed on the DC voltage setpoint. The DC voltage reference signal U_{DC}^{ref} is further used as input in the generator-side converter controller. It is a voltage signal which oscillates around its mean value $U_{DC}^{setpoint}$ with a sinusoidal offset Δu_{osc}. This definition is indicated in Figure 144, by path (1). Once the phase angle is identified, it can be used to realise the phase compensation itself – sketched in Figure 144 by path (2). Note, that the identification of the right phase angle, by using a sinusoidal disturbance as input signal instead of the generator speed is realised in a stable operation condition, namely using a high generator inertia.

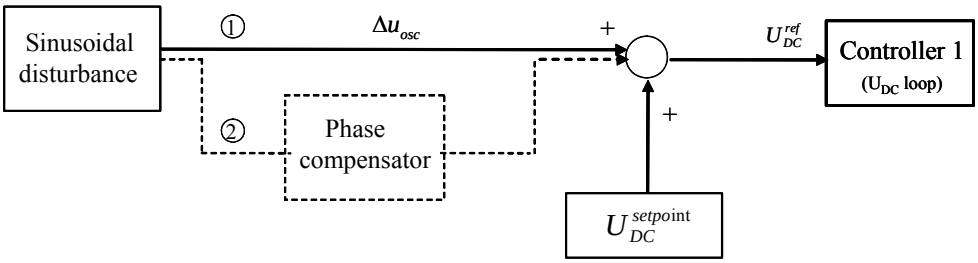

① - sinusoidal disturbance directly without phase compensator
② - sinusoidal disturbance through a phase compensator

Figure 144: Determination of the right phase angle.

Figure 145 illustrates how the electrical torque of the generator caused by the sinusoidal disturbance signal leads by 90 degrees, when no phase compensation is used (i.e. path (1)). Note that when a phase compensator is used (i.e. path (2)) the electrical torque is placed in phase with the sinusoidal disturbance (input signal) – see Figure 145.

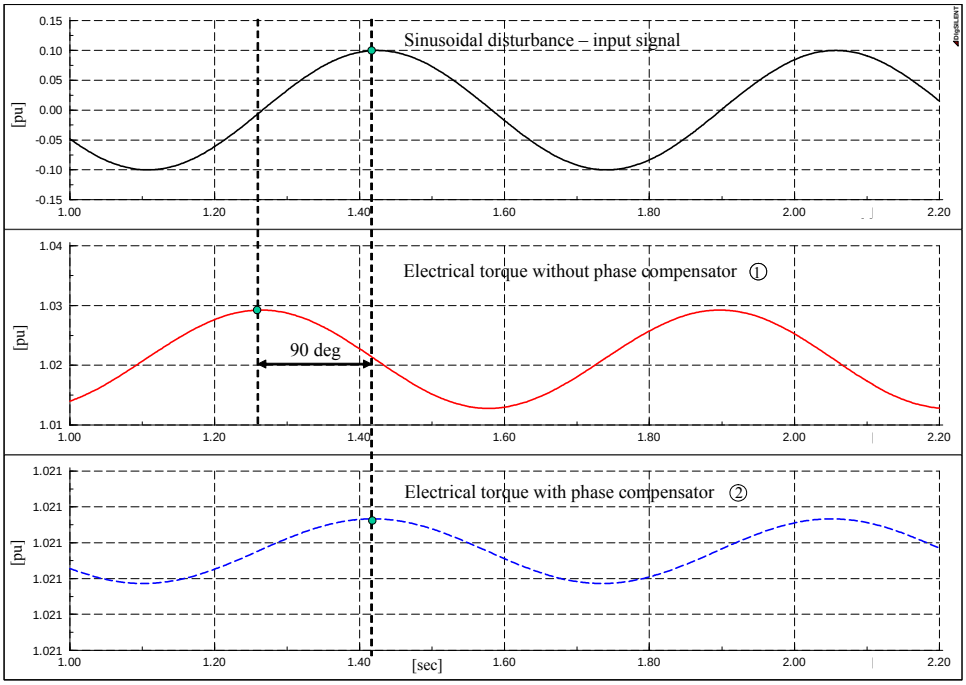

Figure 145: Phase compensation.

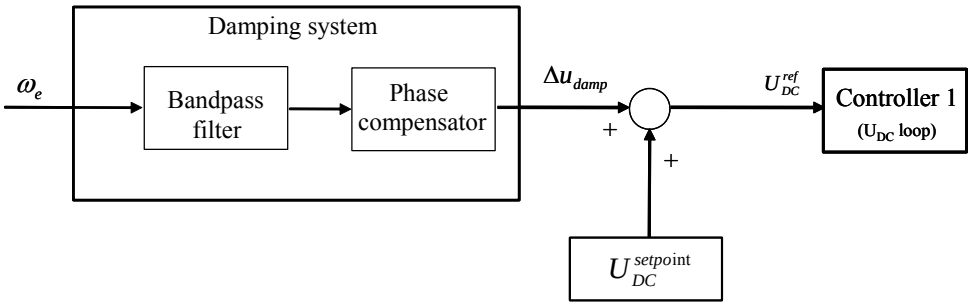

Figure 146: Damping oscillations system.

The idea of the damping system is to translate the speed oscillations into an oscillating DC voltage with the right phase angle and frequency. The result is t that the speed oscillations are damped. Once the frequency and the phase angle of the oscillation to be damped are found, a damping system can be realised.

The damping system is shown in Figure 146. It consists of two blocks: a bandpass filter and a phase compensator. The input in the damping system is the generator speed. The output of the damping system is superimposed on the DC voltage setpoint to provide the DC voltage reference signal for the generator-side converter controller (controller 1), as follows:

$$U_{DC}^{ref} = U_{DC}^{setpoint} + \Delta u_{damp} \qquad (105)$$

In a general setup, a bandpass filter pass a band of desired or specified frequencies, while attenuating those outside the band. In the present work, the bandpass filter of the damping system is designed to pass only oscillations of the free-free frequency (i.e. 10 rad/sec for the considered wind turbine) and to block all the other frequencies. The bandpass filter does not change the phase of the input signal. By designing a very narrow bandwidth, the bandpass filter allows the phase compensator to act exclusively on the oscillations only with the free-free frequency and not also on other existing frequencies in the system.

A low pass filter is used as a phase compensator in order to introduce a -90 degrees phase at the free-free frequency. The design of the low pass filter is based on the transfer function between DC voltage and electrical torque.

Figure 147 shows the Bode diagram of the designed bandpass and low-pass filters of the damping system. The position of the free-free frequency which have to be damped is also indicated.

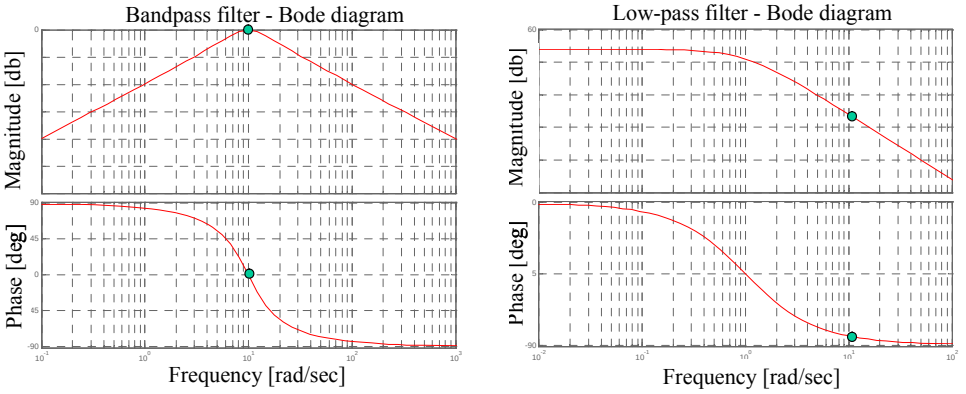

Figure 147: Bode diagram of bandpass filter and low pass filter.

Figure 148 illustrates the effect of the damping system on the multi-pole PMSG wind turbine with full-scale converter, when the system gets excited by for example a sudden change of 1 m/s in the wind speed. The wind speed, the generator speed and the active power production are illustrated for the situations with and without damping system respectively. Note that without damping system, the wind speed change provokes large oscillations with increasing oscillation amplitude in the generator speed and as result the system becomes unstable. It is clearly visible that these oscillations are quickly damped when the damping system is used. Such an additional damping system ensures thus a stable operation of the multi-pole PMSG with full-scale converter configuration, which otherwise would be unstable even under normal grid conditions.

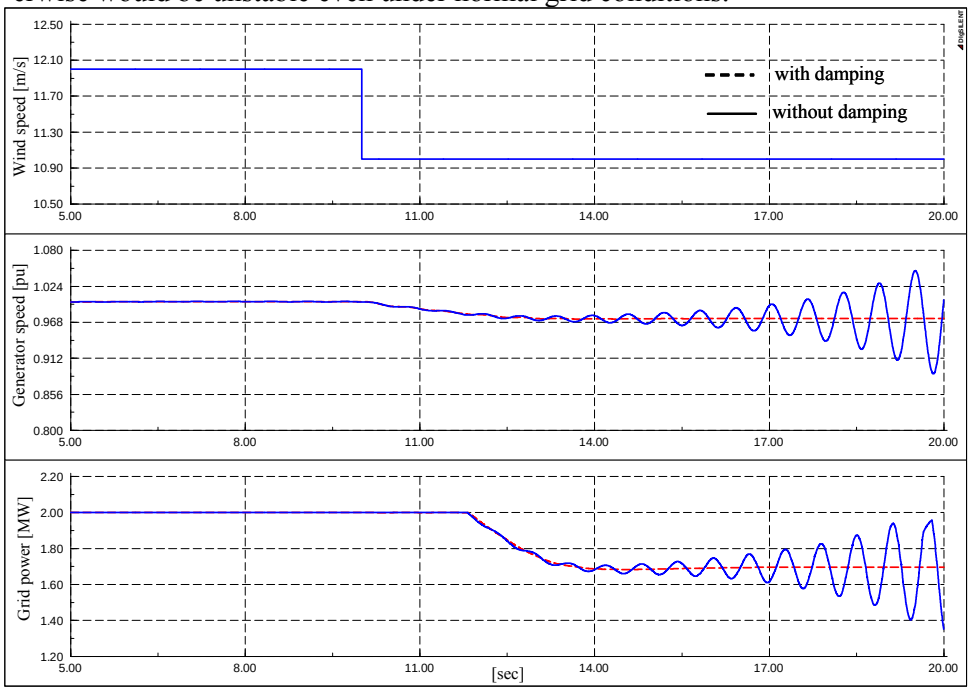

Figure 148: The effect of the damping system.

9.6.4 Converter control strategy

Different control strategies of the full-scale power converter, with their own advantages and disadvantages, can be applied. The strategies are typically based on the control of one of the following signals:

- ***generator stator voltage U_S to its rated value*** – it provides a robust control of the generator fluctuations, it keeps the ratio U_S/U_{DC} in a reasonable and controlled range, it avoids the risk of overvoltage and saturation of the converter in case of overspeeds. The disadvantage of this control strategy is that it implies a variable reactive power demand from the generator. This must be delivered by the power converter which has to have an increased rated power.

- ***generator reactive power Q_{gen} to zero*** - it implies a varying stator voltage, less losses and current rating. It may however results in stator voltages that challenges the saturation of the converter.

The converter control strategy implemented in the present work is based on to control the generator stator voltage to its rated value. This has the advantage that the generator and the power converter always operate at the rated voltage, for which they are designed and optimised. Figure 149 shows, as an example, the phasor diagram of this control strategy in case of two different operational points. At low wind speeds, if the generator speed increases, the active power increases according to the MPT characteristic with $P \sim \omega_e^3$, while the torque increases with $T_e \sim \omega_e^2$. Because $T_e \sim \sin\delta$ the load angle δ increases stronger than the magnitude of E, which increases linearly with the speed ($E=j\,\omega_e\,\Psi_{PM}$). It follows, that the reactive power demand increases as well and the generator starts to operate underexcited. For higher wind speeds the MPT control increases the power linearly with the generator speed ($P \sim \omega_e$). Thus the torque and the load angle stay constant. As the magnitude of E increases further the reactive power demand of the generator starts then to decrease. The reactive power demand of the generator can be thus limited by controlling the generator stator voltage depending on the generator speed.

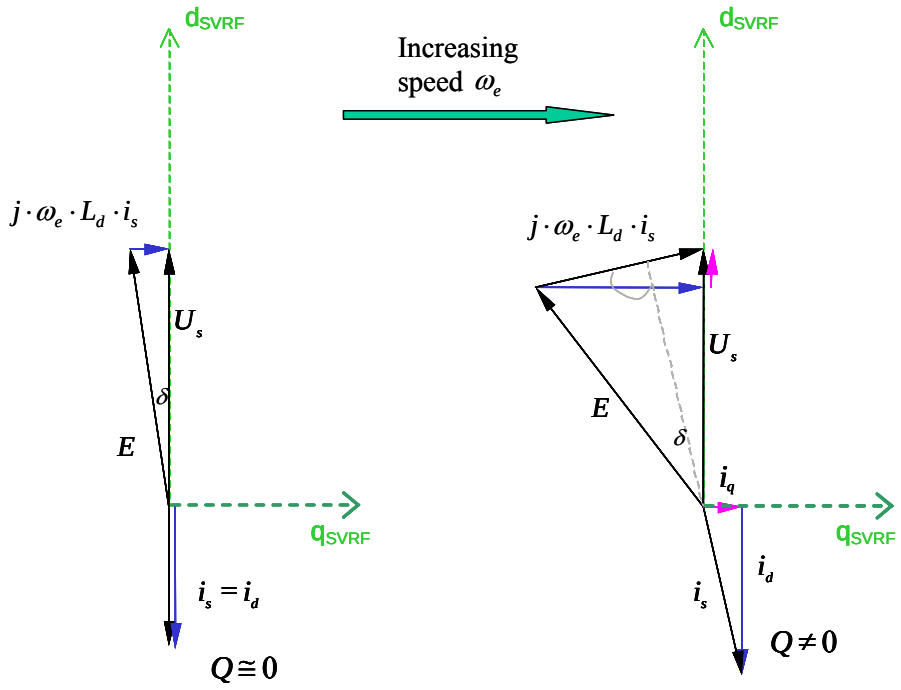

Figure 149: Generator stator voltage U_S control strategy – two operation points (at low wind speeds).

The control strategy used in this work is based on the idea that the generator-side converter controls the generator stator voltage U_S and the DC-link voltage constant, while the grid-side converter controls independently the active and reactive power flow to the grid.

Similar to the control of DFIG (see Chapter 7), the control of both converters existing in the direct-driven PMSG wind turbine concept is also based on two control loops in cascade: a very fast inner current controller regulating the currents to the reference values that are specified by the outer slower power controller. The current controller provides reference signals in d- and q-axis, which are sent further to the PWM-controlled power converter.

Generator-side converter control (controller 1)

The generator-side converter controls the DC-link voltage U_{DC} and the generator stator voltage U_S in the stator voltage oriented reference frame (SVRF). Hence, the DC voltage is controlled with the d-component of the stator current, while the stator AC voltage is controlled by the q-component of the stator current. The stator voltage is controlled to its rated value in order to avoid overvoltage or saturation effects in the converter. The DC-link voltage is also kept constant, but small variations of the DC-link voltage are allowed when the electrical damping of the system is necessary. The DC-link voltage is controlled to its reference value U_{DC}^{ref}, provided by the damping system, described in Section 9.6.3.

The generic control structure of the generator-side converter is shown in Figure 150.

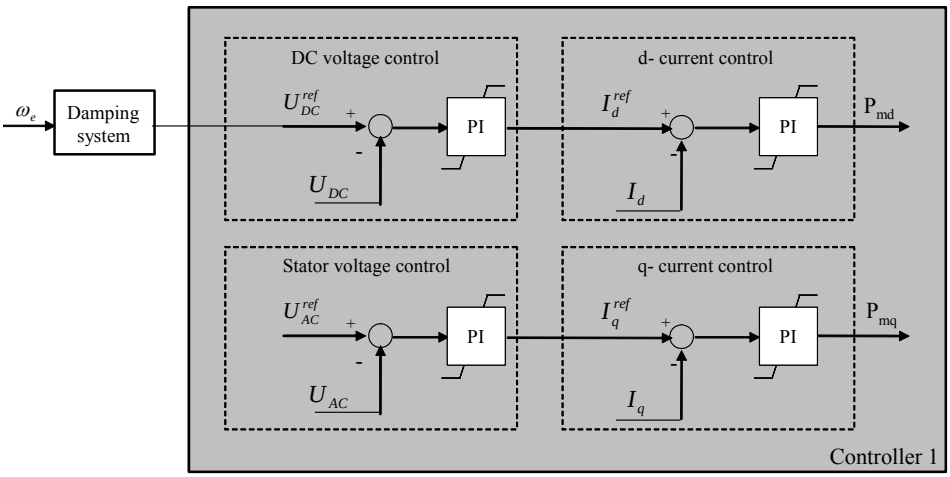

Figure 150: Generator-side converter control (controller 1).

As the generator-side converter balances the DC link voltage, it ensures the power transport from the PMSG terminals to the power grid. Notice that the control of active power and of constant DC-link voltage is closely related.

Grid-side converter control (controller 2 and MPT)

The grid-side converter controls active and reactive power in a grid voltage oriented reference frame. Hence, the active power P_{grid} is controlled by d- component of the converter current whereas the reactive power Q_{grid} is controlled by the q-component of the converter current. The generic control of the grid-side converter is illustrated in Figure 151.

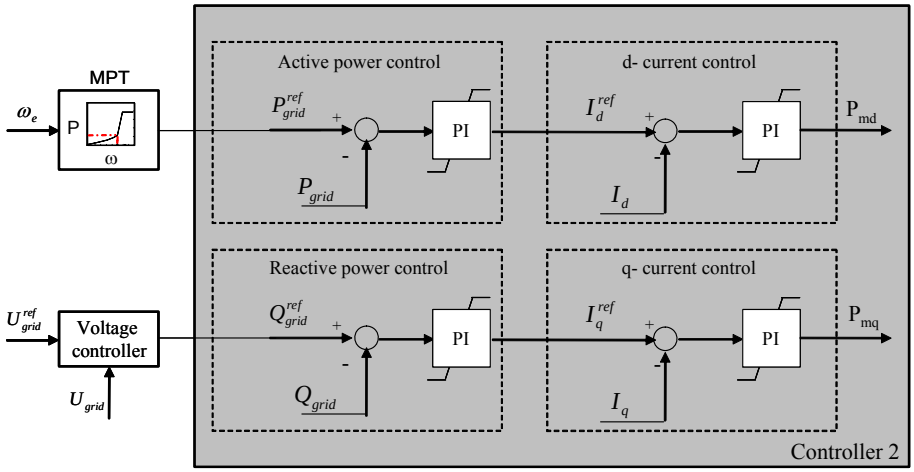

Figure 151: Grid-side converter control (controller 2).

Notice that the power reference P_{grid}^{ref} is defined by the speed-power MPT characteristic. The objective of MPT characteristic, illustrated in Figure 152, is to drive the wind generator automatically in the operation point of highest efficiency at any time.

As known, the variable speed wind power generators can be operated at a constant power factor or can support with reactive power. The reactive power reference Q_{grid}^{ref} is in generally set to zero. However, in the cases when the grid voltage is disturbed from its rated value and voltage grid support is required

from the wind turbine, the reactive power reference Q_{grid}^{ref} can be provided by a voltage controller, as indicated in Figure 151.

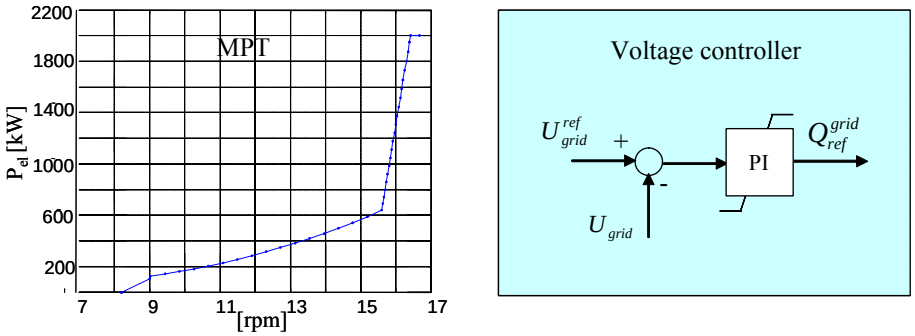

Figure 152: Maximum power tracking (MPT) characteristic and voltage controller used for direct-driven PMSG wind turbine.

The voltage controller, sketched in Figure 152, is realised by a PI controller with antiwind-up and controls the grid voltage to its rated value. The input of the controller is the error signal between the measured grid voltage and the rated grid voltage.

The parameters of the converter controllers are determined based on the wind turbine response to steps in deterministic wind speeds.

A potential advantage of this converter control strategy is that it does not need any special treatment to handle grid faults. During a grid fault, the generator - side converter is less affected by the fault since it is not directly coupled to the grid. It can therefore, during grid faults, continue unaffected to control the generator stator voltage and the DC voltage to their rated values, while the active and reactive power supply to the grid are directly controlled at the wind turbine terminals by the grid-side converter. However one may pay attention on the DC-link voltage reference value provided by the damping controller. Only small variations from its rate value are acceptable for the DC-link voltage. During a grid fault the wind turbine starts to accelerate due to the unbalance between the electromagnetic torque and mechanical torque. In this situation, the damping controller reacts immediately trying to damp the speed oscillations by controlling the DC voltage reference. This action can generate an oscillating DC voltage reference itself, up and down outside a reasonable range for the converters control. This phenomenon can lead to instability, especially for very low U_{DC} reference values. This can be avoided by simply limiting the DC voltage reference signal or by using a chopper. It is beyond the scope of this report to focus on the fault-ride-through capability of PMSG wind turbine concept. However, a simple simulation, where the DC voltage reference provided by the damping controller is limited, is illustrated in Section 9.7 in order to underline the strength of the described converter control strategy also in case of grid faults.

9.7 Simulations results

In this section, different studies are carried out in order to illustrate and evaluate the performance of the control system for the variable speed multi-pole PMSG wind turbine concept. The controller performance is assessed and discussed by means of normal operation simulations of a 2MW PMSG wind turbine connected to the grid through a 2.5MW power converter.

The network layout of the variable speed multi-pole 2MW PMSG wind turbine is illustrated in Figure 153.

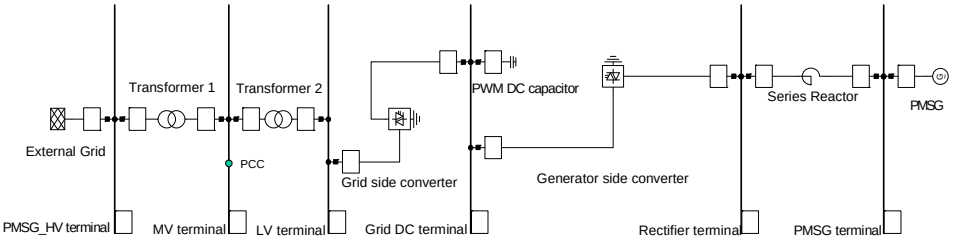

Figure 153: Electrical layout of the PMSG wind turbine with full-scale converter.

The wind turbine is connected to the external grid through a full-scale converter consisting of a generator-side converter, a dc-link capacitor and a grid side converter. The control of active and reactive power is based on the measured power at the PCC placed on the MV terminal.

9.7.1 System performance under deterministic wind speeds

In order to evaluate the performance of variable speed direct-driven PMSG wind turbine controller, described in this chapter, a set of step response simulations with deterministic wind speed (no turbulence, no tower shadow) are performed. Typical quantities of the turbine system, as wind speed in [m/s], pitch angle in [deg], generator speed in [rpm] and the active generator power in [MW], are shown in Figure 154 for steps in wind of 1m/s every 20 seconds.

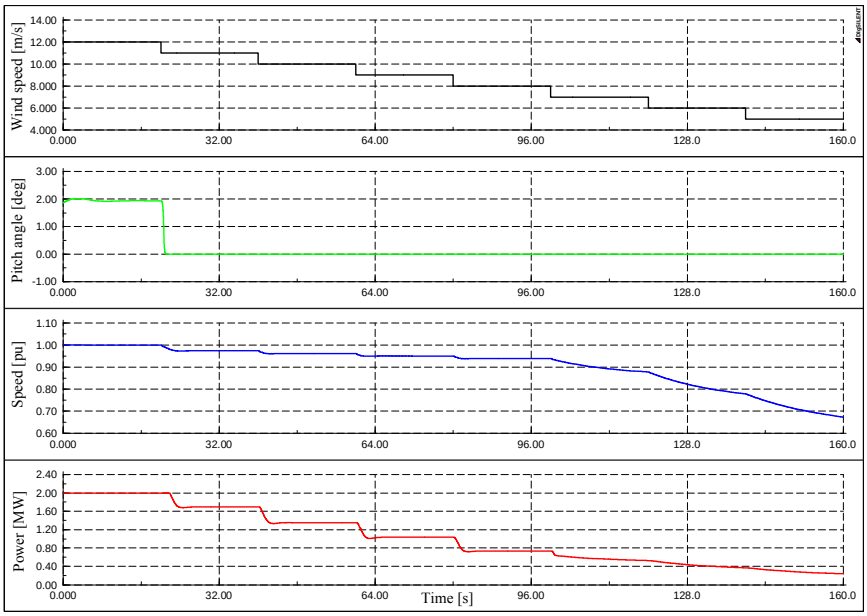

Figure 154: Wind speed, pitch angle, generator speed and active power for steps in wind of 1m/s from 12m/s down to 5m/s.

In the power optimization strategy (i.e.at low wind speeds less than 12m/s), the speed controller is passive, keeping the pitch angle constant to the optimal value (i.e. zero for the considered wind turbine). Meanwhile, the power controller controls the active power to the active power reference signal provided by the maximum power tracking look-up table. The generator speed is continuously adapted to the wind speed, in such a way that it is extracted maximum

power out of wind. Notice that the response time in the steps is bigger at lower wind speeds then at higher wind speeds.

Figure 155 shows the performance of the generator side converter control during the simulated case. The illustrated signals are: the Dc-link voltage, the stator voltage, the generator reactive power and the reactive power to the grid. The DC-link voltage is kept constant to its reference value of 5.9 kV. However, the damping of the system causes small variations of the DC-link voltage around its reference value. Notice that the stator voltage is also controlled to its rated value, too.

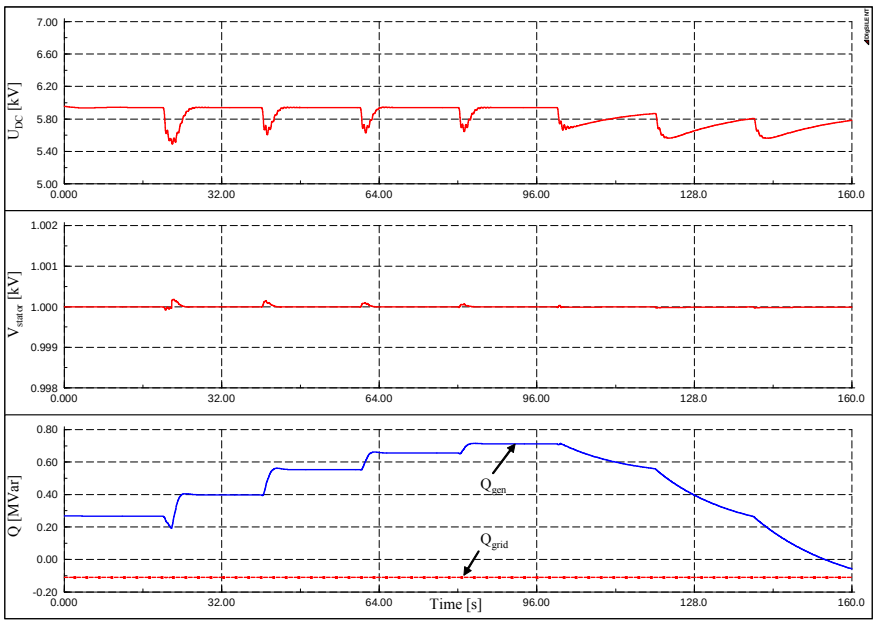

Figure 155: DC-link voltage, stator voltage, generator reactive power and the grid reactive power for steps in wind of 1m/s from 12m/s down to 5m/s.

Notice that the reactive power production of generator and grid side converter is independently controlled.The reactive power demand of the generator varies, while the grid side converter reactive power production is zero. As expected, by using the control strategy described in this chapter, the generator reactive power varies while the stator voltage is kept constant.

As long as the wind speed is bigger than 8m/s, the generator works in an underexcitated operation. In this speed range, according to the linear ramp in the MTP characteristic, the active power of the generator P_{gen} decreases linearly with the speed. Meanwhile, the internal voltage E=j$\omega\Psi_{PM}$ decreases also linearly with the speed. In this situation, the stator current q-component starts to increase in order to keep the stator voltage constant. Hence, the reactive power increases. After 100 s the wind speed steps down to 7 m/s. From this moment, the active power is controlled according to the MPP tracking with $P \sim \omega^3$. The torque and the load angle start to decrease stronger ($T_e \sim \omega^2$) than the amplitude of E, which finally leads to a decrease of reactive power. In contrast to this, the grid-side converter reactive power production does not vary. The grid side converter only satisfies the small reactive power demand of the transformer.

A similar simulation, performed for steps in the wind speed from 12m/s up to 20m/s, is illustrated in Figure 156 and Figure 157. Notice that both the speed controller and the active power controller are active for wind speeds higher that 12m/s.

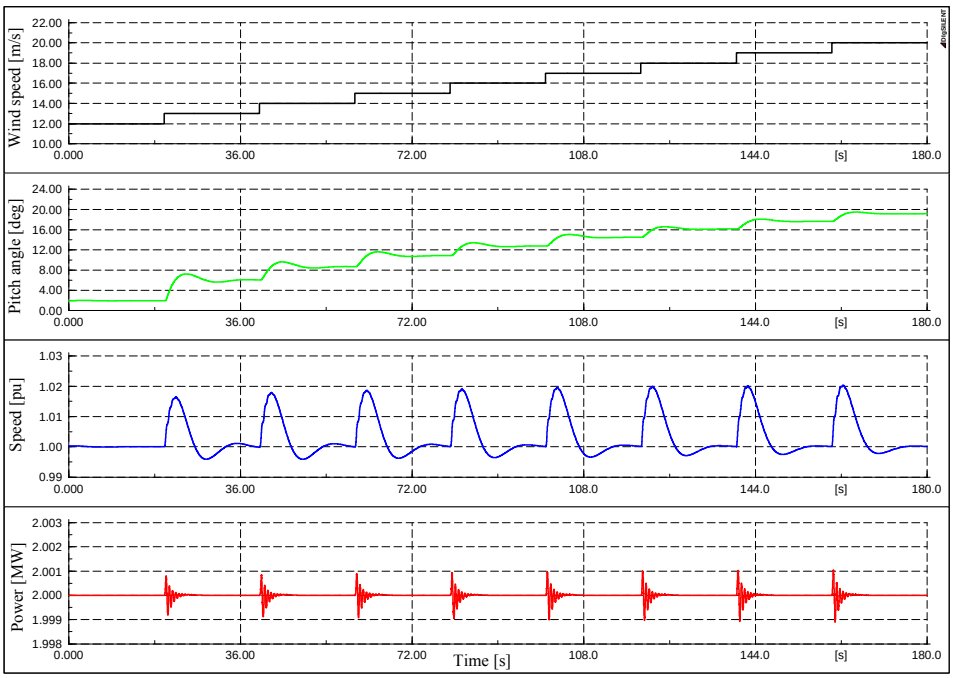

Figure 156: Wind speed, pitch angle, generator speed and active power for steps in wind of 1m/s from 12m/s up to 20m/s.

The steps in the wind speed yield changes in both the pitch angle and the generator speed. The step response of the pitch angle and generator speed does not present big overshoots and oscillations (fast in steady state). Remark also that the response of the generator speed is almost identical over the whole wind range between 12m/s and 20m/s, a fact that indicates that the gain scheduling in the speed controller is working properly. The power controller keeps the active power to 2MW with a small deviation about 1%. Since the pitch mechanism reacts slowly compared to the power controller, dynamic variation in the generator speed and so in the rotational speed of the turbine rotor are allowed in order to absorb fast wind gusts and to store rotational energy in the turbine's inertia.

The stator voltage is kept constant, while the DC-link voltage varies according to the damping signal, which is modulated on the constant reference value od U_{DC}. Notice that the generator reactive power is almost constant in this case.

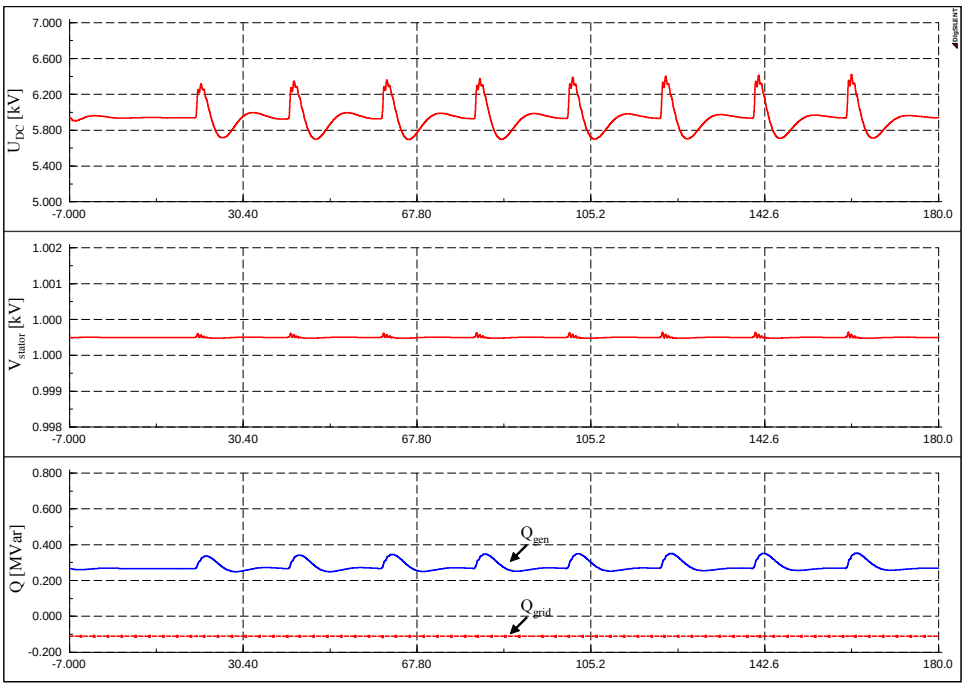

Figure 157: DC-link voltage, stator voltage, generator reactive power and the grid reactive power for steps in wind of 1m/s from 12m/s up to 20m/s.

9.7.2 System performance under stochastic wind speeds

The performance of the PMSG wind turbine control system, designed and described in this chapter, is now illustrated for the case of stochastic wind speeds. Two set of simulations are considered: one for mean wind speed 8m/s and another for mean wind speed 12m/s.

Figure 158 illustrates the case when the mean speed is 8 m/s and the turbulence intensity of 10%.

The generator speed is tracking the slow variation in the wind speed. As expected for this wind speed range, the pitch angle is passive, being kept constant to its optimal value (i.e. zero for the considered wind turbine). The active power delivered to the grid does reflect the variation in the wind speed. Notice that the fast oscillations in the wind speed are completely filtered out from the electrical power.

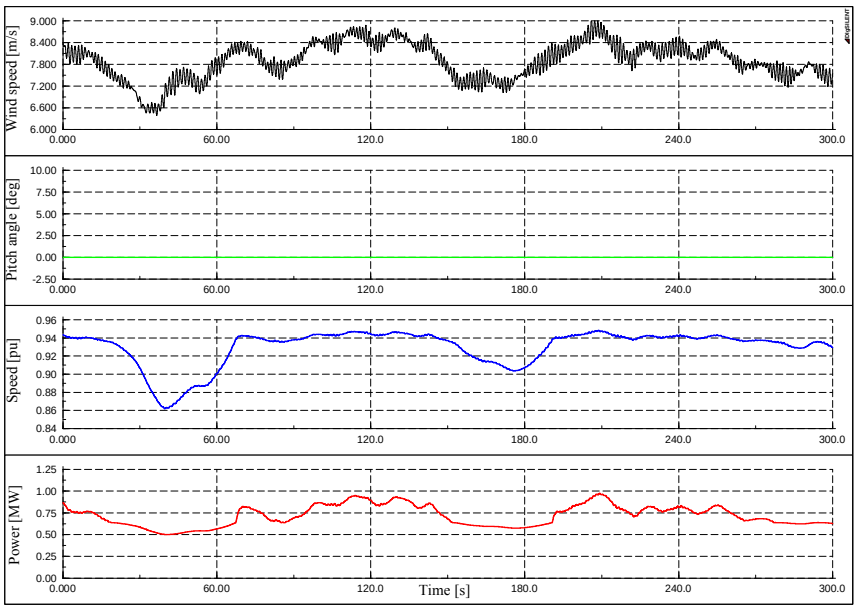

Figure 158: Wind speed, pitch angle, generator speed and active power under stochastic wind speed with a mean wind speed of 8m/s.

Figure 159 illustrates the simulation with turbulent wind, where the mean speed is 12 m/s and the turbulence intensity of 10%. The turbine operates partly at rated conditions and partly at partial load. As soon as rated wind speed is exceeded, the pitch angle increases and limits the speed. The power is kept to the rated power as long as the energy in the wind permits that.

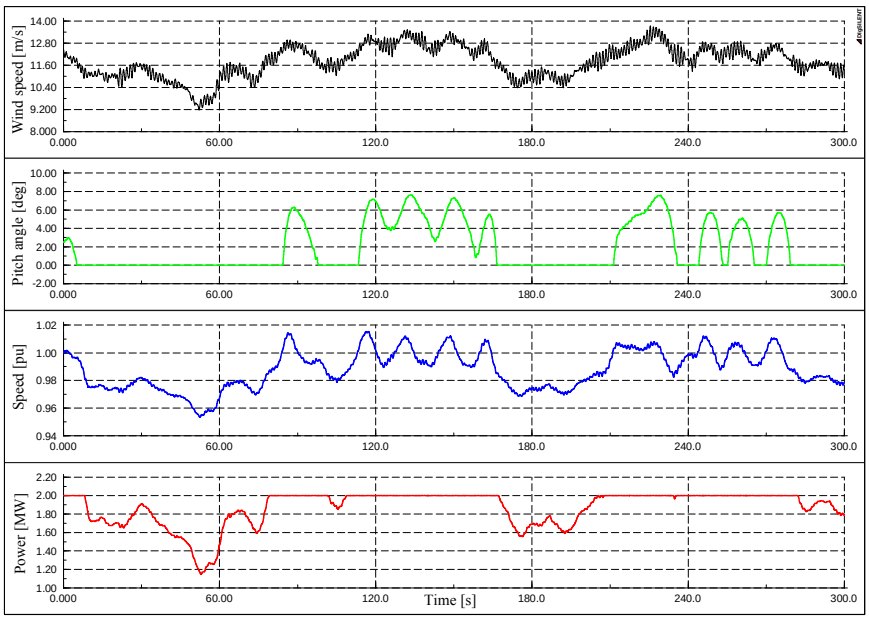

Figure 159: Wind speed, pitch angle, generator speed and active power under stochastic wind speed with a mean wind speed of 12m/s.

9.7.3 Voltage controller effect

The following simulation shows the performance of the voltage controller during normal operation conditions. The grid voltage and the reactive power supplied to the grid by the grid-side converter are illustrated for the situations with and without voltage controller respectively. It is assumed that the 2MW PMSG wind turbine operates at its rated capacity (i.e. at wind speeds higher than 12m/s), as this is worst for the voltage stability.

Figure 160 illustrates how the voltage controller, presented in Figure 152, adjusts the reactive power demand Q_{grid}^{ref} for the grid-side converter controller in the case when a reactive power sink is connected and then disconnected at the MV terminal of the PMSG wind turbine in Figure 153. It is assumed that first 1MVar reactance and than 1.5MVar, respectively, is connected to the MV terminal and disconnected after 1 second, successively as illustrated in Figure 160.

Notice that the connection of each reactance implies a modification in the grid voltage U_{grid}. When no voltage control is enabled (case 1), no reactive power support is delivered to the grid by the grid-side converter. The grid voltage is therefore not re-established as long as no matter which reactance is connected to the PMSG wind turbine's grid.

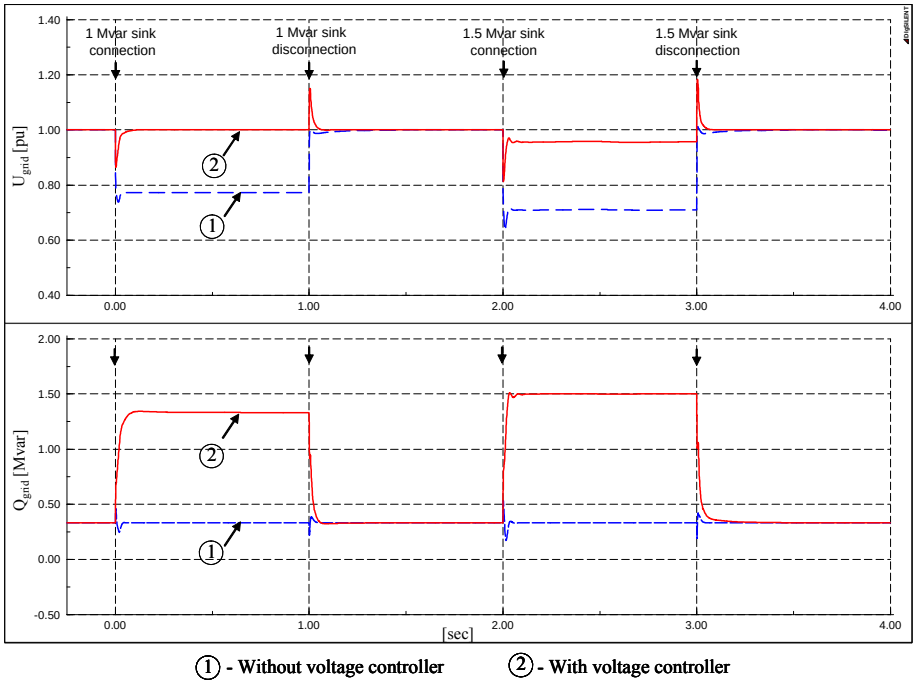

Figure 160: PMSG voltage controller performance ((a) – without voltage control (b) with voltage control) -when a reactive power sink of 1Mvar and 1.5Mvar respectively, is connected and disconnected

On the other hand, when the voltage controller is used (case 2), the grid-side converter supports the grid by supplying reactive power – as illustrated in Figure 160. In this case, the grid voltage is quickly re-established to 1pu when the first 1MVar reactance is connected. The connection of the 1.5MVar reactance leads, as expected, to a deeper drop in the grid voltage and therefore the PMSG wind turbine has to produce more reactive power to re-establish the grid voltage. The 2MW PMSG wind turbine connected to the grid through the 2.5MVar converter has a reactive power reserve about 1.5MVar in the case of a 12m/s wind speed. The grid-side converter produces therefore its maximum limit of 1.5MVar to the grid when the second reactance is connected. Notice that it is however not sufficient to re-establish the grid voltage due to the reac-

tive power absorbed by the transformer placed between the grid-side converter and the PCC – see Figure 153.

10 CONCLUSIONS

This report presents a collection of models and control strategies developed and implemented in the power system simulation tool PowerFactory DIgSILENT for different wind turbine concepts. It is a second edition of Risø-R-1400(EN) and it gathers and describes a whole wind turbine model database built-op and developed during several research projects. The report contains thus an overview over some electrical models (induction generator, synchronous generator, power converters, transformers), already integrated components in the power system tool, but also over the newly developed and implemented wind turbine models (mechanical model, aerodynamical model, wind model, control model).

The wind turbine dynamic model includes the main effects that contribute to the fluctuation of the power from a wind turbine. It comprises the mechanical model, the aerodynamic model (improved with a model for dynamic stall effects) and the electrical model: induction generator, power converter (converter, soft-starter, capacitor bank) and transformer.

The built-in electrical models in DIgSILENT are initialised automatically by the load flow calculation, while the user developed models, must be initialised by the user. If the initialisation is not done properly, it results in large fictive transients, which must decay before the actual dynamics can be simulated. This costs simulation time and in some cases the fictive transients even can cause numerical instabilities. An initialisation method is therefore developed and implemented. This method allows immediately an accurate simulation of the dynamic performance, without fictive transients in the beginning of the simulation.

The main attention in the report is drawn to the modelling at the system level of the following wind turbine concepts:

1. Fixed speed active stall wind turbine concept
2. Variable speed doubly-fed induction generator wind turbine concept
3. Variable speed multi-pole permanent magnet synchronous generator wind turbine concept

These wind turbine concept models can be used or even extended for the study of different aspects, e.g. assessment of power quality, control strategies, connection of the wind turbines at different types of grid.

The goal of the model database process has been to build generic models, without focusing on a particular design of a manufacturer. They are not restricted by confidentiality, but as a consequence, the performance of the simulation models may differ some from the performance of a specific wind turbine.

Since wind turbine controllers can be designed in several ways, and since the design details are normally confidential, new control methods have been proposed and implemented, their performance assessed and discussed by means of simulations. The design as well as the evaluation of the controllers was carried out for normal continuous operations (for both power optimisation and power limitation operations), but grid fault conditions operation has been also treated. As in the near future, wind turbines are required to replace more or less other generating units in the power system, grid support power and voltage controller have been also designed and presented.

Fixed speed active stall wind turbine concept

A dynamic model of an active stall wind turbine connected to the grid, has been implemented in the power system simulation tool Power Factory-DIgSILENT. Different control strategies depending on the connection type (AC or DC) of the active stall wind turbine have been presented.

AC connection case:

The simulation model, presented in this report, of the active stall wind turbine with AC grid connection, regards wind turbines similar to the ones in Nysted. Two control strategies for the active stall wind turbine with AC connection have been designed and presented in the report.

The first designed controller is a traditional active stall wind turbine controller where the goal is to achieve electrical power with a minimum of pitch actions. Such a controller is very slow, as it tries to reduce the pitch activity as much as possible to limit the stress of the pitch system. The simulations conducted show that the controller manages to run the turbine efficiently in many conceivable wind speed situations. The system has no tendency to become unstable in which situation ever, since the controller does not attempt to respond to fast transients instantaneously. However such a controller design is not optimal for grid support, since in this case the wind turbine is asked to act as a fast active element in the power system. To speed up the power control, a second control design for the active stall wind turbine has been purposed and presented.

The second controller is a grid support power controller. The aim of this controller, is to enable fast control of the wind turbine power, which is necessary especially in case when specific and fast power demands are imposed to wind turbines by the system operator. It has to be as fast as possible to power reference changes, but still with physical limits on pitch activity. This characteristic of the controller enables better grid integration for active stall wind turbines with AC connection, as it manages a relatively fast response to changes in the active power demand. Simulations show that a sudden change in the active power set point for an active stall wind turbine can be reached fully within a few seconds when this fast controller is used.

Notice that this second controller for active stall wind turbine is also attractive in case of grid faults operation, when a quick reduction of the aerodynamic power production is necessary as soon as a grid fault is detected. In case of grid fault operation, the wind turbine power has to be reduced as soon as a grid fault occurs, in order to prevent it from going overspeed, and by doing so, assists in voltage recovery. When a grid fault is detected, the controller gets for example a zero power reference. Riding through grid faults implies that the active stall wind turbine has to change its pitch angle as quickly as possible (maximum pitch rate).

DC connection case:

The grid support control capabilities of an active stall wind turbine can be even more improved in case when it is connected to the grid via an HVDC/VSC. A DC grid connection via HVDC/VSC transmission of an active stall wind farm has been therefore designed and presented in this report. Such a system has special regulating properties e.g. decoupled control of active and reactive power, continuous AC voltage regulation, variable frequency control, black-start capability, etc. Moreover the market interest for this concept may increase if it is proved that using a DC transmission system the wind farm/park can develop power plant characteristics as the turbine itself is cost-efficient and very reliable.

A new control strategy for an active stall wind farm station has been proposed and implemented in DIgSILENT. Using this control strategy an active

stall wind farm can operate both with fixed voltage/frequency or variable voltage/frequency situations. In the second situation the set point frequency is calculated based on the maximum average wind speed inside the wind farm. Since the reactive power necessary for the operation of squirrel-cage induction generator is provided by this power converter the wind turbines use a fixed capacitor bank instead of a variable one in both cases. The variable voltage/frequency control strategy implies also a simplification in the active stall controller and reduces the pitching of the blades for low wind speeds. The simulation results show a good response of the implemented system in both situations.

Variable speed doubly-fed induction generator wind turbine concept

A dynamic model of a variable speed, variable pitch wind turbine with DFIG, has been also implemented in the power system simulation tool Power Factory-DIgSILENT.

The overall control system of a variable speed DFIG wind turbine is built up with a hierarchical structure. There are two hierarchical control levels, strongly connected to each other, i.e. DFIG control level (control of active and reactive power) and wind turbine control level. A vector control approach is adopted for the control of the power converter, while the control of the wind turbine is a result of two cross-coupled controllers: a speed and a power limitation controller. The control of the power converter is essential for the behaviour of the DFIG wind turbine both in normal and during grid fault conditions.

This report proposes and presents the design of different control strategies for a DFIG wind turbine for both normal operation and for operation during grid fault conditions.

Normal operation

The overall control of the variable speed, variable pitch wind turbine with DFIG during normal operation has as goal to track the wind turbine optimum operation point, to limit the power in the case of high wind speeds and to control the reactive power interchanged between the wind turbine generator and the grid.

In normal operation, the power converter control has the following goals:

- the rotor-side converter has to control independently the active and reactive power on the grid.
- the grid-side converter has to maintain the dc-link capacitor voltage in a set value regardless of the magnitude and the direction of the rotor power and to guarantee a converter operation with unity power factor (zero reactive power).

The control of the wind turbine generates the pitch angle of the wind turbine and the reference of the active power for the power converter control. In this report two of the most frequent control strategies for variable speed wind turbines have been implemented and described:

- Control strategy I - where the power converter is used to control the generator speed, while the pitch system limits the power.
- Control strategy II - where the power converter controls the power, while the pitch system prevents the overspeeding of the generator, i.e. the pitch angle limits the generator speed to its rated value in case of high wind speeds. It provides a fast power control.

Both control strategies are implemented and presented. Their good performance is assessed and discussed by means of simulations. Notice that the second control strategy is expected to be closer to the real controllers implemented in the industry.

Operation during grid fault

A dynamic model of variable speed DFIG wind turbines with the fault ride-through control and protection has been also implemented in DIgSILENT.

The fault ride-through and voltage controller of the DFIG wind turbine presented in this report is built-on as an extension of the control structure of the DFIG during normal operation.

In contrast to its very good performance in normal operation, the DFIG wind turbine concept is quite sensitive to grid faults and requires special power converter protection. The protection system of the converter (i.e. crowbar resistance) is triggered when high transient currents and voltages occur in the generator and converter, otherwise the power converter device would be damaged during grid faults. When the crowbar is triggered, DFIG behaves as a conventional squirrel cage induction generator (SCIG) and therefore its controllability is temporarily lost. The crowbar resistance, which value is strictly dependent on the generator data sheet, has influence on the rotor current and on the reactive power demands of the generator during grid faults.

The goal of the implemented fault ride-trough controller for a DFIG wind turbine is to provide the wind turbine the control ability, required in the technical specifications by the power system operator, namely to operate uninterrupted at disturbances in the power system, such as short-circuit faults, and to contribute to the voltage control. Such control of DFIG during a grid voltage dip enables:

- Voltage recovery assistance by the wind turbine during the fault
- Reduced demand of other dynamic reactive compensation units
- Reduced standby power generation, because of uninterrupted wind turbine operation at disturbances
- Return to normal operation conditions after the fault.

The implemented voltage control is based on a strategy where the control of both rotor side converter (RSC) and grid side converter (GSC) is designed in a coordinated manner. RSC controls the voltage on the grid as long as it is not blocked due to heavy disturbances, case when GSC is that which is used to control the voltage. However its generation is limited by GSC rating.

Besides these controllers, a damping controller has been also implemented and tuned in order to damp possible torsion oscillations excited at a fault in the drive-train system. From the transient stability point of view, the drive train of the wind turbine has to be represented by a two-mass model in order to be able to simulate the torsional oscillations excited in the drive train system during grid faults. A damping controller has to be implemented and tuned to damp actively these oscillations, which otherwise might lead to self-excitation and high mechanical stress of the drive train system.

Studies regarding DFIG fault ride-through and voltage grid support capability in a realistic power transmission system model.

Several studies regarding DFIG fault-ride through and voltage grid support capability in a realistic power transmission system model have been carried out. The Danish Transmission System Operator Energinet.dk. has developed and delivered such a realistic power system model for educational and research purposes. This has been a great opportunity for the project to investigate in a realistic power system frame the performance of the designed and implemented DFIG fault-ride through and voltage grid support controller. The simulation results have been shown that the DFIG equipped with the developed voltage grid support control manages to re-establish rapidly the voltage after a severe grid fault. Moreover, it was also concluded that a DFIG wind farm equipped with voltage

control can help a nearby active stall wind farm to ride through a grid fault, without implementation of any additional ride-through control strategy in the active stall wind farm.

Variable speed multi-pole permanent magnet synchronous generator wind turbine concept

A model for a variable speed wind turbine with multi-pole permanent magnet synchronous generator has been developed and implemented in DIgSILENT.

The model contains representations of a permanent magnet generator, a back-to-back voltage source converter and its control, the aerodynamic rotor, a two mass model representation of the shaft system and the pitch angle control.

A control method has been designed for normal operation conditions. The objectives of the control system are:

- to track the maximum power operation point in case of small wind speeds;
- to limit the power in case of large wind speeds;
- to stabilize and damp actively the drive train oscillations existing in the multipole PMSG wind turbine system

The strongest feature of this control method is that it enables the system to stay stable in any operating condition. It has been observed that the wind turbine configuration with multipole PMSG behind a full scale converter is quite an unstable system. There are several reasons for that: 1) PMSG has no damper windings 2) the drive train shaft becomes soft in case of large number of multipoles 3) SG behind a full scale converter (electrical decoupling between turbine and grid). The damping oscillations in the generator speed has been realized by periodically charging and discharging the dc-link, having thus no negative impact on the power quality in the grid.

The performance of designed and implemented control strategy for the multipole PMSG with full-scale converter has been assessed and illustrated by means of simulations for different operating conditions (up and down steps in low and large wind speeds, deterministic as well as stochastic). A future research step is to investigate and enhance the fault-ride through and voltage grid support controller's capabilities of the multipole PMSG full scale converter system.

The three implemented wind turbine concept models are an important step towards the long-term objective of developing tools for study and improvement of the dynamic interaction between wind turbines/wind farms and power systems to which they are connected. These models can be easily extended to model different kinds of wind turbines or wind farms.

Acknowledgements

This work was carried out by the Wind Energy Department at Risø National Laboratory in co-operation with Aalborg University. The Danish Energy Agency is acknowledged for funding this work in contract numbers ENS 1363/04-0008 and ENS-1363/01-0013.

REFERENCES

Akhmatov V. (2002), *Variable-speed wind turbines with doubly-fed induction generators. Part II: Power System Stability.* Wind Engineering, Vol. 26, No. 3, pp 171-188.

Akhmatov V. (2003), *Analysis of dynamic behavior of electric power systems with largeamount of wind power,* PhD thesis, 2003, Ørsted DTU.

Akhmatov V. (2003a), *Variable-speed wind turbines with doubly-fed induction generators. Part IV: Uninterrupted operation features at grid faults with converter control coordination*. Wind Engineering, Vol. 27, No. 6, pp 519-529.

Akhmatov V., Nielsen A.H., Pedersen J. K., Nymann O., 2003, *Variable-speed wind turbines with multipole synchronous permanent magnet generators. Part I. Modelling in dynamic simulation tools*. Wind Engineering, Volume 27, No. 6, pp 531-548.

Akhmatov V. (2004), *An aggregated model of a large wind farm with variable-speed wind turbines equipped with doubly-fed induction generators,* Wind Engineering, Vol 28, No 4, pp 479-488.

Akhmatov V., Nielsen A.H. (2006), *Simulation model of the transmission grid for a large offshore windfarm*, used in education and research at the Technical University of Denmark, Wind Eng.; 30(3), pp 255-263.

A. van Kaick Neu-Isenburg GmbH&Co. KG (a). *AvK – Manual. Self regulating brushless alternators*.

A. van Kaick Neu-Isenburg GmbH&Co. KG (b). *AvK Self regulating brushless alternators. Technical Data*.

Bahrman M.P., Johansson J.G., Nielsen B.A. (2003) *Voltage source converter transmission technologies – the right fit for the application*, IEEE Proceed. on Power Eng. Soc. General Meeting, vol.3, pp.1840-1847.

Binder A., Schneider T. (2005), *Permanent magnet synchronous generators for regenerative energy conversion – a survey.* European Conference on Power Electronics and Applications, EPE 2005, 11-14 September, Dresden, Germany.

Bindner H., Rebsdorf A., Byberg W. (1997) *Experimental investigation of combined variable speed/variable pitch controlled wind turbines.* EWEC, Dublin, 4p.

Blaabjerg F, Chen Z, Kjaer SB. (2004) *Power Electronics as efficient interface in dispersed power generation systems.* IEEE Trans. on Power Electronics, Vol.19, No.5, pp.1184-1194.

Bolik S.M. (2003), *Grid requirements challenges for wind turbines*, Proc. of the Fourth Int. Workshop on Large-Scale Integration on wind power and transmission networks for offshore wind farms, Billund, Denmark, 6p.

Bossany, E.A. (2000) *The design of closed loop controllers for wind turbines.* Wind Energy, vol. 3, p. 149-163.

Cigre (2003) *Modelling of gas turbines and steam turbines in combined cycle power plants,* Task Force C4.02.25.

DEFU (1998). *Connection of wind turbines to low and medium voltage networks*, Report no. KR111-E, Elteknikkomiteen (1998-10-09).

DIgSILENT GmbH, *DIgSILENT Technical Documentation - PowerFactory DSL Models*, August 2006.

Eltra (2000). *Specifications for Connecting Wind Farms to the Transmission Network.* ELT 1999-411a, Eltra, http://www.eltra.dk.

E.ON.(2006) *Netzanschlussregeln Hoch-und Hoechst-spannung.* 2003, Report ENENARHS2006, April 2006, 46 pages, www.eon-netz.com

Energinet.dk (2004) *Wind turbines connected to grids with voltages above 100 kV - Technical regulations for the properties and the control of wind turbines.* Energinet.dk, Transmission System Operator of Denmark for Natural Gas and Electricity, Technical Regulations TF 3.2.5, 2004, 35 p. Available: www.energinet.dk

Eping C., Stenzel J., Poeller M., Mueller H., (2005) *Impact of Large Scale Wind Power on Power System Stability*, Fifth INternational Workshop on Large-Scale Integration of Wind Power and Transmission Networks, April 7-8, Glasgow, Scotland, 9p.

Gjengedal T. (2003) *Integration of wind power and the impact on power system operation*, IEEE, pp. 76-83.

Grauers A.(1996), *Efficiency of three wind energy generator systems.* IEEE Transactions on Energy Conversion, Vol. 11, No. 3, pp. 650-657.

Grauers A., Landström S., (1999), *The Rectifiers Influence on the Size of Direct-driven Generators*. European Wind Energy Conference 1999, p. 829-832, 1-5 March Nice, France

Hansen, L.H.,Helle L., Blaabjerg F., Ritchie E., Munk-Nielsen S., Bindner, H., Sørensen, P. and Bak-Jensen, B. (2001) *Conceptual survey of Generators and Power Electronics for Wind Turbines*, Risø-R-1205(EN).

Hansen A. D., Bindner H., Rebsdorf A. (1999) *Improving transition between power optimisation and power limitation of variable speed/variable pitch wind turbines*. European Wind Energy Conference, Nice, France, 1-5 March, p. 889-892.

Hansen A. D., Sørensen P., Blaabjerg F., Bech J. (2002) *Dynamic modelling of wind farm grid interaction*. Wind Engineering, Vol. 26, No.4, p. 191-208.

Hansen A. D., Sørensen P., Iov F., Blaabjerg F. (2003) *Initialisation of grid-connected wind turbine models in power-system simulations*. Wind Engineering, Vol. 27, No.1, p. 21-38.

Hansen A.D., Iov F., Blaabjerg F., Hansen LH. (2004) *Review of Contemporary Wind Turbine Concepts and their Market Penetration.* Wind Engineering, 2004, Vol. 28, No.3, pp. 247-263.

Hansen A.D. (2005), *Generators and Power Electronics for Wind Turbines.* Chapter in *Wind Power in Power Systems*, Editor Thomas Ackermann, John Wiley &Sons, Ltd, 24 p.

Hansen A.D., Sørensen P., Iov F., Blaabjerg F. (2006a) *Grid support of a wind farm with active stall wind turbines and AC grid connection.* Wind Energy, vol. 6, pp 341-359.

Hansen A.D., Sørensen P., Iov F., Blaabjerg F. (2006b) *Power control of a wind farm with active stall wind turbines and AC grid connection*, EWEC, Athene, 6p.

Hansen A.D., Hansen L.H., (2007) *Wind turbine concepts market penetration over ten years (1995 to 2004)*, Wind Energy, Vol. 10, No. 1, pp 81-97

Heier S. (1998). *Grid Integration of Wind Energy Conversion Systems*, ISBN 0 471 97143.

Holdsworth L., Charalambous I., Ekanayake J.B., Jenkins N. (2004) *Power system fault ride through capabilities of induction generator based wind turbines*, Wind Engineering, Vol. 28, No 4, pp 399-412.

IEC 61400-21 (2001). *Wind turbine generator systems - Part 21: Measurement and assessment of power quality characteristics of grid connected wind turbines.* Final Draft International Standard 88/144/FDIS International Electrotechnical Commission, IEC 2001-07-01, Ed.1.

IEEE Std 421.5-1992. *IEEE Recommended Practice for excitation System Models for Power System Stability Studies*, IEEE Press, 1992, ISBN 1-55937-218-4;

Jauch C., Sørensen P., Bak-Jensen B. (2004) *International review of grid connection requirements for wind turbines.* Nordic wind Power Conference,1-2 March 2004, Chalmers University of Technology, 6p.

Jauch C. (2006), PhD thesis "Stability and Control of Wind Farms in Power Systems". Risø-PhD-24, Risø National Laboratory.

Jenkins N., Allan R., Crossley P., Kirschen D., Strbac G. (2000) – Embedded Generation, IEE Press, ISBN 085296 774 8;

Jöckel S., Hagenkort B., Hartkopf T., Schneider H.(2001), *Direct-Drive Synchronous Generator System For Offshore Wind Farms with Active Drive Train Damping by Blade Pitching*. European Wind Energy Conference EWEC 2001, 2nd-6th July, Copenhagen, Denmark, pp. 991-994.

Jöckel S. (2002), *Calculations of Different Generator Systems for Wind Turbines with Particular Reference to Low-Speed Permanent-Magnet Machines*. PhD thesis, Technical University Darmstadt.

Jöckel S., (2006), *High energy production plus built-in reliability – The new Vensys 70 / 77 gearless wind turbines in the 1.5 MW class,* European Wind Energy Conference EWEC, Athens.

Karlsson P. (2002). *DC Distributed Power Systems. Analysis, Design and Control for a Renewable Energy system*, PhD Dissertation, Lund University, Sweden, 2002, ISBN 91-88934-25-X;

Kayikci M., Anaya-Lara O., Milanovic J.V., Jenkins N. (2005) *Strategies for DFIG voltage control during transient operation*, CIRED, 18th Int. Conference on Electricity Distribution, Turin, 5p.

Krause P.C., Wasynczuk O., Sudhoff S. D. (2002) *Analysis of Electric machinery and drive systems*, IEEE Press

Kundur P. (1994), *Power System Stability and Control,* McGraw Hill.

Langreder W. (1996) *Models for variable speed wind turbines* CREST, Dept. of Electrical Engineering, Loughborough University, UK and Risø National Laboratory, Denmark.

Lasseter R. H. (2002) *Microgrids*, IEEE Power Engineering Society Winter Meeting, 2002, Vol. 1, 27-31, pp. 305 - 308;

Lehnhoff M., Böhmeke G., Trede A. (1998) *Active-Stall / Passive-Stall Vergleich und Betriebsergebnisse*, aerodyn Energiesysteme GmbH, Husumer Schiffswerft, DEWEK'98 Tagungsband, p. 78-81

Leonhard, W. (2001) *Control of electrical drives*, Springer Verlag, ISBN 3540418202.

Lindholm M. (2004), *Doubly-fed Drives for Variable Speed Wind Turbines - A 40kW laboratory setup*. PhD thesis, Ørestad-DTU, Denmark.

Pöller, M. (2003) *Doubly-Fed Induction Machine Models for Stability Assesment of Wind Farms*, Power Tech. Conf., Bologna.

Mohan N., Undeland, T.M. and Robbins, W.P. (1989) *Power Electronics: converters, applications and design*.

Novak P., Ekelund T., Jovik I., Schmidtbauer B. (1995) *Modelling and control of variable speed wind turbine-drive-system dynamics.* IEEE Control Systems, August.

Novotny D.W., Lipo T.A. (1998) *Vector control and dynamics of AC drivers*, Oxford University Press.

Pena, R., Clare, J.C. and Asher, G.M. (1996) *Doubly-fed induction generator using back-to-back PWM converters and its application to variable speed wind-energy generation*. IEE proceedings on electronic power application, 143(3), p. 231-241.

Poeller M., Achilles S. (2003), *Aggregated Wind Park Models for Analyzing Power System Dynamics*, Fourth International Workshop on Large-Scale Integration of Wind Power and Transmission Networks, October 20-21, Billund, Denmark, DIgSILENT, 10pp.

Rosas P.A.C. (2003) *Power Quality and Stability Issues of Integration of Large Wind Farms.* Ph.D. thesis.

Schettler F., Huang H., Christl N. (2000) *HVDC transmission systems using voltage sourced converters – Design and applications*, IEEE Proceed. on Power Eng. Soc. General Meeting, vol.2, pp. 715-720;

Skytt A.K., Holmberg P., Juhlin L.E. (2001) *HVDC Light for connection of wind farms*, Proceed. on 2nd International WorkShop on Transmission Networks for Offshore Wind Farms, Royal Institute of Technology Stockholm, Sweden, March 29-30.;

Slootweg JG, Kling WL. (2001) *Modelling and analysing impacts of wind power on transient stability of power systems*, Wind Engineering, Vol. 25, No.6, pp. 3-20.

Sun T., Chen Z., Blaabjerg F. (2005) *Transient stability of DFIG Wind Turbines at an External Short-circuit fault*, Wind Energy, No 8, pp 345-360.

Søbrink K.H., Sørensen P.L.(1999) *DC Feeder for connection of a wind farm*, Proceeed. On Cigre Symposium, Kuala Lumpur, Malaysia, September;

Sørensen P., Bak-Jensen B., Kristiansen J., Hansen A.D., Janosi L., Bech J. (2000) *Power plant characteristics of wind farms*. Wind Power for the 21st Century. Proceddings of the International Conference held at Kassel, Germany 25-27 September.

Sørensen P., Hansen A.D., Janosi L., Bech J., Bak-Jensen B. (2001a) *Simulation of interaction between wind farm and power system.* Risø-R-1281, Risø National Laboratory.

Sørensen P., Hansen A.D., Rosas P.A.C. (2001b) *Wind models for prediction of power fluctuations from wind farms.* Journal of Wind Engineering no 89, p. 9-18 .

Sørensen, P.; Hansen, A.D.; Christensen, P.; Meritz, M.; Bech, J.; Bak-Jensen, B.; Nielsen , H. (2003), *Simulation and Verification of Transient Events in Large Wind Power Installations.* Risø-R-1331 (EN), 80p.

Sørensen P, Iov F, Blaabjerg F, Skaarup J, (2004) *Test and simulation of dynamic phase compensation from Mita-Teknik A/S*, Risø-R-1438 (EN).

Westlake A. J. G., Bumby J.R., Spooner E. (1996) *Damping the power-angle oscillations of a permanent-magnet synchronous generator with particular reference to wind turbine applications*. IEE Proceedings, Electr. Power Appl., Vol 143, No 3, May.

Wortmann B., Hansen L.H. (2000) *Multi-pole generator wind energy converter without gearbox and with variable speed*. Project EFP 96 report. Partners: Risø national Laboratory, Elkraft AmbA, Siemens A.G., NEG Micon A/S.

Øye,& S. (1991). *Dynamic stall - simulated as time lag of separation.* In Vol. Proceedings of the 4th IEA Symposium on the Aerodynamics of Wind Turbines, McAnulty, K.F- (Ed.), Rome, Italy.

Risø's research is aimed at solving concrete problems in the society.

Research targets are set through continuous dialogue with business, the political system and researchers.

The effects of our research are sustainable energy supply and new technology for the health sector.